Nuno Alberto Marques Mendes

ROBOTIC FRICTION STIR WELDING OF POLYMERS

Doctor of Philosophy Thesis in Mechanical Engineering, specialization in Control and Management, supervised by Professor Joaquim Norberto Cardoso Pires da Silva and Professor Altino de Jesus Roque Loureiro and submitted to the Mechanical Engineering Department of the Faculty of Sciences and Technology of the University of Coimbra

July 2014

· U C ·

UNIVERSIDADE DE COIMBRA

ROBOTIC FRICTION STIR WELDING OF POLYMERS

Nuno Mendes

PhD Thesis

Printed in Coimbra, Portugal

UNIVERSIDADE DE COIMBRA

It is not knowledge, but the act of learning, not possession but the act of getting there, which grants the greatest enjoyment.

Carl Friedrich Gauss, 1777-1855.

To my family and friends.

Acknowledgements

The preparation of this dissertation was only possible thanks to the contribution and support of many people.

First of all, I would like to express my gratitude to my doctoral advisor Professor Norberto Pires for introducing me into the field of robotics. I would also like to express my appreciation and gratitude to my doctoral co-advisor, Professor Altino Loureiro, for his guidance, support and availability. They both trusted me and provided encouragement and freedom to investigate my own ideas, having good advices and providing me very good feedback. I would like to give a special thanks to Professor Carla Martins, MSc Anaísa Costa of the University of Minho (IPC/I3N – UM), Professor Pedro Vilaça, PhD João Gandara of the Instituto Superior Técnico (IST), PhD David Verdera and MSc José Sotelo of the Asociación de Investigación Metalúrgica del Noroeste (AIMEN) for their invaluable assistance. I would further like to thank all the staff and students, past and present, at the Industrial Robotics Laboratory of the University of Coimbra for creating such an easy going and inspiring atmosphere over the years, my colleagues and friends Pedro Neto, Nélio Mourato, Paulo Vaz, André Castelhano and Dário Pereira.

My appreciation and gratitude also goes out to the University of Coimbra's Mechanical Engineering Research Centre (CEMUC), with special thanks to the members of the Advanced Manufacturing Systems Group. I also wish to extend my thanks to all the professors and staff of the Department of Mechanical Engineering of the University of Coimbra (DEMUC), who all contributed in their own way to make my years at DEMUC a very pleasurable experience. Last but not least, I am extremely grateful to my family and close friends. They have been a constant source of encouragement.

This thesis was made possible thanks to the support of the Portuguese Foundation for Science and Technology (FCT), grant SFRD/BD/62485/2009.

Nuno Mendes

Coimbra, July 2014

Abstract

In the last few years, there has been a tendency in the way factories have evolved. Increasingly, manufacturing companies are changing and reinventing their production systems. The automation of some technological processes is today a major factor for the success of a manufacturing company. Owing to its flexibility, programmability and efficiency, industrial robots are a fundamental element of modern flexible manufacturing systems, promoting productivity when successfully implemented. In addition, automation can open the door of such processes to more companies, especially small and medium sized companies (SMEs).

This thesis is dedicated to study methods that will conduct to the definition of a robotic platform for a relatively new joining process, friction stir welding (FSW). There is a lot of room for improvements concerning the robotization of the FSW process. In fact, this is an important topic due to the enormous advantages that a robot can bring to the FSW process when compared with dedicated FSW machines. In this scenario, the advantages of robots over dedicated FSW machines are multiple: flexibility, cost, faster setup and easier to programme. On the other hand, they present some relative disadvantages: the reduced stiffness of the robotic arm in the presence of the high forces involved into the process and the positional error associated to this kind of machine.

The first axis of research focuses on the off-line definition of nominal robot trajectories with a high-level of abstraction from the robot specific language. This was achieved by directly interfacing with a common computer-aided design (CAD) package to extract nominal data. There follows a proposal for the discretization of the nominal robot trajectories in small sections. These small sections will then be on-line adjusted according to the inputs from sensory-feedback. Trajectory adjustments are required because the real robot operates in a dynamic environment involving contact between the FSW tool and the work pieces, a partially unknown environment (PUE). Thus, robotic systems must have autonomy to overcome this situation. It is proposed a method for robot self-recognition and self-adaptation through the analysis of the contact between the robot end-effector and its surrounding environment. The proposed force/motion control system has an external

control loop based on forces and torques being exerted on the robot end-effector and an internal control loop based on robot motion. The external control loop is tested with a proportional integrative (PI) and a fuzzy-PI controller. Finally, connecting all the dots, it is defined a complete concept and design of a novel FSW robotic platform for welding polymeric materials. The platform is composed by three major groups of hardware: a robotic manipulator, a FSW tool and a system that links the manipulator wrist to the FSW tool (support of the FSW tool). Experimental tests proved the versatility and validity of the proposed solution.

The produced welds on acrylonitrile butadiene styrene (ABS) plates were tested in order to study the influence of rotational speed, traverse speed and axial force on the quality of the welds. It is presented a comparison between welds produced in the robotic FSW system and in a dedicated FSW machine. Strength and strain properties of the welds are evaluated and correlated with the morphology of the welded zone. It was concluded that the welds produced in the robotic system present similar or better appearance and mechanical properties than the welds produced in the dedicated FSW machine.

Keywords: Robotics; Friction stir welding; Hybrid force/motion control; Polymers; Off-line programming.

Resumo

Nos últimos anos tem-se verificado uma tendência na forma como as fábricas têm evoluído. Cada vez mais, as empresas de manufatura estão a mudar e reinventar os seus sistemas de produção. A automatização de alguns processos tecnológicos é hoje um fator muito importante para o sucesso de uma empresa de manufatura. Devido à sua flexibilidade e eficiência, os robôs industriais são hoje vistos por muitos como um elemento chave dos sistemas de manufatura modernos, promovendo a produtividade quando corretamente implementados. Estes aspetos podem facilitar a introdução de novos processos tecnológicos nas empresas, especialmente nas pequenas e médias empresas.

Esta tese foca-se no estudo de metodologias que possam conduzir à definição de uma plataforma robótica para um processo tecnológico relativamente recente, a soldadura por fricção linear (SFL). Existe um enorme espaço para melhorias nos sistemas robóticos relativamente à sua aplicação no processo de SFL. De facto, este é um tópico bastante importante devido às vantagens que um robô pode trazer ao processo de SFL. Neste cenário, as vantagens dos robôs sobre as máquinas dedicadas de SFL são diversas: flexibilidade, custo, instalação mais rápida e facilidade de programação. Por outro lado, os robôs apresentam algumas desvantagens: a baixa rigidez do manipulador quando sujeito a elevados esforços e o erro posicional associado aos robôs.

O primeiro eixo de investigação foca-se na definição off-line das trajetórias nominais do robô de uma forma intuitiva para o utilizador, ou seja, com um elevado nível de abstração da linguagem do robô. Isto é conseguido interagindo diretamente com um pacote de computer-aided design (CAD) comercial e extraindo dai os dados nominais necessários. Segue-se uma proposta para a discretização das trajetórias nominais em pequenas secções. Estas pequenas secções serão depois ajustadas on-line de acordo com os inputs recebidos do feedback sensorial. Os ajustamentos de trajetória são requeridos devido ao robô operar num ambiente dinâmico que envolve contacto entre a ferramenta de SFL e as peças a soldar, um ambiente parcialmente desconhecido. Assim, o sistema robótico deverá apresentar autonomia para ultrapassar esta situação. É proposto um método para o auto reconhecimento e a auto adaptação do robô através da análise do contacto entre o robô e o

ambiente envolvente. O método de controlo de força/movimento apresenta um ciclo de controlo externo baseado nas forças e momentos exercidos na ferramenta do robô e um anel de controlo interno baseado no movimento do robô. O anel externo é testado com um controlador proporcional integrativo (PI) e um controlador fuzzy-PI. Finalmente, juntando o anterior referido, é definido o conceito de uma nova plataforma robótica para SFL de materiais poliméricos. A plataforma é composta por três grupos de hardware: um manipulador robótico, uma ferramenta de SFL e um sistema de suporte da ferramenta. Testes experimentais provaram a versatilidade e validade desta solução.

As soldaduras realizadas foram testadas de modo a estudar a influência da velocidade de rotação, da velocidade transversal e da força axial na qualidade das soldaduras levadas a cabo em placas de acrilonitrilo butadieno estireno (ABS). É apresentada a comparação entre as soldaduras produzidas pelo sistema robótico e as soldaduras produzidas pela máquina dedicada de SFL. As propriedades de tensão e deformação foram medidas, avaliadas e correlacionadas com a morfologia da zona soldada. Foi concluído que as soldaduras produzidas pelo sistema robótico apresentam aparência e propriedades mecânica similares ou superiores as soldaduras produzidas pela máquina dedicada de SFL.

Palavras-chave: Robótica; Soldadura por fricção linear; Controlo híbrido força/movimento; polímeros; Programação off-line.

Contents

Figures

Tables

Acronyms and abbreviations

1-D – one-dimensional

2-D – two-dimensional

3-D – three-dimensional

ABS – acrylonitrile butadiene styrene

CAD – computer-aided design

CEMUC – University of Coimbra's Mechanical Engineering Research Centre

DEMUC – Department of Mechanical Engineering of the University of Coimbra

DOF – degrees of freedom

EU – European Union

F/T – force/torque

FCT – Portuguese Foundation for Science and Technology

$\mathbf{f}_d$ – set force

$\mathbf{f}_e$ – measured force

FSW – friction stir welding

F_x – traverse force

F_y – side force

F_z – axial force

GMAW – gas metal arc welding

HDPE – high-density polyethylene

J – jacobian matrix

MDPE – medium-density polyethylene

M_z – torque

OLP – off-line programming

PETG – polyethylene terephthalate

PI – proportional integrative

PI – proportional integrative

PID – proportional integrative derivative

PP – polypropylene

PTFE – polytetrafluoroethylene

PUE – partially unknown environment

r – radius of the tool pin

R – radius of the tool shoulder

R/T – rotational to traverse speed

RSP – resistive spot welding

SFL – soldadura por fricção linear

SMEs – small and medium sized enterprises

t – length of the tool pin

σ – shear flow stress

1. INTRODUCTION

1.1. Friction stir welding

Welding is one of the main application areas for industrial robotics and during several decades was the main technological process that was performed by robots. Nowadays, robotic welding is used in three fundamental welding processes: gas metal arc welding (GMAW), resistive spot welding (RSP) and laser welding. All of these processes have gained flexibility and became more attractive in industry when applied by robots. The same flexibility is intended to be reached in the process of friction stir welding (FSW) aided by robots, becoming this welding process appealing from an economical and technological point of view. Since this welding process displays a lot of advantages over other welding processes in terms of weld quality as well as simplicity of the process, it is expected that robotic FSW creates new opportunities of application to FSW.

FSW was initially developed by Thomas et al. (1991) in the early nineties for joining soft metals, as aluminium alloys such as those of series 2XXX and 7XXX, which were generally considered difficult or impossible to weld using fusion welding techniques at that time. In the last decade a lot of progresses have been done in this welding process enabling FSW of metals, polymers and dissimilar materials. This process has been used in several industries such as aeronautics, aerospace, railway, automotive and shipbuilding mainly in welding of aluminium alloys. The FSW process takes place in the solid-phase, at

temperatures below the melting point of the material. As a result, the weld seams produced by this method are free from defects such as shrinkage, embrittlement, cracking or porosity. The reduced welding temperature during this process makes possible lower distortion and residual stresses, enabling improved mechanical properties. FSW is also an energy efficient process that requires no filler material and, in most cases, does not require the use of a shielding gas. Furthermore, the process lacks fumes, arc flash, spatter, and pollution associated with most fusion welding techniques. This makes FSW a very attractive welding process. Welding poses serious threats to health and safety of workers. Smoke and fumes generated by welding are the most common health risks, as they are extremely toxic. These health risks are found mainly in fusion welding. However, as the process of FSW is a solid state process, it does not present this kind of risk. This is a topic that worries society, which can mean that in some years important technological restrictions can be imposed to the most dangerous welding processes.

The traditional FSW process consists of a rotational tool, formed by a pin and a shoulder, which is inserted into the abutting surfaces of pieces to be welded and moved along the weld joint, as illustrated in Fig. 1.1. During the process, the pin located inside the weld joint, generating heat through both friction and plastic deformation softens the material and enables plastic flow, causing the mixture of materials. At the same time, the shoulder placed on the surface of the seam heats and drags material from the front to the back side of the tool, preventing leakage of material out of the welding joint and becoming smooth the crown seam, providing a smooth surface. During the welding process the FSW tool can be tilted backward (travel angle) and sideways (work angle), as shown in Fig. 1.2. While travel angles different from zero are mainly applied when a rotational shoulder tool is used, work angles different from zero are applied in dissimilar-thickness butt weld applications. This process is applied mainly to butt, lap and T-butt weld joints but other joint geometries can be welded.

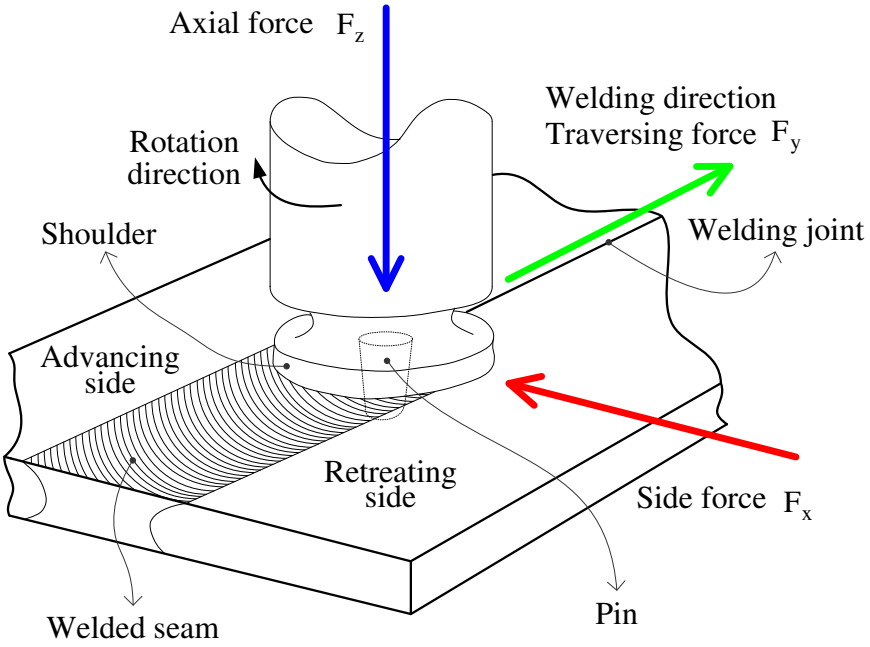

Figure 1.1 – Schematic representation of the FSW process.

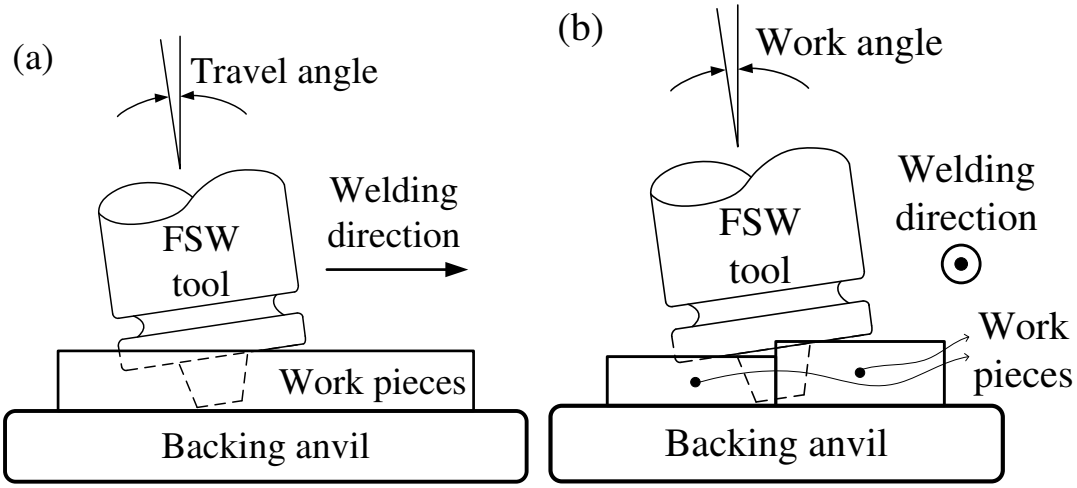

Figure 1.2 – Tilt angles used in the FSW process: (a) travel angle, (b) work angle.

1.2. Limitations of friction stir welding process

The process of FSW is restricted by several constraints which are preventing the expansion of the process in industrial application. The most influent constraint of the process is the high loads (forces and toques) involved in the process which does require heavy duty machinery. The most common machines used to perform FSW are conventional machine tools, such as milling machines, and custom-built machines; while the former are widely

used in industry and most workers are familiarized with them, the latter have high costs and a long learning curve associated due to the programming/control software. Both of these kinds of machines present low flexibility, limited work volume and few different welding paths are possible to be performed, often restricted to straight or circumferential welding, besides that most applications are presently restricted to two-dimensional planes by such machine tools. Industrial articulated robots are machines that excel by its great flexibility and relatively large work volume beyond which they begin to be widely used in industry. However, these robots are neither stronger nor stiffer machines to support the high loads involved in the process. The high loads acting on the manipulator cause large and unpredictable positional errors during the FSW process. There are some techniques that can be used to reduce the required loads without loss of weld quality. As shown in section 2, these techniques are related with accurate control of welding parameters avoiding their sharp variations. Furthermore, an appropriate FSW tool design also benefits load requirements.

The work pieces must be rigidly clamped during welding, by means of suitable jigging bars and a backing anvil, in order to prevent the abutting pieces moving apart or material breaking through the underside of the joint.

The hole left at the end of the weld when tool is withdrawn is often quoted as impediment to FSW, although the use of run-on/run-off plates or the friction hole filling techniques, such as taper plug and friction hydro pillar welding can be considered. The absence of filler in FSW is an advantage in many cases, but can also be a disadvantage since it hampers the process being used for fillet welds. When polymeric materials are welded, the force and torque required are less than those used in welding steel or aluminium alloys, however, the requirements of fixing parts should be maintained.

The most common defects associated with FSW of metals are cavities or voids, lack of penetration (kissing bond), root flaws, oxide alignment, plates thinning, bad surface appearance or hooking in the case of lap joints. On the other hand, the main defects in FSW of polymers are cavities, root defects and bad surface appearance. These defects are due to inappropriate tool design and definition of welding parameters as well as inaccurate control of welding process, specially the control of those parameters related with the maintenance of continuous and uniform flow of soften material, maintenance of temperature and pressure in the material flow, and the appropriate mixing of material.

Although the FSW process can be carried out in all positions (Fig. 1.3) and 3D paths, most of the scientific or industrial studies only have approached the flat position in 2D paths, because few equipment designs allow welding in positions different from flat position and 2D paths. In fact, such machines are customised for specific applications having associated high costs and low flexibility, and being hardly applicable to other industrial settings. The use of industrial articulated robots can solve these drawbacks due to their high flexibility. For this to happen it is necessary to solve several problems related to the control of the robot and the welding process, as well as developing tools and devices adapted to robots that allow for the completion of the welding process.

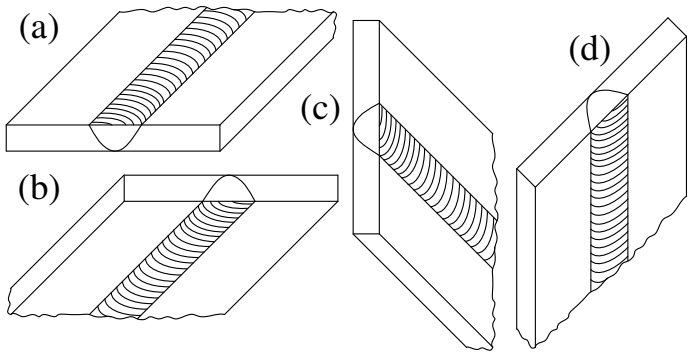

Figure 1.3 – Welding positions: (a) flat, (b) overhead, (c) horizontal, (d) vertical positions.

Process conditions must be established and optimized to the different materials in order they can be pre-set and the subsequent in-process monitoring can be used in production and quality control. The use of modern sensors and artificial intelligent methods associated to robotic systems will allow FSW process to reach its full potential. An additional difficulty to take into account in the industrial application is that programming of robots is often a tedious and time-consuming task which demands significant technical expertise requiring workers with knowledge in the field, so that all simplification that can be introduced in this area will be helpful.

1.3. Objectives

The first objective in this thesis is therefore to design and validate a FSW tool suitable to perform FSW of polymers. This tool must be flexible in order to be used either in robotic systems or in dedicated FSW machines.

The second objective is to design a simple and lightweight welding device adaptable to robotic systems and capable to operate with the FSW tool developed. Such robotic solution would probably decrease the costs of FSW of polymers becoming this kind of welding more attractive and create new application opportunities to polymers, expanding its use in industry.

The third objective is the development of a hybrid force/motion control system capable to cope with positional errors and instability of FSW process. This strategy is extremely important to avoid positional errors (which have their origin in the robotic system) and to avoid weld defects such as the voids and porosity. The use of an additional force control loop in the robot control system is studied in order to achieve good weld quality and allow the use of robots with lower payload to perform FSW.

Additionally, the improvement of weld quality and reduction of payload are studied by varying welding parameters, such as rotational and traverse speeds of the tool and introducing external heating in the weld joint. Therefore, the fourth objective of this thesis is the optimization of the welding parameters (axial force, rotational and traverse speeds) as well as heating temperature in FSW of acrylonitrile butadiene styrene (ABS) plates.

The fifth objective of this thesis is the validation of the robotic solution which is made by comparison between welds preformed in the robotic system and welds carried out in a dedicated FSW machine, taking in consideration the weld quality and the control of process parameters such as the axial force required.

Finally, the sixth objective of this thesis is to present a simple and intuitive virtual platform capable to program the industrial robot to perform FSW. On this stage robot code is generated taking into account robot nominal-paths and the integration of positional adjustments provided by the force control loop. Besides the general advantage presented by this programming process, such as increase robot time availability, increase of work safety, etc., when applied to FSW application this programming process enables low effort to create FSW paths and avoids contact between FSW tool and work pieces during the programming task.

The major challenges in this thesis can therefore be summarized in the following questions:

- Is it possible to perform FSW of polymers in an articulated industrial robot with reduced payload capacity?

- Can force control help to achieve welds of high quality?
- Does the optimization of the parameters of the welding process allow produce welds with good quality and simultaneously reduce the required load capacity of the robot?

1.4. Structure of the thesis

Besides this introductory chapter, the organization of this thesis includes a second chapter dedicated to the state of the art of FSW tools used to weld polymeric materials and machines used in FSW. The third chapter focuses on the development of the robotic solution and all its functionalities. This is followed by a fourth chapter dedicated to the influence of welding parameters as well as the influence of the FSW system, a dedicated FSW machine and the robotic system developed, on the weld quality. In the end, the fifth chapter with the outputs of the thesis and further research topics is presented. This thesis synthesizes the research work done in each field in a short text, supported by the papers published by the author.

2. LITERATURE REVIEW

2.1. Friction stir welding of polymers

In spite of the fact that the FSW process for metals is highly developed and is increasingly used in industry, the FSW of polymers is recent, so it requires a lot of research on appropriate tools and welding parameters. In fact the success of welding of polymers has not been achieved with the developments done for FSW of metals because of the different physical and mechanical properties of polymers and metals. The most important differences between thermoplastics and metals that restrict the application of FSW process in polymers are their low thermal conductivity, the low melting temperature range and the viscoelastic properties. Using conventional tools for metals in welding of polymers results in welds with several defects such as cavities, being the polymeric material ejected from the weld joint (Nelson et al., 2004). Consequently, these welds have non-uniform crown appearance and low tensile strength. Actually, the rotating tool shoulder ejects the material instead of retaining it as in welding of metals. Furthermore, the heat generated by the tool is not sufficient to promote the polymer melting and mixing because of the low thermal conductivity of polymers. In order to solve these difficulties several FSW tools have been developed and explored. Five types of tools have been proposed:

- The Hot Shoe tool (Bagheri et al., 2013; Kiss and Czigány, 2012b; Nelson et al., 2004; Strand, 2004);
- The conventional FSW tool with an extremely large shoulder (Aydin, 2010; Panneerselvam and Lenin, 2014);
- The Viblade tool (Scialpi et al., 2007, 2009);
- The conventional milling tool (Kiss and Czigány, 2007);
- The self-reacting tool (Pirizadeh et al., 2014).

The thermoplastics investigated include various grades of polyethylene (PE), polypropylene (PP), polyamide (PA), polycarbonate (PC), polymethyl methacrylate (PMMA), polytetrafluoroethylene (PTFE), acrylonitrile butadiene styrene (ABS), polyethylene terephthalate glycol (PETG) and polyvinylidene fluoride (PVDF).

2.1.1. Hot shoe tool

Among all the FSW tools explored to weld thermoplastics the one that has presented better results is the Hot Shoe tool (Nelson et al., 2004), an illustrative schematic representation of this tool is illustrated in Fig. 2.1. This tool consists on a rotating pin surrounded by a long stationary (non-rotating) shoulder also called shoe. The shoulder works as a constraining surface that inhibits ejection of melted material and retains polymer in the weld region as well as assists in reconsolidation of the polymer by applying forging pressure. Another beneficial function of the shoulder is the increase of the cooling time, as stated by Strand (2004), a uniform cooling rate throughout the weld volume reduces defect formation such as voids. It is very important to promote a uniform cooling and solidification rate in whole weld. If the outer material cools much quicker than the inner, a hard shell is formed. As the inner layers then cool, the material contracts and pulls away from the shell and large voids are formed, leading to the deterioration of mechanical performance of the weld. Increasing the shoe length allows to maintain pressure for a longer time as the weld cools. Consequently, the more cooling and solidification of the weld occur under pressure the material shrinkage is more uniform and voids formation is reduced (Strand, 2004). The shoulder also provides thermal energy to the in-contact surface increasing the heat input into the weld joint. This additional energy is provided by an external heating system. A special attention must be paid to the shoulder when the design of the FSW tool. The

shoulder must be designed such that lateral forces are not translated into the pin from the shoulder. These forces may lead to failure of the pin.

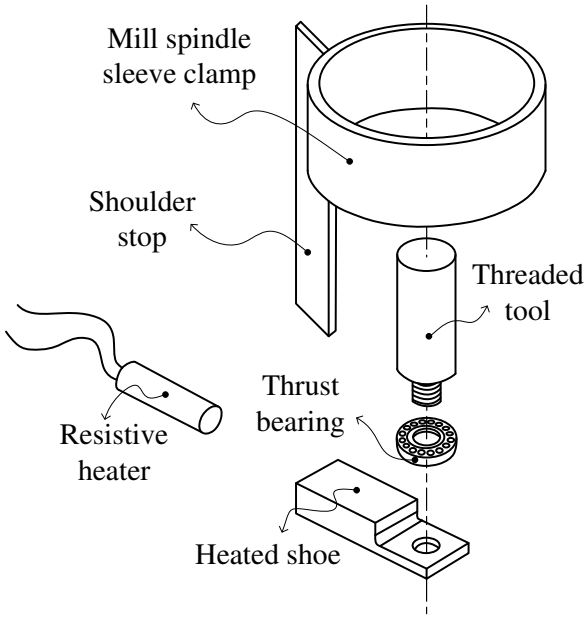

Figure 2.1 – Hot Shoe tool (Source: (Nelson et al., 2004)).

Strand (2004) and Nelson et al. (2004) performed FSW in several thermoplastics using a Hot Shoe tool heated by electrical resistances. Both of these studies have reported welds with good quality for some specific welding parameters, although for others welds have presented poor surface finishing and voids.

In recent studies, Kiss and Czigány (2012a) have proposed the use of a non-heated stationary shoulder, made of polytetrafluoroethylene (PTFE), connected with a milling tool (similar to the Hot Shoe tool). This new tool has demonstrated promising results, despite not having been adequately explored yet.

Mostafapour and Azarsa (2012) have used a Hot Shoe tool, with an aluminium shoulder and an electrical resistance as external heating element, in the welding of high-density polyethylene (HDPE). It was observed that the heat generated during the welding process was concentrated in the weld nugget, resulting in the formation of a pool of melted polymer around the pin. The size of the melted pool was increased by increasing the rotational speed, resulting in improved tool stirring conditions and weld quality. In general, higher tool rotational speed (1600 (rpm)) and shoulder tool temperature (140 (ºC)) result in high weld mechanical performance. These authors report that when not suitable welding

conditions are met (insufficient heat input in the welding joint), defects such as incomplete root penetrations and lack of bonding between stirred polymer and base material are observed.

Rezgui et al. (2010) have also assessed the feasibility of a Hot Shoe tool in FSW of HDPE. The shoulder of this Hot Shoe tool version is made of wood, which prevents that the heat generated by the pin be spread in the shoulder and consequently transmitted to the upper surface of the polymeric work piece, because of the low thermal conductivity of wood materials. It was concluded that with this tool the heat generated is concentrated in the weld joint where the HDPE melts, leading to the formation of defects in the weld, which cause specimens failure for very small strains.

2.1.2. Conventional FSW tool with large shoulder

The FSW tool with extremely large rotating shoulder, see Fig. 2.2, also has been reported as a good solution to perform FSW on thermoplastics (Aydin, 2010). This tool behaves in the same way as a conventional FSW tool with the particularity that the extremely large shoulder in-contact with the upper surface of the work piece, which generates much more frictional heat than a conventional tool, is an important heating source. Since the friction and conduction coefficients of a polymer are remarkably low, a large shoulder with large surface in-contact with polymer surface benefits welds quality by generation of higher amount of heat, promoting polymer melting and bonding. Another function of the shoulder is to retain melted material on the joint line avoiding ejection of material. However, although the published studies (Arici and Sinmazçelýk, 2005; Bozkurt, 2012; Panneerselvam and Lenin, 2012, 2014; Payganeh et al., 2011), reporting the use of this tool, do not refer the production of flash during FSW process, it is likely that the production of flash and ejection of melted material occur, due to the high linear speed on the periphery of the tool. In fact, the surface appearance of the welds is very rough presenting large defects with valley-like structures, although this tool provides welds with good mechanical properties.

Figure 2.2 – Conventional FSW tool with large shoulder (Source: (Aydin, 2010)).

Aydin (2010) developed a conventional FSW tool with a larger shoulder, compared to the conventional FSW tool used to weld metallic materials, and a heating system placed at the root of the seam, which enables the production of defect-free welds with a basin-like nugget zone. However, the seam welded surface was very rough with non-aesthetic appearance. The same tool concept without heating system has been used in other studies (Arici and Sinmazçelýk, 2005; Bozkurt, 2012; Panneerselvam and Lenin, 2012, 2014; Payganeh et al., 2011) to investigate the influence of some welding parameters in welded seams quality (this topic is presented in section 2.1.7). The main drawback of the welds produced by this kind of tool has been bad crown surface quality of the seams.

2.1.3. Viblade

Scialpi et al. (2007) presented a new concept of FSW tool called Viblade tool, which is shown in Fig. 2.3. The Viblade tool consists in a blade and a shoulder animated with reciprocated motion (vibration) in the direction of the weld. While the blade remains within the weld joint generating heat by friction to melt the polymer and provides suitable flow to melted material, the shoulder is in-contact with the upper surfaces of the polymer generating heat by friction to melt the polymer and avoiding ejection of material from the weld joint. Moreover the shoulder applies forging pressure provided by vertical load (axial

force) to aid consolidation of the melted material. Likewise, a horizontal load (side force) guarantees contact between work pieces to be welded avoiding formation of defects and promoting bonding. The melted material flows around both sides of the blade into a cavity emptied by the blade itself as it advances along the joint line. Although the results of this technique were promising, it presented several drawbacks because of the complexity of the mechanism required to operate the tool, and the short working life-time of the blade, as concluded by Scialpi et al. (2009). Furthermore, this tool can be used only in welding joints of linear trajectory and in butt or corner joint geometries.

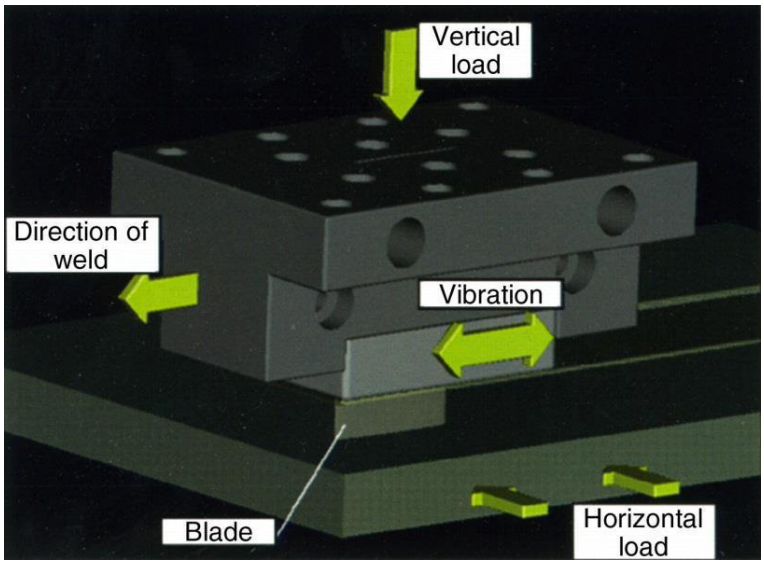

Figure 2.3 – Viblade tool (Source: (Scialpi et al., 2009)).

2.1.4. Conventional milling tool

Conventional milling tools rotating in opposite direction to the milling direction (avoiding the milling of the raw material and promoting mixing) were explored to perform FSW in polypropylene (PP) by Kiss and Czigány (2007). The welds produced by the tools were reported as successful but their mechanical properties were poor. Two milling tools were used in this study, Fig. 2.4.

Figure 2.4 – Conventional milling tool (Source: (Kiss and Czigány, 2007)).

2.1.5. Self-reacting tool

The most recent FSW tool presented in literature of FSW of polymeric materials was a Self-reacting tool style (also known as Bobbin tool) (Pirizadeh et al., 2014). A schematic representation of this tool is illustrated in Fig. 2.5. This tool consists of two non-rotating shoulders, one on the top surface and one on the bottom surface of the work piece, connected by a pin fully contained within the work piece. While the pin rotates to produce frictional heat and mix the melted material, the shoulder avoids expelling material from the welding joint. This tool has provided satisfactory welds, but further research is needed to exploit all its potential. The Self-reacting tool presents some advantages over the other tools such as no need for a backing anvil. Additionally, a machine used to operate a Self-reacting tool does not need to be as robust in the axial direction as to operate any of the FSW tools mentioned above. This is because the major part of the axial force is supported by the two shoulders, forming a pair action-reaction, and hence axial force supported by the machine tends to zero. An inconvenient of this tool is the way that the tool gets into contact with the work pieces. In order to pass the pin through the work pieces, a hole must be drilled in the work pieces. This is to avoid undesired collisions among the Self-reacting tool and fixtures or work pieces, and to allow that the weld starts at a different point from the extremity of the work piece. Alternatively, the welding process should start and end out of the work piece.

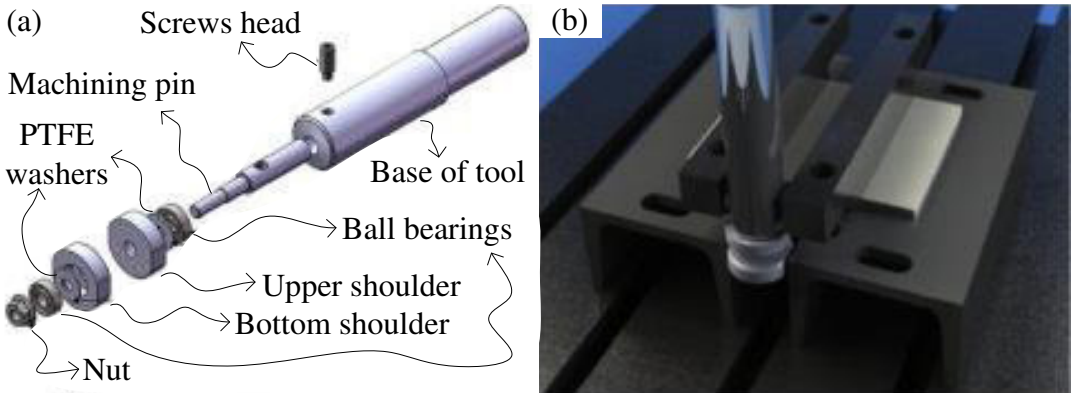

Figure 2.5 – Self-reacting tool: (a) disassembled tool; (b) tool in-operation (Source: (Pirizadeh et al., 2014)).

2.1.6. Tool features

2.1.6.1.Pin shape

The shape of the pin of a FSW tool plays an important role in the FSW process of thermoplastics. The geometry of the pin can be specially designed to produce higher frictional forces in the polymer to input additional energy into the welding joint and controlling the flow of melted polymer (Panneerselvam and Lenin, 2012). Several pin geometries are feasible being preferable a non-circular cross-section because the rate of heat generation as well as peak temperatures are relatively higher in the case of non-circular pin profiles. However, shapes that promote a cutting action on the thermoplastic must be avoided in order to prevent the milling of the work piece. In an illustrative way, some of the non-circular cross-sections of the pin may be polygonal, star-shaped, lobed, dumb-bell-shaped, ovoid, bladed, s-shaped, crossed, or a combination thereof (Fig. 2.6). Additionally, the pin geometry can be improved with shear or friction producing protuberances placed on pin's surface. These characteristics can be threads (Fig. 2.7(a)), grooves, flutes, ridges, or the like. These features of the FSW tool shear the polymer in the joint as the pin rotates and advances through the polymer. Shearing adds more energy to the joint area, thus melting the polymer faster and more efficiently. A tapered pin has advantages over other pin shapes (Fig. 2.7(b)). This feature increases the contact surface between the tool and the polymer causing more frictional heating. Payganeh et al. (2011) studied the influence of the pin tool geometry on a PP composite with 30 (%) glass fibre. It

is reported that a taper pin with groove provides better results than other pin shapes (triangle pin with screw thread, triangle pin, and cylindrical pin with grooves).

Panneerselvam and Lenin (2013) have studied the influence of tool pin geometry on weld quality of PP. This study has approached several pin geometries (square, triangular, threaded and tapered) which their performances were assessed for sets of welding parameters (rotational and traverse speeds). Depending on the tool pin geometry and welding parameters, several defects were observed such as porosity, cavities, lack of consolidation and inclusions. The best welds were obtained by the threaded pin profile.

The influence of the pin geometry (straight cylindrical, taper cylindrical, square, triangular, threaded cylindrical, and grooved with square) in traversing force (F_x in Fig. 1.1) generated by FSW of PP plates was studied by Panneerselvam and Lenin (2012). It was found that the welds produced by the threaded pin profile require less amount of axial force to produce welds than the other pin profiles, besides that, the square, triangular and grooved with square pin profile produce defect free welds. The triangular pin profile was considered the best solution since the traversing force developed during the FSW process was low and the welds were free of defects (voids and blow defects) for welds produced at different welding parameters (traverse speed).

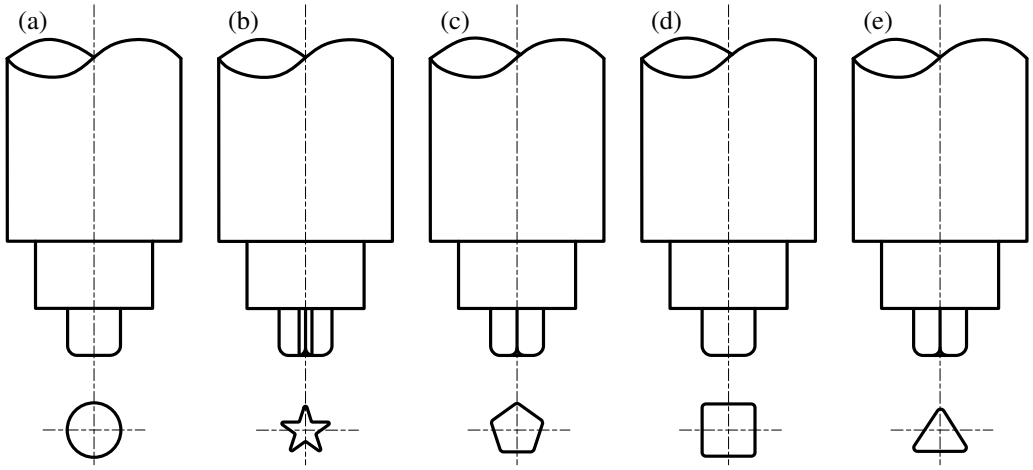

Figure 2.6 – Pin profile: (a) straight cylindrical; (b) star-shaped; (c) pentagonal; (d) squared; (e) triangular.

2.1.6.2. Pin's thread

A non-threaded pin is undesirable because it promotes low volume retention even when a stationary shoulder is used to constrain the flow (Panneerselvam and Lenin, 2014). Thus,

without threads to direct the material flow to the root of the weld the melted polymer flows out of the weld area from underneath the shoulder reducing the volume of polymer in the weld zone. The same phenomenon happens if the thread direction of the pin directs the material flow to the upper surface. Besides the thread direction of the pin, the tool rotational direction is of the same importance because it also controls the material flow. If both the threads of the pin and the tool rotation are in the same direction poor weld quality is obtained. Thus, they must be in opposite directions in order to direct the material flow downwards to the weld root, preventing defect formation. Another problem of the non-threaded pin is excessive stress generated in the FSW process that is transmitted to the machine. Thus, a stiffer machine is required which increases the costs.

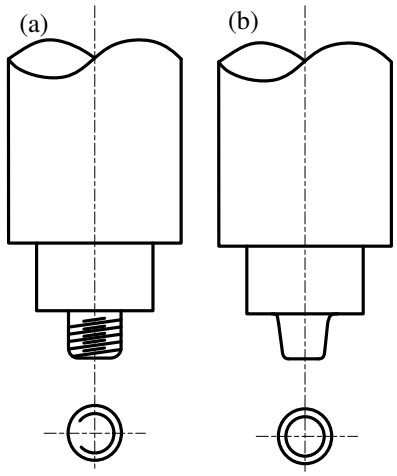

Figure 2.7 – Pin with: (a) threaded; (b) tapered geometry.

2.1.6.3. Other features

It is also reported in literature (Nelson et al., 2004) that the length to diameter ratio of the tool pin is an important design consideration. Ratios greater than 2:1 lead to shortening tool life because the pin undergoes rapid cyclic fatiguing from the high side loads placed on it. In order to avoid this problem, tools must be designed with the shortest pin possible, but it depends on the thickness of the plates to be welded.

It is highly recommended that the shoulder of a FSW tool must be coated. A coated shoulder reduces residual stress concentration on weld crown caused by sticking melted material to tool. As a result, welds produced by a coated tool present higher joint performance and good crown surface quality. Mostafa and Azarsa (2012) have performed

FSW in PE making use of a Hot Shoe tool surface coated with PTFE, achieving welds with good crown surface quality and improved mechanical properties.

2.1.7. Welding parameters

The welding parameters play also an important role in weld quality of polymeric materials. The most referred welding parameters are the tool design (mentioned above) the tool rotational and traverse speeds, the axial force (vertical load), the tool temperature, the horizontal load, the plunge depth, the tilt angle, the dwell time[1] and the tool offset[2] (for welding of dissimilar materials).

The tool rotational speed is an important parameter in the FSW of PP sheets as shown by Kiss and Czigány (2012b). A Hot Shoe tool with a non-heated shoulder made of PTFE was used to produce welds at 2000 and 3000 (rpm) of rotational speed, and 60 (mm/min) of traverse speed. The welds produced at higher rotational speed were reported as presenting the highest tensile strength, 86 (%) of the base material tensile strength, while the welds produced at 2000 (rpm) just presented 55 (%) of the base material tensile strength. Furthermore, it was observed that the morphology archived in the nugget of the welds was similar to the base material, which was attributed to the slow cooling rate of the welds.

Kiss and Czigány (2012a) succeeded in joining PP as well as polyethylene therephthalate (PETG) by using a Hot Shoe tool. High tensile strength welds were achieved in both materials reaching 90 (%) of the base material tensile strength. This study proposed a K factor depending on the rotational speed, traverse speed and tool diameter, see equation (1), as a key condition for obtaining good quality welds.

$$K = \frac{\text{rotational speed (rpm)}}{\text{traverse speed (mm/min)}} \cdot \text{tool diameter (mm)} \tag{2.1}$$

The K factor should range from 150 to 400, with each parameter ranging inside maximum and minimum operational limits, which depend on the material to weld. However, the K factor does not account for the effect of external heating or the axial force, a parameter

[1] Dwell time - consists in heating the work piece locally by frictional heating. In this phase the FSW tool is animated with rotating motion and no translation movement. This technique is usually used in the beginning of the weld.
[2] Offset - Misalignment between tool centre point and joint line.

which greatly influences the formation of defects at least in FSW of metals. Kim et al. (2006) proved that increasing the tool plunge axial force (F_z in Fig. 1.1) in FSW of aluminium die casting alloy the weld defect size is reduced or removed.

The influence of welding parameters in weld quality of HDPE was show by Saeedy and Givi (2011) and Rezgui et al. (2011) who studied the welding parameters rotational speed, traverse speed and tilt angle. It was shown that high strength welds are just achieved for an optimized set of welding parameters, which are interdependent. The optimum set of welding parameters provided the highest tensile strength weld, 75 (%) of the base material tensile strength.

Bozkurt (2012) studied the influence of parameters rotational speed, traverse speed and tilt angle on FSW of HDPE plates. The resulting welds presented low mechanical performance which was attributed to voids and root cracks formed in the welds. It was concluded that rotational speed is the most influent parameter in the seam quality while tilt angle is the least influent parameter. Payganeh et al. (2011) studied the influence of the same parameters investigated by Bozkurt on PP composite with 30% glass fibre. They showed that large rotational speed, low traverse speed and large tilt angle allows to do welded seams with better quality. In this study was clearly shown that when larger tilt angles are used, better mechanical properties of the welded seams are obtained. As easily understood, when the tilt angle increases, the axial force (F_z in Fig. 1.1) applied in the welding joint increases too (while the welded seam is being formed). Thus, this study suggests that when higher axial force is used to perform FSW of thermoplastics, higher quality seams are reached. A study proposed by Arici and Selale (Arici and Selale, 2007) further explored the influence of tool tilt angle on weld quality. In this study were performed butt welds with double passes on medium-density polyethylene (MDPE) with the following welding parameters: tilt angle ranging between 0 and 5 (º); traverse speeds of 12.5, 25 and 40 (mm/min); and rotational speed of 1000 (rpm). It was reported that tool tilt angles higher than 1 (º) results in the production of larger amount of flash (material ejected to the outside of the welding joint) reducing the thickness of the welding zone which in turn affects the tensile strength of the welds. The best tensile strength welds were obtained at 1 (º) tilt angle reaching the maximum tensile strength efficiency of 87 (%) relatively to the base material tensile strength. On the whole, the traverse speed does not seem to affect weld quality. In fact, these two later studies can seem to contradict each other but they

converge to the same effect. When a tilt angle different from zero is used, the rear of the tool is placed on a lower position than the work piece surface and the front of the tool is placed on a upper position than the work piece surface leaving a gap between the tool and the work pieces in the front side of the tool. This gap itself is directly proportional to the size of the tilt angle, the higher the tilt angle, the higher the gap. Taking this in consideration it can be concluded that both studies present the same results, i.e. for low tool tilt angles (about 1 or 2 (º)) the ejection of material from the welding zone is prevented while for higher tool tilt angles the reduction in thickness of the welding zone is inevitable, affecting drastically the weld properties. Additionally, it is likely that the tool dimensions have influence on the gap created which may also contribute to the slight difference in results obtained for the welding of the two materials, since it was not used the same tool in the both studies.

A study approaching FSW of PE was presented by Arici and Selale (2007). This study made use of a conventional FSW tool with large shoulder to investigate the effect of tool tilt angle on the weld performance and it was concluded that the tensile strength decreased with increasing tool tilt angle, because of the weld thickness decrease.

Arici and Sinmazçelýk (2005) showed that defects on the seam root can be removed by double passes of tool on FSW of medium density polyethylene (MDPE). It is mentioned that an adequate amount of heat must be provided to the joint in order to melt the polymeric material, however, when too much heat is provided to the weld joint some melted material is expelled from the joining area during welding.

A conventional FSW tool with large shoulder was also used by Squeo et al. (2009) in a study that approaches pre-heating of the tool as well as pre-heating of the weld joint in PE. Several combinations of welding parameters (rotational and traverse speeds and two different tool pin diameters) were investigated and it was proved that pre-heating improves weld quality.

A recent study carried out by Bagheri et al. (2013) on ABS have shown the influence of pre-heating of a threaded Hot Shoe tool and rotational and traverse speeds on weld quality. Three levels of welding parameter were considered, i.e. pre-heating tool: 50, 80 and 100 (ºC); rotational speed: 800, 1250 and 1600 (rpm); and traverse speed: 20, 40 and 80 (mm/min). The increase in rotational speed is responsible for increasing material joint temperature, which is a key factor to achieve good quality welds. However, when the heat

provided to the weld joint is too high the temperature reached in the polymer is excessive, causing burning of the weld surface. The same authors also claimed that lower traverse speed leads to welds with higher tensile strength, because welding zone is heated for longer time. A negative aspect of this study was the low traverse speeds used in the production of the welds, i.e. the welds which presented significant improvement in tensile strength were performed at 20 (mm/min), that from an industrial point of view is unattractive. In conclusion, the maximum tensile strength was reported for the welds performed with the maximum heat input, i.e., maximum tool rotation speed and shoe temperature and the lowest traverse speed.

2.2. Machines and control systems for FSW

Three kinds of machines are reported in literature as viable to perform FSW. These machines are:

- conventional machine tools such as milling machines (Longhurst et al., 2010; Longhurst, Strauss, and Cook, 2010);
- dedicated FSW machines or custom-built machines (Okawa et al., 2006);
- industrial robots (Smith, 2000; Soron and Kalaykov, 2006).

Each of these machines has different technical capabilities in terms of force, stiffness, accuracy, sensing, decision-making, and flexibility.

2.2.1. Force capability

A challenging issue in FSW is to have a machine able to support the high loads generated during the welding process, which depends greatly on the type of material and thickness of the work pieces. The most relevant loads acting on a machine during the FSW process are the axial force (F_z), the traverse force (F_x), the side force (F_y), and the torque (M_z). The directions of these loads are displayed in Fig. 1.1.

Axial force (F_z) is one of the main process parameters. It is responsible for the friction between the FSW tool and the work pieces, contributing to heat generation in the FSW process. Furthermore, axial force is responsible for applying forging pressure which is vital to obtain good weld formation.

Traverse force (F_x) is responsible for supporting material resistance to the tool movement along the joint line.

Side force (F_y) arises due to the asymmetry of the FSW process, caused by the direction of tool rotation. The advancing side of the weld is warmer than the retreating side of the weld (Zhang et al., 2005), consequently, the material on the advancing side is softer and less resistant. This force has the direction from the retreating side to the advancing side of the weld.

Torque (M_z) is also responsible for friction between the FSW tool and the work pieces. This friction is one of the main heating sources for the process of FSW.

All of these loads play an important role in the process. They are a prerequisite to choose or develop FSW equipment. They also play an important role in the control the FSW process, for example maintaining a given axial force or torque allows conferring a good quality to welded seams.

2.2.2. Stiffness capability

This is the ability of a FSW equipment withstands loads without undergoing deformation or deflexion. When a FSW machine presents low stiffness its FSW tool does not reach the desired welding path, strongly affecting the weld quality. Moreover, low stiff machines tend to cause excessive vibration which in turn can lead to FSW process instability.

2.2.3. Accuracy capability

In general FSW machines present high levels of accuracy however, if machines have low stiffness, their accuracy is reduced due to the same reasons pointed out in the section 2.2.2.

2.2.4. Sensing capability

Sensing consists on the machine ability to be aware of some phenomena that are occurring in the weld joint, i.e. states and values of direct and indirect welding variables involved in FSW process that reflect the evolution of the welding material and consequent welding formation. In this thesis, it is considered as direct welding variables the welding parameters that somehow can be actuated in a direct way. Some of the welding parameters that compose the direct variables are the rotational and traverse speeds, the tilt angle and the

external heat input. On the other hand, it is considered as indirect variables all those variables that cannot be actuated in a direct way, they depend on other variables. This group of variables is composed by the loads involved in the welding process (axial force, traverse force, side force and torque), the temperature reached in the welding area, the stirred material flow and the stirred material mixture, between others.

2.2.5. Decision-making capability

Control methods can be implemented in the control system of the equipment in order to allow process self-adaptation. The data provided from sensors (values of the direct and indirect variables) are used as feedback to the control system. Therefore, indirect monitored variables converge to desired states and values in which FSW process provides good quality weld.

2.2.6. Flexibility capability

The flexibility of a machine limits the complexity of a welding path that can be performed. The number of axes that a machine possesses usually establishes the flexibility of the machine. A one-dimensional (1D) welding path is the least complex requiring the least flexibility (axes number). The simplest version of this machine possesses just two axes. On the other hand, a two-dimensional (2D) welding path requires more flexibility, not only to move the FSW tool through the two directions but also to maintain work and travel angles. A three-dimensional (3D) welding path is the most demanding in flexibility, a machine to perform the simplest 3D path must have at least five axes. In addition, in many applications multiple welds with multiple directions and with multiple orientations are required, which demands the required flexibility of the machine.

2.2.7. Conventional machine tools

The process of FSW is similar in terms of principle of operation of the equipment to other technological manufacturing processes such as machining, deburring, grinding and drilling. Basically, all of these processes consist in moving a rotating tool through a work piece, producing movement of material which constitutes the work piece. Thus, it is plausible to assume that a conventional machine tool, such as a milling machine, can be used to

perform FSW. However, the loads generated during the FSW process gain more relevance when this equipment is used. The loads involved in FSW are higher than the loads generated in the milling process (Backer, 2012; Longhurst et al., 2010). By this reason, conventional machine tools have to be strengthened in order to increase their load and stiffness capabilities. Thus, there are potential opportunities to modify existing equipment to perform FSW. The modifications can be made on several levels: structural, flexibility, decision-making and sensing (Yavuz, 2004). The structural modifications are performed in order to make the equipment more robust (some parts of equipment can be replaced such as ways, guides, rails, motors, spindles, etc.). The flexibility can be increased by the introduction of additional motors that provide additional degrees of freedom to the equipment. Owing to the high loads involved in the FSW process, the majority of the solutions have implemented force control to prevent equipment damage and ensure human safety and to achieve good weld quality. The decision-making of the equipment can still be improved providing movement in more directions at the same time. Besides that, the machine can be equipped with multiple sensors to collect different information which will be used to control the equipment through an embedded control solution.

These machines are very popular due to the fact that they are widely used in industry for machining purposes, which is one of the most common technologic processes used in industry. Therefore, the existence of this kind of equipment in industry is guaranteed as well as knowledge to operate it. In FSW the use of modified machine tools is recommended for:

- prototyping and small series production of:
    - welding long or small work pieces;
    - welding thick or thin work pieces;
- applications where high stiffness is required;
- single- or multi-axis applications.

It must be expected low production performance. An example of a modified milling machine is presented in Fig. 2.8 (Longhurst, 2009).

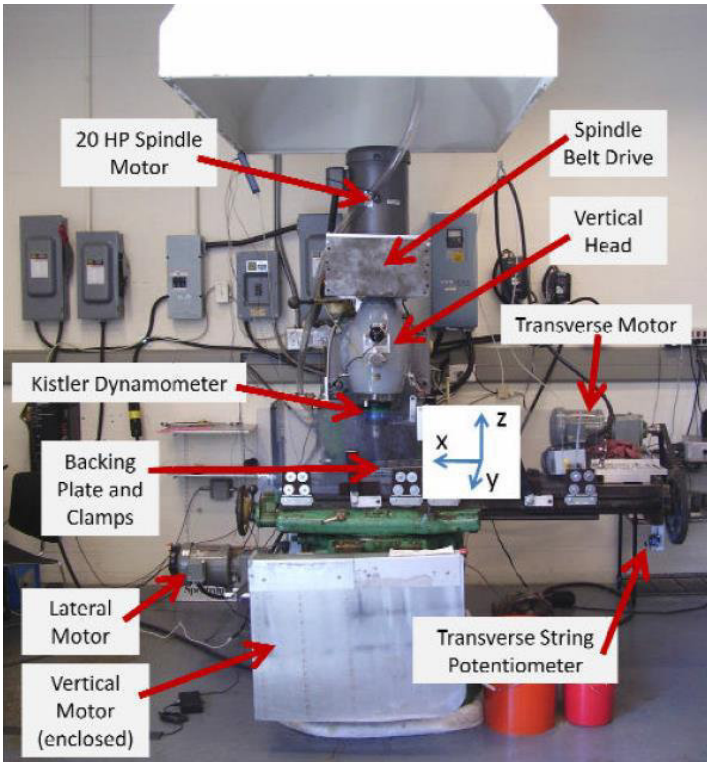

Figure 2.8 – Modified milling machine for FSW (Source: (William Russell Longhurst, 2009)).

2.2.8. Dedicated FSW machines

Dedicated FSW machines tend to have the highest load capability, stiffness, accuracy and availability (Okawa et al., 2006). They can assume different configurations presenting distinct levels of flexibility. In this family of machines are inserted the custom-built machines that are machines developed specifically to satisfy final application requirements (Smith et al., 2001). A requalification of these machines to other applications is difficult in several cases. Typically, dedicated FSW machines are relatively expensive and their cost increases with increase in flexibility.

The use of dedicated FSW machines is recommended for high series production of the same part types as conventional machine tools:

- welding long or small work pieces;
- welding thick or thin work pieces;
- applications where high stiffness is required;
- single- or multi-axis applications).

Additionally, the use of custom-built machines must be considered for applications where the alternative solution does not exist or is relatively expensive. An example of a dedicated FSW machine is presented in Fig. 2.9.

Figure 2.9 – Dedicated FSW machine – FSW Legio^{TM} (ESAB, 2014).

2.2.9. Robotic FSW machines

A third family of machines that has recently been introduced in FSW of metals concerns to robotic machines (industrial robots). During several years low load capability (payload) and low stiffness of industrial robots have prevented the use of robots in FSW applications. However, recent developments have led to development and consequent release in the market of robotic equipment with high payloads which are capable of performing FSW on material of thin-to-moderate thickness. The main advantages presented by robotic machines are flexibility and process automation which allow for significant productivity improvements. As an example, consider a work piece with welds on multiple sides. A robotic solution can allow for welding on multiple sides of the work piece in a single setup (for instance the work piece shown in Fig. 2.10). This reduces non-value-added materials handling applications and can yield a lot of improvements in productivity, consequently reducing net welding cost. Applications recurring to 3D welding paths have become

increasingly attractive and feasible with the use of a robotic system for FSW. A great range of this kind of application just needs an industrial robot with five degrees of freedom which becomes the use of industrial robots more appealing since the most common robots in the market possess five or six degrees of freedom.

The robotic-based solutions are available in two basic categories:

- articulated arm robots (Marcotte and Vanden-Abeele, 2010; Smith, 2000; Soron and Kalaykov, 2006);
- parallel-kinematic robots (Zhao et al., 2007).

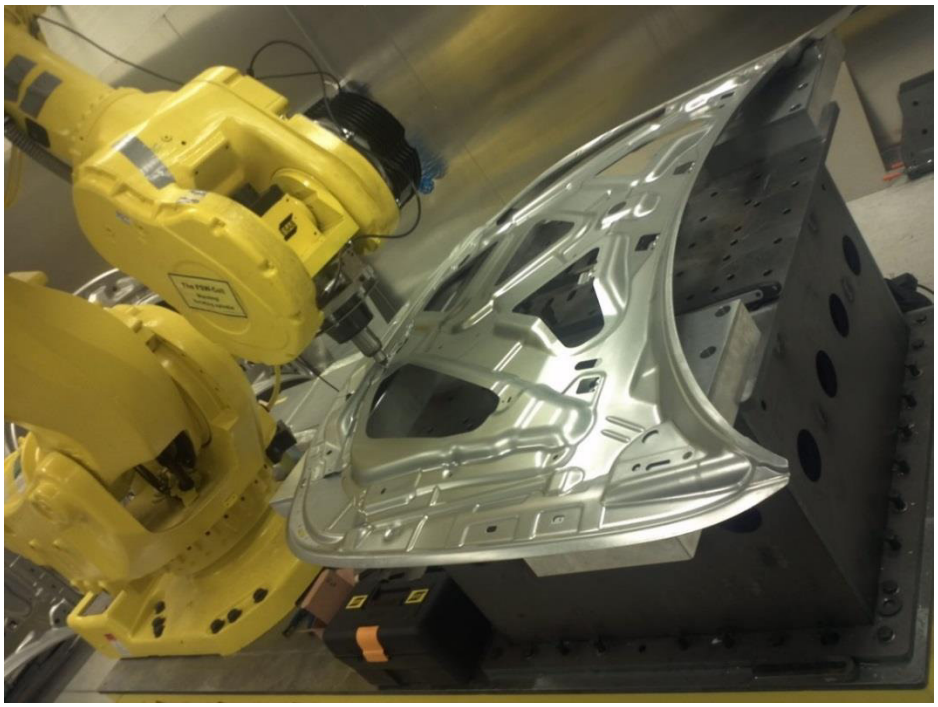

Figure 2.10 – Robotic FSW of a multi welding part (Source: (Backer et al., 2012)).

Articulated arm robots present high repeatability and flexibility but low accuracy that worsens when they are subjected to high loads. Comparing articulated robots to dedicated FSW machines, generally these robots display higher flexibility and decision-making capability besides they are remarkably lower in cost. However, these types of robots have relatively low stiffness and moderate load capability which limits their application. Given their flexibility and relative low cost, they can be the lowest-cost solution by far but have a limited range of materials on which they can perform FSW due to the high loads required to weld some materials. As a general rule, the most robust robots are capable of welding up

to 6 (mm) thick aluminium material (Marcotte and Vanden-Abeele, 2010; Shultz et al., 2013). Their capability in higher-melting-point materials tends to be somewhat less. The drawbacks are related to high compliance, which cause process stability issues.

The use of articulated arm robots is recommended for:

- relatively thin material;
- applications having multiple welds that would otherwise require multiple setups;
- dissimilar-thickness butt welds (tailor-welded blanks), these kinds of welds require both a travel angle and a work angle (more flexibility is required). Robots are ideal solutions for this application;
- applications where multi-axis capability is required (different tool orientations are needed);
- higher work volume applications where productivity is an important factor.

Marcotte and Abeele (2010) have developed a robotic FSW system based on an articulated arm robot. In this study was successfully reported the production of aluminium welds of 1D, 2D and 3D welding paths. Fig. 2.11 presents an articulated arm robot capable to perform FSW of 1D, 2D and 3D welding paths. The friction stir spot welding (FSSW), a variant process of FSW, have also been reported as feasible and appealing when performed by an articulated arm robot (Hinrichs et al., 2004).

Figure 2.11 – Articulated arm robot performing FSW (TUM, 2014).

The other basic robotic configuration is the parallel-kinematic robot. They can support higher loads and have significantly higher stiffness than an articulated arm robot. However, their cost can be notably higher, and their work volume is significantly less than the articulated arm robots, as well as the allowed range of orientation. A typical example of this family of robots is the Tricept, shown in Fig. 2.12. Parallel-kinematic robots should be considered in similar applications to the articulated arm robots with the following particular characteristics:

- the work volume of the work pieces is relatively small;
- the work piece can be welded near or close to the horizontal plane;
- the load or stiffness requirements are somewhat higher.

Shi et al. (2012) have developed a 3-PRS (Prismatic, Revolute and Spherical joint) parallel mechanism to perform FSW of 3D welding paths. Table 1 displays a comparative analysis among the different machines.

Figure 2.12 – Parallel-kinematic robot (Tricept) performing FSW (PKM TRICEPT, 2014).

Table 2.1 – FSW equipment features.

Characteristics ↓	Equipment			
	Milling machine	**FSW machine**	**Parallel robot**	**Articulated robot**
Flexibility	low	low/medium	high	high
Cost	medium	high	high	low
Stiffness	high	high	high	low
Work volume	medium	medium	low	high
Setup time	low	high	medium	medium
Number of programming options	low	medium	high	high
Capacity to produce complex welds	low	medium	high	high
Control type	motion	motion/force	motion	motion

2.2.10. Limitations of articulated arm robots

Owing to the high loads involved in the FSW process and low stiffness presented by articulated arm robots, they cannot guarantee the same robustness as either a conventional machine tool or a dedicated FSW machine (Gibson et al., 2014). Articulated arm robots are composed by joints and links that have associated servomotors, gearboxes and transmission axes. All of these elements are subjugated to non-predictable phenomena such as backlash, vibration, bearing run-out, between others that attribute compliance[3] to articulated arm robots leading to deflexions in the robot's joints and links (Leali et al., 2014; Schneider et al., 2014). Thus, encoders mounted to robots' linkage motors to read their position cannot detect such deflexions. The encoder readings are than fed back to the robots control system determining erroneously the position of their end-effectors (i.e. FSW tool). While robots are moving in the free air, these deflexions are negligible small as pre-known loads and mass can be account for, but when tool comes in contact with work pieces all these joints and links cause deviations between predefined robot path and the actual followed path. This leads to deviations away from the welding joint which affect negatively weld quality.

[3] A robot is said compliant when it is not completely rigid and when it can sense and control the forces it applies to work pieces.

2.2.11. Improving robotic FSW accuracy

In order to enable articulated arm robots, which present low stiffness, to perform FSW, it has been proposed in several studies (Bres et al., 2010; Cook et al., 2004; Smith et al., 2003; Soron and Kalaykov, 2006) to control the loads involved in the process instead of to control the robot's position. In this way it is possible to obtain the same weld quality using an articulated arm robot as when a stiff FSW machine is used and at the same time work at lower loads reducing load requirements of the machines used. When load control is used excessive loads and loss of contact between FSW tool and work pieces are prevented. As a result, damage of the actors involved in the process (FSW tool, machine, work pieces, etc.) and formation of welding defects are avoided and worker safety is guaranteed.

2.2.12. Welding parameters affecting stiffness machine requirements

As pointed out above, welding parameters affect resulting weld. Moreover, these parameters also affect each other, allowing achieve welds of similar quality in the presence of different sets of parameters. It is demonstrated in literature of FSW of thermoplastics as well as metals that the amount of provided heat to welding joint is a key point to achieve quality welds. Such amount of provided heat depends on a number of parameters such as: rotational speed, traverse speed, axial force, torque, plunge depth, external heating provided to the joint, type of material, thickness of the work pieces, etc. Taking into account the exposed above, it is expectable to reduce loads generated in the welding process as well as the required level of machine stiffness by keeping the same amount of heat dissipated in the joint. This is achieved by changing the other welding parameters.

Welds performed in a milling machine controlled in motion control have shown a significant reduction of axial force when the rotational speed is increased (Longhurst et al., 2010). This is a result of the increased heat input, which causes the material to soften more. This important conclusion suggests that the deflections in the robot can be significantly reduced by welding at higher rotational speed and at a lower axial force. However, the friction coefficient between tool and material is a limiting factor for the rotational speed. There will not be a proper material flow since a certain rotational speed is reached, which can cause welding defects. Within a certain parameter range, the reaction forces can be

reduced through proper setting of the process parameters including tool design to make it possible to apply robots for FSW.

Cook et al. (2004) used a milling machine to perform FSW on aluminium concluding that the heat input generated by the axial force, rotational speed and traverse speed together with the tool design, must be selected in a proper way. Too high heat input and axial force together with too low traverse speed will simply cause the tool to melt down into the material. On the other hand, a high heat input will produce a softer material during the FSW process, which is beneficial for the robot. This study is summarizing as the axial force requirements imposed to the robot can be reduced by operating at high tool rotational speed and low traverse speed. Crawford et al. (2006) have shown by simulation of the robotic FSW process that axial force and torque decrease as rotational speed is increased. The FSW plunging stage was studied by Zimmer et al. (2010) concluding that it is feasible to decrease axial force and torque by increasing generated energy (higher rotational speed and lower plunging speed) and/or using control force instead motion control.

2.2.13. Sensing methods to improve weld quality

In FSW of metal materials the robotization of the process and the use of force control have encouraged a number of studies to improve weld quality. A good example is the study presented by Fleming et al. (2008) that investigated automatic fault detection in robotic friction stir lap welds. In order to overcome faults as worm-holes (voids in the weld), real-time analysis of axial force though a methodology based on principal component analysis (PCA) are proposed.

Side FSW tool deviation has been an issue that has been studied in robotic FSW of aluminium. In order to prevent excessive side deviation from joint line, several studies have been carried out (Backer et al., 2012, 2010; Fleming et al., 2010, 2009). A method for automatic seam-tracking in FSW of lap joints is presented by Fleming et al. (2010). In this method, tracking is accomplished by weaving the FSW tool back-and-forth perpendicular to the traverse direction and monitoring force and torque signals. This approach showed to be efficient and weaving does not reduce weld quality. It can be utilized in robotic and non-robotic FSW process. The same method has been studied for FSW of T-joints by Fleming et al. (2009). The feasibility of the method was shown as well as the improvement of weld quality. Backer et al. (2012, 2010) demonstrated that side deviations are caused by

robot deflexion. Compensation of these side deviations are pointed out as irrelevant during welding of thin and/or soft materials but are necessary for butt-joint welding of high-strength aluminium alloys. Online sensing through vision and laser sensors were used to measure robot deviations. Three different approaches proved to be efficient:

- Using a seam-tracking system based on vision;
- Implementing compensations in the pre-programmed robot paths (off-line);
- Using pre-heating techniques of welding joints.

2.3. Control of robotic system

Over the last years, robot force control has assumed an increasingly important role in the performance of some robotic tasks. It is not only used in tasks where it is sufficient to maintain the contact forces and torques within certain limits but also on tasks where the deflexion of the robot is a major factor. The first case is the most common in robotic applications such as deburring, polishing and assembly. In the second case, applications such as milling, grinding, drilling and friction stir welding are typical examples where stiffness and payload come into play. Even though these two cases can seem different, the approach to deal with them is always the same, i.e. controlling force and moment of interaction between robot end-effector and environment in an appropriate way. Depending on the robotic task, a control technique should be chosen such as:

- Passive force control when the contact forces should be controlled to achieve task success, but it is sufficient to keep them inside some safety domain giving to the end-effector some freedom to adapt to environment (Siciliano and Villani, 2000);
- Active force control when the contact forces should be carefully controlled because they contribute directly to the success of the task (Gatland, 1995; Kwang and Jay Louis, 2006; Nagata et al., 2007; Pires et al., 2007, 2004, 2002; Lin and Huang, 1998; Siciliano and Villani, 2000; Tang and Kwong, 2001).

In the first case, contact forces produce an undesirable effect on the task. They are not necessary for the process to be carried out. In the second case, the contact forces are necessary to finish the task correctly, i.e., the contact forces should be controlled, making them assume some particular value or to follow a force profile.

Active force control is the most used in industrial applications. Although it requires higher investment, both monetary and information processing, it can guarantee that high contact forces will never occur. In order to afford disturbance rejection capability, several studies have been carried out. From the more common methods presented in literature: motion control, force control and hybrid force/motion control, one that has been pointed out by the scientific community as one of the most suitable to deal with robot deflexion and force/torque feedback is the hybrid force/motion control (Siciliano and Villani, 2000). This method allows controlling the non-constrained task directions in motion control and the constrained task directions in force control. Hybrid force/motion control architecture consists of an external force control loop closed around an internal motion control loop. To deal with robot deflexion this approach is the most suitable because the force controller is designed so as to dominate the motion controller. Hence, a position error is tolerated along the constrained task directions in order to ensure force regulation. Fig. 2.13 and Fig. 2.14 illustrate two different versions of this controller.

Up to now, many different kinds of robotic systems using force control strategies have been developed and successfully applied to various industrial processes such as polishing (Nagata et al., 2007) and deburring (Pires et al., 2007, 2002). A large number of force control techniques (fuzzy, PI, PID, etc.) with varying complexity have been proposed thus far (Kwang and Louis, 2006; Pires et al., 2004; Lin and Huang, 1998; Tang and Kwong, 2001).

According to the current state of the art, there are four different ways to control the robotic FSW process:

- Adjusting the plunge depth according to a given set force (Longhurst et al., 2010; Smith et al., 2003; Soron and Kalaykov, 2006; Zhao et al., 2009; 2007);
- Adjusting the plunge depth according to a given set torque for the robot motors (Smith, 2000);
- Adjusting the plunge depth according to a given set torque for the tool (Longhurst et al., 2010);
- Adjusting the traverse speed according to a given set force (Longhurst, Strauss, and Cook, 2010; Longhurst, 2009).

2.3.1. Adjusting the plunge depth according to a given set force

This approach proposes the use of force control where the plunge depth (penetration of the FSW tool along axial direction (z-axis)) is adjusted as the tool traverses along the welding joint. Thus, axial force (F_z) converges to a set force ensuring proper forging and consolidation of stirred material. In order to implement this system, a force sensor to collect force readings about loads acting in the FSW tool is needed. These force readings are fed back into a control system that in turn controls robot servomotors attributing proper position to the FSW tool. This control architecture is called direct force control, shown in Fig. 2.13, where $\mathbf{f}_d$ is the set force and $\mathbf{f}_e$ is the measured force. A force sensor is relatively easy to integrate but can be expensive and susceptive to noise disturbance.

The axial force has been the most used control parameter because it is the highest load acting on the FSW tool. Therefore, preventing axial force to reach extremely high values, all the hardware system and the FSW process itself are safe.

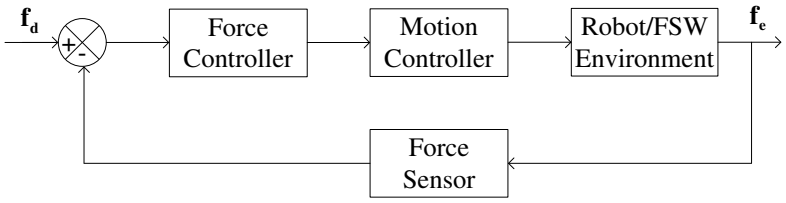

Figure 2.13 – Direct force control for a FSW robotic system.

2.3.2. Adjusting the plunge depth according to a given set torque for the robot motors

The second approach is closely similar to the first one, just differing in raw data. In this case the data consists of readings of robot motors torques that are processed to estimate loads acting on the FSW tool. Recurring to the robot Jacobian matrix (**J**), the applied axial force can be calculated based upon the measured current supplied to each motor in a serially configured articulating arm robot. This control architecture is shown in Fig. 2.14. The major advantage of this solution is the elimination of expensive force sensors, reducing implementation costs. This solution, called indirect force control, just allow to achieve a rough control of the contact force due to the compliance nature of the articulated robot, only an approximated model of the robot and stiffness is possible to formulate

(Siciliano and Villani, 2000). Smith (2000) has been quite successful in performing FSW on aluminium using an articulated arm robot with embedded indirect force control, however, the update time was limited to 2 (Hz) because of the computational burden of computing the manipulator Jacobian.

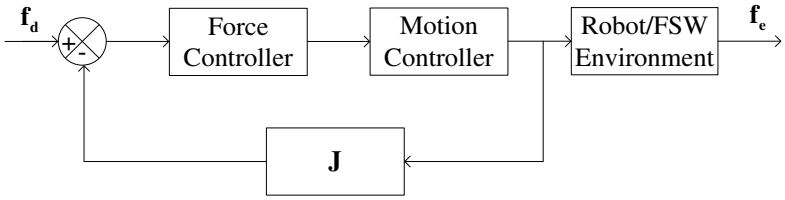

Figure 2.14 – Indirect force control for a FSW robotic system.

2.3.3. Adjusting the plunge depth according to a given set torque for the tool

This approach takes into account the torque exercised on the tool to feed back the robot control system. Axial displacements are sent to the robot arm to change the previous programmed robot welding path in order to reach a set torque. It is referred in literature (Longhurst et al., 2010) that the control of the torque provides more stable results than the control of the axial force when the actuating variable is the plunge depth. In fact, the torque is a more representative variable of the loads acting in the FSW tool than the axial force. The control method is based upon the mathematical model of welding torque given by:

$$Torque = \int_r^R 2\pi r^2 dr + 2\pi r^2 t\sigma + \int_0^r 2\pi r^2 \sigma dr \tag{2.2}$$

Where σ is the shear flow stress (N/m^2) at the shear interface boundary, i.e. tool surface, R is the radius of tool shoulder (m), r is the radius of tool pin (m), and t is the length of tool pin (m). The model predicts that welding torque is a function of plunge depth. The major benefits of torque control in relation to force control are simplicity and lower cost. A procedure to collect torque readings is recurring to a force/torque sensor. An alternative economical way to collect torque data can simply be using indirect measuring via the supplied current to the spindle motor or in the case of a hydraulic motor, the pressure difference across the motor. Torque control has been successfully demonstrated for the

automation of a conventional milling machine. No similar study was found to articulated robots. Further research is needed to assess feasibility of this solution.

Torque control may not be an attractive control procedure to FSW of thermoplastics because this process is very susceptible to concentrate excessive energy (reaching high temperatures and even melting of material) in some stages of the welding joint promoting excessive tool penetration on these stages. In this situation, the axial force tends to increase and may reach too high values that may endanger the integrity on the equipment involved in the FSW process. An excessive tool penetration phenomenon for force control similar to torque control can occur however, excessive values of axial force are avoided by the control system.

2.3.4. Adjusting the traverse speed according to a given set force

This approach consists of force control using traverse speed as the actuating variable, therefore similar to the approach presented in section 2.3.1. It is used a force sensor to collect force readings about loads acting in the FSW tool. This approach was proposed by Longhurst et al. (Longhurst, Strauss, and Cook, 2010; Longhurst, 2009) in the automation of a milling machine to perform FSW along one of its actuation axes (one motor), i.e. welding direction is aligned with one of the axes of the milling machine. It was reported that this system is more robust and stable when compared with a force controller that uses plunge depth as the actuating variable. However, when the traverse speed is used as actuating variable, the plunge depth must be kept constant (not change relative to the position of the work piece surface). This kind of approach is difficult to apply to articulated robots due to its compliance nature. For instance, if a six axis articulated arm robot is used to control axial force via traverse speed, more than one linkage must be adjusted simultaneously as the tool continuously traverses along the welding joint. Any simultaneous multi-linkage adjustment possibly could result in small fluctuations in the plunge depth of the tool. This will further lead to fluctuations in the axial force and possibly negating the advantages of using traverse speed as the controlling variable. This solution has associated the same investment costs as force control via plunge depth.

3. ROBOTIC FRICTION STIR WELDING SYSTEM

3.1. Overview

The research and development phases that conducted to the definition of the robotic system for FSW were elaborated having in mind that the final solution should be innovative when compared with other solutions using industrial robots for FSW. Thus, the work was divided into four phases, each leading to a partial solution. The integration of these solutions led to the final solution, shown in Fig. 3.1.

First, it was developed a solution for intuitive off-line definition of robot trajectories from available raw CAD data. After this, the previously defined nominal trajectories were discretized in order to allow them to be adjusted on-line. This on-line adjustment of discretized trajectories is managed by a force/motion controller that has force and torque feedback as input. This controller gives the robot the necessary autonomy to adapt to the real and dynamic working environment during robot welding. It was also developed a FSW tool for welding polymeric materials. Finally, all the above systems were integrated to create the robotic platform for friction stir welding proposed in this thesis. A number of tests were performed in order to tune and validate the system to achieve maximum performance.

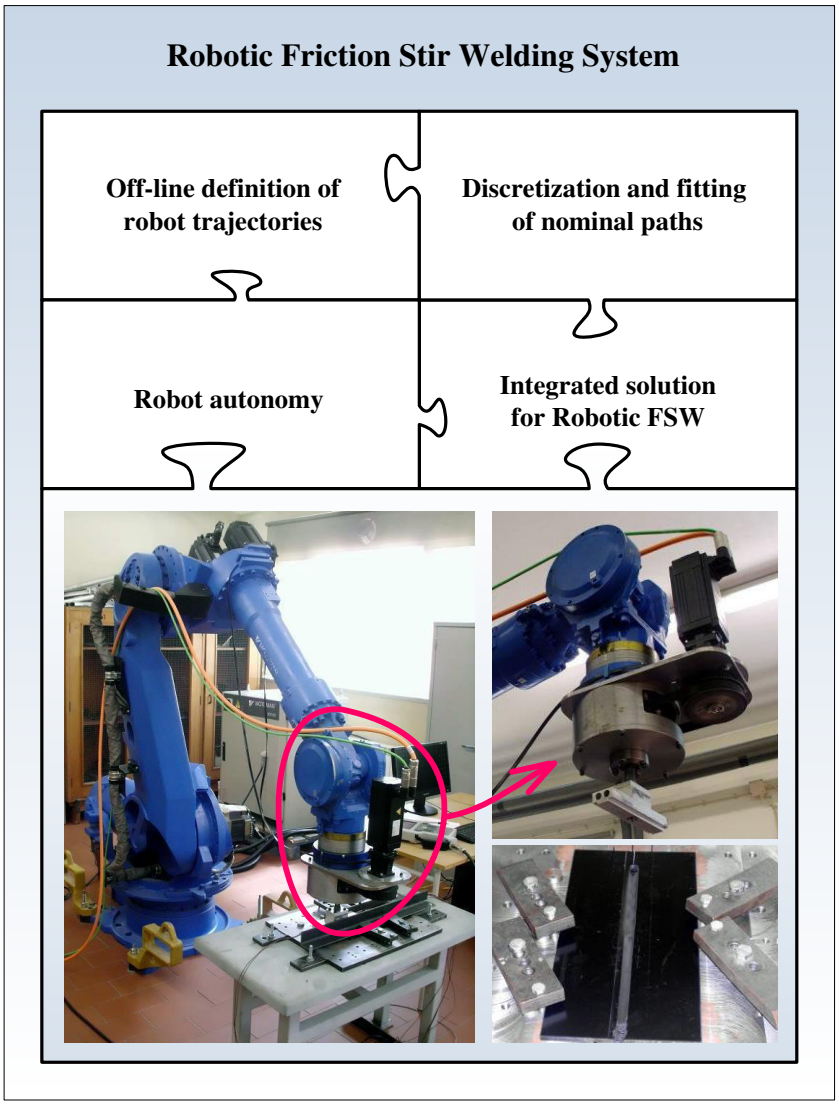

Figure 3.1 – Relationship between major research and development topics to create the final robotic solution for FSW.

3.2. Off-line definition of robot trajectories

The automation and robotization of the process of FSW is desirable due to the several reasons highlighted in previous chapters. Nevertheless, such process presents advantages and disadvantages. An important disadvantage is related with the non-intuitive nature of the common methods to define robot trajectories off-line (nominal paths). In off-line robot programming (OLP) nominal robot paths are usually extracted from CAD data. These data are the base for all the software solutions for OLP that exist. The development of novel and more intuitive CAD-based solutions for OLP appear as an effective way to make robots more accessible to industries.

Since OLP software solutions for robot programming are not intuitive and difficult to customize, it is proposed to directly extract such nominal paths from CAD drawings running on a common 3D CAD package. The aim is to automatically generate robot motion sequences (programs) from a graphical description of the robot paths over a 3D CAD model of a given robotic cell. A unified treatment of CAD and robot programming methods may involve very important advances in versatility and autonomy of the platform; in other words, product design and robot programming can be integrated seamlessly. It is explored the most suitable way to represent robot motion in a CAD drawing, how to automatically extract such motion data from the drawing, make the mapping of data from the virtual (CAD model) to the real environment and the process of automatic generation of robot paths/programs.

Results indicate that we can successfully extract and automate the process of extracting nominal robot paths from a CAD drawing running in a common CAD package. Robotic cell design and OLP are embedded in the same interface and work through the same platform, a common commercial CAD package. In addition, the experiments showed that the proposed system is intuitive to use and has a short learning curve, allowing user with basic knowledge in robotics and CAD to create robot programs in just few minutes.

Detail about this process can be found in **Appendix A1**.

3.3. Discretization and fitting of nominal paths

Robot OLP presents some adversities. An important one is related with the differences in alignment and geometry between the real environment and the virtual environment. This is even more evident when there is contact between the robot tool and the surrounding environment (work pieces) as in the process of FSW. In order to deal with the uncertainty and inaccuracy of the robot working environment, the introduction of sensory-feedback in the robotic system for FSW was studied and implemented. The robot should be able to ensure recognition of their work environment and make appropriate adjustments (on-line) in the pre-programmed paths. However, ordinary industrial robots are not able to easily incorporate sensory-feedback and some special care needs to be taken to ensure proper running of the system. A possible approach is to discretize the nominal path in small paths.

After that, some appropriate adjustments should be done on these small paths while the robot is performing them.

It is proposed the use of sensory-feedback through the implementation of a hybrid force/motion control system. The function of this control system is to keep the contact between robot tool and work-piece. Nevertheless, even though not all commercial robots are ready to incorporate sensory-feedback in an easy way, most are prepared to make adjustments in the pre-programmed path, when the robot programs are being executed. Having this capability in mind, we propose the discretization of the nominal robot path in small sections and then make the adjustments that are desirable in these small sections (path adjustment). Some techniques of path discretization are presented, namely: linear paths, circular paths and curvilinear paths (Nagata patch). In addition, an interpolation technique is presented to interpolate end-effector orientation (Slerp).

Linear and circular discretization are exact methods so that they have no errors, this analysis was done taking into account the robot Cartesian space. On the other hand, the Nagata patch is a numerical method and presents small errors, which do not put the robot task at risk. With regard to the orientation interpolation method, it interpolates the orientation proportionally to the number of points generated, being constant the increment of orientation. This works very well to linear and circular paths but when used with curved paths, where the linearity is not verified, some slight disproportionality can occur.

Detail about this process can be found in **Appendix A2**.

3.4. Robot autonomy

Often, in off-line robot programming, the idealized robotic environment (the virtual one) does not reflect accurately the real one. In this situation, we are in the presence of a partially unknown environment (PUE). Thus, robotic systems must have some degree of autonomy to overcome this situation, especially when contact exists. These differences between the idealized robot environment and the real robotic environment can have different origins: the unpredictable dynamic behavior of the real environment after contact with the robot or other equipment, robotic arm deflection, errors from the robot calibration process, an incorrect mapping of data from the virtual to the real environment, the roughness of contact surfaces, poorly representative CAD models and the presence of

foreigner objects in the work environment. It follows from this that in order to have total control over the OLP process, the robot has to know in real time the actual configuration of its surrounding environment. This has been achieved by incorporating sensors into the robotic systems.

It was proposed a method for robot self recognition and self-adaptation through the analysis of the contact between the robot end effector and its surrounding environment. The idea behind this is to control the end-effector pose (position and orientation) in real time and in accordance with the forces and torques from the contact of the robot end effector with its surrounding environment. This allows the robot to keep a given contact force and avoid undesirable impacts. The proposed force/motion control system has an external control loop based on forces and torques being exerted on the robot end effector and an internal control loop based on robot motion. The external control loop is tested with a proportional integrative (PI) and a fuzzy-PI controller. The system performance is validated with real-world experiments involving contact in PUEs.

Results indicate that the proposed hybrid force/motion control system allows to increase robot autonomy. The system proved to be a valuable tool to help robots to adapt to PUEs, especially when contact exists. The external control loop of the hybrid controller was tested with a PI and a fuzzy-PI controller. Real-world experiments involving contact in PUEs demonstrated that we cannot say that the fuzzy-PI controller is better than the PI controller. Both showed similar behaviors, with some disturbance around the set points. Another conclusion that can be drawn from experiments is that the proposed system only works properly if the data transfer between the F/T sensor and the robot controller is done in real time. Future work will focus on performing more real world experiments with different materials in contact.

Detail about this process can be found in **Appendix A3**.

3.5. Integrated solution for robotic FSW

The proposed methods in previous sections can be integrated to create a new robotic FSW solution. The complete concept and design of a novel FSW robotic platform for welding polymeric materials is here defined. It was conceived to have a number of advantages over common FSW machines: it is more flexible, cheaper, easier and faster to setup and easier

to programme. On the other hand, it presents some relative disadvantages: the reduced stiffness of the robotic arm in the context of the high forces involved into the process and the positional error associated to this kind of machine (clearance in motor and geared transmission mechanisms, backlash, bearing run-out, vibration, etc.)

The platform is composed by three major groups of hardware: a robotic manipulator, a FSW tool and a system that links the manipulator wrist to the FSW tool (support of the FSW tool). This system is also responsible for supporting a force/torque (F/T) sensor and a servo motor that transmits motion to the tool. During the process, a hybrid force/motion control system adjusts the robot trajectories to keep a given contact force between the tool and the welding surface. The controller has as input the contact forces between the tool and the work piece in each instant of time. A FSW tool with tapered and threaded pin profile was developed. This tool has an external heating system and a static shoulder. The rotational motion of the shoulder needs to be restricted by external constraints (more detail is in appendix A4).

The platform is tested and optimized in the process of welding ABS plates. Experimental tests proved the versatility and validity of the proposed solution. They demonstrate that it is possible to weld plastics with an acceptable level of quality using a robotic FSW platform aided by force/motion control and tuned with appropriate process parameters. On the other hand, it was concluded that it is virtually impossible to produce quality welded seams without force/motion control (for robotic FSW). Robotic FSW has a number of advantages over common FSW machines: it is more flexible, cheaper, easy and fast to setup and easy to programme.

Detail about this process can be found in **Appendix A4**.

4. EVALUATION OF PRODUCED WELDS

4.1. Influence of FSW parameters in weld quality

The purpose of this research is to study the influence of rotational and traverse speeds and axial force on the FSW quality of ABS plates. Welds were carried out in a FSW machine, using a tool with a stationary shoulder and no external heating system. This study takes into account the reduction of axial force required to obtain good quality welds, in order to develop robotic systems adapted to industrial welding of polymers. The effect of external heating is not considered in this stage of the study. The aim of this study is to examine the effect of main FSW parameters on the quality of ABS plate welds.

The welding parameters studied were the tool rotational speed which varied between 1000 and 1500 (rpm); the traverse speed which varied between 50 and 200 (mm/min), and the axial force ranging from 0.75 to 4 (kN). A major novelty is to study the influence of the parameter axial force on FSW of polymers. Produced welds have always a tensile strength below the base material, reaching the maximum efficiencies of above 60 (%) for welds made with higher rotational speed and axial force.

Based on the experimental results and discussion, the following conclusions can be drawn:

- It is feasible to produce good quality welds without any external heating;

- Tool rotational speed and axial force values above a certain threshold (rotational speed higher than 1250 (rpm) and axial force higher than 1.5 (KN)) are required to produce welds free of defects;
- Tool rotational speed generates the heat for plasticizing the polymer and promotes adequate material mixing;
- The axial force contributes to material mixing and prevents the formation of cavities in the retreating side of stir zone;
- The tensile strength and strain at break of welds is always below that of the base material;
- Welds of high strength efficiency and strain at break are achieved only when high rotational speed and high axial force are used;
- The main influence of traverse speed, when external heating is not used, is on the weld crown appearance. Good weld crown appearance is obtained when sufficient heat is provided to the welding joint. Thus, ratios of rotational / traverse speeds (R (rpm)/T (mm/min)) higher than 10 lead to good weld crown appearance.

Detail about this process can be found in **Appendix B1**.

4.2. Robotic FSW results and comparison

In this section it was studied the main factors affecting FSW of ABS plates, performed by the developed robotic system for FSW. Welds were carried out using a tool with stationary shoulder and an external heating system. The welding parameters studied were the axial force, rotational and traverse speeds and temperature of the tool. Furthermore, the influence of tool temperature in weld crown appearance is also analysed. Strength and strain properties of the welds are evaluated and correlated with the morphology of the welded zone. A comparison between welds produced in the robotic FSW system and in a dedicated FSW machine is presented.

It was studied the influence of welding parameters on the microstructure and mechanical properties of welds produced in the robotic system. The presented welds were performed in the proposed robotic system which may introduce some perturbations in the FSW process due to the reduced stiffness of the mechanical structure of an anthropomorphic robot when it operates with relatively high contact forces. Because of

that, robotic welds were compared with welds performed in a dedicated FSW machine, in order to analyse the influence of the robotic system on the weld quality.

It is shown the feasibility of robotic FSW of ABS without deteriorating the mechanical properties of the welds in relation to those produced in the dedicated FSW machine. Based on the experimental results and discussion, the following conclusions can be drawn:

- It is feasible to produce good quality welds in a robotic FSW system;
- A tool temperature of 115 (ºC) improves weld quality, specially the weld crown surface;
- High axial force promotes the squeeze of the molten polymeric material, preventing introduction of air into the weld and helps cooling of the weld, avoiding shrinkage and voids formation.
- High axial force improves tensile strength and strain of welds;
- The rotational speed is primarily responsible for heat generation, promoting adequate plasticizing and mixing the polymer;
- High tool rotational speed improves tensile strength and strain of welds;
- Welds free of defects present the same hardness as base material;
- To prevent lack of heat or overheating of the tool the R/T ratio must range between 10 and 20;
- A quality weld is obtained for tool temperature of 115 (ºC), axial force higher than 1.5 (kN), rotational speed higher than 1250 (rpm) and low traverse speed (ranging between 50 and 100 (mm/min));
- The welds produced in the robotic system present similar or better appearance and mechanical properties than the welds produced in the dedicated FSW machine.

Detail about this process can be found in **Appendix B2**.

5. CONCLUSIONS AND FURTHER WORK

5.1. Conclusions

We are now in position to answer to the major challenges pointed out in the beginning of this thesis. It was proved that it is possible to perform FSW of thermoplastics in a robotic solution that makes use of an articulated arm robot to produce the movement of the FSW tool and support the high loads generated in the FSW process. It was shown that it is feasible to produce welds at low axial force keeping a reasonable weld quality (visual appearance and mechanical performance). However, the welds that presented the highest mechanical performance, in particular the highest strain, were performed at the highest axial force. This leaves the idea that a stronger machine (articulated arm robot with higher payload capacity) parameterized at higher axial force can provide welds with better mechanical properties. It is recommended to use a different tool that does not transmit the whole axial force to the machine, instead of this, the tool should absorb much of such axial force. The control of axial force allowed avoiding excessive and too low values for this welding parameter, at the same time, the loss of contact and the reduction of possible gaps between FSW tool and work pieces were also eliminated. In some way, it can be said that the control of axial force allowed reducing the robot required payload. The developed robotic solution, that has low load capacity, produces welds of similar or better quality

(superficial appearance and mechanical properties) than those produced in a dedicated FSW machine, which has higher load capacity but much lower flexibility.

The overall conclusions of this thesis can be summarized as:

- OLP of industrial robots through an off-the-shelf CAD package is feasible, intuitive to use and has a short learning curve;
- Discretization of robot paths allows force control integration in order to constitute an hybrid force/motion control system. The linear and circular path discretization methods are exact methods presenting no theoretical errors. On the other hand, the curvilinear path (Nagata patch) presents small theoretical errors, however, these errors do not put the robot task at risk. The orientation interpolation method works well to linear and circular paths but when used with curved (non-linear) paths some slight disproportionalities can occur;
- The implementation of hybrid force motion control allows on-line robot adjustments. The fuzzy-PI controller and the PI controller showed similar performance. Both controllers allow supressing/reducing disturbing effect;
- Welds with good quality are obtained when the hybrid force motion control system is aided to the robotic FSW platform and parameterized with appropriated welding parameters;
- It is virtually impossible to produce welded seams with good quality in the FSW robotic system without force/motion control;
- High axial force promotes the squeeze of the molten polymeric material, preventing introduction of air into the weld and helps cooling of the weld, avoiding shrinkage and voids formation. Moreover, high axial force improves tensile strength and strain of welds;
- A quality weld is obtained for tool temperature of 115 (ºC), axial force higher than 1.5 (kN), rotational speed higher than 1250 (rpm) and low traverse speed (ranging between 50 and 100 (mm/min)).

5.2. Further work

Welding parameters (such as traverse speed, rotational speed, temperature and vibration) can be integrated in the force/motion control system. To reduce the overshoot in the beginning of the weld, it is intended to use different control parameters in the beginning of the weld and when stationary conditions are reached. The development of FSW tools for complex welding in 3D space will be a target for further research.

The welding of other materials such as other thermoplastics, dissimilar materials and composites will be tried. The FSW of these materials bring the necessity of refinement of

welding parameters since the optimal welding parameters are dependent on the physical and mechanical properties of each material.

References

Arici, A., and Selale, S. (2007). Effects of tool tilt angle on tensile strength and fracture locations of friction stir welding of polyethylene. Science and Technology of Welding and Joining, 12(6), 536–539.

Arici, A., and Sinmazçelýk, T. (2005). Effects of double passes of the tool on friction stir welding of polyethylene. Journal of Materials Science, 40(12), 3313–3316.

Aydin, M. (2010). Effects of Welding Parameters and Pre-Heating on the Friction Stir Welding of UHMW-Polyethylene. Polymer-Plastics Technology and Engineering, 49(6), 595–601.

Backer, J. De. (2012). Robotic friction stir welding for flexible production. Lund University.

Backer, J. De, Christiansson, A.-K., Oqueka, J., and Bolmsjö, G. (2012). Investigation of path compensation methods for robotic friction stir welding. Industrial Robot: An International Journal, 39(6), 601–608.

Backer, J. De, Soron, M., Ilar, T., and Christiansson, A.-K. (2010). Friction stir welding with robot for light weight vehicle design. In 8th International Symposium on Friction Stir Welding (pp. 14–24). Timmendorfer, Germany.

Bagheri, A., Azdast, T., and Doniavi, A. (2013). An experimental study on mechanical properties of friction stir welded ABS sheets. Materials & Design, 43, 402–409.

Bozkurt, Y. (2012). The optimization of friction stir welding process parameters to achieve maximum tensile strength in polyethylene sheets. Materials & Design, 35, 440–445.

Bres, A., Monsarrat, B., Dubourg, L., Birglen, L., Perron, C., Jahazi, M., and Baron, L. (2010). Simulation of friction stir welding using industrial robots. Industrial Robot: An International Journal, 37(1), 36–50.

Cook, G. E., Crawford, R., Clark, D. E., and Strauss, A. M. (2004). Robotic friction stir welding. Industrial Robot: An International Journal, 31(1), 55–63.

Crawford, R., Cook, G. E., Strauss, A. M., and Hartman, D. A. (2006). Modelling of friction stir welding for robotic implementation. International Journal of Modelling, Identification and Control, 1(2), 101–106.

ESAB. (2014). Legio Friction Stir Welding.

Fleming, P. A., Hendricks, C. E., Cook, G. E., Wilkes, D. M., Strauss, A. M., and Lammlein, D. H. (2010). Seam-Tracking for Friction Stir Welded Lap Joints. Journal of Materials Engineering and Performance, 19(8), 1128–1132.

Fleming, P. A., Hendricks, C. E., Wilkes, D. M., Cook, G. E., and Strauss, A. M. (2009). Automatic seam-tracking of friction stir welded T-joints. The International Journal of Advanced Manufacturing Technology, 45(5-6), 490–495.

Fleming, P., Lammlein, D., Wilkes, D., Fleming, K., Bloodworth, T., Cook, G., … Prater, T. (2008). In-process gap detection in friction stir welding. Sensor Review, 28(1), 62–67.

Gatland, H. B. (1995). A new methodology for designing a fuzzy logic controller. IEEE Transactions on Systems, Man, and Cybernetics, 25(3), 505–512.

Gibson, B. T., Lammlein, D. H., Prater, T. J., Longhurst, W. R., Cox, C. D., Ballun, M. C., … Strauss, A. M. (2014). Friction stir welding: Process, automation, and control. Journal of Manufacturing Processes, 16(1), 56–73.

Hinrichs, J. F., Smith, C. B., Orsini, B. F., DeGeorge, R. J., Smale, B. J., and Ruehl, P. C. (2004). Friction Stir Welding for the 21st Century Automotive Industry. In Fifth International Conference on Friction Stir Welding (pp. 1–13). Metz, France: TWI.

Kim, Y. G., Fujii, H., Tsumura, T., Komazaki, T., and Nakata, K. (2006). Three defect types in friction stir welding of aluminum die casting alloy. Materials Science and Engineering: A, 415(1-2), 250–254.

Kiss, Z., and Czigány, T. (2007). Applicability of friction stir welding in polymeric materials. Periodica Polytechnica Mechanical Engineering, 51(1), 15.

Kiss, Z., and Czigány, T. (2012a). Effect of welding parameters on the heat affected zone and the mechanical properties of friction stir welded poly(ethylene-terephthalate-glycol). Journal of Applied Polymer Science, 125(3), 2231–2238.

Kiss, Z., and Czigány, T. (2012b). Microscopic analysis of the morphology of seams in friction stir welded polypropylene. Express Polymer Letters, 6(1), 54–62.

Kwang, L., and Jay Louis, P. (2006). Feasibility Study of a Force Feedback Controlled Robotic System for Bone Milling. In 2006 IEEE Conference on Cybernetics and Intelligent Systems (pp. 1–6). IEEE.

Leali, F., Vergnano, A., Pini, F., Pellicciari, M., and Berselli, G. (2014). A workcell calibration method for enhancing accuracy in robot machining of aerospace parts. The International Journal of Advanced Manufacturing Technology.

Longhurst, W. R. (2009). Force control of friction stir welding. Vanderbilt University.

Longhurst, W. R., Strauss, A. M., and Cook, G. E. (2010). Enabling Automation of Friction Stir Welding: The Modulation of Weld Seam Input Energy by Traverse Speed Force Control. Journal of Dynamic Systems, Measurement, and Control, 132(4), 041002.

Longhurst, W. R., Strauss, A. M., Cook, G. E., Cox, C. D., Hendricks, C. E., Gibson, B. T., and Dawant, Y. S. (2010). Investigation of force-controlled friction stir welding for manufacturing and automation. Proceedings of the Institution of Mechanical Engineers, Part B: Journal of Engineering Manufacture, 224(6), 937–949.

Longhurst, W. R., Strauss, A. M., Cook, G. E., and Fleming, P. A. (2010). Torque control of friction stir welding for manufacturing and automation. The International Journal of Advanced Manufacturing Technology, 51(9-12), 905–913.

Marcotte, O., and Vanden-Abeele, L. (2010). 2d and 3d friction stir welding with articulated robot arm. In 8th International Symposium on Friction Stir Welding 2010 (pp. 778–797).

Mostafapour, A., and Azarsa, E. (2012). A study on the role of processing parameters in joining polyethylene sheets via heat assisted friction stir welding: Investigating microstructure, tensile and flexural properties. International Journal of the Physical Sciences, 7(4), 647–654.

Nagata, F., Kusumoto, Y., Fujimoto, Y., and Watanabe, K. (2007). Robotic sanding system for new designed furniture with free-formed surface. Robotics and Computer-Integrated Manufacturing, 23(4), 371–379.

Nelson, T. . W., Sorenson, C. D., and Johns, C. J. (2004). Friction stir welding of polymeric materials. USA.

Okawa, Y., Taniguchi, M., Sugii, H., and Marutani, Y. (2006). Development of 5-Axis Friction Stir Welding System. In 2006 SICE-ICASE International Joint Conference (pp. 1266–1269). IEEE.

Panneerselvam, K., and Lenin, K. (2012). Investigation on Effect of Tool Forces and Joint Defects During FSW of Polypropylene Plate. Procedia Engineering, 38, 3927–3940.

Panneerselvam, K., and Lenin, K. (2013). Effects and defects of polypropylene plate for different parameters in friction stir welding process. International Journal of Research in Engineering and Technology, 2(2), 143–152.

Panneerselvam, K., and Lenin, K. (2014). Joining of Nylon 6 plate by friction stir welding process using threaded pin profile. Materials & Design, 53, 302–307.

Payganeh, G. H., Arab, N. B. M., Asl, Y. D., Ghasemi, F. A., and Boroujeni, M. S. (2011, September 16). Effects of friction stir welding process parameters on appearance and strength of polypropylene composite welds. International Journal of Physical Sciences. Academic Journals.

Pires, J. N., Afonso, G., and Estrela, N. (2007). Force control experiments for industrial applications: a test case using an industrial deburring example. Assembly Automation, 27(2), 148–156.

Pires, J. N., Godinho, T., and Araújo, R. (2004). Force control for industrial applications using a fuzzy PI controller. Sensor Review, 24(1), 60–67.

Pires, J. N., Ramming, J., Rauch, S., and Araújo, R. (2002). Force/torque sensing applied to industrial robotic deburring. Sensor Review, 22(3), 232–241.

Pirizadeh, M., Azdast, T., Rash Ahmadi, S., Mamaghani Shishavan, S., and Bagheri, A. (2014). Friction stir welding of thermoplastics using a newly designed tool. Materials & Design, 54, 342–347.

PKM TRICEPT. (2014). Friction stir welding & processing.

Rezgui, M. A., Ayadi, M., Cherouat, A., Hamrouni, K., Zghal, A., and Bejaoui, S. (2010). Application of Taguchi approach to optimize friction stir welding parameters of polyethylene. EPJ Web of Conferences, 6, 07003.

Rezguia, M.-A., Trabelsib, A.-C., Ayadic, M., and Hamrounic, K. (2011). Optimization of friction stir welding process of high density polyethylene. International Journal of Production and Quality Engineering, 2(1), 55–61.

Saeedy, S., and Givi, M. K. B. (2011). Investigation of the effects of critical process parameters of friction stir welding of polyethylene. Proceedings of the Institution of Mechanical Engineers, Part B: Journal of Engineering Manufacture, 225(8), 1305–1310.

Schneider, U., Drust, M., Ansaloni, M., Lehmann, C., Pellicciari, M., Leali, F., … Verl, A. (2014). Improving robotic machining accuracy through experimental error investigation and modular compensation. The International Journal of Advanced Manufacturing Technology.

Scialpi, A., Troughton, M., Andrews, S., and De Filippis, L. A. C. (2007). In-line reciprocating friction stir welding of plastics. Joining Plastics/Fügen von Kunststoffen, 1, 42–51.

Scialpi, A., Troughton, M., Andrews, S., and De Filippis, L. A. C. (2009). Viblade^{TM}: friction stir welding for plastics. Welding International, 23(11), 846–855.

Shi, J., Wang, Y., Zhang, G., and Ding, H. (2012). Optimal design of 3-DOF PKM module for friction stir welding. The International Journal of Advanced Manufacturing Technology, 66(9-12), 1879–1889.

Shih-Tin Lin, and Ang-Kiong Huang. (1998). Hierarchical fuzzy force control for industrial robots. IEEE Transactions on Industrial Electronics, 45(4), 646–653.

Shultz, E. F., Fehrenbacher, A., Pfefferkorn, F. E., Zinn, M. R., and Ferrier, N. J. (2013). Shared control of robotic friction stir welding in the presence of imperfect joint fit-up. Journal of Manufacturing Processes, 15(1), 25–33.

Siciliano, B., and Villani, L. (2000). Robot Force Control. Springer.

Smith, C. B. (2000). Robotic friction stir welding using a standard industrial robot. In 2nd Friction Stir Welding International Symposium. Gothenburg, Sweden.

Smith, C. B., Crusan, W., Hootman, J. R., Hinrichs, J. F., Heideman, R. J., and Noruk, J. S. (2001). Friction stir welding in the automotive industry. In Proceedings of the 2001 TMS Annual Meeting Automotive Alloys and Joining Aluminum Symposia (Aluminum 2001) (pp. 175–185).

Smith, C. B., Hinrichs, J. F., and Crusan, W. A. (2003). Robotic friction stir welding: the state-of-the-art. In 4th Friction Stir Welding International Symposium. CD-ROM.

Soron, M., and Kalaykov, I. (2006). A Robot Prototype for Friction Stir Welding. In 2006 IEEE Conference on Robotics, Automation and Mechatronics (pp. 1–5). IEEE.

Squeo, E. A., Bruno, G., Guglielmotti, A., and Quadrini, F. (2009). Friction stir welding of polyethylene sheets. In *The Annals of "DUNĂREA DE JOS" University of* Galati Fascicle V, Technologies in Machine Building (pp. 241–146).

Strand, S. (2004). Effects of friction stir welding on polymer microstructure. Brigham Young University.

Tang, K. S., and Kwong, S. (2001). An optimal fuzzy PID controller. IEEE Transactions on Industrial Electronics, 48(4), 757–765.

Thomas, W., Nicholas, E., Needham, J., Murch, M., Temple-Smith, P., and Dawes, C. (1991). Friction-stir butt welding. UK: GB Patent No. 9125978.8.

TUM. (2014). Robotic Friction Stir Welding.

Yavuz, H. (2004). Function-oriented design of a friction stir welding robot. Journal of Intelligent Manufacturing, 15(6), 761–775.

Zhang, H. W., Zhang, Z., and Chen, J. T. (2005). The finite element simulation of the friction stir welding process. Materials Science and Engineering: A, 403(1-2), 340–348.

Zhao, X., Kalya, P., Landers, R. G., and Krishnamurthy, K. (2007). Design and Implementation of a Nonlinear Axial Force Controller for Friction Stir Welding Processes. In 2007 American Control Conference (pp. 5553–5558). IEEE.

Zhao, X., Kalya, P., Landers, R., and Krishnamurthy, K. (2009). Path force control for friction stir welding processes (pp. 1–8). Wright-Patterson, USA.

Zimmer, S., Langlois, L., Laye, J., and Bigot, R. (2010). Experimental investigation of the influence of the FSW plunge processing parameters on the maximum generated force and torque. The International Journal of Advanced Manufacturing Technology, 47(1-4), 201–215.

A.1. APPENDIX A1

Robotics and Autonomous Systems 61 (2013) 896–910

Contents lists available at SciVerse ScienceDirect

Robotics and Autonomous Systems

journal homepage: www.elsevier.com/locate/robot

Direct off-line robot programming via a common CAD package

Pedro Neto *, Nuno Mendes

CEMUC, Department of Mechanical Engineering - POLO II, University of Coimbra, 3030-708 Coimbra, Portugal

HIGHLIGHTS

- A novel CAD-based off-line robot programming solution.
- Robot programs are automatically generated from a CAD drawing.
- Robot cell design and robot programming are embedded in the same interface.
- The system is intuitive to use and presents a short learning curve.

ARTICLE INFO

Article history:
Received 13 July 2012
Received in revised form
30 January 2013
Accepted 8 February 2013
Available online 2 April 2013

Keywords:
Intuitive robot programming
CAD
Off-line programming

ABSTRACT

This paper focuses on intuitive and direct off-line robot programming from a CAD drawing running on a common 3-D CAD package. It explores the most suitable way to represent robot motion in a CAD drawing, how to automatically extract such motion data from the drawing, make the mapping of data from the virtual (CAD model) to the real environment and the process of automatic generation of robot paths/programs. In summary, this study aims to present a novel CAD-based robot programming system accessible to anyone with basic knowledge of CAD and robotics. Experiments on different manipulation tasks show the effectiveness and versatility of the proposed approach.

1. Introduction

Robot programming through the conventional teaching process (using the teach pendant) is often a tedious and time-consuming task that demands significant technical expertise. Many companies, especially small and medium-sized enterprises (SMEs), are not using robots and/or other automatic systems in their facilities because the configuration and programming process of this type of equipment is time-consuming and requires workers with knowledge in the field [1]. Nevertheless, most industrial robots are still programmed using the conventional teaching process. Thus, new and more intuitive approaches to robot programming are required. In fact, teach pendants are not intuitive to use [2–5] and some authors have presented solutions to this problem. This may involve the introduction of mechanisms for collision avoidance and automatic path planning in the robot teaching process [3,4]. Off-line robot programming (OLP) has increased in popularity over the years, with advantages and disadvantages over lead-through methods (see Section 2) [6–8].

Drawing inspiration from the way humans communicate with each other, this paper explores and studies methodologies that can help robot users to interact with a robot in an intuitive way, with a high-level of abstraction from the robot specific language. In fact, a human being can be taught in several different ways, for example, through drawings. As an example, it is very common to see a human being explaining something to another human being with base on a CAD drawing. In practice, CAD data have been used in robot programming with some degree of reliability since the 1980s; see Section 2.1.

In this paper, we present a novel system for CAD-based OLP, Fig. 1. Robot programs are directly generated from a 3-D CAD drawing running on a commonly available 3-D CAD package and not from commercial OLP or CAM software. The aim is to automatically generate robot motion sequences (programs) from a graphical description of the robot paths over a 3-D CAD model of a given robotic cell. A unified treatment of CAD and robot programming methods may involve very important advances in versatility and autonomy of the platform; in other words, product design and robot programming can be integrated seamlessly. It is explored the most suitable way to represent robot motion in a CAD drawing, how to automatically extract such motion data from the drawing, make the mapping of data from the virtual (CAD model) to the real environment and the process of automatic generation of robot paths/programs. A major goal is to create a CAD-based OLP system accessible to anyone with basic knowledge of CAD and robotics. Since today's CAD packages are rather widespread, are

* Corresponding author. Tel.: +351 239 790 700.
E-mail address: pedro.neto@dem.uc.pt (P. Neto).

0921-8890/$ – see front matter
http://dx.doi.org/10.1016/j.robot.2013.02.005

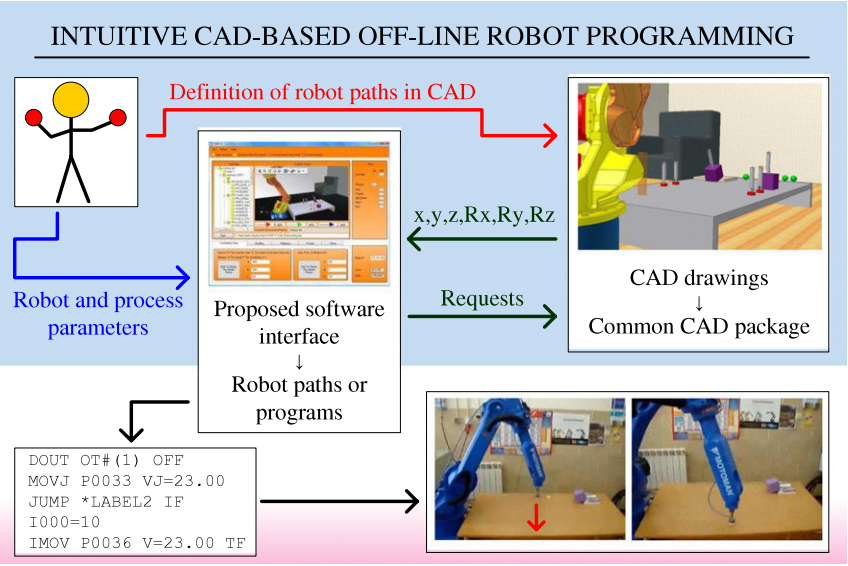

Fig. 1. Overview of the proposed approach.

relatively easy to use and have affordable prices, this can open the door to new robot users and thus contribute to increase in the number of existing robots in companies. Some algorithms with running code are presented, allowing readers to replicate and improve the work done so far. Experiments on different manipulation tasks show the effectiveness and versatility of the proposed approach.

2. Off-line robot programming

OLP is not a "fully automatic" programming process, it may involve manual editing of robot code and/or the definition of the robot programs by means of computer software that simulates the real robotic scenario. Some major advantages of OLP include the following:

- Robot programming without stopping/disturbing robot production, Fig. 2. Robots can be programmed before installation and stay in production while being re-programmed for a new task [6]. This means that robot programming can be carried out in parallel with robot production (production breaks are shortened).
- The programming efforts are moved from the robot operator in the workshop (factory floor) to the engineer/programmer in the office.
- Increase of work safety. During the programming process the user is not in the robot working area.
- Robot programs can be tested using simulation tools. This is very important to anticipate the real robot behavior and in this way to optimize working processes.

On the other hand, some disadvantages can be pointed out:

- Relatively high initial investment in software and workers' training. This investment is difficult to justify for most SMEs.
- Error associated with robot calibration. Robot calibration requires highly expensive measurement hardware, software and technical knowledge.
- The task calibration process requires experienced operators. A rough task calibration can lead to tremendous inaccuracies during robot operation.
- Robot programs created off-line need to be tested in the real robot in order to verify if they run correctly. In this context, calibration errors can lead to robot crashes.

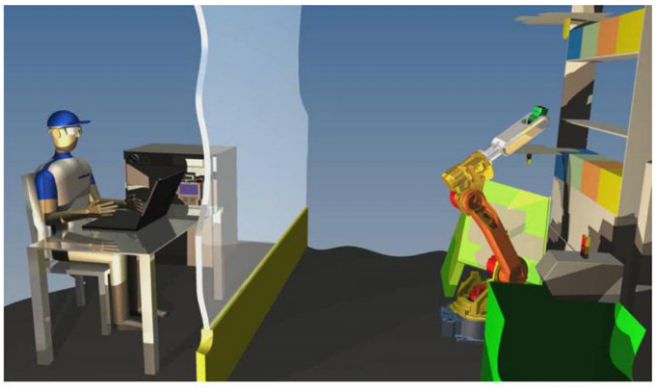

Fig. 2. OLP concept.

- Process information is required in advance.
- OLP methods rely on accurate modeling of the robotic cell.

Software packages dedicated to OLP are usually called OLP software or computer-aided robotics (CAR) software. Some OLP packages are able to operate with robots from different manufacturers (generic OLP packages). Three of the most common generic OLP packages are *Delmia* from *Dassault Systémes*, *RobCAD* from *Technomatix Technologies* and *Robotmaster* from *Jabez Technologies*. These software packages provide a set of modeling and simulation tools capable to represent graphically a robot manipulator and its attendant equipment, generate programs, and hence simulate a given robotic task [7,8]. On the other hand, almost every robot manufacturer has its own OLP software. Examples are *KUKA.Sim* from *KUKA*, *RobotStudio* from *ABB Robotics* and *MotoSim* from *Motoman*. Early versions of OLP software were based on simple wireframe models of the robot's kinematics. However, in recent years, robot simulation techniques have seen a rise in realism and popularity, possibly coinciding with the advancement of computing and graphical animation technologies. OLP packages of today are more graphically powerful, modular (with modules for specific processes such as coating and welding) and standard (with capacity for example to import standard CAD formats).

All of these capabilities come at a cost. A license for OLP software can cost thousands of Euros, an investment difficult to justify for most SMEs. Advantages of OLP software are tempered by some limitations in existing systems. In fact, they are not intuitive to use

and can only be applied in situations where the robot surrounding environment is known a priori and well modeled [9]. In addition, high absolute positioning accuracy can only be achieved with correctly calibrated robots [10–12]. If the robot poses (positions and orientations) are manually taught, repeatability is an important factor and positioning accuracy is not [12]. On the contrary, in OLP, positioning accuracy is a factor of crucial importance because robot paths are defined in a virtual space with respect to a given coordinate system. The positioning accuracy of an industrial robot varies with the manufacturer, age and robot type. The error magnitude can be as low as a tenth of a millimetre or as high as several centimetres. An appropriate calibration can reduce it to less than a millimetre. The international standard ISO 9283 recommends procedures for a correct calibration process. Different hardware and techniques have been applied in robot calibration, for example the ROSY system that uses a calibration ball and digital cameras to calculate kinematic errors and the resulting correction values (compensatory parameters) [10]. Another study shows how the accuracy of an ABB IRB 1600 industrial robot is improved using a 29-parameter calibration model [11]. Measures are acquired with a laser tracker. Most robot manufacturers provide robot calibration services.

2.1. CAD-based robot programming

In recent years, CAD technology has become economically attractive and easy to work with. Today, millions of SMEs worldwide are using CAD technology to design and model their products. Nevertheless, the CAD industry has to face significant technical challenges in future [13].

Already in the 1980s, CAD was seen as a technology that could help in the development of robotics [14]. Since then, a variety of research has been conducted in the field of CAD-based robot planning and programming. Over the years some researchers have explored CAD technology trying to extend its capabilities to the robotics field. Today, it is possible to extract information from CAD drawings/files to generate robot paths/programs for many different applications [15–18].

A series of studies have been conducted using CAD as an interface between robots and humans. Diverse solutions have been proposed for the processes of spray painting and coating. A review of CAD-based robot path planning for spray painting is presented by Chen et al. [19]. A CAD-guided robot path generator is proposed for the process of spray painting of compound surfaces commonly seen in automotive manufacturing [20]. Arikan and Balkan propose a CAD-based robotic system addressing the spray painting process of curved surfaces (OLP and simulation) [21] and Chen et al. a CAD-based automated robot trajectory planning system for spray painting of free-form surfaces [22].

An important study in the field of CAD-based robotics presents a method to generate 3-D robot working paths for a robotic adhesive spray system for shoe outsoles and uppers [23]. An example of a novel process that benefits from robots and CAD versatility is the so-called incremental forming process of metal sheets. Without using any costly form, metal sheets are clamped in a rigid frame and the robot produces a given 3-D contour by guiding a tool equipped with a high-frequency oscillating stamp over the metal surface. The robot's trajectories are computed from the CAD model on the basis of specific material models. Prototype panels or customized car panels can be economically produced using this method [24]. Pulkkinen et al. present a robot programming concept for applications where metal profiles are processed by robots and only a 2-D geometrical representation of the workpiece is available [25].

Nagata et al. propose a robotic sanding platform where robot paths are generated by CAD/CAM software [26]. A robotic CAD/CAM system that allows industrial robots to move along CL data without using any robot language is presented by Nagata et al. [27,28]. A recent study discusses robot path generation from CAM software for rapid prototyping applications [29]. Feng-yun and Tian-sheng present a robot path generator for a polishing process where CL data are generated from the postprocessor of a CAD system [30]. Other previous studies report the development of robotic systems for rapid prototyping in which cutting data are extracted from CAD drawings [31,32]. A CAD-based system to generate deburring paths from CAD data is proposed by Murphy et al. [33]. A method for manufacturing prototype castings using a robot-based system in which manufacturing paths are generated from CAM software is proposed by Sallinen and Sirviö [34]. In a different kind of application, CAD drawings are used for robot navigation purposes, namely for large scale path planning [35].

As we have seen above, a variety of research has been conducted in the fields of CAD-, CAM- and VRML-based OLP. However, none of the studies so far has an effective solution for an intuitive and low-cost OLP solution using raw CAD data and directly interfacing with a commercial CAD package. Research studies in this area have produced great results, some of them already implemented in industry, but limited to a specific industrial process (welding, painting, etc.). Even though a variety of approaches has been presented, a cost-effective and standard solution has not been established yet.

3. CAD-based approach

3.1. CAD packages

CAD technology has become economically attractive and easy to work with so that today there are millions of companies worldwide using it to design and model their products. While the prices of CAD packages have decreased, their features and functionalities have been upgraded, with improved and simplified user interfaces, user-oriented functionalities, automatic design of standard products, etc. Nowadays, most CAD packages provide a wide range of associated features (integrated modules or standalone solutions) that not only help in the effective design process, but also help in other tasks such as mechanical simulation and the physical simulation of dynamic processes. Robot programming and simulation has been seen as another feature that CAD packages can integrate.

Autodesk Inventor, which is one of the most common 3-D CAD packages of today, was chosen to serve as interface with the proposed solution. It incorporates all the functionalities of modern CAD packages, design, visualization, simulation, and user-friendly interface, and provides a complete application programming interface (API) for customization purposes, allowing developers to customize their CAD-based applications [36]. In terms of file formats, besides all the standard formats, *Autodesk Inventor* has proprietary file formats to define single *part model* files (ipt file) and *assembly model* files (iam file).

3.2. Extracting data from CAD drawings

The base of the proposed CAD-based OLP platform is the ability to automatically extract robot motion data from CAD drawings running on *Autodesk Inventor*. The *Autodesk Inventor API* is used for that purpose. It exposes the *Inventor's* functionalities in an object-oriented manner using a technology from *Microsoft* called *Automation*. In this way, developers can interact with *Autodesk Inventor* using current programming languages such as Visual Basic (VB), Visual C# and Visual C++. The *API* allows developers to create a software interface that performs the same type (kind) of operations that a user can perform when using *Autodesk Inventor* interactively. Summarizing, the *API* provides a set of routines that

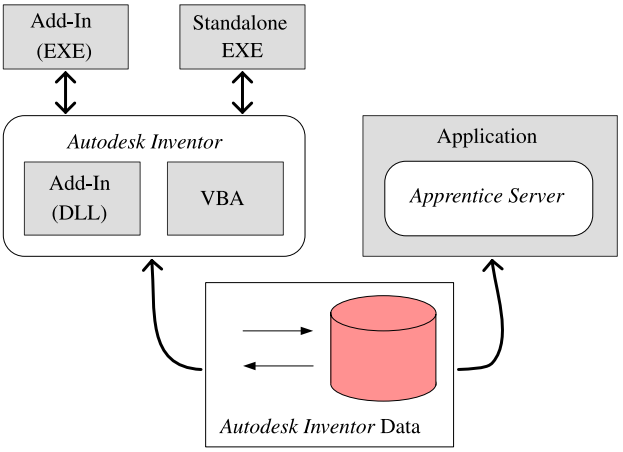

Fig. 3. Accessing the Autodesk Inventor's API.

may be used to build a software interface based on resources from *Autodesk Inventor*.

There are different ways to access the *Autodesk Inventor API*, Fig. 3. The white boxes represent components provided by the *API* (*Autodesk Inventor* and *Apprentice Server*) and the gray boxes represent programs written by developers. When one box encloses another box, this is an indication that the enclosed box is running in the same process as the box which is enclosing it. Thus, an "in-process" program will run significantly faster than a program running out of the process.

In the context of this paper, a standalone application is proposed to access the *API* and subsequently *Inventor* data. This choice was due to the necessity to integrate in the main application not only the process of interaction with CAD but also other software components for other tasks, for example, robot communications.

The *API* provided by *Autodesk* has a number of functionalities that were explored to be used in robotics. As an example, it is possible through a standalone application to open *Autodesk Inventor* in visible mode, Fig. 4, and open an *Inventor* document, Fig. 5. The properties of the document can then be easily accessed, Fig. 5.

There are a great number of data that can be extracted from a CAD drawing. The question is: What data are required to achieve our goal (OLP)? In practice, we need to have robot motion from CAD drawings, i.e., a sequence of target points representing the robot end-effector poses with respect to a known coordinate system (in Cartesian space). Thus, given the capacity of the *Autodesk Inventor API*, it was established that we need to extract positions and orientations of objects in 3-D space from proper CAD drawings representing a given robotic cell.

1. Positions—positional data can be acquired from a CAD drawing in different ways, for example, acquiring *WorkPoints* positional data (points that can be placed in the CAD drawing—see Section 3.3), Fig. 6. In other situations, positional data come from the points that characterize each one of the different lines representing virtual robot paths in a CAD drawing, Fig. 7. For example, in a specific situation, if the robot paths assume the geometry of a spline in the CAD drawing, the *API* provides all the points necessary to define such geometry. All these data are defined in relation to the origin of the CAD *assembly model* of the robotic cell.
2. Orientations—the *API* provides information about the transformation matrix (or homogeneous transform) of each *part model* represented in a CAD *assembly model*, Fig. 8. The transformation matrix contains the rotation matrix and the position of the origin of the *part model* to which it refers, both in relation to the origin of the CAD *assembly model* of the robotic cell.

3.3. CAD models

The process of creating the CAD *part models* that compose the CAD *assembly model* of the robotic cell should respect some rules. Since it was previously established that we need to have

Algorithm 1. Opening Autodesk Inventor (coded in VB).

```
1  ' Get object.
2  Private oApp As Inventor.Application
3  Try
4  |  oApp =
   |  System.Runtime.InteropServices.Marshal.GetActiveObject("Inventor.Application")
5  Catch ex As Exception
6  |  MessageBox.Show("A problem occurs")
7  End Try
8  ' Open Inventor (oApp).
9  Dim InventorAppType As Type = System.Type.GetTypeFromProgID("Inventor.Application")
10 oApp = System.Activator.CreateInstance(InventorAppType)
11 ' Make Inventor visible.
12 oApp.Visible = True
```

Fig. 4. Opening *Autodesk Inventor* (coded in VB).

Algorithm 2. Opening an Autodesk Inventor document (coded in VB).

```
1  ' Open an Inventor document (InventorDoc).
2  Private oApp As Inventor.Application
3  Private InventorDoc As Inventor.Document
4  InventorDoc = oApp.Documents.Open("document name")
5  ' Properties of the document.
6  Dim oPropsets As PropertySets
7  oPropsets = InventorDoc.PropertySets
```

Fig. 5. Opening an *Inventor* document and extracting their properties (coded in VB).

Algorithm 3. Extracting data from a selected WorkPoint (coded in VB).

```
' Select an item.
Dim oSelectSet As SelectSet
oSelectSet = ThisApplication.ActiveDocument.SelectSet
' Check if the selected item is a WorkPoint.
If TypeOf oSelectSet.Item(i) Is WorkPoint Then
    Dim wp1(i) As WorkPoint
    wp1(i) = oSelectSet.Item(i)
    ' WorkPoint data (name, X, Y, Z).
    WorkPointPos(i).oName = wp1(i).Name
    WorkPointPos(i).x = wp1(i).Point.X
    WorkPointPos(i).y = wp1(i).Point.Y
    WorkPointPos(i).z = wp1(i).Point.Z
Else
    MsgBox("You must select a WorkPoint.")
    Exit Sub
End If
```

Fig. 6. Extracting data from a selected *WorkPoint* (coded in VB).

Algorithm 4. Extracting data from a selected virtual line (coded in VB).

```
'Extracting straight line data.
If TypeOf oSelectSet.Item(i) Is SketchLine3D Then
    'Defining an object type SketchLine3D.
    Dim Line_ As SketchLine3D
    Line_ = oSelectSet.Item(i)
    'Start and end points of the SketchLine3D.
    Dim start_point_x, start_point_y, start_point_z As Double
    Dim end_point_x, end_point_y, end_point_z As Double
    start_point_x = Line_.StartSketchPoint.Geometry.X 'The same for y and z.
    end_point_x = Line_.EndSketchPoint.Geometry.X 'The same for y and z.
'Extracting spline data.
ElseIf TypeOf oSelectSet.Item(i) Is SketchSpline3D Then
    'Defining an object type SketchSpline3D.
    Dim Spline_ As SketchSpline3D
    Spline_ = oSelectSet.Item(i)
    'Start, medium and end points of the SketchSpline3D.
    Dim s_start_point_x, s_start_point_y, s_start_point_z As Double
    Dim s_mid_point_x, s_mid_point_y, s_mid_point_z As Double
    Dim s_end_point_x, s_end_point_y, s_end_point_z As Double
    s_start_point_x = Spline_.StartSketchPoint.Geometry.X 'The same for y and z.
    s_mid_point_x = Spline_.FitPoint(2).Geometry.X 'The same for y and z.
    s_end_point_x = Spline_.EndSketchPoint.Geometry.X 'The same for y and z.
End If
```

Fig. 7. Extracting data from a selected virtual line (coded in VB).

Algorithm 5. Transformation matrix (coded in VB).

```
' Get an occurence from the selected item.
Dim oOccurrence As ComponentOccurrence
oOccurrence = ThisApplication.ActiveDocument.SelectSet.Item(i)
' Get the transformation matrix.
Dim oTransform As Inventor.Matrix
oTransform = oOccurrence.Transformation
' Get matrix data, for example cell (1, 3).
Dim mt13 As Double
mt13 = oTransform.Cell(1, 3)
```

Fig. 8. Extracting the transformation matrix of a selected item (coded in VB).

represented in the CAD *assembly model* of the robotic cell all the required robot paths (end-effector poses), it becomes necessary to study the most suitable way to have that information represented in CAD drawings. This can be achieved in two different ways.

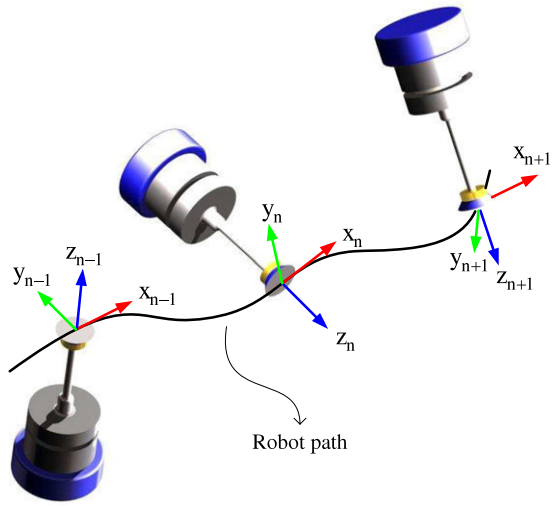

Fig. 9. Simplified tool models defining the robot end-effector pose in each path segment.

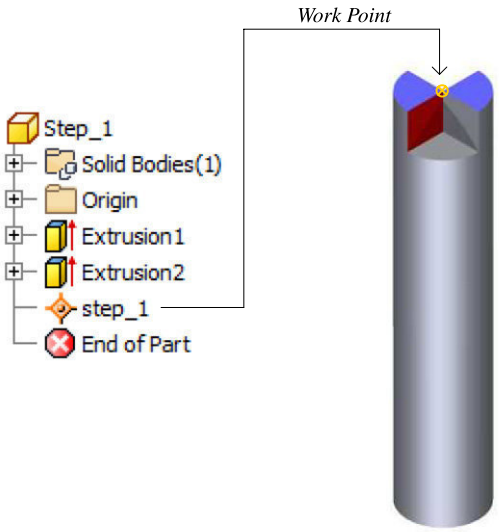

Fig. 10. A *WorkPoint* attached to a tool model in a location where the tool is connected to the robot wrist.

1. Introducing extra robot tool (end-effector) models within the *assembly model*. These models represent the desired robot end-effector pose in each segment of the path, Fig. 9. Positional data are achieved by placing a *WorkPoint* attached to any part of the tool model, Fig. 10. The *WorkPoint* data (x, y, z) are provided by the *API* in relation to the origin of the CAD *assembly model*. Orientation data are achieved from the tool models orientation in the drawing (transformation matrix).
2. Drawing lines (in the *assembly model*) representing the desired robot path (positional data) and defining the robot end-effector orientation by placing simplified tool models along the path lines (in each segment of the path), as in the above topic, Fig. 9.

The CAD *assembly model* does not need to accurately represent the real cell in all its aspects. On the contrary, it can be a simplified model containing all the necessary/important information for the programming process (target points and relations between them). As an example, the robot tool length, robot path positions and relative positioning of CAD models have to accurately represent the real environment. However, the models appearance does not need to be exactly the same as the real objects. It means that, for example, chamfers or rounded edges are expendable. These simplifications allow us to speed up the modeling process. Fig. 11 shows a real robot tool (a) and two CAD models of that tool, (b) and (c), with the same length *l*. These two models were created with different levels of detail.

1. Model (b) was created with more detail than model (c). It represents more accurately the real tool, with advantages in terms of visualization. Nevertheless, the process of drawing this model is more time consuming than drawing model (c);
2. Model (c) is a simpler version but accurate at the same time in terms of total length of the tool. It can be drawn in seconds and used where only the length of the tool is a factor of importance.

It is important to note that the best model is the simplest model that still serves its purpose.

3.3.1. Process/path planning

The process/path planning task occurs during the construction of the CAD *assembly model*, in which the user is planning in advance the "best" process parameters and paths. Depending on the type and complexity of the process in study, the planning task can include several factors.

1. Models selection/construction and definition of the layout of the cell. Some CAD models can be accessed from libraries provided by manufacturers (robots and other peripheral equipment).
2. Robot motion. Robot motion can be indirectly defined by placing simplified tool models and/or virtual paths within the CAD *assembly model*. The desired movement type (linear, circular or spline) is defined by the geometry of the virtual paths or in the software interface.
3. Operation sequences. Robot operation sequences are defined by the name of the tool models. The first five characters of the name of a tool model should be "step_" (simple robot motion). The sixth character and following should be a number defining the ordering sequence for robot motion. Following the sequence number the tool name can have or not a character type letter indicating a specific robot operation, for example, "step_1A" can indicate robot motion plus the activation of a digital output of the robot.
4. Collisions. Collisions should be predicted by the designer during the creation of the CAD model of the cell. The designer should ensure that there are no collisions between the robot and other objects within the workspace. Fig. 12 shows a CAD drawing with two tool models (initial and target pose) and an obstacle. If the robot end-effector is linearly moved from the initial to the target pose a collision occurs. The designer should anticipate this situation and introduce into the drawing "intermediate" tool models to allow the robot to avoid the obstacle, Fig. 13.
5. Grasping and re-grasping/repositioning. These are common situations in industrial robotics, especially in pure manipulation tasks. Many times, in order to properly perform a task, there is a need for re-grasping or repositioning a given workpiece. Fig. 14 shows a re-grasping process in which a grasping location is changed from an initial pose defined by the tool model step_1 to a target pose defined by step_5. Moreover, during the planning phase, it has to be ensured that the robot is operating with valid tool locations, including valid contact conditions between the gripper and the workpiece. Note that as in Figs. 13 and 14 some "intermediate" tool models are used to avoid collisions during the re-grasping process.

A robot simulation system can be a valuable help in this planning phase, helping us to visualize the robotic process (robot motion, possible collisions and the re-grasping operations) and detect existing robot kinematic singularities or robot joint limits.

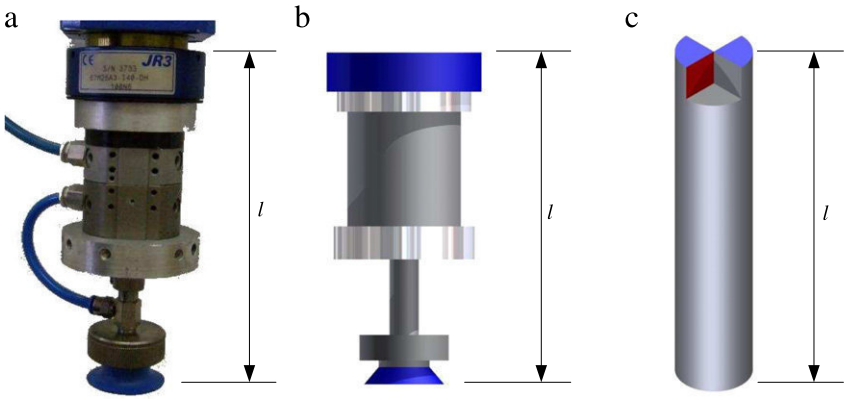

Fig. 11. Real robot tool (a), and simplified models (b) and (c).

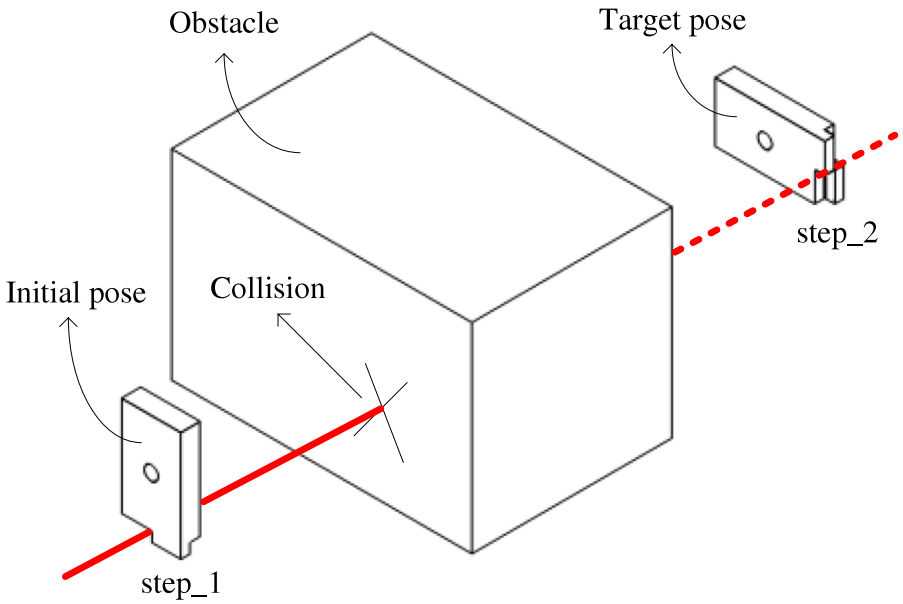

Fig. 12. Collision.

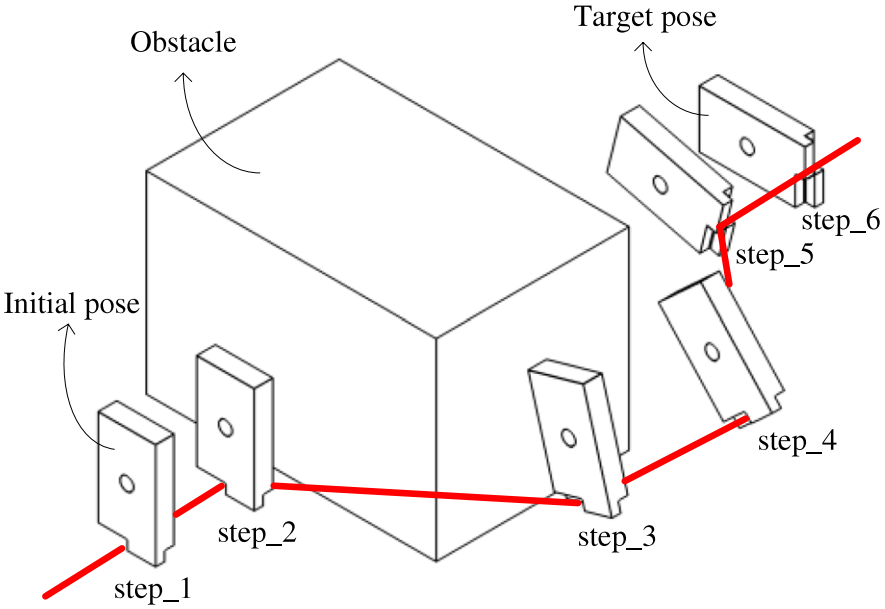

Fig. 13. Avoiding an obstacle.

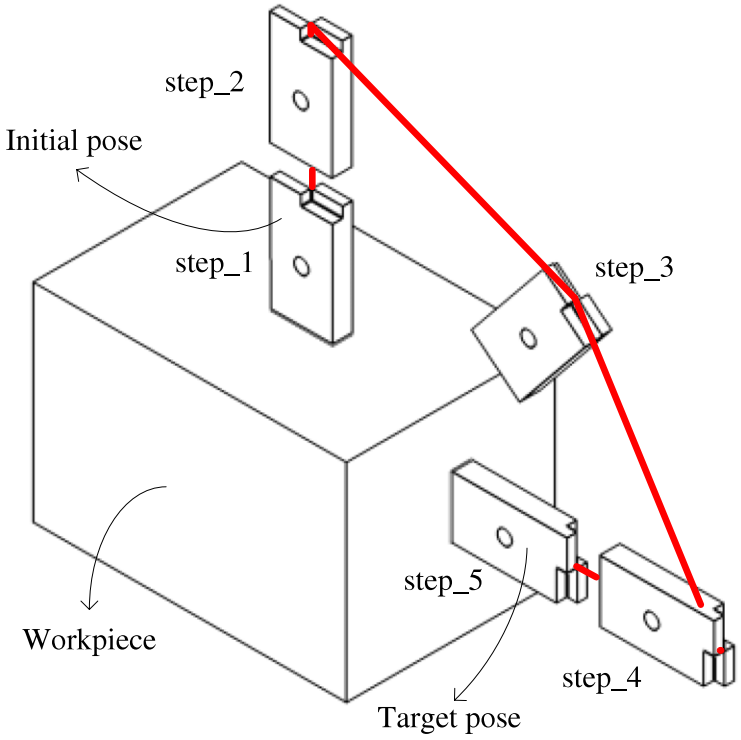

Fig. 14. Re-grasping.

3.4. Mapping and calibration

Many times it is necessary to express the same quantity in relation to different coordinate systems, i.e., change descriptions from frame to frame, mapping. These capabilities can be used for the task calibration process, making the CAD model of the cell in study to match with the real robotic cell. All robot end-effector positions and orientations extracted from CAD have to be known with respect to one or more reference frames known a priori in the space of the real robot. These frames have to be defined within the CAD drawing of the cell by placing invisible *part models* with the desired poses into the CAD *assembly model* (note that each *part model* has a frame associated). Then, the real robot is taught about that frame(s)' pose in the real environment through the conventional way, using the teach pendant. Essentially, the process consists in the definition of one or more frames within the CAD drawing of the cell and the corresponding frame(s) in the robot controller. This makes the task calibration process a relatively simple and non-time consuming process. Nevertheless, complex robotic scenarios can require the definition of a significant number of different frames. In this case, the task calibration process can be lengthy and prone to error. This is because the user has to remember the pose of each frame previously defined within the CAD drawing and at the same time to define such frames in the real scenario.

As mentioned before, the *Autodesk Inventor API* provides all the information (transformation matrices, *WorkPoints* and path lines data) with respect to the origin of the CAD *assembly model*, here defined by frame $\{U\}$, Fig. 15. Frame $\{B\}$ is defined in the robot controller during the calibration process (in the real robot), and at the same time the *API* provides the transformation matrix of $\{B\}$ relative to $\{U\}$, ${}^{U}_{B}\mathbf{T}$. This means that frame $\{B\}$ "makes the link" between the virtual and real world. Note that, as mentioned above, it is possible to define more than one frame if necessary, as the process is similar.

Since *Autodesk Inventor* considers the tool models (with a *WorkPoint* attached) and the path lines as a constituent of a single *part model* within in the CAD *assembly model*, the transformation matrix (relative to $\{U\}$) of that single *part model* defines the pose of tool models and path lines. For the general case presented in Fig. 15 the path line is part of the table top model. The table top model has the origin and orientation defined by $\{E\}$. However, it is not necessary to know the orientation of the path lines because the *API* gives all the necessary points to define the path lines relative to $\{U\}$, for example the initial path point ${}^{U}\mathbf{P}_{ini}$, Fig. 15. Thus, it is necessary to achieve the path line points relative to frame $\{B\}$. The same for the tool models in which we need to have orientations and *WorkPoint* positional data relative to $\{B\}$.

The generic tool models that incorporate $\{C\}$ and $\{D\}$, Fig. 15, help to define the end-effector pose in each path segment, as well as the *WorkPoint* positions (if they have a *WorkPoint* attached). The *API* provides the transformation matrix of these models relative to $\{U\}$, ${}^{U}_{C}\mathbf{T}$ and ${}^{U}_{D}\mathbf{T}$. Given our purpose (robot programming), we wish to express $\{C\}$ and $\{D\}$ in terms of $\{B\}$, ${}^{B}_{C}\mathbf{T}$ and ${}^{B}_{D}\mathbf{T}$. For ${}^{B}_{C}\mathbf{T}$ we have that

$$ {}^{B}_{C}\mathbf{T} = {}^{B}_{U}\mathbf{T} + {}^{U}_{C}\mathbf{T}. \tag{1} $$

To find ${}^{B}_{U}\mathbf{T}$, we must compute the rotation matrix that defines frame $\{U\}$ relative to $\{B\}$, ${}^{B}_{U}\mathbf{R}$, and the vector that locates the origin of frame $\{U\}$ relative to $\{B\}$, ${}^{B}\mathbf{P}_{Uorg}$:

$$ {}^{B}_{U}T = \left[\begin{array}{ccc|c} & {}^{B}_{U}R & & {}^{B}P_{Uorg} \\ 0 & 0 & 0 & 1 \end{array}\right] \tag{2} $$

Let us consider a generic vector/point defined in $\{U\}$, ${}^{U}\mathbf{P}$. If we wish to express this point in space in terms of frame $\{B\}$ we must compute

$$ {}^{B}\mathbf{P} = {}^{B}_{U}\mathbf{R}\,{}^{U}\mathbf{P} + {}^{B}\mathbf{P}_{Uorg}. \tag{3} $$

Given the characteristics of a rotation matrix, ${}^{B}_{U}\mathbf{R} = {}^{U}_{B}\mathbf{R}^{T}$, and as we know ${}^{U}_{B}\mathbf{T}$, there follows the computation of ${}^{B}\mathbf{P}_{Uorg}$. From the process

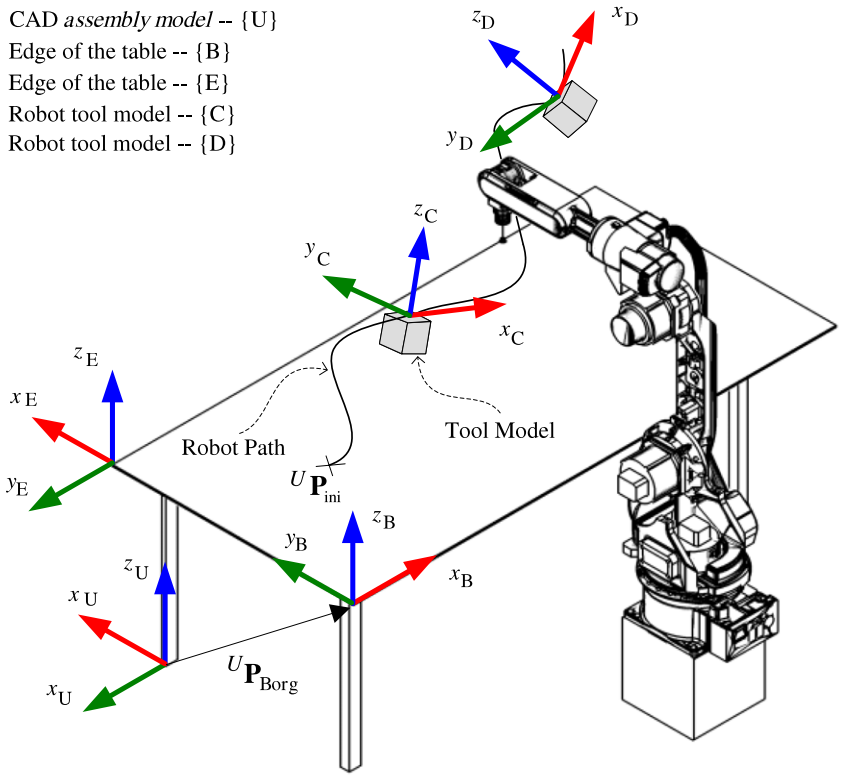

Fig. 15. Coordinate frames.

of inverting a transform we have that

$$ {}^{B}_{U}T = \left[\begin{array}{ccc|c} & {}^{U}_{B}R^{T} & & -{}^{U}_{B}R^{T\,U}P_{Borg} \\ 0 & 0 & 0 & 1 \end{array}\right] \tag{4} $$

Thus, from (2) and (4):

$$ {}^{B}\mathbf{P}_{Uorg} = -{}^{U}_{B}\mathbf{R}^{T\,U}\mathbf{P}_{Borg}. \tag{5} $$

At this stage, from (1) and (4) we can compute ${}^{B}_{C}\mathbf{T}$. The same methodology can be applied to achieve ${}^{B}_{D}\mathbf{T}$ and any other transformation. This means that all positions and orientations extracted from CAD can be referred with respect to the reference frame(s) defined in the real environment at the moment of the calibration process.

3.5. X–Y–Z Euler angles

After having obtained from CAD drawings the rotation matrices defining robot end-effector orientations in relation to a given frame, such matrices are transformed into effective end-effector rotations, usually Euler angles or quaternions.

The description of the orientation of a generic frame $\{B\}$ with respect to a generic frame $\{A\}$ in the form of X–Y–Z Euler angles (α, β, γ) can be represented by a rotation matrix composed of the multiplication of the rotation matrices around each angle: ${}^{A}_{B}\mathbf{Rot}_{xyz} = \mathbf{Rot}_{x}(\alpha)\,\mathbf{Rot}_{y}(\beta)\,\mathbf{Rot}_{z}(\gamma)$. It is now possible to compute the X–Y–Z Euler angles. If $\beta \neq \pm(\pi/2)$:

$$ \beta = A\tan 2\left(r_{1,3}, \sqrt{r_{1,1}^2 + r_{1,2}^2}\right) \tag{6} $$

$$ \alpha = A\tan 2\left(\frac{r_{2,3}}{-\sqrt{r_{1,1}^2 + r_{1,2}^2}}, \frac{r_{3,3}}{\sqrt{r_{1,1}^2 + r_{1,2}^2}}\right) \tag{7} $$

$$ \gamma = A\tan 2\left(\frac{r_{1,2}}{-\sqrt{r_{1,1}^2 + r_{1,2}^2}}, \frac{r_{1,1}}{\sqrt{r_{1,1}^2 + r_{1,2}^2}}\right) \tag{8} $$

where $r_{a,b}$ are the elements of ${}^{A}_{B}\mathbf{Rot}_{xyz}$ and $A\tan 2(y, x)$ is a two argument arc tangent function. When $\beta = \pm(\pi/2)$, the process to compute Euler angles is more complex. In this situation both the x and z axes are aligned with each other and one degree of freedom is lost. This phenomenon is mathematically unsolvable and is known as gimbal lock. In this scenario, α and γ cannot be calculated separately but together:

$$ \alpha \pm \gamma = A\tan 2\left(r_{3,2}, r_{2,2}\right). \tag{9} $$

The gimbal lock phenomenon does not make Euler angles "wrong" but makes them unsuited for some practical applications. Some methods have been proposed to deal with the gimbal lock phenomenon, for example, solutions based on the representation of rigid body orientation through quaternions [37]. However, some robot manufacturers force the use of Euler angles so that in these cases the option for quaternions is ruled out. Pollard et al. propose to locate regions near gimbal lock and compute a restricted degree of freedom solution within those regions [38]. In practice, a typical approach is to set an angle equal to zero and compute the remaining angle. In this case, if $\beta = (\pi/2)$, and assuming that $\alpha = 0$, we have

$$ \gamma = A\tan 2\left(r_{2,1}, -r_{3,1}\right). \tag{10} $$

On contrary, if $\beta = -(\pi/2)$ and assuming that $\alpha = 0$, we have

$$ \gamma = A\tan 2\left(r_{2,1}, r_{3,1}\right). \tag{11} $$

3.6. Interpolation for end-effector orientations

When an industrial robot is performing a pre-programmed movement and this one requires abrupt end-effector orientation changes, we must take special care because it can come into a situation where no one has total control over the end-effector orientation. In other words, we have no control over the interpolation made by the robot controller between two given poses. This is particularly true when robot programs are generated off-line. In

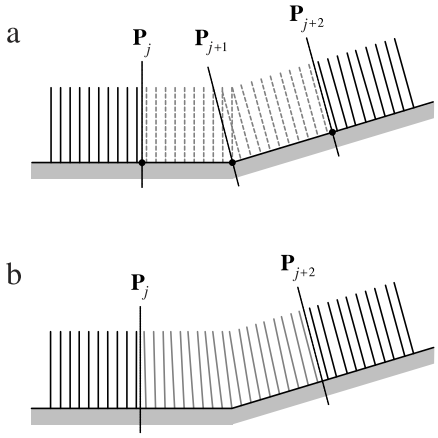

Fig. 16. End-effector poses: (a) before interpolation and (b) after interpolation.

some situations this could be a major problem, leading to the appearance of defects in the work produced by the robot [39]. The proposed solution to circumvent this problem is based on the implementation of linear smooth interpolation of end-effector positions and orientations [30]. The process involves the following steps:

1. Identification of risk areas. This is achieved by analyzing the CAD drawing of the cell and manually defining those areas in the drawing (abrupt end-effector orientation changes).
2. Discretization of the risk robot path in equally spaced intervals.
3. Computation of end-effector orientations for each interpolated path point. The new path is smoother than the initial, Fig. 16.

For the profile shown in Fig. 16, interpolation was divided in two sections $S_1 \in \left[\mathbf{P}_j, \mathbf{P}_{j+1}\right]$ and $S_2 \in \left[\mathbf{P}_{j+1}, \mathbf{P}_{j+2}\right]$. The calculations are presented for section S_1 but for other sections the procedure is similar. For a sampling width Δt the interpolated position $\mathbf{r}(k) = (r_x, r_y, r_z)^T$ is

$$r_i(k) = r_i(0) + v_i(k)\, k\, \Delta t, \quad \begin{cases} (i = x, y, z) \\ k = 1, \ldots, n-1 \end{cases} \tag{12}$$

where $v_i(k)$ is a directional velocity profile and n represents the number of interpolated points.

A spherical linear interpolation (SLERP) algorithm was implemented for the purpose of quaternion interpolation. Given two known unit quaternions, $\mathbf{Q}_0$ (from $\mathbf{P}_j$) and $\mathbf{Q}_n$ (from $\mathbf{P}_{j+1}$) with parameter k moving from 1 to $n-1$, the interpolated end-effector orientation $\mathbf{Q}_k$ can be obtained as follows:

$$\mathbf{Q}_k = \frac{\sin\left(\left(1 - \frac{k-1}{n-1}\right)\theta\right)}{\sin\theta}\mathbf{Q}_0 + \frac{\sin\left(\frac{k-1}{n-1}\theta\right)}{\sin\theta}\mathbf{Q}_n,$$
$$k = 1, \ldots, n-1 \tag{13}$$

where

$$\theta = \cos^{-1}\left(\mathbf{Q}_0 \cdot \mathbf{Q}_n\right). \tag{14}$$

This method for quaternion interpolation is also used when we want to interpolate Euler angles, simply by transforming Euler angles into quaternions and vice versa.

3.7. Generation of robot programs

The search for new and more intuitive methods to program machines has led to the emergence of techniques to generate machine code. In the last few decades, several code generation techniques have been developed. The most prominent example is the use of commercial CAD/CAM systems to generate reliable CL data for CNC machining [40]. CNC tool paths can also be generated from

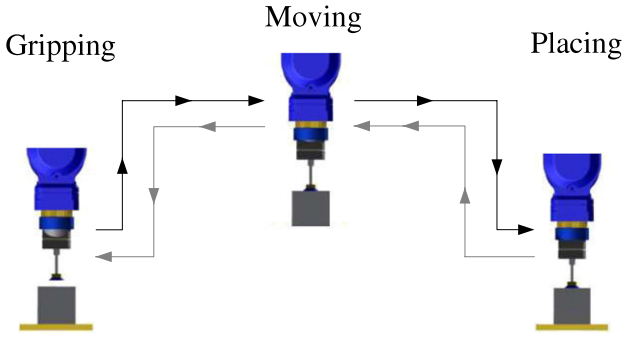

Fig. 17. The different phases of a manipulation task.

standard CAD formants [41–43]. Nevertheless, these systems to generate code tend to have some drawbacks such as their ability to generalize from different situations and respond to unseen problems. During the elaboration of an algorithm to generate code, the keyword is "generalize" and never "particularize", the algorithm must be prepared to cover a wide range of variations in the process. For particular applications with a limited and well known number of process variations this kind of algorithms presents acceptable performance [44].

Robot controller specific languages have seen only minor advances in the last few years. Some authors have devoted attention to create methodologies capable to generalize robot programs around a task but which at the same time can be customized as necessary [45]. An operation can be customized in terms of type of robot operation or shape of the workpiece. Intrinsically, this allows us to profit from previously similar work, incorporating the programmers' experience and process knowledge [46]. Thus, the time to create robot programs for related products/tasks can be reduced and non-specialists can create robot programs by themselves. These systems follow the same logic as the well known macros or scripts in the world of computer science. Translators for robot programming languages have also been matter of concern [47], as well as the development of robotic system that operates without using a specific robot language [27,28].

In this paper, we propose an algorithm to automatically generate robot programs with information extracted from CAD drawings. The way the process to generate robot code is applied differs with the robotic task under study. Nevertheless, there is a common point in all robot programs. It means that since robots usually perform manipulation tasks, the process to generate a robot program does not differ greatly from application to application, containing common tasks like gripping, moving and placing, Fig. 17.

The automatic generation of a robot program is no more than writing robot commands in a text file, line by line. In this paper, this process is managed by the software interface (Section 3.8) that extracts data from CAD drawings, interprets that data and finally generates robot programs. The process to generate a robot program is divided into two distinct phases:

1. Definition and parameterization of robot end-effector poses, frames, tools and constants. The algorithm in Fig. 18 summarizes the process of data acquisition from tool models and/or path lines and the generation of robot code. The following equation represents a common definition of a robot pose in a robot program:

$$P = x, y, z, \begin{cases} \alpha, \beta, \gamma \longrightarrow \textit{Euler angles} \\ q_w, q_x, q_y, q_z \longrightarrow \textit{Quaternions}. \end{cases} \tag{15}$$

In addition to robot poses, specific process and robot parameters (coordinate systems, tools, etc.) are specified in this phase. This information comes from the parameters introduced in the software interface, for example, robot home position, number of working cycles, approaching distances, etc.

Algorithm 6 Data extraction from CAD drawings and generation of robot paths/programs

Input: CAD drawing
Output: robot paths/programs

```
Begin
  For Each tool model Do
    Get WorkPoint position, Algorithm 3
    Get transformation matrix, Algorithm 5
    Compute frame correlations, eq (1) to (5)
    Compute Euler angles, eq (6), (7), (8), (10), (11)
    If (tool name = step_n) Then
      Generate code for simple robot motion
    Else If (tool name = step_n...) Then
      Generate code for a given robot operation/task
    End If
  End For
  For Each selected path line in CAD Do
    Get path position, Algorithm 4
    Get end-effector orientation (from tool models)
    Generate robot code
  End For
End
```

Fig. 18. Extracting data from CAD and generation of robot code.

2. Body of the program. A robot program contains predominantly robot motion instructions: linear, joint, circular or spline robot movement. These movement instructions respect the type of motion established in the CAD drawing and/or the software interface. For example, if a segment of a path is drawn as a straight line, the generated code will contain a robot instruction that makes the robot end-effector move linearly in that path segment. In this phase the algorithm also has to deal with particular situations associated with each robotic task such as the generation of IO commands to communicate with other machines and the definition of approaching distances.

The proposed algorithm is able to generate robot programs for *Motoman* robot controllers (INFORM language), Fig. 19. However, as all robot programs are based on the same principle, the proposed algorithm can be adapted to generate code in other programming languages.

3.8. Software interface

The developed software interface makes the link between the user, the CAD package and the robot. The functionalities and global architecture of the proposed software interface are schematically shown in Fig. 20. This software interface runs under *Microsoft Windows* operating systems (*XP* or above) and in any industrial or personal computers with processing and graphical capacity to host *Autodesk Inventor*, Fig. 21. It was mainly written in VB.

4. Experiments

The CAD-based OLP system was validated in two different experimental setups, both representing practical scenarios of application of robots (manipulation tasks). The first experiment involves a robot manipulating objects from a location to another one and the second experiment a robot transporting an object between obstacles.

4.1. Experiment I

This experimental setup was designed to accomplish a simple object manipulation task. Robot programs are generated from a CAD *assembly model* of the robotic cell in study, Fig. 22, where

```
...0064=489.3844...
75.050253609301,0,0,0
P00070=489.38445479391,166.36209915648,
775.050253609301,0,0,0
//INST
///DATE 2010/06/29 16:28
///ATTR SC,RW
///GROUP1 RB1
NOP
SET D001 0
SET I005 1
SET I000 10
DOUT OT#(1) OFF
MOVJ P0033 VJ=23.00
MOVJ P001 VJ=23.00
JUMP *LABEL2 IF I000=10
IMOV P0036 V=23.00 TF
*LABEL2
ADD P0036 P0043
DOUT OT#(1) ON
TIMER T=1.00
MOV...VJ=23.00
```

Fig. 19. A snippet of a robot program generated for a *Motoman* robot (INFORM).

simplified robot tool models represent the target poses for robot motion (initial poses and target poses). The robot task from which a robot program is generated consists in having the robot handling three objects from an initial to a final pose, Fig. 23 [48].

4.2. Experiment II

In this experiment, robot programs are generated from a CAD *assembly model* in which the virtual paths (positional data) are represented in the form of straight lines, arcs and splines. The end-effector orientation is defined by placing tool models along the above mentioned virtual paths. These models define the orientation of the robot end-effector in each segment of the path, Fig. 24. The robot program generated from CAD is tested in a real scenario. As shown in Fig. 25 the real robot performs the manipulation task with success bypassing the obstacles without hitting them [49].

4.3. Results and discussion

The experiments demonstrated the versatility of the proposed CAD-based OLP system. Robotic cell design and robot programming are embedded in the same interface and work through the same platform, *Autodesk Inventor*, without compatibility issues. In terms of accuracy, as in the case of commercial OLP software, the error that may exist comes from the robot and/or task calibration process and inaccuracies in the construction of the CAD models. In fact, error is always present, which may or may not be acceptable, depending on their magnitude and application under consideration. Often, task calibration errors arise from the little time and attention devoted to the calibration process. This situation is increasingly common as companies are constantly being asked to change production for new products. The above is true for all the robot programming and simulation systems based on virtual representation of objects in space, OLP. It is also important to note that after generating a robot program, it should be simulated in

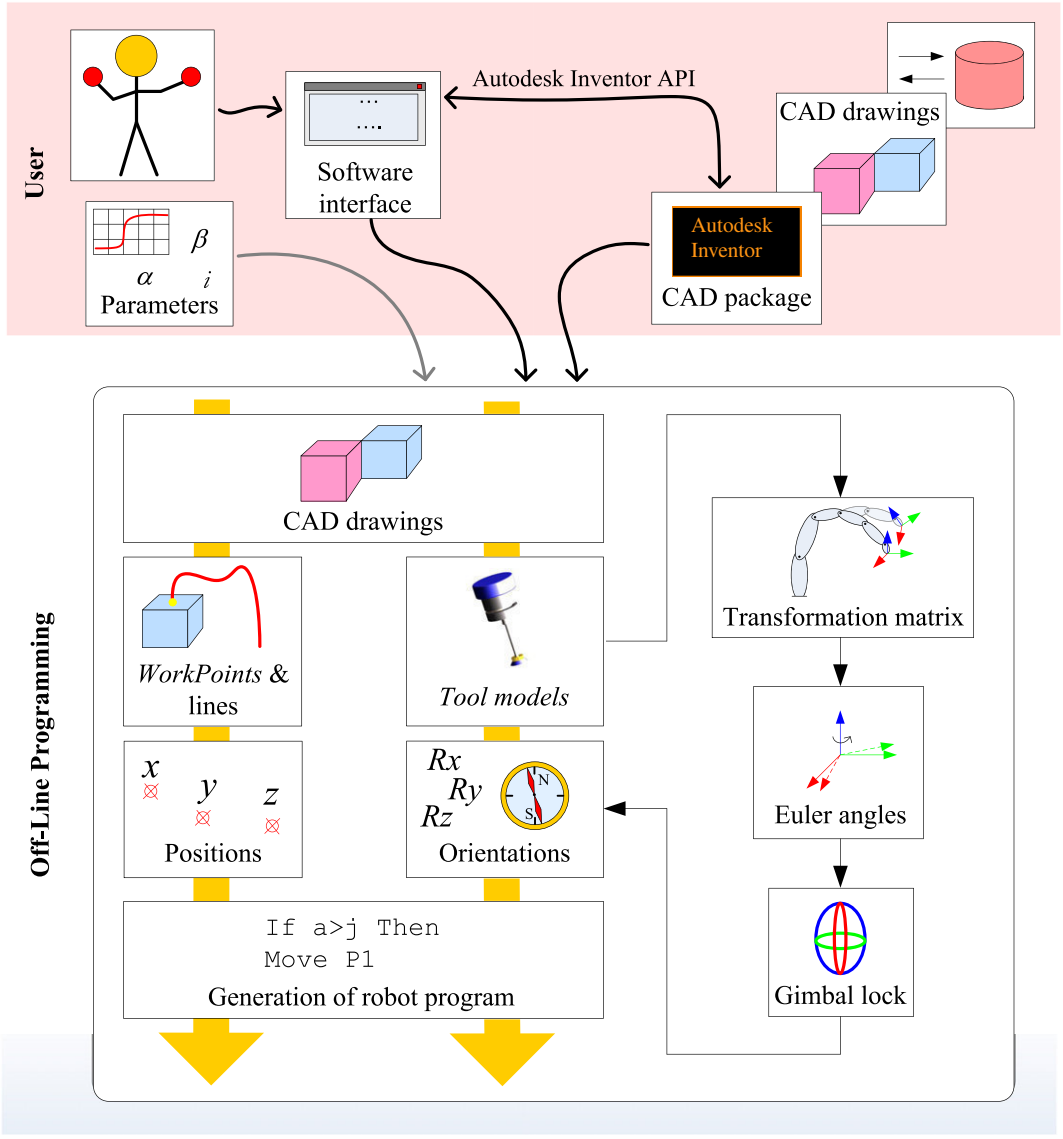

Fig. 20. Functionalities and architecture.

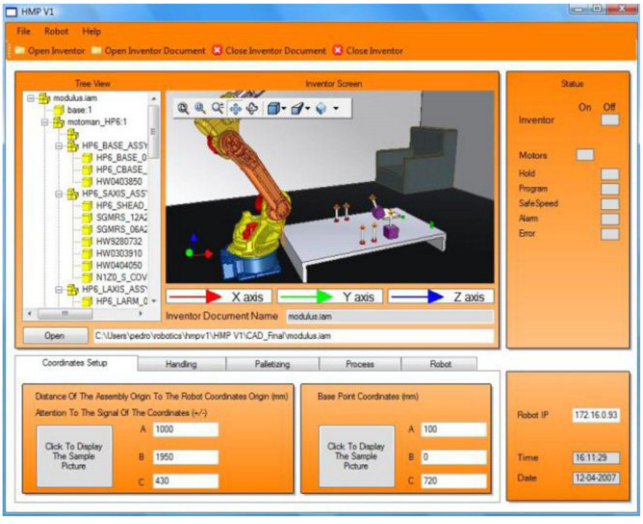

Fig. 21. Graphical user interface of the developed software.

order to better visualize the robotic process (robot motion, possible collisions, the re-grasping operations, kinematic singularities, robot joint limits). Moreover, in order to be cautious with respect to possible errors, the robot programs generated off-line have to be tested (and adjusted if necessary) in the real robot (in the shop floor).

The proposed CAD-based HRI system is not the definitive solution for OLP. Nevertheless, it is an original contribution to the field, with pros and cons. The proposed system is limited in some aspects, for example in the level of sophistication and ability to generalize from particular situations. On the other hand, the intuitiveness of use, short learning curve and the low-cost nature of the system appear as positive aspects, making it more accessible than common OLP software. All of these characteristics are fundamental when the objective is to spread the utilization of this kind of systems in SMEs or use it for educational and training purposes.

5. Conclusions and future work

A novel CAD-based OLP platform has been presented. Robotic cell design and OLP are embedded in the same interface and work

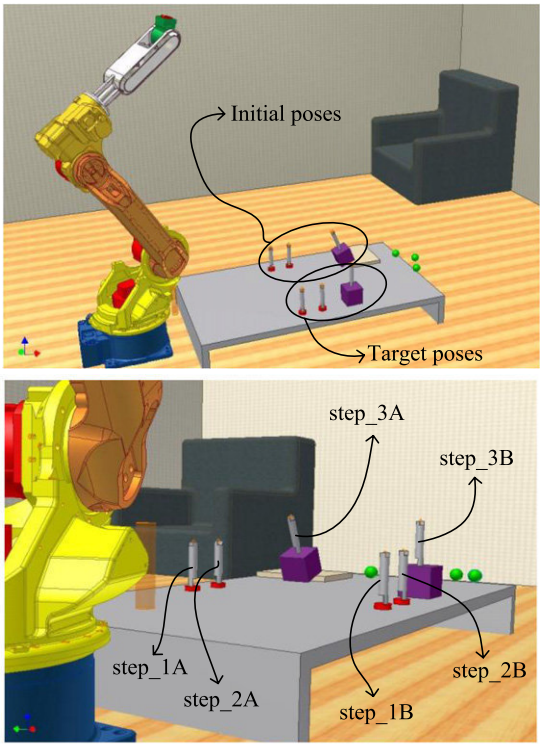

Fig. 22. Two different perspectives of the CAD *assembly model*.

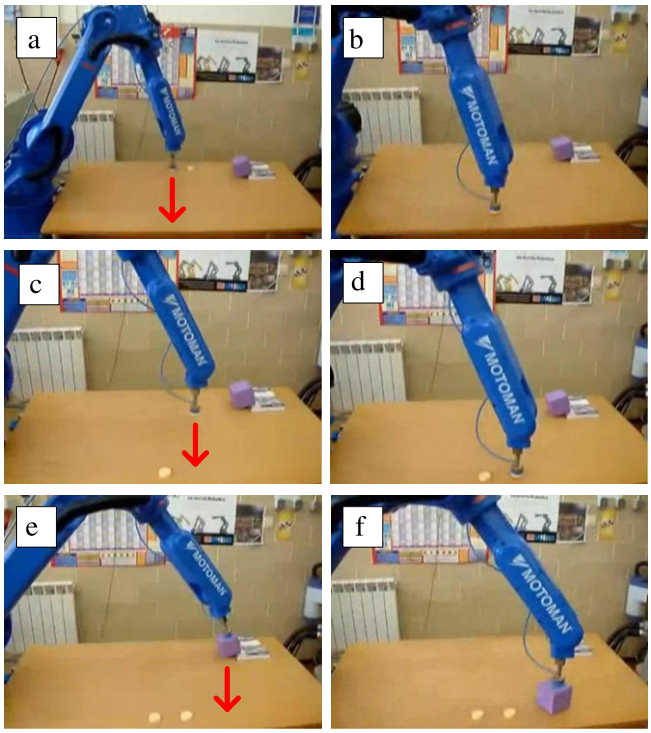

Fig. 23. Robot running the program generated from CAD.

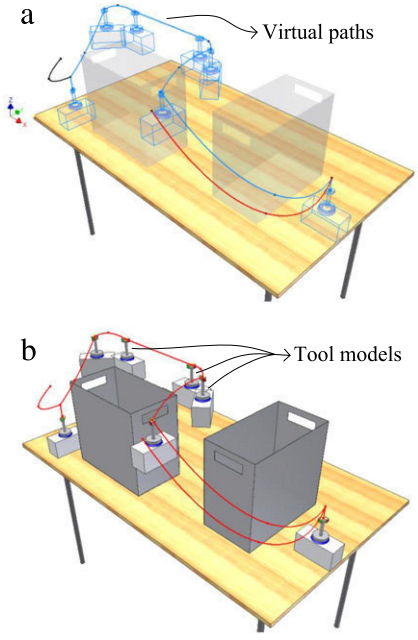

Fig. 24. CAD *assembly model* of the cell in study: with obstacles in invisible mode (a) and in visible mode (b).

through the same platform, a common commercial CAD package. It was proposed a method to extract robot paths (positions and orientations) from a CAD drawing of a given robotic cell. Such data are then treated and transformed into robot programs. In addition, the experiments showed that the proposed system is intuitive to use and has a short learning curve, allowing user with basic knowledge in robotics and CAD to create robot programs in just few minutes. In terms of accuracy, the error that may exist in the processes of OLP comes from inaccuracies in the robot/task calibration processes inherent to OLP and from situations where the CAD models do not reproduce properly the real robotic environment.

There are some aspects of the proposed CAD-based solution that can be improved in future. One aspect has to do with the algorithm to generate code; it has to be more generalist, flexible and easier to

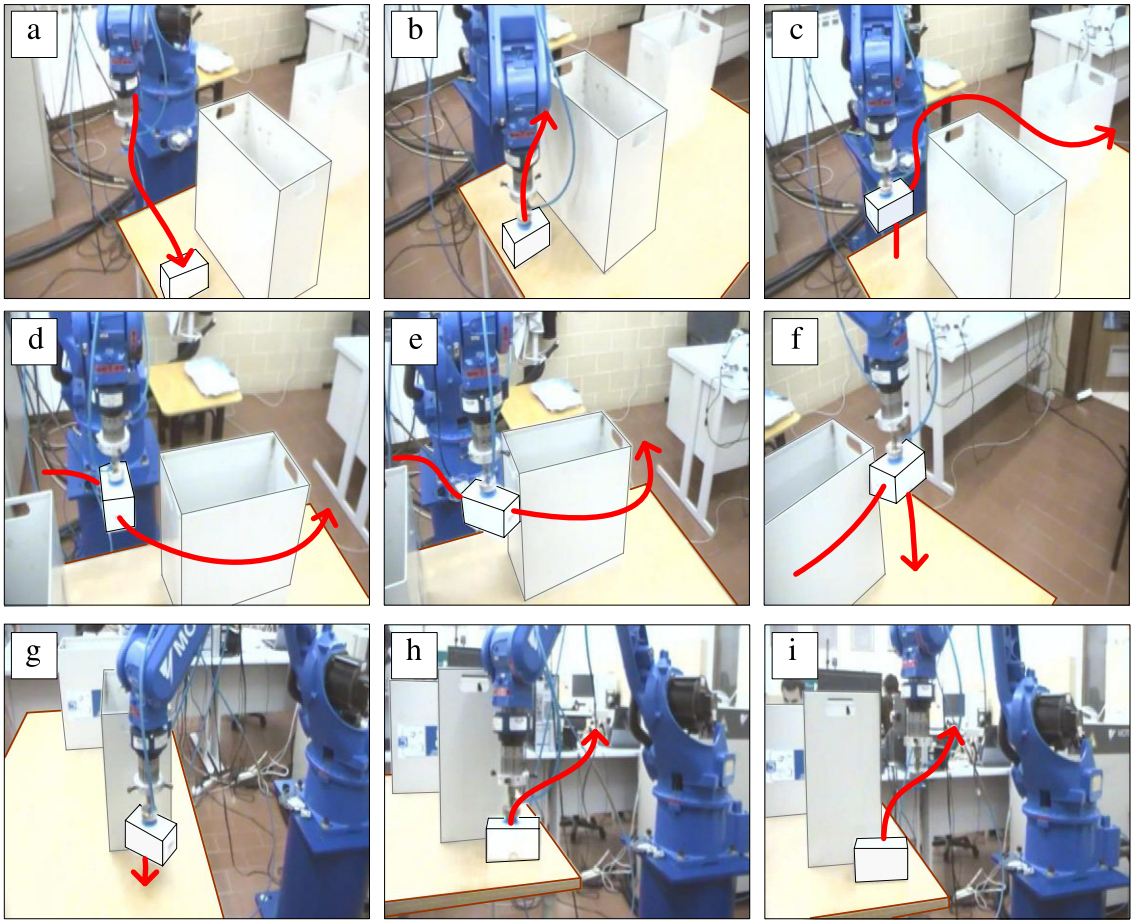

Fig. 25. Robot running the program generated from CAD.

tune. An idea for future work is to have a graphical- or icon-based interface to tune the algorithm to generate code in a more intuitive way and independently of the robot language. The other aspect has to do with the existing error in the process. External sensing (force sensing for example) can help to deal with this situation by increasing the accuracy of the processes, making it less susceptible to error and simpler.

References

[1] S. Forge, C. Blackman, A helping hand for Europe: the competitive outlook for the EU robotics industry, in: Publication Office of the European Union, 2010.
[2] L. Qi, D. Zhang, J. Zhang, J. Li, A lead-through robot programming approach using a 6-DOF wire-based motion tracking device, in: Proceedings of the 2009 IEEE International Conference on Robotics and Biomimetics, 2009, pp. 1773–1777.
[3] B. Hein, M. Hensel, H. Wörn, Intuitive and model-based on-line programming of industrial robots: a modular on-line programming environment, in: Proceedings of the 2008 IEEE International Conference on Robotics and Automation, 2008, pp. 3952–3957.
[4] B. Hein, H. Wörn, Intuitive and model-based on-line programming of industrial robots: new input devices, in: Proceedings of the 2009 IEEE International Conference on Intelligent Robots and Systems, 2009, pp. 3064–3069.
[5] V.S. Bottazzi, J.F.C. Fonseca, Off-line robot programming framework, in: Proceedings of the Joint International Conference on Automatic and Autonomous Systems and International Conference on Networking and Services, 2005, pp. 71–76.
[6] S. Mitsi, K.D. Bouzakis, G. Mansour, D. Sagris, G. Maliaris, Off-line programming of an industrial robot for manufacturing, The International Journal of Advanced Manufacturing Technology 26 (3) (2004) 262–267.
[7] X.F. Zha, H. Du, Generation and simulation of robot trajectories in a virtual CAD-based off-line programming environment, The International Journal of Advanced Manufacturing Technology 17 (8) (2001) 610–624.
[8] Z. Pan, J. Polden, N. Larkin, S.V. Duin, J. Norrish, Recent progress on programming methods for industrial robots, Robotics and Computer-Integrated Manufacturing 28 (2) (2012) 87–94.
[9] E. Freund, D. Rokossa, J. RoBmann, Process-oriented approach to an efficient off-line programming of industrial robots, in: Proceeding of the 24th Annual Conference of the IEEE Industrial Electronics Society, 1998, pp. 208–213.
[10] L. Beyer, J. Wulfsberg, Practical robot calibration with ROSY, Robotica 22 (5) (2004) 505–512.
[11] A. Nubiola, I.A. Bonev, Absolute calibration of an ABB IRB 1600 robot using laser tracker, Robotics and Computer-Integrated Manufacturing 29 (1) (2013) 236–245.
[12] J. Muelaner, Z. Wang, P. Maropoulos, Concepts for and analysis of a high accuracy and high capacity (HAHC) aerospace robot, Proceedings of the Institution of Mechanical Engineers, Part B: Journal of Engineering Manufacture 255 (8) (2011) 1393–1399.
[13] D.J. Kasik, W. Buxton, D.R. Ferguson, Ten CAD challenges, Computer Graphics and Applications 25 (2) (2005) 81–92.
[14] B. Bhanu, CAD-based robot vision, IEEE Computer 20 (8) (1987) 12–16.
[15] C.I. Lin, T.F. Lu, CAD-based intelligent robot workcell, in: Proceedings of the 3rd International Conference on Computer Integrated Manufacturing, 1995, pp. 437–444.
[16] P. Neto, N. Mendes, R. Araújo, J.N. Pires, A.P. Moreira, High-level robot programming based on CAD: dealing with unpredictable environments, Industrial Robot 39 (3) (2012) 294–303.
[17] M. Ferreira, A.P. Moreira, P. Neto, A low-cost laser scanning solution for flexible robotic cells: spray coating, The International Journal of Advanced Manufacturing Technology 58 (9) (2012) 1031–1041.
[18] P. Neto, J.N. Pires, A.P. Moreira, CAD-based off-line robot programming, in: Proceedings of the 4th IEEE International Conference on Robotics, Automation and Mechatronics, 2010, pp. 516–521.
[19] H. Chen, T. Fuhlbrigge, X. Li, A review of CAD-based robot path planning for spray painting, Industrial Robot 36 (1) (2009) 45–50.
[20] W. Sheng, N. Xi, M. Song, Y. Chen, P. MacNeille, Automated CAD-guided robot path planning for spray painting of compound surfaces, in: Proceedings of the IEEE/RSJ International Conference on Intelligent Robots and Systems, 2000, pp. 1918–1923.

[21] M.A.S Arikan, T. Balkan, Process modeling, simulation, and paint thickness measurement for robotic spray painting, Journal of Robotic Systems 17 (9) (2000) 479–494.
[22] H. Chen, W. Sheng, N. Xi, M. Song, Y. Chen, CAD-based automated robot trajectory planning for spray painting of free-form surfaces, Industrial Robot 29 (5) (2002) 426–433.
[23] J.Y. Kim, CAD-based automated robot programming in adhesive spray systems for shoe outsoles and uppers, Journal of Robotic Systems 21 (11) (2004) 625–634.
[24] T. Schaefer, D. Schraft, Incremental sheet metal forming by industrial robot, Rapid Prototyping Journal 11 (5) (2005) 278–286.
[25] T. Pulkkinen, T. Heikkilä, M. Sallinen, S. Kivikunnas, T. Salmi, 2D CAD based robot programming for processing metal profiles in short series manufacturing, in: International Conference on Control, Automation and Systems, 2008, pp.156–162.
[26] F. Nagata, T. Hase, Z. Haga, M. Omoto, K. Watanabe, CAD/CAM-based position/force controller for a mold polishing robot, Mechatronics 17 (4/5) (2007) 207–216.
[27] F. Nagata, S. Yoshitake, A. Otsuka, K. Watanabe, M.K. Habib, Development of CAM system based on industrial robotic servo controller without using robot language, Robotics and Computer-Integrated Manufacturing 29 (2) (2013) 454–462.
[28] F. Nagata, S. Yoshitake, A. Otsuka, K. Watanabe, M.K. Habib, CAM system without using robot language for an industrial robot RV1A, in: Proceedings of the 2012 IEEE International Symposium on Industrial Electronics, 2012, pp. 1529–1534.
[29] E. Cerit, I. Lazoglu, A CAM-based path generation method for rapid prototyping applications, The International Journal of Advanced Manufacturing Technology 56 (1/4) (2011) 319–327.
[30] L. Feng-yun, L. Tian-sheng, Development of a robot system for complex surfaces polishing based on CL data, The International Journal of Advanced Manufacturing Technology 26 (2005) 1132–1137.
[31] Y.H. Chen, Y.N. Hu, Implementation of a robot system for sculptured surface cutting – part 1 – rough machining, International Journal of Advanced Manufacturing Technology 15 (9) (1999) 624–629.
[32] Y.N. Hu, Y.H. Chen, Implementation of a robot system for sculptured surface cutting – part 2 – finish machining, International Journal of Advanced Manufacturing Technology 15 (9) (1999) 630–639.
[33] K. Murphy, R. Norcross, F. Proctor, CAD directed robotic deburring, in: 2nd International Symposium on Robotics and Manufacturing Research, Education, and Applications, 1988.
[34] M. Sallinen, M. Sirviö, Robotized system for prototype manufacturing of castings and billets, in: E. Arai, T. Arai (Eds.), Mechatronics for Safety, Security and Dependability in a New Era, Elsevier, Oxford, 2006, pp. 277–280.
[35] A. Murarka, B. Kuipers, Using CAD drawings for robot navigation, in: IEEE Systems, Man and Cybernetics Conference, 2001, pp. 678–683.
[36] Q.H. Wang, J.R. Li, B.L. Wu, X.M. Zhang, Live parametric design modifications in CAD-linked virtual environment, The International Journal of Advanced Manufacturing Technology 50 (9) (2010) 859–869.
[37] T.K. Yoo, W.H. Lee, Blend shape with quaternions, in: International Conference on Convergence Information Technology, 2007, pp. 776–780.
[38] N. Pollard, J.K. Hodgins, M.J. Riley, C. Atkeson, Adapting human motion for the control of a humanoid robot, in: IEEE International Conference on Robotics and Automation, 2002, pp. 1390–1397.
[39] N. Mendes, P. Neto, J.N. Pires, A. Loureiro, Discretization and fitting of nominal data for autonomous robots, Expert Systems with Applications 40 (4) (2013) 1143–1151.
[40] H.F. Wang, Y.L. Zhang, CAD/CAM integrated system in collaborative development environment, Robotics and Computer-Integrated Manufacturing 18 (2) (2002) 135–145.
[41] M. Liang, S. Ahamed, B. van den Berg, A STEP based tool path generation system for rough machining of planar surfaces, Computers in Industry 32 (2) (1996) 219–231.
[42] X.W. Xu, Q. He, Striving for a total integration of CAD, CAPP, CAM and CNC, Robotics and Computer-Integrated Manufacturing 20 (2) (2004) 101–109.
[43] X.W. Xu, Realization of STEP-NC enabled machining, Robotics and Computer-Integrated Manufacturing 22 (2) (2006) 144–153.
[44] Z. Liu, W. Bu, J. Tan, Motion navigation for arc welding robots based on feature mapping in a simulation environment, Robotics and Computer-Integrated Manufacturing 26 (2) (2010) 137–144.
[45] E. Freund, B. Luedemann-Ravit, A system to automate the generation of program variants for industrial robot applications, in: IEEE/RSJ International Conference on Intelligent Robots and System, 2002, pp. 1856–1861.
[46] H. Chen, W. Sheng, Transformative CAD based industrial robot program generation, Robotics and Computer-Integrated Manufacturing 27 (5) (2011) 942–948.
[47] E. Freund, B. Luedemann-Ravit, O. Stern, T. Koch, Creating the architecture of a translator framework for robot programming languages, in: IEEE International Conference on Robotics and Automation, 2001, pp. 187–192.
[48] Available: http://www2.dem.uc.pt/pedro.neto/Video_2012_1.wmv.
[49] Available: http://www2.dem.uc.pt/pedro.neto/Video_2012_2.wmv.

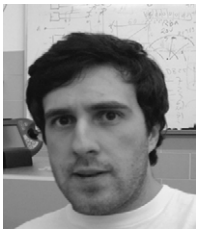

Pedro Neto was born in Coimbra, Portugal, on February 1, 1984. He received the Bachelor degree and Ph.D. degree in Mechanical Engineering from the University of Coimbra in 2007 and 2012, respectively. He has been involved in teaching activities since 2010 as Assistant Professor at the Department of Mechanical Engineering of the University of Coimbra. His research interests include: human–robot interaction, pattern recognition, CAD-based robotics and sensor fusion. Pedro Neto is author of several journal and conference publications. He participated in two European funded R&D projects, FP6 and FP7, and national projects.

Nuno Mendes is currently a Ph.D. student at the University of Coimbra. He received the Bachelor degree in Mechanical Engineering from the University of Coimbra in 2008. His research interests include: CAD-based robotics, sensor fusion, force control, Fuzzy and robotic friction stir welding. Nuno Mendes is author of several journal and conference publications.

A.2. APPENDIX A2

Expert Systems with Applications 40 (2013) 1143–1151

Contents lists available at SciVerse ScienceDirect

Expert Systems with Applications

journal homepage: www.elsevier.com/locate/eswa

Discretization and fitting of nominal data for autonomous robots

Nuno Mendes, Pedro Neto *, J. Norberto Pires, Altino Loureiro

Department of Mechanical Engineering (CEMUC)-POLO II, University of Coimbra, 3030-788 Coimbra, Portugal

ARTICLE INFO

Keywords:
Autonomous robots
Fuzzy logic
PI control
Discretization
Off-line programming
Robotics

ABSTRACT

This paper presents methodologies to discretize nominal robot paths extracted from 3-D CAD drawings. Behind robot path discretization is the ability to have a robot adjusting the traversed paths so that the contact between robot tool and work-piece is properly maintained. In addition, a hybrid force/motion control system based on Fuzzy-PI control is proposed to adjust robot paths with external sensory feedback. All these capabilities allow to facilitate the robot programming process and to increase the robot's autonomy.

1. Introduction and motivation

The process of robot off-line programming (OLP) has become increasingly popular in recent time, mainly inside Small and Medium-Sized Enterprises (SMEs). To this effect has contributed the required knowledge in robot programming which has been replaced by high widespread knowledge within enterprises. One way to use OLP is recurring to CAD drawings of the robotic cell in study (Chen & Sheng, 2011; Kim, 2004; Liu, Bu, & Tan, 2010; Vosniakos & Chronopoulos, 2008). When CAD drawings are used to program a robot, the programming task can become easier, more intuitive and less monotonous. In addition, the knowledge required is high disseminated within enterprises structure because SMEs generally use CAD packages to design and develop their products. Moreover, while a robot is in the production phase the following working setup can be prepared off-line, thereby the setup time is reduced and the management of workers becomes easier.

A series of studies have been conducted using CAD as interface between robots and operators, for example, a review on CAD-based robot path planning for spray painting is presented by Chen, Fuhlbrigge, and Li (2009). Nagata, Kusumoto, Fujimoto, and Watanabe (2007) propose a robotic sanding platform where the robot paths are generated by CAD/CAM software. An example of a novel process that benefits from the robots and CAD versatility is the so-called incremental forming process of metal sheets (Schaefer & Schraft, 2005). The robot paths are achieved from a CAD model on the basis of specific material models. Prototype panels or customized car panels can be economically produced using this method. Feng-yun and Tian-sheng (2005) present a robot path generator for the polishing process, where cutter location data are generated from the postprocessor of a CAD system. A CAD-based robot programming system where is referred the use of a sequence of virtual robot tool models to define the robot paths is presented by Neto, Mendes, Araújo, Pires, and Moreira (2012). Nevertheless, the CAD-based robot programming systems have found some adversities. The major of them is calibration, i.e., the differences in alignment between the real environment and the virtual environment (CAD). These differences always exist and are almost impossible to determine because their origin is unpredictable. In order to deal with the uncertainty and inaccuracy of the robot working environment, the introduction of sensory-feedback in robotic systems has been studied and implemented (Mendes, Neto, Pires, & Moreira, 2010; Neto, Mendes, Pires, & Moreira, 2010). However, many of the robots are not able to easily incorporate sensory-feedback and some special care needs to be taken to ensure proper running of the system. One of the possible approaches is to discretize the path in small paths (Nagata, Kusumoto, et al., 2007). After that, some appropriate adjustments should be done on these small paths while the robot is performing them (Pires, Afonso, & Estrela, 2007). Several studies about robot path discretization have been proposed, such as Nagata, Hase, Haga, Omoto, and Watanabe (2007), which presents a CAD/CAM-based position/force controller. This study addresses a calculation method of robot orientation from cutter location data. Some algorithms for robot path discretization have been proposed to smooth robot paths (position and orientation) (Feng-yun & Tian-sheng, 2005; Neto, Mendes, et al., 2012). Nielson (2004) proposes an algorithm for nonlinear smoothly interpolating orientation, which showed excellent results when used in Spline curves. Sheng, Xi, Song, and Chen (2001) present a method for robot path planning where nominal data are extracted from a CAD surface. A methodology for robot path planning from 3-D CAD models by means of the linear and circular discretization is presented by Berger and May (2005). Kuffner (2004) addresses some implementation issues and techniques in rigid body path planning using the

* Corresponding author. Tel.: +351 239 790 700; fax: +351 239 790 701.
E-mail addresses: nuno.mendes@dem.uc.pt (N. Mendes), pedro.neto@dem.uc.pt (P. Neto).

0957-4174/$ - see front matter © 2012 Elsevier Ltd. All rights reserved.
http://dx.doi.org/10.1016/j.eswa.2012.08.023

Lei group SE(3). Nagata (2005) presents a completely local algorithm for surface discretization. The main idea is the discretization of a curve segment supporting itself on the position and normal vectors at endpoints.

This paper aims to promote the OLP of industrial robots, in which nominal data (obtained for example from CAD drawings) are adapted to robot motion for industrial processes such as Friction Stir Welding (FSW) (Cook, Crawford, Clark, & Strauss, 2004; Fleming, Hendricks, Wilkes, Cook, & Strauss, 2009; Soron & Kalaykov, 2006). The idea is to provide to users, with basic skills in CAD and robot programming, the tools to off-line generate reliable robot programs. However, as there are usually discrepancies between the virtual and real environment, the robot should be able to ensure recognition of their work environment and make appropriate adjustments (on-line) in the pre-programmed paths. In this way, we propose the use of sensory-feedback through the implementation of a hybrid force/motion control system. The function of this control system is to keep the contact between robot tool and work-piece. Nevertheless, even though not all commercial robots are ready to incorporate sensory-feedback in an easy way, most are prepared to make adjustments in the pre-programmed path, when the robot programs are being executed. Having this capability in mind, we propose the discretization of the nominal robot path in small sections and then make the adjustments that are desirable in these small sections (path adjustment). In this paper, some techniques of path discretization are presented, namely: linear paths, circular paths and curvilinear paths (Nagata patch). In addition, an interpolation technique is presented to interpolate end-effector orientation (Slerp). In order to perform the adjustments in the pre-programmed paths, a hybrid force/motion control system is presented, with special attention to the force control loop which is developed using Fuzzy reasoning and traditional Proportional Integrative control (PI).

The paper is further organized as followed. The second section focuses on the extraction of information from CAD. The third section presents some path discretization methods. The fourth section presents the hybrid force/motion control system used to produce adjustments in the pre-programmed path. The methods presented in the previews sections are evaluated through an experiment that is presented in section fifth. Finally, in the sixth section, conclusions are dawn and future work highlighted.

2. Acquisition and processing of nominal data from CAD

2.1. Case study

For this study, which is performed in the Cartesian space, nominal data are directly extracted from a commercial CAD package, Autodesk Inventor. Each CAD model consists in a robotic cell, points (representing robot paths also known as robot end-effector positions) and poses (representing orientations of the robot tool also known as robot end-effector orientations) (Fig. 1). The data extracted from a CAD model are transformation matrices, consisting in rotation matrices and coordinates of points, both in relation to the origin of the CAD model of the cell. The information needed to program the robot will be extracted from the CAD environment by using an application programming interface (API) provided by Autodesk. This API allows the data transfer between the Autodesk Inventor and a Software Interface (which is the application that manages the entire process). Later, the information extracted from CAD is converted into robot code. A diagram with the procedure to extract nominal data from a CAD model and their conversion into a robot program is presented in Fig. 2.

In order to extract information from a CAD model, all the components belonging to the model (robot, work-pieces, conveyors, etc.) must be drawn and assembled like in the real cell in their real

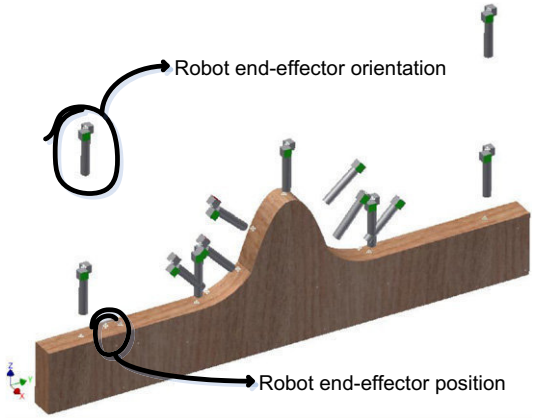

Fig. 1. A CAD model.

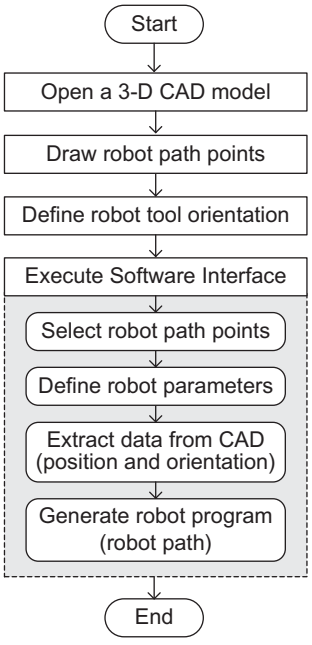

Fig. 2. Procedure to extract nominal data and generate robot programs from CAD.

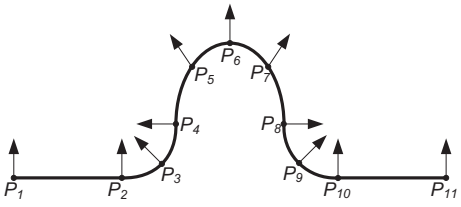

Fig. 3. Schematic representation of a 3D CAD path to extract nominal data.

dimensions and shapes. Furthermore, the points must define the beginning and the end of the robot path. Nevertheless, it is the user that defines the type of path (linear, circular or curvilinear). Fig. 3 represents schematically a robot path. The arrows represent the robot tool orientation in each discretized position and the *P*s represent robot positions.

2.2. Transformation between coordinate systems

In order to establish a match between the real environment and the virtual environment (CAD environment) some geometric

references have to be provided. In other words, it is necessary to have all robot end-effector positions and orientations with respect to one or more reference frames (local coordinate systems) known a priori by the robot. These frames are made known to the robot through a calibration process. Generally, this is a simple and non-time consuming process where the user needs to define the frame(s) within the CAD environment by selecting three positions within the CAD drawing. Then, the user has to teach the real robot about that frame(s)' pose in the real scenario (off-line to on-line mapping). These three positions, which define a reference frame, have to follow some rules:

- The first position should be the origin of the frame.
- The second position should be a position in the frame x-axis and non-coincident with the frame origin.
- The third position should be a position in the frame positive xOy quadrant and non-coincident with the x-axis of the frame.

Aiming to convert a positional vector expressed in the coordinate system $\{L\}$ into a positional vector expressed in the coordinate system $\{M\}$, the transformation matrix from $\{L\}$ into $\{M\}$, ${}^{M}_{L}\mathbf{T}$, must be calculated. Being A, B and C the first, second and third positions, respectively, defined in the three-dimensional space through coordinate system $\{L\}$ and defining the vectors $\overrightarrow{\mathbf{AB}}$ and $\overrightarrow{\mathbf{AC}}$ from these positions as shown in Fig. 4. We can calculate ${}^{L}_{M}\mathbf{T}$ following the procedure below:

1. Calculate the vectors $\overrightarrow{\mathbf{AB}}$ and $\overrightarrow{\mathbf{AC}}$.
2. Calculate $\vec{\mathbf{E}} = \overrightarrow{\mathbf{AB}} \times \overrightarrow{\mathbf{AC}}$.
3. Calculate $\vec{\mathbf{F}} = \vec{\mathbf{E}} \times \overrightarrow{\mathbf{AB}}$.
4. Normalize the vectors $\overrightarrow{\mathbf{AB}}$, $\vec{\mathbf{E}}$ and $\vec{\mathbf{F}}$.

Being $\overrightarrow{\mathbf{ab}}$, $\vec{\mathbf{e}}$ and $\vec{\mathbf{f}}$ the normalized vectors of $\overrightarrow{\mathbf{AB}}$, $\vec{\mathbf{E}}$ and $\vec{\mathbf{F}}$, respectively, the rotation matrix from $\{L\}$ into $\{M\}$ is defined as ${}^{L}_{M}\mathbf{R} = \left[\overrightarrow{\mathbf{ab}} \quad \vec{\mathbf{f}} \quad \vec{\mathbf{e}}\right]$. The transformation matrix can be represented by:

$$ {}^{L}_{M}\mathbf{T} = \begin{bmatrix} \overrightarrow{\mathbf{ab}} & \vec{\mathbf{f}} & \vec{\mathbf{e}} & A \\ 0 & 0 & 0 & 1 \end{bmatrix} \tag{1} $$

As our goal is to transform coordinate vectors expressed in coordinate system $\{L\}$ into the new defined coordinate system $\{M\}$, the transformation matrix appears:

$$ {}^{M}_{L}\mathbf{T} = \begin{bmatrix} {}^{L}_{M}\mathbf{R}^{T} & -{}^{L}_{M}\mathbf{R}^{T} \cdot A \\ 0 & 1 \end{bmatrix} \tag{2} $$

To transform a robot position P expressed in a coordinate system $\{L\}$ into a coordinate system $\{M\}$ we have:

$$ \overrightarrow{{}^{M}\mathbf{P}} = {}^{M}_{L}\mathbf{T} \cdot \overrightarrow{{}^{L}\mathbf{P}} \tag{3} $$

3. Information processing and path discretization

When we want to discretize a robot path, two important factors should be taken in consideration: the type of movement and the orientation assumed by the robot when it performs such movement. In this study, it is assumed that the variation of orientation is proportional to the variation of position. However, this assumption cannot be true if the robot path is a curve with non-constant curvature (irregular arc segment). Such situation can lead to the existence of some small errors.

The paths analyzed in this work were linear, circular and curvilinear with one concavity, which are the most used in common robotic applications. A method of orientation discretization is also presented.

3.1. Linear discretization

If the path to be followed by the robot end-effector is a linear path, the discretization method should be as follows. Considering two robot end-effector positions P_A and P_B, if we want to move from P_A to P_B by a linear movement, as shown in Fig. 5, the first thing we need to do is to define how long the distance between the discretized positions, k, should be. Consequently, the number of intermediate positions, n, should be calculated by:

$$ n = \frac{\left\|\overrightarrow{P_A P_B}\right\|}{k} \tag{4} $$

Now, the intermediate positions, P_j, can be calculated:

$$ \begin{aligned} &P_j = P_{j-1} + k \cdot \overrightarrow{p_A p_B}, \quad j \in \aleph \wedge j \subset [1, n-1] \\ &P_0 = P_A \\ &P_n = P_B \end{aligned} \tag{5} $$

where $\overrightarrow{p_A p_B}$ is the normalized vector of $\left\|\overrightarrow{P_A P_B}\right\|$.

Linear discretization demonstrated to be a good method to apply in any situation of linear path (Cartesian space) because it is computational efficient (in terms of computation time) and it is an exact method (it does not present any residual error). Furthermore, it is simple and easy to implement because only a few calculations are involved. In this way, linear discretization is suitable to be incorporated into the robot programming code. Nevertheless, there is a curiosity that concerns to the "last movement". This one can be smaller than the other movements, Fig. 5. This phenomenon occurs because we define the distance between positions, called k, and not the number of discretized positions, n. However, this is not a problem, it is a difference between movements' length, which does not put the task in risk.

3.2. Circular discretization

In order to have a versatile circular discretization method, three positions belonging to the nominal path should be provided (P_1, P_2 and P_3). The first one should be the starting position, the second

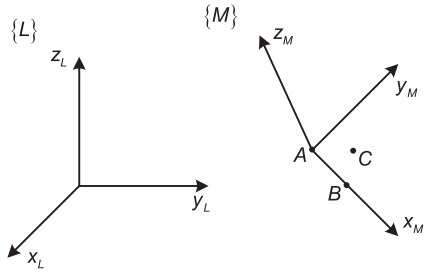

Fig. 4. Defining a frame.

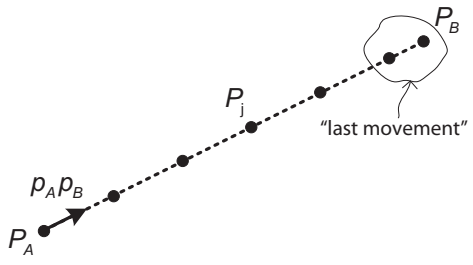

Fig. 5. Representation of the linear discretization method.

one should be an intermediate position and finally the third position should be the finishing position, as represented in Fig. 6. Through these positions the centre of the arc $P_0 = (x_0, y_0, z_0)$ and the radius r can be calculated by:

$$\begin{cases} (x_1 - x_0)^2 + (y_1 - y_0)^2 + (z_1 - z_0)^2 = r^2 \\ (x_2 - x_0)^2 + (y_2 - y_0)^2 + (z_2 - z_0)^2 = r^2 \\ (x_3 - x_0)^2 + (y_3 - y_0)^2 + (z_3 - z_0)^2 = r^2 \\ \begin{vmatrix} x_1 - x_0 & y_1 - y_0 & z_1 - z_0 \\ x_2 - x_0 & y_2 - y_0 & z_2 - z_0 \\ x_3 - x_0 & y_3 - y_0 & z_3 - z_0 \end{vmatrix} = 0 \end{cases} \tag{6}$$

The generation of the discretized positions using circular discretization is processed between P_1 and P_3. In the first step, a local coordinate system is defined, in which its origin is P_0 and the direction along the x-axis is the same direction as $\overrightarrow{P_0P_1}$. The direction of the y-axis is defined by P_2, which is located in the first quadrant of the xOy plane as shown in Section 2.2. In the second step it is computed the angle θ formed between $\overrightarrow{P_0P_1}$ and $\overrightarrow{P_0P_3}$, (7), θ_{inc}, (8) (where l_0 is the increment of distance travelled in the arc) and the number of generated positions n, (9).

$$\theta = \cos^{-1}\left(\frac{\overrightarrow{P_0P_1} \cdot \overrightarrow{P_0P_3}}{\left\|\overrightarrow{P_0P_1}\right\| \cdot \left\|\overrightarrow{P_0P_3}\right\|}\right) \tag{7}$$

$$\theta_{inc} = \frac{l_0}{r} \tag{8}$$

$$n = \frac{\theta}{\theta_{inc}} \tag{9}$$

In the third step the discretized positions are generated by:

$$\begin{cases} x_i = r \cdot \cos(\theta_{inc} \cdot i) \\ y_i = r \cdot \sin(\theta_{inc} \cdot i)\ ,\ i \in \aleph \wedge i \subset [0, n] \\ z_i = 0 \end{cases} \tag{10}$$

In the fourth and last step, the generated positions are transformed from the local coordinate system to the global coordinate system as presented in Section 2.2.

This circular discretization method presents a very similar behaviour to the method presented in Section 3.1. Once again, it is an exact method and thus there is no theoretical error. Furthermore, the "last movement" is smaller in some situations for the same reasons that were pointed out in the previous method. However, the task is not put in jeopardy. Fig. 6 presents the discretized positions through the circular discretization method.

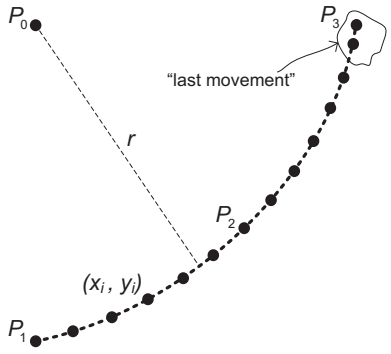

Fig. 6. Nominal data for circular discretization.

3.3. Curvilinear discretization (Nagata patch)

In order to obtain an efficient computational method for curvilinear discretization we decided to use a numerical method which was recently proposed by Nagata (2005) and has already been applied successfully to diverse engineering problems (Boschiroli, Fünfzig, Romani, & Albrecht, 2011; Neto, Oliveira, Alves, & Menezes, 2010; Neto, Oliveira, Menezes, & Alves, 2012; Sekine & Obikawa, 2010). The main idea behind this parametric surface description (subsequently named Nagata patch) is the quadratic discretization of a curved segment from the position and normal vectors at the end points. The method here presented was initially developed for high-precision milling (Lin, Watanabe, Morita, Uehara, & Ohmori, 2007). However, this study aims to show that Nagata patch can be applied to robot path definition.

This method starts with the calculation of the rotation centre P_0, (6). For this purpose, three positions belonging to the curve have to be provided (P_1, P_2, P_3), Fig. 7. After that, the discretization is processed, in a first phase among the positions P_0, P_1 and P_2. In a second phase the second part of curve is discretized among the positions P_0, P_2 and P_3. Owing to the repetition of the method, in this document is only presented in detail the first phase of discretization. Fig. 8 shows the centre of curvature, P_0, the initial position, P_1 and the final position, P_2. The directional vectors $\vec{\mathbf{n}}_1$ and $\vec{\mathbf{n}}_2$ are then calculated (11) and (12), as well as the shortest vector connecting P_1 to P_2, $\vec{\mathbf{d}}$ (13).

$$\vec{\mathbf{n}}_1 = \frac{P_1 - P_0}{\|P_1 - P_0\|} \tag{11}$$

$$\vec{\mathbf{n}}_2 = \frac{P_2 - P_0}{\|P_2 - P_0\|} \tag{12}$$

$$\vec{\mathbf{d}} = P_2 - P_1 \tag{13}$$

Before applying the curvilinear discretization method using Nagata patch (16), $\vec{\mathbf{c}}$ (15) and a (14) have to be calculated. The angle among the centre of curvature and the initial and final positions, α, is limited to a value lower than 180°, Fig. 8.

$$a = \vec{\mathbf{n}}_1 \cdot \vec{\mathbf{n}}_2 = \cos(\alpha) \tag{14}$$

$$\vec{\mathbf{c}} = \begin{cases} \frac{1}{1-a^2} \cdot \begin{bmatrix} \vec{\mathbf{n}}_1 & \vec{\mathbf{n}}_2 \end{bmatrix} \cdot \begin{bmatrix} 1 & -a \\ -a & 1 \end{bmatrix} \cdot \begin{Bmatrix} \vec{\mathbf{n}}_1^T \cdot \vec{\mathbf{d}} \\ -\vec{\mathbf{n}}_2^T \cdot \vec{\mathbf{d}} \end{Bmatrix}, & a \neq \pm 1 \\ \vec{\mathbf{0}}, & a = \pm 1 \end{cases} \tag{15}$$

$$P(\eta) = P_0 + (\vec{\mathbf{d}} - \vec{\mathbf{c}}) \cdot \eta + \vec{\mathbf{c}} \cdot \eta^2, \quad \eta \in \Re \wedge \eta \subset [0, 1] \tag{16}$$

In order to estimate the parameter η we have to determine the number of movements (position increments), n, by calculating the total curve length to be travelled. To this end, we do an approximation of the curve to a perfect arc (17)–(20).

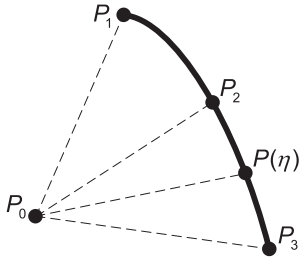

Fig. 7. Nominal data for Nagata patch.

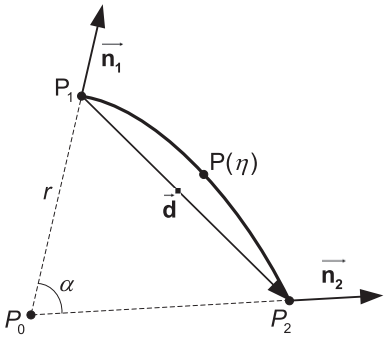

Fig. 8. Representation of the Nagata patch.

$$\alpha = \cos^{-1}(a) \tag{17}$$

$$\alpha_0 = \frac{l_0}{r} \tag{18}$$

$$n = \frac{\alpha}{\alpha_0} \tag{19}$$

$$\eta_i = \frac{1}{n} \tag{20}$$

where α is the total curve angle to be travelled, α_0 is the curve angle to be travelled in each increment, l_0 is the curve length to be travelled in each increment and η_i is the increment of the η in each increment.

The Nagata patch proved to be a very good method for representing curves with a concavity. To illustrate the power of the Nagata method, it was used to represent two well-defined curves, a parabolic curve and an arc, using only three positions for each one. The results can be seen in Figs. 9 and 10, and Tables 1 and 2. Since both curves are symmetric, in the tables are only shown the results for the first halves of the curves. The analysis allowed concluding that there are small differences in the generated positions and the well-defined curves. In order to generalize these differences, they are presented in Tables 1 and 2 as a function of the radius of the curvature because of the influence of this parameter in the magnitude of the differences. Another parameter that influences the difference between the curves is the rotated angle α, i.e., higher angles (larger distances between positions) lead to major differences. The maximum difference occurs in the half angle of the total angle, i.e., for an angle of 90°, the maximum error occurs at an angle of 45°. Although the formulation presented above is only defined for a specific kind of curvature orientation, it is

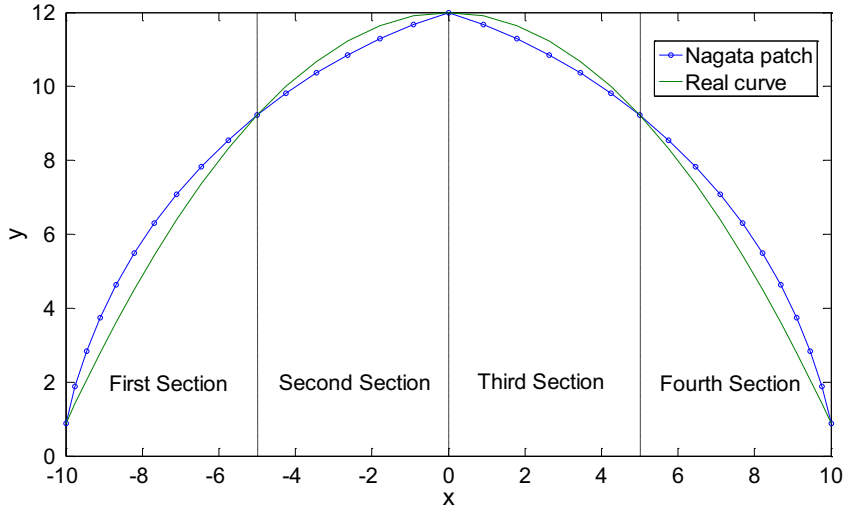

Fig. 9. Error presented in a circular path generated by Nagata patch.

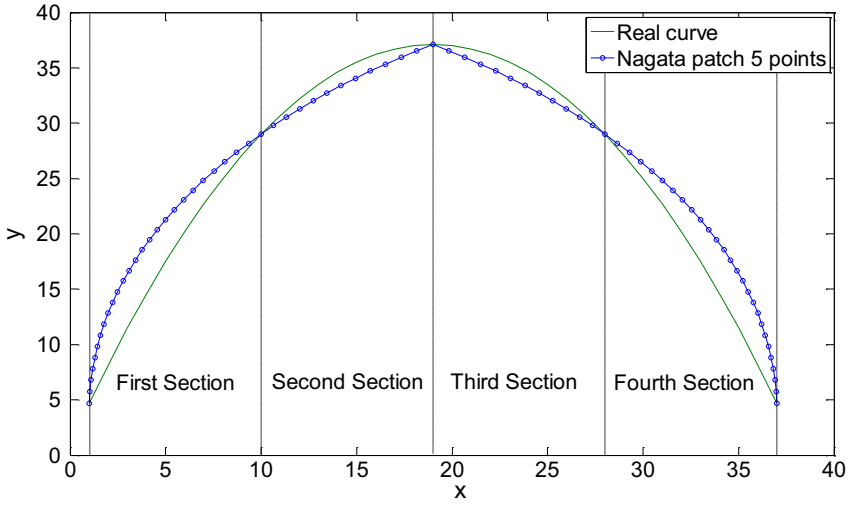

Fig. 10. Error presented in a curvilinear path generated by Nagata patch.

Table 1
Error present in a Nagata patch test.

	First section ($\alpha \approx 33^o$)									
% Path per section	0	10.3	20.5	30.7	40.7	50.7	60.7	70.6	80.4	90.2	100
Error/radius (%)	0	−3	−5.1	−6.4	−6.8	−6.6	−5.8	−4.6	−3.1	−1.5	0
	Second section ($\alpha \approx 21^o$)										
% Path per section	0	−3.4	−6.6	−9.8	−12.8	−15.8	100				
Error/radius (%)	0	1.2	2.1	2.5	2.4	1.6	0				

Table 2
Error presented in a parabolic path generated by Nagata patch.

	First section									
% Path per section	0.0	11.5	23.1	38.5	42.3	46.2	61.5	69.2	76.9	88.5	100
Error/radius (%)	0.0	−6.1	−10.2	−12.4	−12.5	−12.4	−10.4	−8.6	−6.6	−3.2	0.0
	Second section										
% Path per section	0.0	8.3	16.7	25.0	33.3	50.0	58.3	66.6	83.3	91.7	100
Error/radius (%)	0.0	0.9	1.7	2.4	2.9	3.5	3.5	3.3	2.2	1.2	0.0

possible to increase or decrease the curvature of the curve by defining the vectors $\vec{\mathbf{n}}_1$ and $\vec{\mathbf{n}}_2$ in a different way.

The major advantages of the Nagata patch are:

- Computationally efficient.
- It works over a local coordinate system.
- The method uses only a variable and this one is dimensionless.
- It is compact, fast and easy to implement.

The errors obtained in a path discretization through this method are acceptable when used in robotic tasks that do not require very strict accuracy, for example in FSW. In spite of the good results presented by this method in the representation of curves with a concavity, Nagata patch should not only be seen as a method of representation of paths which were previously generated by other methods. The Nagata patch is a different method for path generation and it should be faced as well, an advanced method that enables the generation of a given type of path.

3.4. Orientation interpolation (Slerp)

A quaternion interpolation algorithm (spherical linear interpolation – Slerp) to interpolate smoothly a sequence of end-effector orientations is here presented (Fig. 11). Given two known unit quaternion, Q_0 and Q_n, with parameter k moving from 1 to $n-1$, the interpolated end-effector orientation Q_k can be computed:

$$Q_k = \frac{\sin\left(\left(1-\frac{k-1}{n-1}\right)\cdot\theta\right)}{\sin\theta}\cdot Q_0 + \frac{\sin\left(\frac{k-1}{n-1}\cdot\theta\right)}{\sin}\theta\cdot Q_n, \quad k\in\aleph\wedge k\subset[1\ n-1] \tag{21}$$

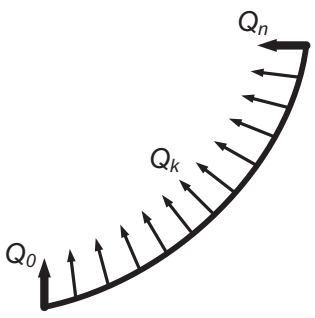

Fig. 11. Orientation interpolation.

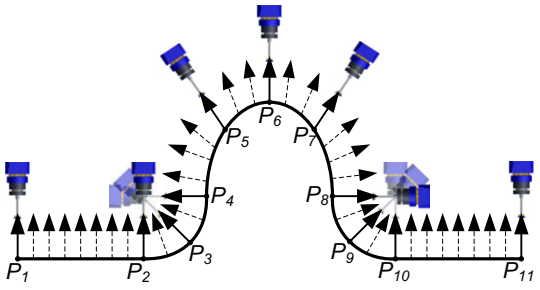

Fig. 12. Orientation interpolation of robot paths.

where:

$$\theta = \cos^{-1}(Q_0\cdot Q_n) \tag{22}$$

The method used to interpolate the orientation is very efficient and reliable for this kind of robotic application. If we have two robot positions which belonging to an arc and the orientation of these positions is perfectly perpendicular to the arc, the orientation of these discretized positions will be perfectly perpendicular to that arc. This means that the orientation increment is linear. Nevertheless, when this method is used for curved paths the change of orientation along the path should not be linear, in some cases, because the curvature can be more accentuated in the beginning or in the ending of the path. In order to solve this issue another methods should be studied in the future as the v-Spline orientation method (Nielson, 2004). In Fig. 12 is presented some orientation interpolation of robot end-effector path positions for different kinds of robot paths.

4. Hybrid force/motion control system

Since there may be small differences between pre-programmed robot paths, through off-line programming, and real environments, we propose the use of a hybrid force/motion control system to attenuate or even avoid the influence of these differences. This strategy is based on sensory-feedback in which a force/torque sensor feeds the controller. The controller consists in an external force control loop which in turn feeds an internal position control loop as in Fig. 13. The external control loop receives force and torque data about the contact between robot and its environment and sends robot displacement data (adjustments) to the internal control loop, as can be seen in Fig. 14. The Fuzzy reasoning and the

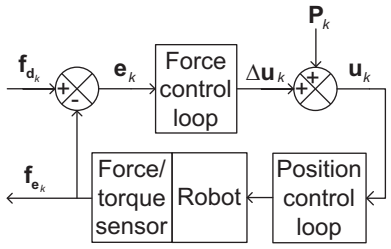

Fig. 13. Hybrid force/motion control system.

Proportional Integrative Control (PI) were used to obtain a powerful and simple control framework.

The characteristics of this controller should be simplicity, flexibility and fast to compute. A null steady state error is pretended to be achieved and in this way a PI-type control was chosen. The association of the two powerful mathematical tools, Fuzzy logic and PI control, allow to use the intuitive knowledge from users and the good performance of the PI control already so well known. Thus, a Fuzzy logic controller type Mamdani (Bingül & Karahan, 2011; Mamdani, 1974) based on the traditional PI controller was implemented. This kind of controller is easy to implement, since it does not need a precise mathematical model of the system. The controller is implemented only using linguistic variables to model the intuitive knowledge of the operator. The implementation of the Fuzzy controller should respect the following order:

- Definition of input and output variables.
- Fuzzification.
- Definition of a group of rules to model the application in study (knowledge base).
- Design of the computational unit that accesses the Fuzzy rules.
- Defuzzification.

The force control loop collects inputs from the force/torque sensor and processes these inputs according to the rules specified in the Fuzzy logic memberships (Section 4.2). The outputs $\Delta\mathbf{u}$ are presented as displacement of the end-effector at which the robotic arm should be moved to obtain the desired contact range of forces and torques.

4.1. Fuzzy-PI controller

In our system, the controller input variables are the force/torque error **e** and change of the error **de**:

$$\mathbf{e}_k = \mathbf{f}_{\mathbf{d}_k} - \mathbf{f}_{\mathbf{e}_k} \tag{23}$$

$$\mathbf{de}_k = \mathbf{e}_k - \mathbf{e}_{k-1} \tag{24}$$

where $\mathbf{f_e}$ is the actual wrench and $\mathbf{f_d}$ is the desired wrench (setpoint). The controller output is the position accommodation for the robot (established in terms of robot displacements).

From the discrete version of traditional PI controller:

$$\mathbf{u}_k = \mathbf{u}_{k-1} + \Delta\mathbf{u}_k \tag{25}$$

$$\Delta\mathbf{u}_k = \mathbf{K_P}\mathbf{de}_k + \mathbf{K_I}\mathbf{e}_k \tag{26}$$

where **u** is the robot displacement; and $\mathbf{K_P}$ and $\mathbf{K_I}$ are coefficient constants. If **e** and *de* are Fuzzy variables, (8) and (9) become a Fuzzy control algorithm. A practical implementation of the proposed Fuzzy-PI concept is simplified in Fig. 14. Finally, the centre of area method was selected for defuzzify the output Fuzzy set inferred by the controller:

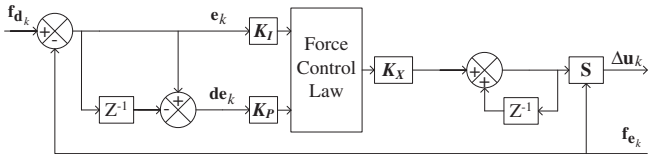

Fig. 14. External force control loop.

$$\Delta U = \frac{\sum_{i=1}^{n} \mu_i \cdot \Delta U_i}{\sum_{i=1}^{n} \mu_i} \tag{26}$$

where μ_i is the membership function, which takes values in the interval [0, 1].

A decision maker $\mathbf{S} \in \Re^{n\times n}$ establishes the axis direction we want to control with force/motion control action. When all the axes are controlled with force and motion actions, the **S** matrix becomes the identity matrix.

4.2. Knowledge base

The knowledge base of a Fuzzy logic controller is composed of two components, namely, a database and a Fuzzy control rule base. Each control variable should be normalized into seven linguistic labels {PL, PM, PS, ZR, NS, NM, NL}. The grade of each label is described by a Fuzzy set. The function that relates the grade and the variable is called the membership function (Fig. 15). The well-known PI-like Fuzzy rule base suggested by MacVicar-Whelan (1977) is used in this paper (Table 3). It allows fast working convergence without significant oscillations and prevents overshoots and undershoots.

4.3. Tuning strategy

Fuzzy logic design is involved with two important stages: knowledge base design and tuning. However, at present there is no systematic procedure to do the tuning. The control rules are normally extracted from practical experience, which may make the result focused in a specific application. The objective of tuning is to select the proper combination of all control parameters so that the resulting closed-loop response best meets the desired design criteria.

In order to adapt the system to different contact conditions, the scaling factors should be tuned. The controller should be adjusted with characteristics representing the working environment to be controlled. These adjustments can be made through the scaling factors, usually applied in any PI controller, namely K_P, K_I and K_X. Lin and Huang (1998) proposes an adjustment where the scaling factors are dynamic and thus they have been adjusted along the task. Similar strategies are proposed in references (Chen, Tung, Tsai, & Fan, 2009; Mudi & Pal, 2000; Yu, 2009). The utilization of different tables of rules accordingly the task to be performed and the materials involved are presented by Pires, Godinho, and Araújo

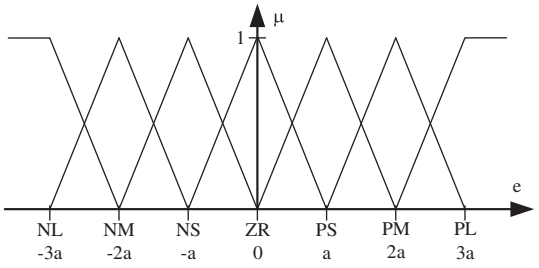

Fig. 15. Membership functions for the input variables.

Table 3
Representation of the rule base.

de	e						
	NL	NM	NS	ZR	PS	PM	PL
PL	nl	nm	ns	zr	pm	pl	pl
PM	nl	nl	nm	zr	pm	pl	pl
PS	nl	nl	ns	zr	ps	pl	pl
ZR	nl	nm	ns	zr	ps	pm	pl
NS	nl	nl	ns	zr	ps	pl	pl
NM	nl	nl	nm	zr	pm	pl	pl
NL	nl	nl	nm	zr	ps	pm	pl

(2004). Dynamic membership functions are proposed by Woo, Chung, and Lin (2000). In this study, the scaling factors are set to appropriate constant values, achieved by the method of trial and error.

5. Experiments

The effectiveness of the proposed approach was evaluated in an experiment, which was repeated 20 times. In this experiment, the robot end-effector should follow a specific robot path keeping the contact between robot end-effector and surface and avoiding excessive contact forces. The robot path was pre-programmed by a CAD drawing, Fig. 1, as presented in Section 2 as well as intended calibrations were done. The real path followed by the robot end-effector is presented in Fig. 16. Note that the surface is highly irregular, which makes this experiment very challenging for any control system. In order to verify the efficiency of the proposed control system two tests of the experiment were checked. In a first test the hybrid control system was implemented to control the normal force to the contact surface. In a second test the robot end-effector execute the pre-programmed path without force control loop, i.e., the robot end-effector path is not adjusted. In both tests the normal force to the contact surface was registered and compared.

Figs. 17 and 18 show the results for the two tests of the experiment, all experimental results presented similar behaviours to these ones. By the analysis of Fig. 17, without make adjustments in the pre-programmed path, we can conclude that the contact between the robot tool and surface is lost several times. Furthermore, the contact force reaches high values as can be seen in the same figure. The experiment failed (excessive contact force) when the discrete time reached the value 323, in which there was the need to stop the experience due to the high contact force values. After that, the experiment only could be restarted for the discrete time 344 (where the safety conditions were satisfied). Notice that even at the point where the experiment was restarted the value of the contact force is very high. The discrete time is directly associated with the positions that compose the robot end-effector path.

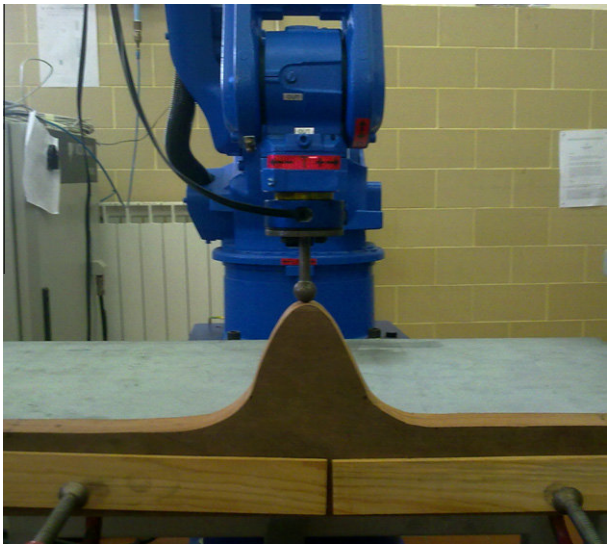

Fig. 16. Experiment layout.

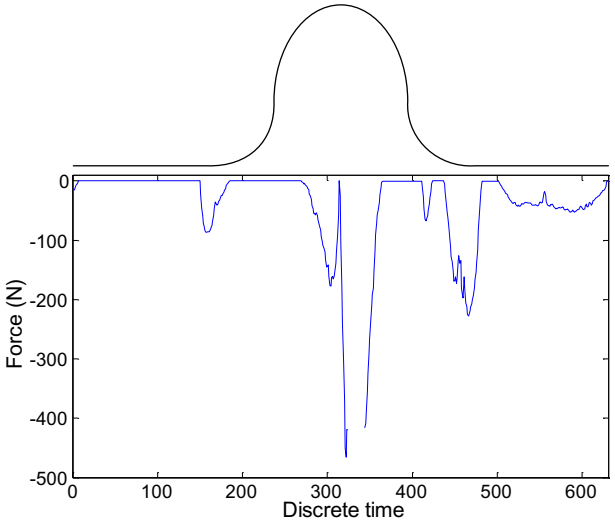

Fig. 17. Measured contact force without adjustments in the pre-programmed path.

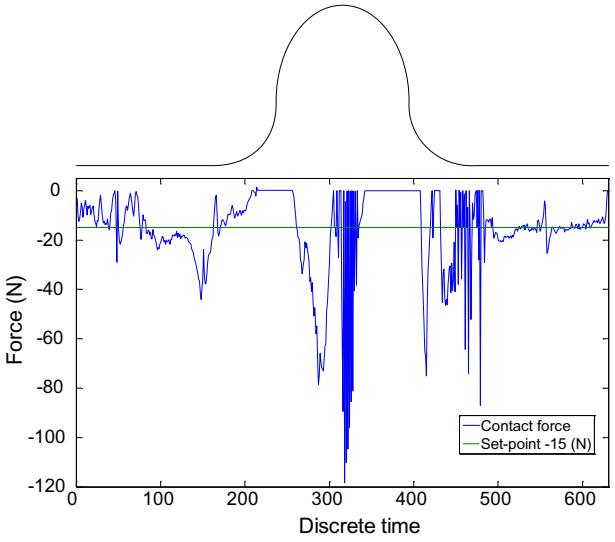

Fig. 18. Measured contact force using the force control loop.

In relation to Fig. 18, which represents the other test, using the force control loop, it can be seen that the contact force is more carefully controlled. Although the contact is lost and the contact force is high in some cases, it is clear the tendency of the contact force to converge to a set-point value. By the comparison between Figs. 17 and 18, the efficiency of the force control loop is evident. With the use of this system the high contact force values are lower and the contact is lost less times. In the analysis of these data it is necessary to take into account that the stiffness of the system is high, the tool is made of steel and the work-piece is made of wood, hence the contact force vary significantly from point to point. These figures do not allow to have a perspective of how far the two interacting parts are one from another and this point can lead to wrong

judgments. When the contact is lost, it is difficult to find a balance between to get in contact quickly and to avoid large overshoots (excessive contact forces). Hence we have chosen to work in the security side, this way large deviations take long times correction.

6. Conclusions and future work

In order to take advantages of CAD-based OLP for robotic applications that require a considerable high degree of accuracy, the self-recognition of the robot work environment (by means of sensory-feedback) should be achieved. However, not all commercial industrial robots allow easy sensory-feedback integration. Our proposal is to discretize all nominal robot end-effector paths, extracted from a 3-D CAD drawing, where it is intended to make adjustments. Then the discretized robot end-effector paths are on-line adjusted by the use of a hybrid force/motion control system. With this idea in mind, some discretization methods were presented, namely: discretization method of linear path, circular path, curvilinear path (Nagata patch) and a method of orientation interpolation (SLERP). The two firsts methods (linear and circular discretization) are exact methods so that they have no errors, this analysis was done taking into account the robot Cartesian space. On the other hand, the Nagata patch is a numerical method and presents small errors, which do not put the robot task at risk. With regard to the orientation interpolation method, it interpolates the orientation proportionally to the number of points generated, being constant the increment of orientation. This works very well to linear and circular paths but when used with curved paths, where the linearity is not verified, some slight disproportionality can occur. In order to solve this issue another methods should be studied in the future between them the v-Spline orientation method.

In order to produce adjustments in the pre-programmed robot paths a hybrid force/motion control system was proposed, a system based on an external force control loop and an internal position control loop. In this study it is only detailed the external control loop, which consists in a Fuzzy-PI controller that receives force/torque data and sends position displacements to the robot end-effector. The effectiveness of this system was tested in an experiment divided in two tests, where in one of the tests a path was traversed by a robot using the hybrid control system and in the other test the same experiment was repeated using a position control system, i.e. using the same hybrid control system without the external force control loop. The benefit of using the proposed system is clear, being the great advantages the reducing number of points of loss of contact and the diminution of the excessive contact forces as well as there was a clear tendency in the contact force to converge to a set-point. The convergence to the set-point can be improved in order to maintain a more stable contact force, with less fluctuation, and more accuracy. For this purpose, more labels and more rules should be incorporated in the Fuzzy-PI controller. General speaking, the presented approach overcame the challenges, thus, OLP becomes more appealing to be used and is a step more to achieve the concept of autonomous robots.

References

Berger, U., & May, M. (2005). An approach for the automatic generation of robot paths from CAD-data. In *Proceedings of the 10th IEEE international conference on emerging technologies and factory automation*, Catania, Italy (Vol. 1, pp. 291–297).

Bingül, Z., & Karahan, O. (2011). A Fuzzy logic controller tuned with PSO for 2 DOF robot trajectory control. *Expert Systems with Applications, 38*(1), 1017–1031.

Boschiroli, M., Fünfzig, C., Romani, L., & Albrecht, G. (2011). A comparison of local parametric C0 Bézier interpolants for triangular meshes. *Computers & Graphics, 35*(1), 20–34.

Chen, H., Fuhlbrigge, T., & Li, X. (2009). A review of CAD-based robot path planning for spray painting. *Industrial Robot, 36*(1), 45–50.

Chen, H., & Sheng, W. (2011). Transformative CAD based industrial robot program generation. *Robotics and Computer-Integrated Manufacturing, 27*(5), 942–948.

Chen, K. U., Tung, P. C., Tsai, M. T., & Fan, Y. H. (2009). A self-tuning Fuzzy PID-type controller design for unbalance compensation in an active magnetic bearing. *Expert Systems with Applications, 36*(4), 8560–8570.

Cook, G. E., Crawford, R., Clark, D. E., & Strauss, A. M. (2004). Robotic friction stir welding. *Industrial Robot, 31*(1), 55–63.

Feng-yun, L., & Tian-sheng, L. (2005). Development of a robot system for complex surfaces polishing based on CL data. *The International Journal of Advanced Manufacturing Technology, 26*(9–10), 1132–1137.

Fleming, P. A., Hendricks, C. E., Wilkes, D. M., Cook, G. E., & Strauss, A. M. (2009). Automatic seam-tracking of friction stir welded T-joints. *The International Journal of Advanced Manufacturing Technology, 45*(5–6), 490–495.

Kim, J. Y. (2004). CAD-based automated robot programming in adhesive spray systems for shoe outsoles and uppers. *Journal of Robotic Systems, 21*(11), 625–634.

Kuffner, J. (2004). Effective sampling and distance metrics for 3D rigid body path planning. In *Proceedings of the 2004 IEEE international conference on robotics & automation*, New Orleans, LA, USA (Vol. 4, pp. 3993–3998).

Lin, S. T., & Huang, A. K. (1998). Hierarchical Fuzzy force control for industrial robots. *IEEE Transactions on Industrial Electronics, 45*(4), 646–653.

Lin, W., Watanabe, Y., Morita, S., Uehara, Y., & Ohmori, H. (2007). Development of a C-CAM system and its application to manufacturing. *Journal of Japan Society for Abrasive Technology, 51*(5), 290–295.

Liu, Z., Bu, W., & Tan, J. (2010). Motion navigation for arc welding robots based on feature mapping in a simulation environment. *Robotics and Computer-Integrated Manufacturing, 26*(2), 137–144.

MacVicar-Whelan, P. J. (1977). Fuzzy sets for man–machine interactions. *International Journal of Man–Machine Studies, 8*(6), 687–697.

Mamdani, E. H. (1974). Application of Fuzzy algorithms for control of simple dynamic plant. In *Proceedings of IEEE institution of electrical engineers* (Vol. 121, No. 12, pp. 1585–1588).

Mendes, N., Neto, P., Pires, J. N., & Moreira, A. P. (2010). Fuzzy-PI force control for industrial robotics. In P. Vadakkepat et al. (Eds.), *Trends in intelligent robotics* (pp. 322–329). Berlin, Heidelberg: Springer-Verlag.

Mudi, R. K., & Pal, N. R. (2000). A self-tuning Fuzzy PI controller. *Fuzzy Sets and Systems, 115*(2), 327–338.

Nagata, T. (2005). Simple local interpolation of surfaces using normal vectors. *Computer Aided Geometric Design, 22*, 327–347.

Nagata, F., Hase, T., Haga, Z., Omoto, M., & Watanabe, K. (2007). CAD/CAM-based position/force controller for a mold polishing robot. *Mechatronics, 17*, 207–216.

Nagata, F., Kusumoto, Y., Fujimoto, Y., & Watanabe, K. (2007). Robotic sanding system for new designed furniture with free-formed surface. *Robotics and Computer-Integrated Manufacturing, 23*(4), 371–379.

Neto, P., Mendes, N., Pires, J. N., & Moreira, A. P. (2010). CAD-based robot programming: The role of Fuzzy-PI force control in unstructured environments. In *Proceedings of the sixth annual IEEE conference on automation science and engineering*, Toronto, Canada (pp. 362–367).

Neto, D. M., Oliveira, M. C., Alves, J. L., & Menezes, L. F. (2010). Local interpolation for tools surface description. In *Proceedings of the 10th international conference on numerical methods in industrial forming processes*, Pohang, Republic of Korea (pp. 479–486).

Neto, P., Mendes, N., Araújo, R., Pires, J. N., & Moreira, A. P. (2012). High-level programming based on CAD: Dealing with unpredictable environments. *Industrial Robot, 39*(3), 294–303.

Neto, D. M., Oliveira, M. C., Menezes, L. F., & Alves, J. L. (2012). Interpolation for tool surface description in sheet metal forming simulation. *Computer-Aided Design.*

Nielson, G. (2004). v-Quaternion splines for the smooth interpolation of orientations. *IEEE Transactions on Visualization and Computer Graphics, 10*(2), 224–229.

Pires, J. N., Afonso, G., & Estrela, N. (2007). Force control experiments for industrial applications: A test case using an industrial debussing example. *Assembly Automation, 27*(2), 148–156.

Pires, J. N., Godinho, T., & Araújo, R. (2004). Force control for industrial applications using a Fuzzy PI controller. *Sensor Review, 24*(1), 60–67.

Schaefer, T., & Schraft, D. (2005). Incremental sheet metal forming by industrial robot. *Rapid Prototyping Journal, 11*(5), 278–286.

Sekine, T., & Obikawa, T. (2010). Normal-unit-vector based tool path generation using a modified local interpolation for ball-end milling. *Journal of Advanced Mechanical Design Systems and Manufacturing, 4*, 1246–1260.

Sheng, W., Xi, N., Song, M., & Chen, Y. (2001). CAD-guided robot motion planning. *Industrial Robot, 28*(2), 143–151.

Soron, M., & Kalaykov, I. (2006). A robot prototype for friction stir welding. In *Proceedings of the 2006 IEEE conference on robotics automation and mechatronics*, Bangkok, Thailand (pp. 1–5).

Vosniakos, G. C., & Chronopoulos, A. (2008). Industrial robot path planning in constraint-based computer-aided design and kinematic analysis environment. *Proceedings of the Institution of Mechanical Engineers – Part B: Journal of Engineering Manufacture, 223*(5), 523–533.

Woo, Z. W., Chung, H. Y., & Lin, J. J. (2000). PID type Fuzzy controller with self-tuning scaling factors. *Fuzzy Sets and Systems, 115*(2), 321–326.

Yu, F. M. (2009). A self-tuning logic design for perturbed time-delay systems with nonlinear input. *Expert Systems with Applications, 36*(3), 5304–5309.

A.3. APPENDIX A3

Int J Adv Manuf Technol
DOI 10.1007/s00170-013-4741-3

ORIGINAL ARTICLE

An optimal fuzzy-PI force/motion controller to increase industrial robot autonomy

Nuno Mendes · Pedro Neto · J. Norberto Pires · Altino Loureiro

Received: 30 July 2012 / Accepted: 7 January 2013

Abstract This paper presents a method for robot self-recognition and self-adaptation through the analysis of the contact between the robot end effector and its surrounding environment. Often, in off-line robot programming, the idealized robotic environment (the virtual one) does not reflect accurately the real one. In this situation, we are in the presence of a partially unknown environment (PUE). Thus, robotic systems must have some degree of autonomy to overcome this situation, especially when contact exists. The proposed force/motion control system has an external control loop based on forces and torques exerted on the robot end effector and an internal control loop based on robot motion. The external control loop is tested with an optimal proportional integrative (PI) and a fuzzy-PI controller. The system performance is validated with real-world experiments involving contact in PUEs.

Keywords Force control · Fuzzy-PI · Autonomous robots · Robotics · Partly unknown environment

1 Introduction

Today, the robotics market imposes that robots are programmed more quickly, more easily and used in more challenging tasks [1, 2]. In this context, off-line robot programming (OLP) is often considered a good solution. Different approaches to OLP have been proposed, most of them based on CAD data. This includes an OLP system based on a CAD/CAM/CAE software for the shoe-manufacturing industry [3], the definition of robot paths for spray painting processes [4], the generation of robot paths from CAD for a friction stir welding process [5] and direct OLP from a common CAD package [6–8]. In addition, there are also OLP commercial software packages in which CAD drawings serve as its input. The problem is that all data from CAD (the CAD drawings representing the robotic cell in study) are nominal data that often do not reflect accurately the real robotic environment. In this context, we may be planning robot paths for a robotic scenario that does not actually exist, at least in its original configuration. Thus, we are in the presence of a partially unknown environment (PUE). These differences between the idealized robot environment (the virtual one) and the real robotic environment can have different origins: the unpredictable dynamic behaviour of the real environment after contact with the robot or other equipments, robotic arm deflection, errors from the robot calibration process [9, 10], an incorrect mapping of data from the virtual to the real environment, the roughness of contact surfaces, poorly representative CAD models and the presence of foreigner objects in the work environment. It follows from this that in order to have total control over the OLP process, the robot has to know in real time the actual configuration of its surrounding environment. In this way, robotic systems must have some degree of autonomy to overcome this situation. This has been achieved by incorporating sensors into the robotic systems [11–16]. Important studies have been conducted in this area, for example, the incorporation of sensors to increase industrial robot autonomy for welding applications [11, 12] or for a general purpose robotic framework [13]. Sensor integration in task-level programming has also been a matter of study [14]. A number of vision-based solutions have been proposed to face PUEs. Kenney et al. use a vision-based approach to facilitate human–robot interaction and robot operation in unstructured environments [15]. Lopez-Juarez et al. explore force feedback to adapt robot behaviours to changing environments [16].

N. Mendes (✉) · P. Neto · J. N. Pires · A. Loureiro
Department of Mechanical Engineering (CEMUC)-POLO II,
University of Coimbra, Rua Luís Reis Santos
3030-788 Coimbra, Portugal
e-mail: nuno.mendes@dem.uc.pt

Published online: 20 January 2013

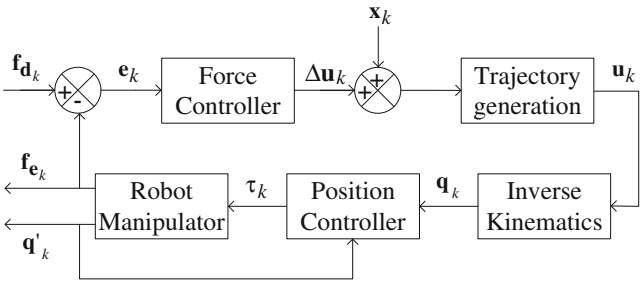

Fig. 1 Hybrid force/motion control system

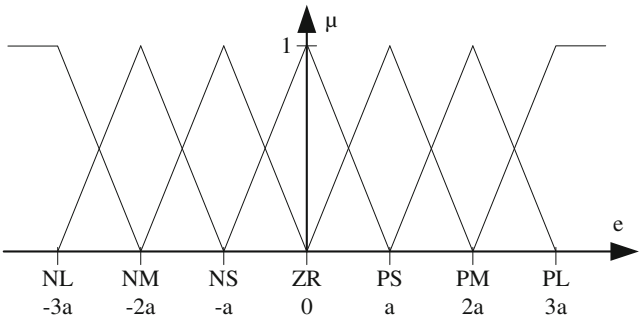

Fig. 3 Membership functions for the input variables

This paper proposes a force/motion control system to increase robot autonomy and thus to achieve a suitable robot performance in a PUE. The idea behind this is to control the end-effector pose (position and orientation) in real time and in accordance with the forces and torques from the contact of the robot end effector with its surrounding environment. This allows the robot to keep a given contact force and avoid undesirable impacts. The proposed force/motion control system has an external control loop based on forces and torques being exerted on the robot end effector and an internal control loop based on robot motion. The external control loop is tested with a proportional integrative (PI) and a fuzzy-PI controller. The system performance is validated with real-world experiments involving contact in PUEs. Finally, results are discussed and some considerations about future work directions are made.

2 Force control applied to robotics

Over the last years, force control applied to robotics has assumed a growing importance in the proper execution of some robotic tasks [17]. These tasks are those in which the robot is required to maintain a given set force (deburring, polishing and assembly tasks) or others in which the deflexion of the robotic arm is a major factor (milling, grinding, drilling and friction stir welding). Even though these two cases appear to be different, both can be treated in the same way by applying a force control technique, passive force control [18] or active force control [18–23]. Hybrid force/-motion control has been presented in literature as one of the most suitable methods to deal with PUEs [18].

Considering the approach proposed in this paper, this method allows controlling the non-constrained task directions (end-effector motion directions) in motion control and the constrained task directions in force control. The system is designed so that force control prevails over motion control. This means that position errors are tolerated to ensure force regulation.

Several robotic solutions using force control techniques have been developed and successfully applied to various industrial processes such as polishing [19] and deburring [20]. A number of force control techniques (fuzzy, PI, PID, hybrid, etc.) with varying complexity have been proposed thus far [20–23].

Fuzzy control was first introduced and implemented in the early 1970s in an attempt to design controllers for systems structurally difficult to model due to naturally existing nonlinearities and other modelling complexities [24]. Hsieh et al. present an optimal predicted fuzzy-PI gain scheduling controller to control the constant turning force process with a fixed metal removal rate under various cutting conditions [25]. Mendes et al. present a hybrid solution exploring robot force/motion control and different modalities of discretization and fitting of nominal data [26, 27]. Lopes at al. present a force–impedance-controlled industrial robot [28]. Gudur and Dixit propose a study in which the roll force and roll torque in a cold flat rolling process are modelled using first-order Takagi–Sugeno (T-S) fuzzy models [29]. Many other studies apply T-S fuzzy models [30–34].

3 Robot control system

3.1 Hybrid force/motion control

Let us consider a rigid robot (manipulator) of n links, the dynamic equation of motion in the joint space is:

$$\mathbf{M}(\mathbf{q})\,\ddot{\mathbf{q}} + \mathbf{C}(\mathbf{q},\dot{\mathbf{q}}) + \mathbf{B}(\mathbf{q},\dot{\mathbf{q}}) + \mathbf{G}(\mathbf{q}) = \boldsymbol{\tau} \tag{1}$$

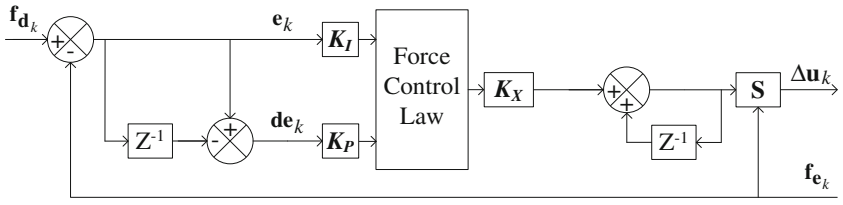

Fig. 2 Fuzzy-based force controller

Table 1 Representation of the rule base

e ed	NL	NM	NS	ZR	PS	PM	PL
PL	nl	nm	ns	zr	pm	pl	pl
PM	nl	nl	nm	zr	pm	pl	pl
PS	nl	nl	ns	zr	ps	pl	pl
ZR	nl	nm	ns	zr	ps	pm	pl
NS	nl	nl	ns	zr	ps	pl	pl
NM	nl	nl	nm	zr	pm	pl	pl
NL	nl	nl	nm	zr	ps	pm	pl

where $\boldsymbol{\tau} \in \Re^n$ is the vector of applied joint torques, $\mathbf{q} \in \Re^n$ is the vector of joint positions, $\mathbf{M} \in \Re^{n\times n}$ is the inertia matrix, $\mathbf{C} \in \Re^n$ is the vector of Coriolis and centrifugal torques, $\mathbf{B} \in \Re^n$ is the vector of torques due to the friction action on the robot joints and $\mathbf{G} \in \Re^n$ is the vector of gravitational torques. When there is an external force applied to the robot end effector, the dynamic Eq. (1) becomes:

$$\mathbf{M}(\mathbf{q})\,\ddot{\mathbf{q}} + \mathbf{C}(\mathbf{q},\dot{\mathbf{q}}) + \mathbf{B}(\mathbf{q},\dot{\mathbf{q}}) + \mathbf{G}(\mathbf{q}) + \boldsymbol{\tau}_e = \boldsymbol{\tau} \tag{2}$$

where $\boldsymbol{\tau}_e \in \Re^n$ is the vector of forces/torques exerted on the environment by the robot end effector expressed in the robot joint space. This vector can be defined as:

$$\boldsymbol{\tau}_e = \mathbf{J}^T\mathbf{f} \tag{3}$$

where $\mathbf{J}^T \in \Re^{n\times n}$ is the transpose of the Jacobian matrix and $\mathbf{f} \in \Re^n$ is the vector of forces and torques exerted on the environment by the robot end effector expressed in Cartesian space. Thus, Eq. (3) may be written as:

$$\boldsymbol{\tau}_e = \mathbf{J}^T\mathbf{K}\mathbf{J}^{\mathrm{T}}\Delta\mathbf{u} \tag{4}$$

where $\mathbf{K} \in \Re^{n\times n}$ is the matrix of stiffness coefficients and $\Delta\mathbf{u} \in \Re^n$ is the vector of correction of displacements and orientations in the Cartesian space.

Traditionally, force/motion control systems applied to a robot manipulator have some end-effector motion directions controlled in motion and others controlled in force. In the proposed hybrid controller, all directions (along *x*, *y* and *z*) are controlled in motion (internal control loop) and some directions in force (external control loop). Contact forces and torques (between the robot tool and the robot working environments) are acquired from a force/torque (F/T) sensor

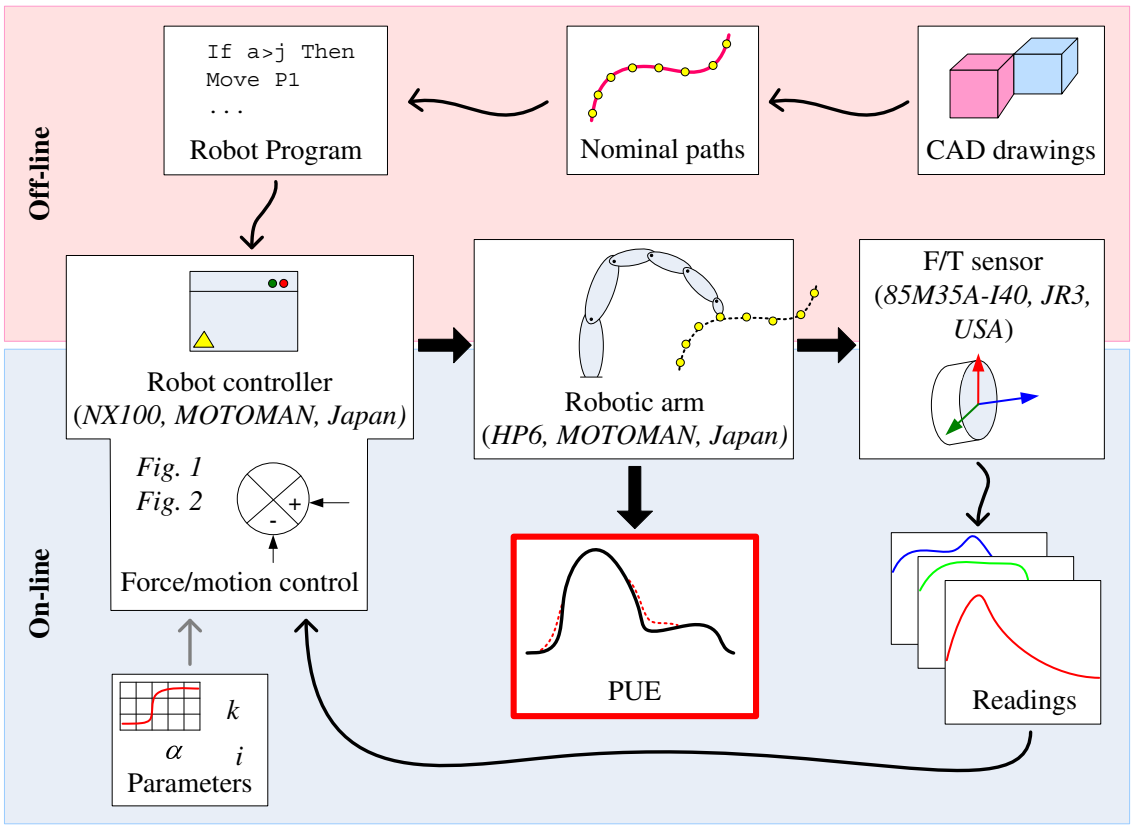

Fig. 4 Overview of the proposed approach and equipment

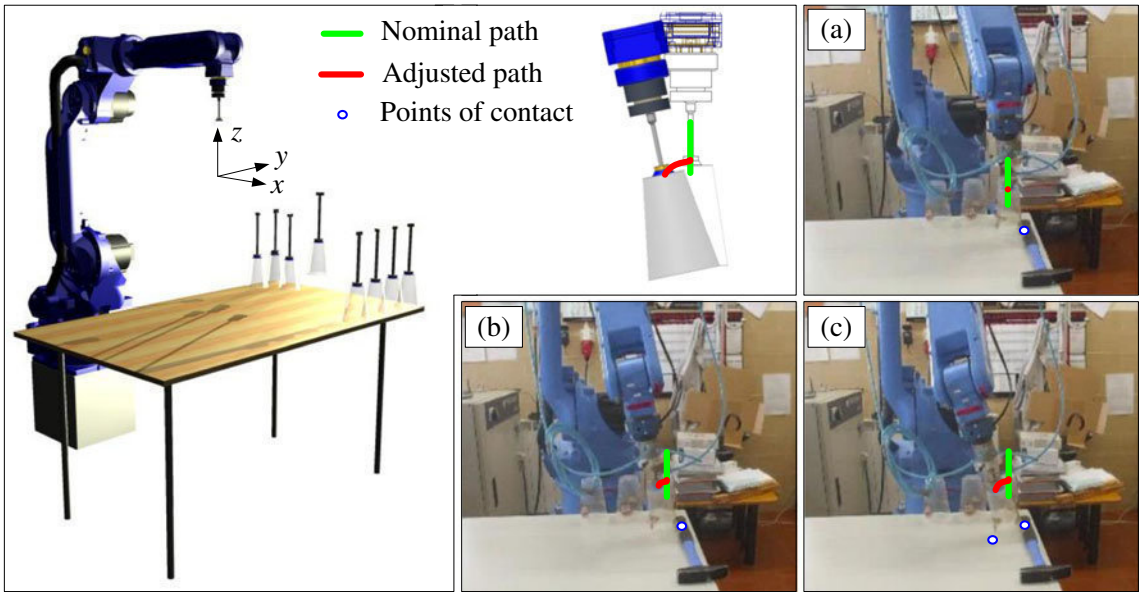

Fig. 5 **a**–**c** Layout of the first experiment

which is between the robot wrist and the tool. The external control loop processes the acquired information using a fuzzy-PI control system and sends end-effector position/-orientation displacement corrections ($\Delta\boldsymbol{\mu}$) to the internal control loop (Fig. 1). The pre-programmed robot paths (nominal data) are then adjusted through the direct control of the servomotors of the robot. In Fig. 1, $q_{\mathrm{k}}^{'}$ is the vector of joint positions in an instant of time previous to the current time.

3.2 Force controller

The proposed force controller associates PI control and fuzzy logic, a fuzzy logic controller type Mamdani [24]. The PI controller has good performance when applied in practical situations. A controller with derivative factor could help to decrease the correction time, but it is very sensitive to noise. With regard to fuzzy, the controller type Mamdani is easy to implement and does not need a rigorous mathematical model of the system in study. Other types of fuzzy controller can require more rigorous mathematical models, for example the T-S controllers [29–34].

3.2.1 Fuzzy control architecture

The controller input variables are the force/torque error **e** and the change of the error **de**:

$$\mathbf{e}_k = \mathbf{f}_{\mathbf{d}_k} - \mathbf{f}_{\mathbf{e}_k} \tag{5}$$

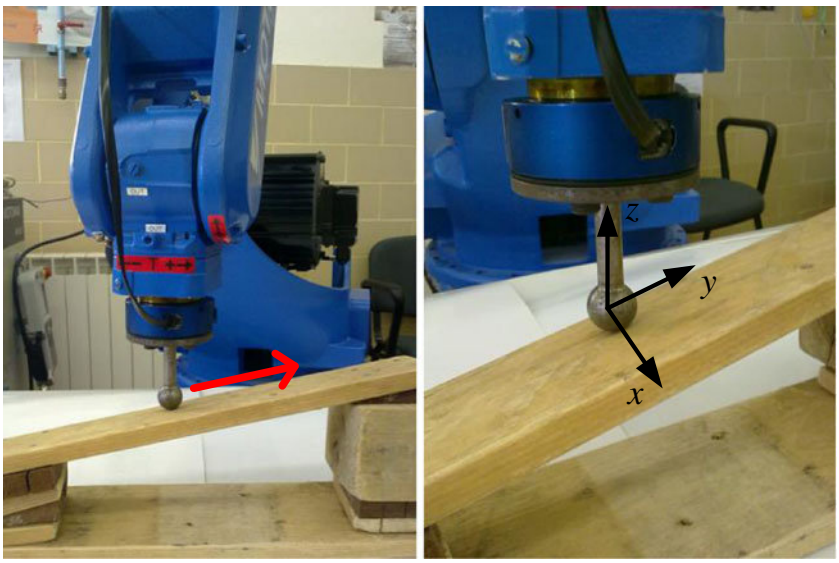

Fig. 6 Layout of the second experiment

$$\mathbf{de}_k = \mathbf{e}_k - \mathbf{e}_{k-1} \tag{6}$$

where $\mathbf{f}_e$ is the actual force/torque and $\mathbf{f}_d$ is the desired force/torque (set points).

3.2.2 Fuzzy-PI

From the conventional PI control algorithm, the robot displacement $\mathbf{u}$ can be computed as:

$$\mathbf{u}(t) = \mathbf{K}_P\,\mathbf{e}(t) + \mathbf{K}_I \int \mathbf{e}(t)dt \tag{7}$$

where $\mathbf{K}_p$ and $\mathbf{K}_I$ are coefficient constants. This can be represented in a discrete version:

$$\mathbf{u}_k = \mathbf{u}_{k-1} + \Delta\mathbf{u}_k \tag{8}$$

$$\Delta\mathbf{u}_k = \mathbf{K}_P\,\mathbf{de}_k + \mathbf{K}_I\,\mathbf{e}_k \tag{9}$$

If **e** and **de** are fuzzy variables, Eqs. (8) and (9) become a fuzzy control algorithm. A practical implementation of the proposed fuzzy-PI concept is in Fig. 2. Finally, the centre of area method was selected to defuzzify the output fuzzy set inferred by the controller:

$$\Delta U = \frac{\sum_{i=1}^{n} \mu_i\,\Delta U_i}{\sum_{i=1}^{n} \mu_i} \tag{10}$$

where μ_i is the membership function which takes values in the range [0, 1]. A decision maker **S**, $\mathbf{S} \in \Re^{n\times n}$, establishes the end-effector directions to control. When all directions are controlled in force and motion, the **S** matrix becomes the identity matrix.

3.2.3 Knowledge base

Each control variable is normalized into seven linguistic labels: positive large (PL), positive medium (PM), positive small (PS), zero (ZR), negative large (NL), negative medium (NM) and negative small (NS). The grade of each label is described by a fuzzy set. The membership function is in Fig. 3. The well-known PI-like fuzzy rule base suggested by MacVicar-Whelan [35] is applied in this study (Table 1).

3.2.4 Tuning strategy

The system can be adjusted to different contact conditions by tuning the scaling factors $\mathbf{K_P}$, $\mathbf{K_I}$ and $\mathbf{K_X}$ according to the characteristics of the environment in study. Lin and Huang propose an adjustment where the scaling factors are dynamic and thus they are adjusted at the same time the task occurs [21]. Also, different tables of rules can be used accordingly the task to be performed and the materials in contact involved in the task [20]. In this paper, the scaling factors are set to appropriate constant values, achieved by trial and error.

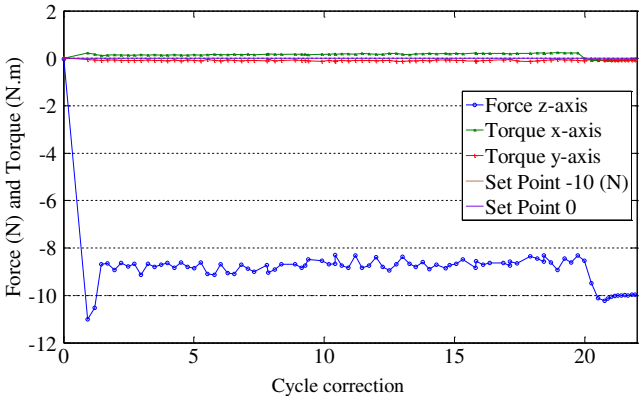

Fig. 7 Results for the first experiment using a fuzzy-PI controller

4 Experiments

The effectiveness of the proposed approach was evaluated in two real-world experiments involving contact in PUEs. In both experiments, the robot is programmed with nominal data from CAD drawings and the external control loop is tested with a PI and a fuzzy-PI controller (Fig. 4).

In the first experiment, the robot is programmed to manipulate plastic cups. A "foreign" object (a hammer) is introduced into the robot working environment, forcing it to become a PUE (Fig. 5). This means that the nominal paths will drive the robot end effector (with the plastic cup attached) to collide with the hammer. In this situation, when contact between the plastic cup and the hammer begins, the force/motion control system assumes the robot control, adjusting the end effector to the PUE and maintaining a given value of contact force (10 N) along the *z* axis and 0 N along the *x* axis.

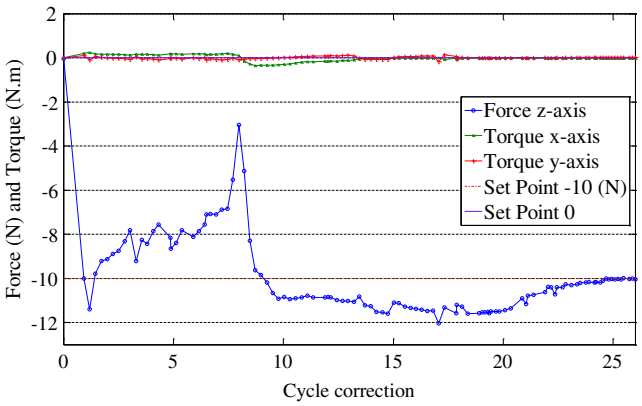

Fig. 8 Results for the first experiment using a PI controller

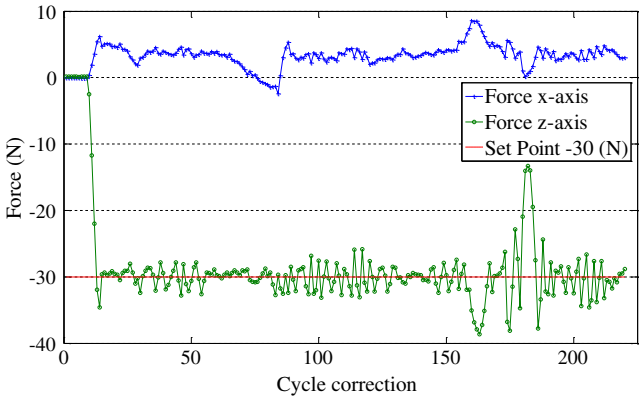

Fig. 9 Results for the second experiment using a fuzzy-PI controller

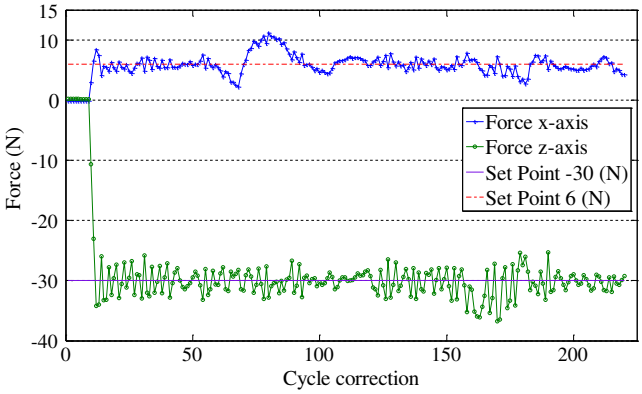

Fig. 11 Results for the third experiment using a fuzzy-PI controller

In the second experiment, the robot is programmed to be moved from a point to another in a straight path and maintaining contact with the workpiece (Fig. 6). In practice, since the contact surface of the workpiece is irregular and there are always calibration errors, it is impossible to properly perform the task described above without force/motion control. The force/motion control system assumes the robot control maintaining a given value of contact force (30 N) along the z axis.

4.1 Results and discussion

For the first experiment, all tests showed similar force control results to those shown in Fig. 7 using a fuzzy-PI controller and those shown in Fig. 8 using a PI controller. Both systems provide acceptable results since the robot adapts to the PUE avoiding excessive contact forces. However, the fuzzy-PI controller performs better than the PI controller because the latter has a large overshoot and needs more time to stabilize (Fig. 8).

Results for the second experiment are shown in Fig. 9 when using a fuzzy-PI controller and in Fig. 10 when using a PI controller. The fluctuation in the controlled forces along the z axis is due to the roughness of the contact surface. Nevertheless, these forces are all around the set point, 30 N. The PI controller has a better resolution (for small disturbances) than the fuzzy-PI controller. On the other hand, it presents a greater overshoot at the beginning of the convergence to the set point (Fig. 10). Since both systems (controllers) have similar results, a third experiment was done to ascertain the best solution. This experiment is similar to the second experiment but applying force/motion control along the x axis and the z axis, with set point forces of 6 and 30 N, respectively. The results are in Figs. 11 and 12. In this context, results obtained along the z axis are similar to those in the second experiment. For the forces controlled along the x axis, it can be stated that the controller behaved the same way as for the control along the z axis. In summary, we cannot say that one controller is better than the other. The results obtained are in line with similar studies in the field that applies fuzzy reasoning to solve force/-motion control problems [20–23].

5 Conclusions

This paper presented a hybrid force/motion control system to increase robot autonomy. The system proved to be a valuable tool to help robots to adapt to PUEs, especially

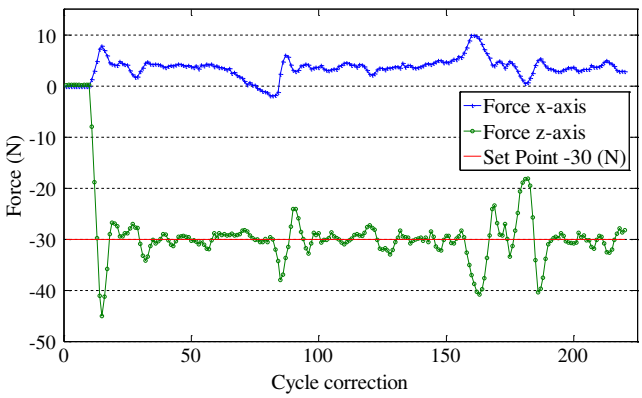

Fig. 10 Results for the second experiment using a PI controller

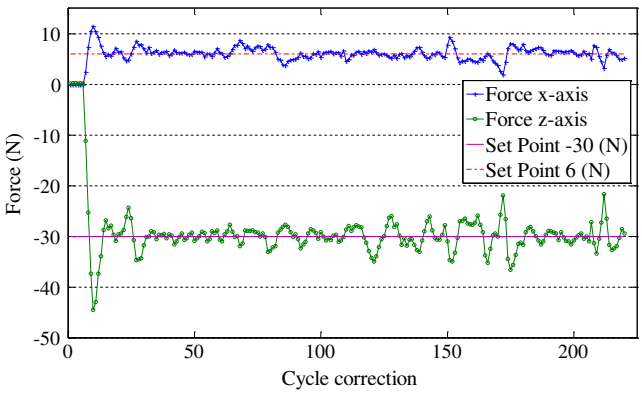

Fig. 12 Results for the third experiment using a PI controller

when contact exists. The external control loop of the hybrid controller was tested with a PI and a fuzzy-PI controller. Real-world experiments involving contact in PUEs demonstrated that we cannot say that the fuzzy-PI controller is better than the PI controller. Both showed similar behaviours, with some disturbance around the set points. Another conclusion that can be drawn from experiments is that the proposed system only works properly if the data transfer between the F/T sensor and the robot controller is done in real time. Future work will focus on performing more real-world experiments with different materials in contact.

References

1. Pan Z, Polden J, Larkin N, Duin SV, Norrish J (2012) Recent progress on programming methods for industrial robots. Robot Comput Integrated Manuf 28(2):87–94. doi:10.1016/j.rcim.2011.08.004
2. Biggs G, MacDonald B (2003) A survey of robot programming systems. In: Proc Australasian Conf Robot Automat 2003 (ACRA 2003), 1 pp 1–10, Brisbane, Australia
3. Kim JY (2004) CAD-based automated robot programming in adhesive spray systems for shoe outsoles and uppers. J Robotic Syst 21(11):625–634. doi:10.1002/rob.20040
4. Chen H, Fuhlbrigge T, Li X (2008) Automated industrial robot path planning for spray painting process: a review. In: Proc 4th IEEE Conf Automation Science Engineering (CASE 2008), Washington DC, USA. doi:10.1109/COASE.2008.4626515
5. Soron M, Kalaykov I (2007) Generation of continuous tool paths based on CAD models for friction stir welding in 3D. In: Proc 2007 Mediterranean Conf Control Automation (MED 2007), Athens, Greece. doi:10.1109/MED.2007.4433944
6. Neto P, Pires JN, Moreira AP (2010) CAD-based off-line robot programming. In: Proc 2010 IEEE Conf Robotics Automation Mechatronics (RAM 2010), Singapore. doi:10.1109/RAMECH.2010.5513141
7. Neto P, Mendes N (2013) Direct off-line robot programming via a common CAD package. Robot Auton Syst, in press
8. Neto P, Pires JN, Moreira AP (2013) Robot simulation: an approach based on CAD-autodesk inventor. IEEE Robot Autom Mag, in press
9. Nubiola A, Bonev IA (2013) Absolute calibration of an ABB IRB 1600 robot using laser tracker. Robot Comput Integrated Manuf 29 (1):236–245. doi:10.1016/j.rcim.2012.06.004
10. Neto P, Mendes N, Araújo R, Pires JN, Moreira AP (2012) High-level programming based on CAD: dealing with unpredictable environments. Ind Robot 39(3):294–303. doi:10.1108/01439911211217125
11. Bolmsjö G, Olsson M (2005) Sensors in robotic arc welding to support small series production. Ind Robot 32(4):341–345. doi:10.1108/01439910510600218
12. Fridenfalk M, Bolmsjö G (2002) Design and validation of a sensor guided robot control system for welding in shipbuilding. Int J Joining Mater 14(3/4):44–55
13. Brink K, Olsson M, Bolmsjö G (1997) Increased autonomy in industrial robotic systems: a framework. J Intell Robotic Syst 19:357–373. doi:10.1023/A:1007909120189
14. Johansson R, Robertsson A, Nilsson K, Brogardh T, Cederberg P, Olsson M, Olsson T, Bolmsjö G (2004) Sensor integration in task-level programming and industrial robotic task execution control. Ind Robot 31(3):284–296. doi:10.1108/01439910410532369
15. Kenney J, Buckley T, Brock O (2009) Interactive segmentation for manipulation in unstructured environments. In: Proc 2009 IEEE Int Conf Robot Autom (ICRA 2009), pp. 1337–1382, Kobe, Japan. doi:10.1109/ROBOT.2009.5152393
16. Lopez-Juarez I, Corona-Castuera J, Peña-Cabrera M, Ordaz-Hernandez K (2005) On the design of intelligent robotic agents for assembly. Inf Sci 171(4):377–402. doi:10.1016/j.ins.2004.09.011
17. Zeng G, Hemami A (1997) An overview of robot force control. Robotica 15(5):473–482. doi:10.1017/S026357479700057X
18. Siciliano B, Villani L (1999) Robot force control. Kluwer, Boston
19. Nagata F, Kusumoto Y, Fujimoto Y, Watanabe K (2007) Robotic sanding system for new designed furniture with free-formed surface. Robot Comput Integrated Manuf 23(4):371–379. doi:10.1016/j.rcim.2006.04.004
20. Pires JN, Ramming J, Rauch S, Araujo R (2002) Force/torque sensing applied to industrial robotic deburring. Sens Rev 22 (3):232–241. doi:10.1108/02602280210433070
21. Lin ST, Huang AK (1998) Hierarchical fuzzy force control for industrial robots. IEEE Trans Ind Electron 45(4):646–653. doi:10.1109/41.704894
22. Li HX, Gatland HR (1995) A new methodology for designing a fuzzy logic controller. IEEE Trans Syst Man Cybern 25(3):505–512. doi:10.1109/21.364863
23. Tang KS, Man KF, Chen G, Kwong S (2001) An optimal fuzzy PID controller. IEEE Trans Ind Electron 48(4):757–765. doi:10.1109/41.937407
24. Mamdani EH (1974) Application of fuzzy algorithms for control of simple dynamic plant. Proc Inst Electr Eng 121(12):1585–1588. doi:10.1049/piee.1974.0328
25. Hsieh CH, Chou JH, Wu YJ (2002) Optimal predicted fuzzy PI gain scheduling controller of constant turning force systems with fixed metal removal rate. Int J Adv Manuf Technol 19(10):714–721. doi:10.1007/s001700200081
26. Mendes N, Neto P, Pires JN, Loureiro A (2013) Discretization and fitting of nominal data for autonomous robots. Expert Syst Appl 40 (4):1143–1151. doi:10.1016/j.eswa.2012.08.023
27. Mendes N, Neto P, Pires JN, Moreira AP (2010) Fuzzy-PI force control for industrial robotics. In: Vadakkepat P et al (eds) Trends in intelligent robotics. Springer, Heidelberg, pp 322–329. doi:10.1007/978-3-642-15810-0_41
28. Lopes A, Almeida F (2008) A force-impedance controlled industrial robot using an active robotic auxiliary device. Robot Comput Integrated Manuf 24(3):299–309. doi:10.1016/j.rcim.2007.04.002
29. Gudur PP, Dixit US (2009) An application of fuzzy inference for studying the dependency of roll force and roll torque on process variables in cold flat rolling. Int J Adv Manuf Technol 42(1–2):41–52. doi:10.1007/s00170-008-1574-6
30. Ho WH, Chou JH (2007) Design of optimal controllers for Takagi-Sugeno fuzzy-model-based systems. IEEE Trans Syst Man Cybern Syst Hum 37(3):329–339. doi:10.1007/s00170-008-1574-6
31. Fanaei A, Farrokhi M (2006) Robust adaptive neuro-fuzzy controller for hybrid position/force control of robot manipulators in contact with unknown environment. J Intell Fuzzy Syst 17(2):125–144
32. Kiguchi K, Fukuda T (1997) Intelligent position/force controller for industrial robot manipulators—application of fuzzy neural networks. IEEE Trans Ind Electron 44(6):753–761. doi:10.1109/41.649935
33. Kucukdemiral IB, Cansever G (2006) Sugeno based robust adaptive fuzzy sliding mode controller for SISO nonlinear systems. J Intell Fuzzy Syst 17(2):113–124
34. Wai RJ, Yang ZW (2008) Adaptive fuzzy neural network control design via a T-S fuzzy model for a robot manipulator including actuator dynamics. IEEE Trans Syst Man Cybern B Cybern 38 (5):1326–1346. doi:10.1109/TSMCB.2008.925749
35. MacVicar-Whelan PJ (1977) Fuzzy sets for man–machine interactions. Int J Man Mach Stud 8(6):687–697

A.4. APPENDIX A4

Int J Adv Manuf Technol
DOI 10.1007/s00170-014-6024-z

ORIGINAL ARTICLE

A novel friction stir welding robotic platform: welding polymeric materials

N. Mendes · P. Neto · M. A. Simão · A. Loureiro · J. N. Pires

Received: 15 September 2013 / Accepted: 27 March 2014

Abstract The relevance, importance and presence of industrial robots in manufacturing have increased over the years, with applications in diverse new and nontraditional manufacturing processes. This paper presents the complete concept and design of a novel friction stir welding (FSW) robotic platform for welding polymeric materials. It was conceived to have a number of advantages over common FSW machines: it is more flexible, cheaper, easier and faster to setup and easier to programme. The platform is composed by three major groups of hardware: a robotic manipulator, a FSW tool and a system that links the manipulator wrist to the FSW tool (support of the FSW tool). This system is also responsible for supporting a force/torque (F/T) sensor and a servo motor that transmits motion to the tool. During the process, a hybrid force/motion control system adjusts the robot trajectories to keep a given contact force between the tool and the welding surface. The platform is tested and optimized in the process of welding acrylonitrile butadiene styrene (ABS) plates. Experimental tests proved the versatility and validity of the proposed solution.

Keywords Friction stir welding · Robotics · Polymers · Force/motion control · ABS · Manufacturing

1 Introduction

The promotion of manufacturing activities is probably one of the most effective ways to encourage economic growth and jobs creation. The question is how to do that? How manufacturing companies in developed countries can compete with low salaries? Much has been discussed around this over the years. However, there seems to be a consensus on the need to make manufacturing companies more flexible, producing what the market needs (small-series and customized products) and less dependent on the cost of labour.

Industrial robots are key elements in flexible manufacturing [1]. The problem is that they are relatively complex machines that need to be reprogrammed to perform a new task. Generally, industrial robots operate in very structured environments, without the capacity to adapt to dynamic scenarios. Thus, there is much research work to do in several different areas related to robotics, for example, in human-robot interaction and robot autonomy. At the same time, the application of robots in new and nontraditional manufacturing processes is another area for further research. This paper introduces and presents the concept and design of a novel friction stir welding (FSW) robotic platform for welding polymeric materials.

FSW was initially developed in the early 1990s for joining soft metals [2]. The welded seams produced by this method are free from defects: cracks, shrinkage and porosity. It also produces low distortion, which is a typical difficulty in fusion welding processes. This makes FSW a very attractive welding process. The traditional FSW process consists of a rotational tool, formed by a pin and a shoulder, which is inserted into the abutting surfaces of pieces to be welded and moved along the weld joint (Fig. 1). During the process, the pin is located inside the weld joint, softening the materials and enabling plastic flow as well as mixing materials. The shoulder is placed on the surface of the seam to create a smooth surface. Although this process is mainly applied to butt weld joints, other joint geometries can be welded. Aluminium, cooper, plastics, composites and dissimilar materials (for example, aluminium and cooper) are examples of materials that can be welded by FSW [3, 4]. The applications are many, but the following industries

Electronic supplementary material The online version of this article (doi:10.1007/s00170-014-6024-z) contains supplementary material, which is available to authorized users.

N. Mendes (✉) · P. Neto · M. A. Simão · A. Loureiro · J. N. Pires
Department of Mechanical Engineering, University of Coimbra, Polo II, 3030-788 Coimbra, Portugal
e-mail: nuno.mendes@dem.uc.pt

Published online: 12 June 2014

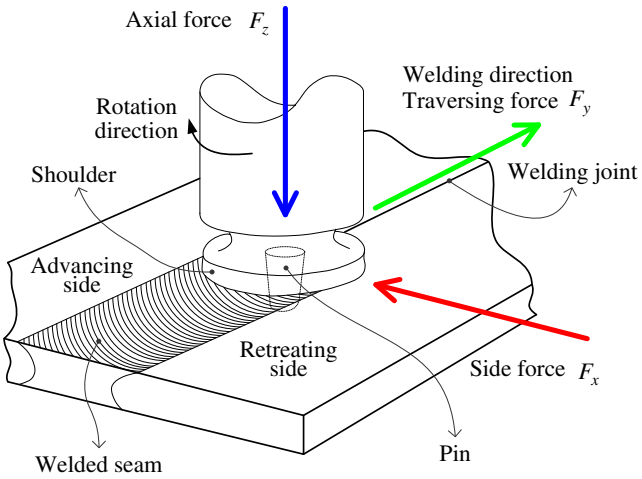

Fig. 1 FSW process

are the most relevant: aerospace, aeronautics, shipbuilding, railway and automotive [5, 6].

The FSW process can be performed using the following equipment: milling machines, FSW machines, parallel robots [7] and anthropomorphic robots [8]. Each of this equipment has its own advantages and disadvantages. They differ in payload capacity, stiffness, workspace, cost, control, etc. [9]. Table 1 resumes the main features of each kind of equipment. Summarizing, it can be stated that the anthropomorphic robots have some important advantages over the other equipment: flexibility, economically competitive, large workspace, fast setup, diverse programming options and capacity to perform multidirectional welds [6]. On the other hand, it presents some relative disadvantages: the reduced stiffness of the robotic arm in the context of the high forces involved into the process and the positional error associated to this kind of machine (clearance in motor and geared transmission mechanisms, backlash, bearing run-out, vibration, etc.) [10–13].

The number of studies in the field of robotic FSW is relatively low but with promising results. Robot prototypes for robotic FSW have been developed, and there are already some solutions in the market [14]. The main problems in using robots performing FSW (reduced stiffness and positional error) and future research directions are discussed in [15, 16]. According to the current state of the art, there are four different ways to control the robotic FSW process:

- Adjusting the plunge depth according to a given set force;
- Adjusting the plunge depth according to a given set torque for the tool;
- Adjusting the plunge depth according to a given set torque for the robot motors;
- Adjusting the traverse speed according to a given set force.

There are a number of approaches to force/motion control applied to robotic FSW [17–20]. The influence of the torque parameter on the control of the FSW process has been studied [21]. An interesting study in the field is dedicated to the development of a CNC milling machine with an integrated force control system. The quantity of heat transferred to the process is controlled through the traverse speed of the tool. It also presented a study in which the force control system (axial force) is linked to the penetration of the tool. These two methods are compared [22]. Another study presents the design and implementation of a FSW force controller [23]. A feedback controller for the path force is designed using the polynomial pole placement technique. The controller is implemented in a Smith predictor-corrector structure to compensate for the inherent equipment communication delay. It is shown that wormhole generation during the welding process is eliminated. Sensory feedback has been used to perform tool trajectory adjustments in welding aluminium plates [24]. Results are compared with the ones produced by a milling machine. The effect of the stiffness of the robot in trajectory compensation (tool deviations) has also been a subject of study [25].

Simulation plays an important role in the development of some controllers for FSW. Robot controller's performance has

Table 1 FSW equipment features

Characteristics ↓	Equipment			
	Milling machine	FSW machine	Parallel robot	Anthropomorphic robot
Flexibility	Low	Low/medium	High	High
Cost	Medium	High	High	Low
Stiffness	High	High	High	Low
Working volume	Medium	Medium	Low	High
Setup time	Low	High	Medium	Medium
Number of programming options	Low	Medium	High	High
Capacity to produce complex welds	Low	Medium	High	High
Control type	Motion	Motion/force	Motion	Motion

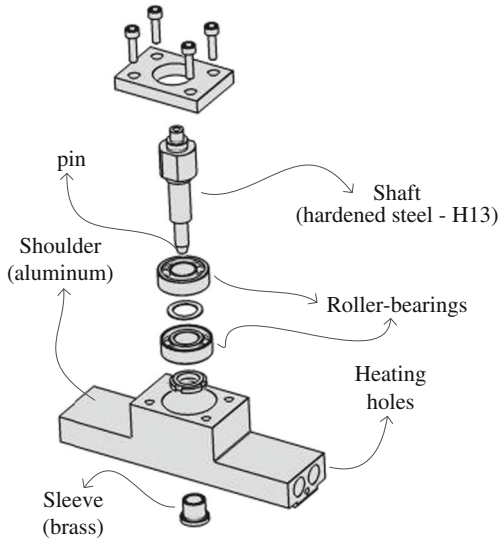

Fig. 2 FSW tool

been tested in simulation environments for the process of FSW. This allows the observation of the controller's behaviour in the presence of perturbations such as tool oscillation and lateral/rotational deviations [26]. Numerical simulation tools have been applied to analyse different FSW parameters [27]. It was achieved that the rotational speed of the tool and the axial force affect mutually the quality of welding [28]. These results have already been proved by real experiments [29].

The FSW process is defined by a number of parameters that influence the robotic process [8, 30–32]. These parameters are rotational speed, traverse speed, axial force, plunge depth, tool geometry, external heating (when used) and dwell time, among others. The investigation of the relationship between the plunge depth and the corresponding axial force is a factor of major importance. Problems in the force controller stability could be caused by the transient response characteristics at the beginning of the welding stage [33]. Some authors have studied the application of seam tracking with base on measured axial forces from the FSW process in order to improve the quality of the welds [34, 35].

In view of the above, it can be seen that a major challenge that hinders further diffusion of robotic FSW is the high forces involved in the process [36]. Nevertheless, force and motion control can attenuate this situation so that since 2000 that anthropomorphic robot is used in FSW [18]. Researchers and engineers rapidly realized that an appropriate robotic system is able to perform FSW with all the advantages highlighted before.

Since robotic FSW is not fully developed yet, there is a lot of room for improvements. In this paper, we concentrate on the concept and design of a novel FSW robotic platform for welding polymeric materials. The platform is composed by three major groups of hardware: a robotic manipulator, a FSW tool and a support for the FSW tool. This last element is also responsible for supporting a force/torque (F/T) sensor and a servo motor that transmits motion to the FSW tool.

During the welding process, a hybrid force/motion control system adjusts the robot trajectories (plunge depth) to keep a given contact force between the tool and the welding surface. The controller has as input the contact forces between the tool and the workpiece in each instant of time. The platform is tested and optimized in the process of welding acrylonitrile butadiene styrene (ABS) plates. Experimental tests proved the versatility and validity of the solution.

2 Concept and design

The main goal of this research was to develop a versatile FSW robotic platform capable to produce quality welds in terms of surface appearance. Thus, in order to support the definition of

Fig. 3 Robotic FSW platform

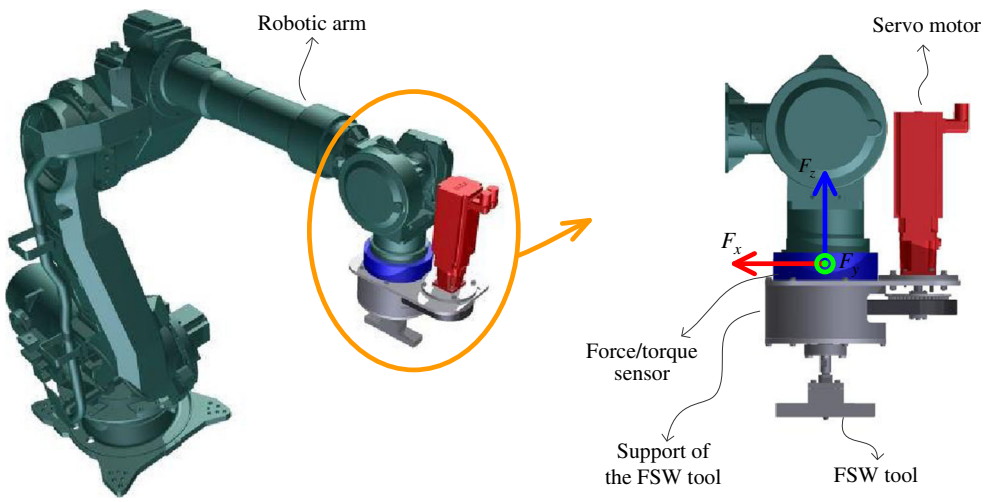

Table 2 FSW parameters threshold

Parameter	Threshold value
Axial force (F_z)	4,000 N
ABS plates thickness	6 mm
Tool rotational speed	1,500 rpm
Traverse and side force $\left(\sqrt{F_x^2 + F_y^2}\right)$	2,000 N
Torque (M)	4 Nm

the concept, it established a set of features that the platform should have:

- Flexibility;
- Robustness;
- Simplicity;
- Easy to programme;
- Adaptability to different force conditions;
- Capability to weld different materials;
- Low setup time;
- Capability to use different tools;
- Easy to tune (change of rotational speed, traverse speed, set forces and set temperature);
- Cheaper than FSW machines;
- Low weight.

The manipulator used is a 6 degrees of freedom (DOF) anthropomorphic robot. The traditional FSW tool (Fig. 1) does not give proper results in terms of weld morphology and tensile strength when applied to polymeric materials. This effect is caused by specific properties of polymeric materials, such as their low melting temperature and low thermal conductivity when compared to metals. The FSW tool was developed with base on previous studies in the field [37] and optimized by trial and error in experimental tests carried out in a FSW machine in the process of welding polymers (Fig. 2) [29]. This tool consists of a stationary shoulder and a conical threaded pin of 5.9 mm length and 10 and 6 mm in diameter, at the base and at the tip of the pin, respectively. A long stationary shoulder was designed in order to allow heating in front of and behind the pin. Furthermore, as in injection moulding of polymers, where during the cooling a minimum threshold of pressure is needed to avoid shrinkage and porosity formation, in FSW of polymers, a minimum

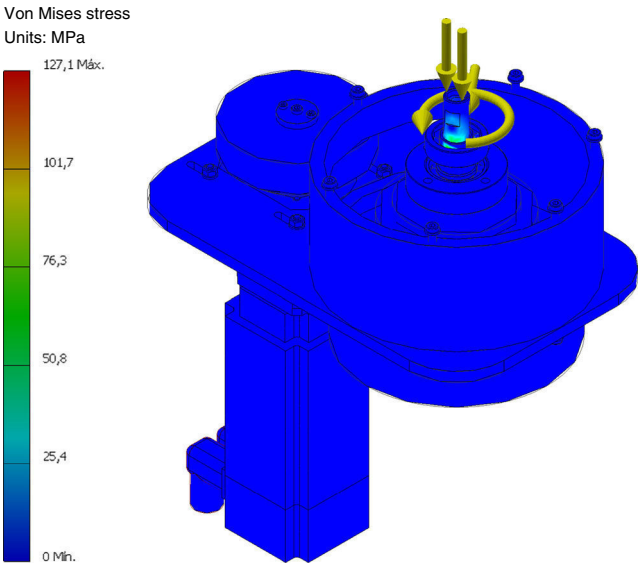

Fig. 5 Stress obtained by FEA

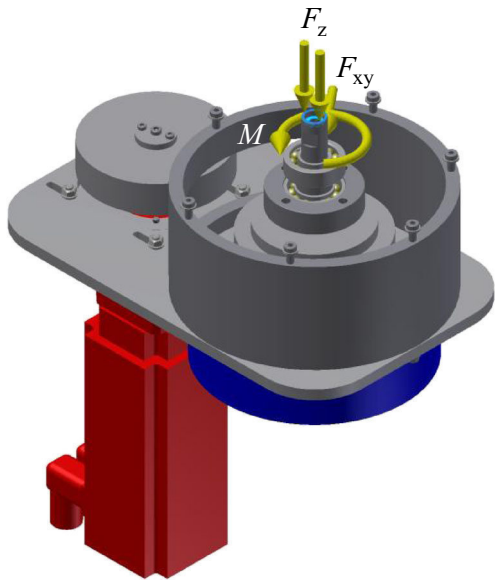

Fig. 4 Major loads acting on the system

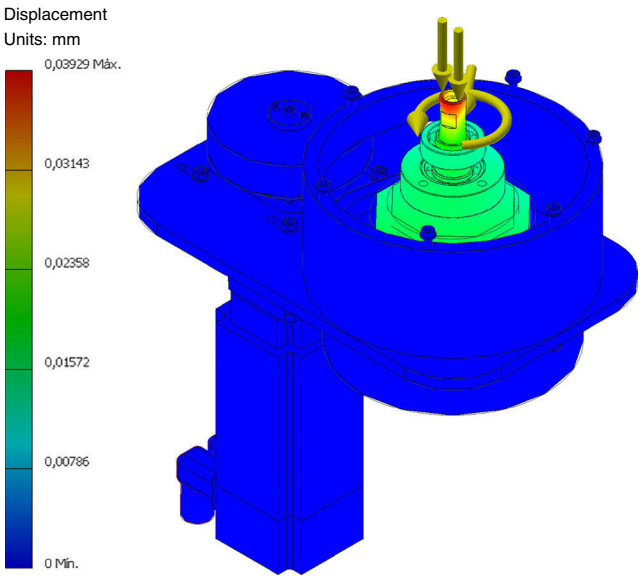

Fig. 6 Displacement obtained by FEA

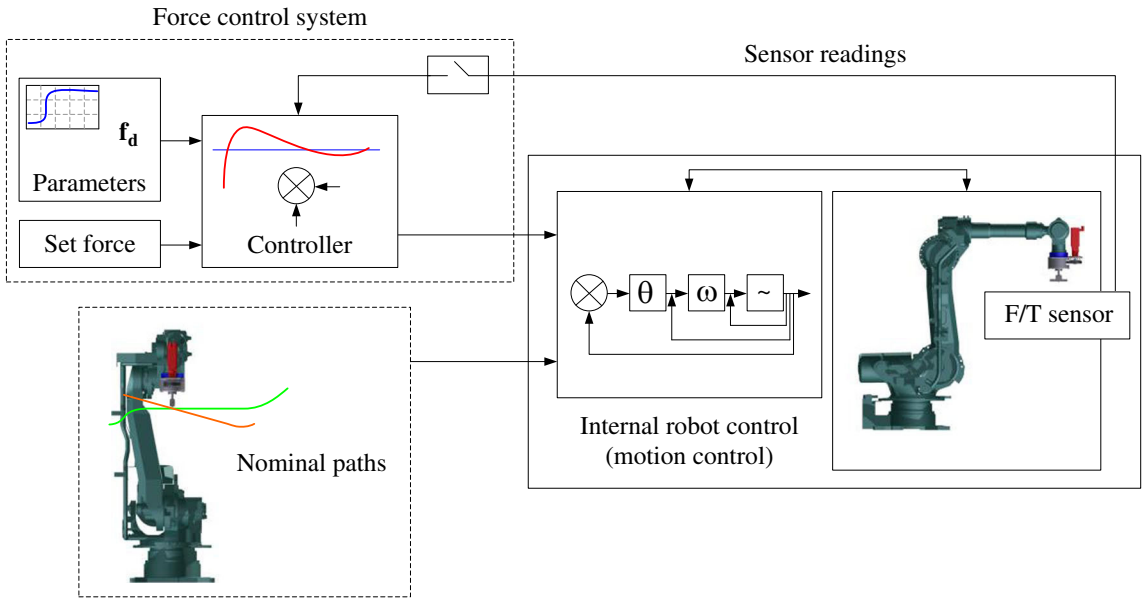

Fig. 7 Control overview of the robotic FSW platform

threshold of axial force is needed to avoid the same defects and improve the mixing of material. This role is played by the long shoulder. Based on previous studies it was decided that the static shoulder must be allowed to move/adapt (during the translation movement of the tool) by itself. In this way, it would be to avoid unnecessary friction, and consequently, loads, inside the tool. Thus, the FSW tool would have a longer life and the required power of the servomotor would be lower. This choice had the disadvantage of requiring an additional support guide to restrict the rotational movement of the shoulder.

This study focuses mainly on the definition of the concept and design of the support of the FSW tool. In terms of concept, it has to have the following functionalities:

- Support the axial forces generated during the process, so that the tool moves in harmony with the robot wrist;
- Transmit power (rotation motion) from the servomotor to the tool;
- Measure forces and torques generated by the welding process (this is necessary for the force/motion control process).

Figure 3 shows the concept. It can be seen that it was decided to align the sixth axis of the robot and the F/T sensor with the FSW tool axis in order to avoid unnecessary shear stress. Rotation motion from the servo motor is transmitted to the tool by means of a belt with a gear ratio i=1.

In terms of mechanical design, the first step was to establish an operating range for the platform according to previous experience and related studies in the field [29–32]. Thus, different threshold values for different parameters were defined (Table 2). The loads acting on the system during the welding process are schematically represented in Fig. 4.

The system design was optimized and validated using finite element analysis (FEA) and considering the loads in Fig. 4 with a factor of safety of 2.5. This optimization was necessary in order to ensure that the solution is mechanically robust without being oversized. Autodesk Simulation was used as FEA software, and the results were obtained with a mesh automatically generated by the software. Figure 5 shows the stress obtained by FEA in which we can see a maximum value of 127 MPa. Since the material is steel with a yield strength of 207 MPa it can be concluded that the system is well designed and has capacity to support the loads involved in the process. Figure 6 shows the maximum displacement obtained by FEA, 0.039 mm, an acceptable value for this kind of equipment.

3 Hybrid force/motion control

As previously mentioned, robotic FSW solutions need force/motion control to produce the desired weld quality. In this

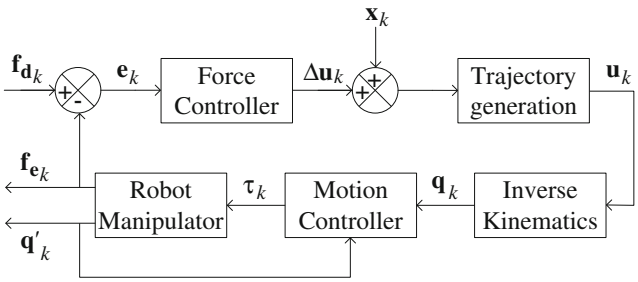

Fig. 8 Hybrid force/motion control system

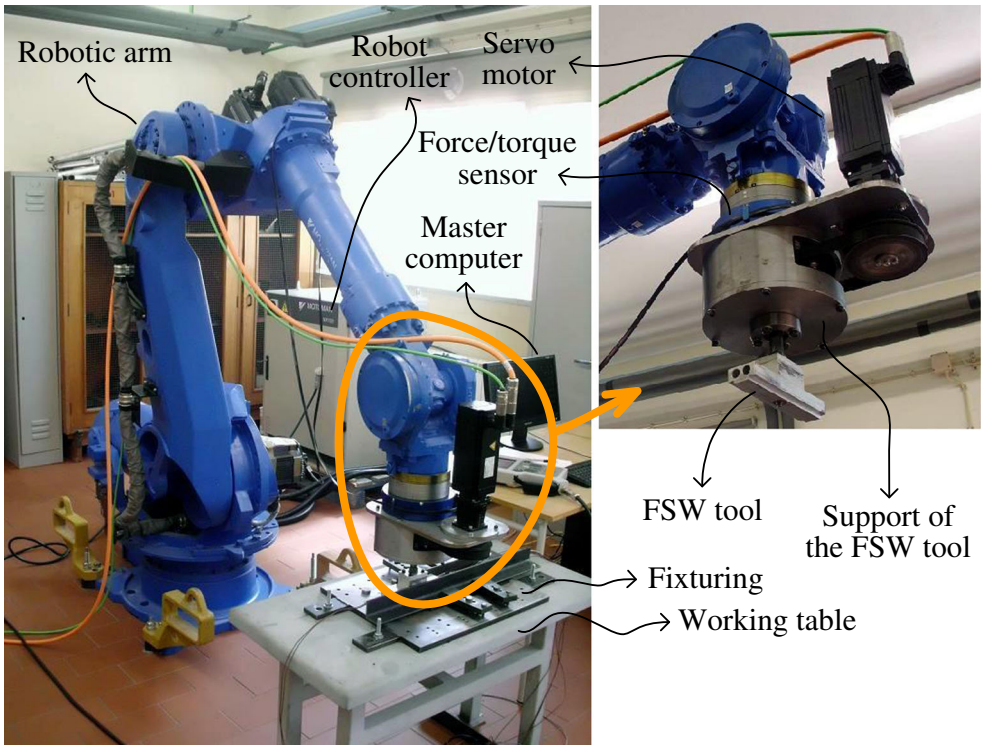

Fig. 9 Hybrid force/motion control system

paper, we are proposing to adjust the plunge depth according to a set axial force. In previous studies, two control methodologies were tested, using a PI and a Fuzzy-PI controller [38, 39]. These controllers showed different behaviours; essentially, the Fuzzy-PI converges faster than the PI controller. On the other hand, the PI controller provides less fluctuation but at the beginning of the process, it has a large overshoot. Figure 7 shows a general control overview of the robotic FSW platform. The process starts with the definition of the nominal robot paths that will be adjusted according to the forces being exerted on the tool during the process [39]. The robot is preprogrammed (nominal paths) by off-line programming as described in previous studies in which target points are extracted from CAD [40]. In order to integrate the force control loop with the motion control loop, the methods presented in [39] are implemented. During the welding process, the forces and torques measured by the F/T sensor and the current pose of the robot end-effector serve as input to the force/motion control system that outputs adjustments for the nominal path. This is done to keep a given set force between the tool and the welding surface. Figure 8 shows the controller in more detail, in which τ is the vector of applied joint torques, q is the vector of joint positions, q' is the vector of actual joint positions, Δu is the vector of correction of displacements and orientations in Cartesian space (plunge depth adjustment), u is the robot displacement in Cartesian space, x is the nominal path, f_d is the desired force (set force) and f_e is the actual force. In addition, the system has incorporated an independent external temperature control system to keep the tool temperature with a desired set value.

4 Implementation

Figure 9 shows the real platform, and Table 3 lists the diverse hardware components applied into the construction of the platform. The servo motor has a maximum rotational speed of 1,500 rpm, a torque of 5.3 Nm and weight of 7 kg (this is a low weight solution). The F/T sensor has a load capacity of 4,000 N along z axis, 2,000 N along x and y axes and a torque of 400 Nm. The robot has a payload of 165 kg and 6 DOF.

Table 3 Hardware components model

Component	Model
Servo motor	SEW PSF221 CMP63M/KY/RH1M/SM1
Servo drive (motor)	MDX61B0014-5A3-4-00/DER11B
F/T sensor	JR3 75E20A-I125-D
Robotic arm	Motoman ES165N
Robot controller	Motoman NX100
Temperature controller	Delta DTD 48
Temperature sensor	Thermocouple J type
Resistances	Resistances of 400 W

Table 4 Parameters used in the welds

Parameter	Weld 1	Weld 2	Weld 3	Weld 4
Type of machine	Robot	Robot	Robot	FSW machine
Set axial force (N)	1,500	Not applied	1,500	1,500
Traverse speed (mm/s)	3.3	3.3	1.6	1.6
Rotational speed (rpm)	1,000	1,000	1,500	1,500
Set temperature (°C)	115	115	115	115

5 Experimental tests and results

Experimental tests were carried out in the process of joining two ABS plates. Butt welds were produced between ABS plates of $300 \times 80 \times 6$ mm^3. The robot is preprogrammed (nominal path) to move the FSW tool linearly along the welding joint. At first, it was necessary to perform some tests to establish what ranges of parameters (control parameters and set temperature) lead to better welds. This is done by trial and error and through visual analysis of the welded seams as well as the analysis of the behaviour of the control system. The ranges for the other parameters (axial force, traverse speed and rotational speed) were analysed and defined in previous studies [29]. From a set of welding tests, four representative tests were chosen to be presented in this manuscript (weld 1, weld 2, weld 3 and weld 4). These tests were performed in the robotic system presented in this manuscript and in a FSW machine with the parameters presented in Table 4. Figure 10 shows a welding being performed in the robotic system.

Figures 11, 12, 13 and 14 show the results of the tests weld 1, weld 2, weld 3 and weld 4, respectively. A visual analysis indicates that Weld 1 presents an acceptable level of quality. In the context of this study, the welded seam quality depends on the following factors:

- Smoothness of the crown seam;
- Quantity of pores or holes in the crown seam;
- Degradation of base material.

In terms of loads applied in the process, after an initial period in which the axial force F_z reaches −1,744 N, it converges to the set force of −1,500 N. It observed a large overshoot which is due to the high weight of the integrative parameter. The value of this parameter is relatively high in order to eliminate any offset. A similar reasoning can be done for the adjustment of the plunge depth Δu. Actually, as shown

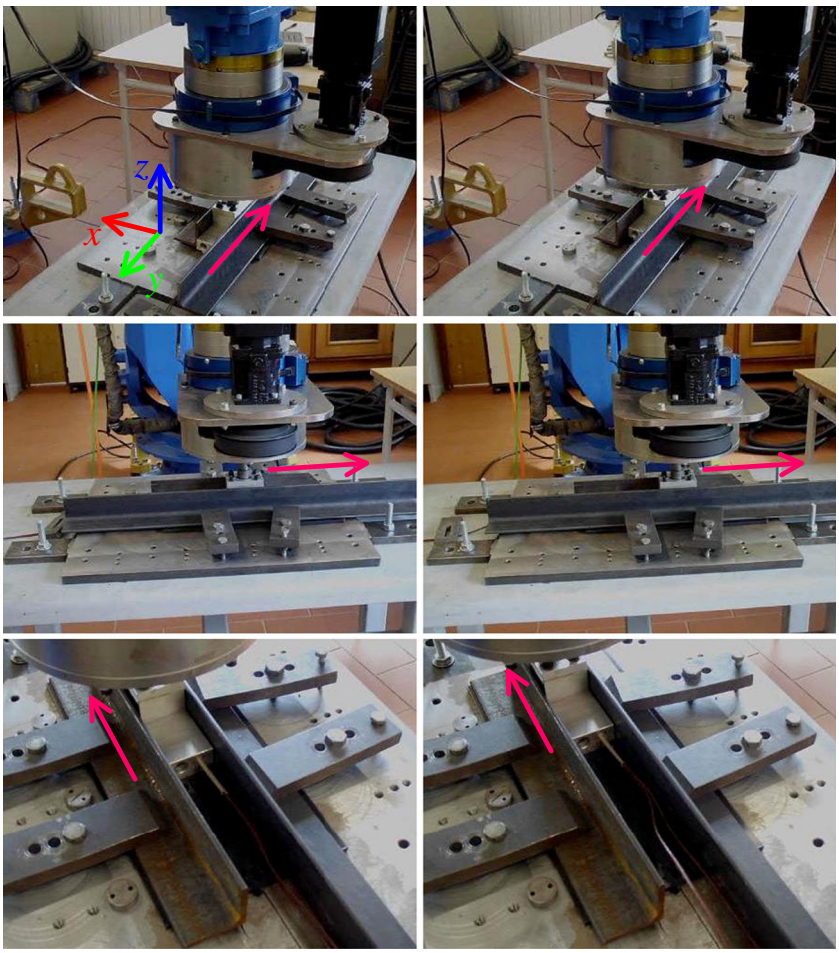

Fig. 10 Experimental tests being performed

in Fig. 11, the adjustment of the plunge depth reached over 3.4 mm. However, these 3.4 mm are not real and are dependent on the inaccuracy of the robot, workpiece deflection and programming error (off-line). In the beginning of the process, the shoulder is not in contact with the upper surface of the workpiece because, as mentioned above, when the robot is programmed in relative coordinates, there are usually positional inaccuracies. Furthermore, by the same reason when a displacement of 3.4 mm is asked to be performed by the robot, the robot does not perform the 3.4 mm exactly. It performs a different quantity which depends on the robot and environment characteristics. The performed displacement quantity is usually lower than the asked quantity [10–13]. It can be observed in Fig. 11 that the output F_z presents a low fluctuation around the set point (less than 5 N) and no offset. This fluctuation comes from noise and some disturbances generated in the robot joints. Since the plates are perfectly flat, they do not introduce disturbances in the system.

As a means of comparison, it was performed a test (weld 2) with no force control, just moving the robot tool linearly along the welding joint according to the parameters in Table 4. From Fig. 12, it can be concluded that the axial force is not enough to compress the melted plastic, producing a welded seam without the desired quality. The welded seam is rough and has an external cavity in almost whole of its depth. Thus, there is a material that was thrown out of the welding joint, and the joining is only established on the root of the seam. The cause of this phenomenon is the existence of a little gap between the shoulder and the welding joint; hence, part of the tool pin volume is out of the welding joint. This leads to less heat generation by friction and hinders heat transfer by conduction between the heating system and the welding joint. Thus, the material of the welding joint is less heated, which means that we have a traverse force with a higher value than when force/motion control is used. In this scenario, the shoulder does not

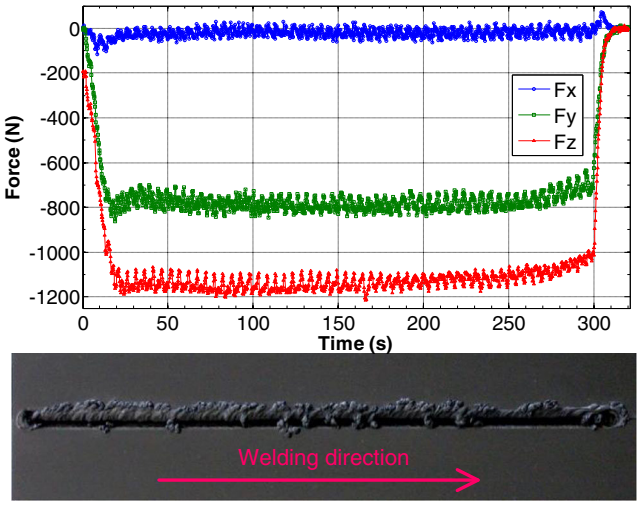

Fig. 12 Resulting weld 2: welded seam and measured loads during robotic FSW process using motion

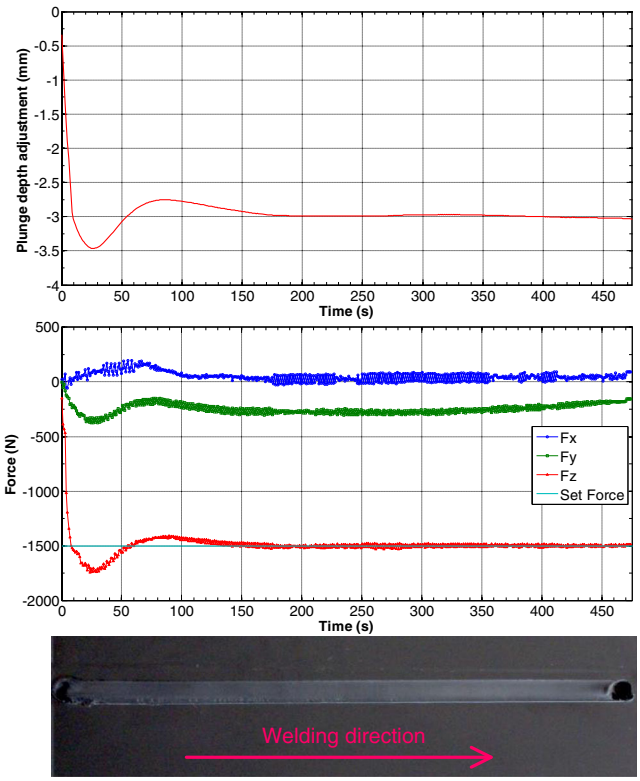

Fig. 11 Resulting weld 1: welded seam, measured loads and plunge depth adjustment during robotic FSW process using force/motion control

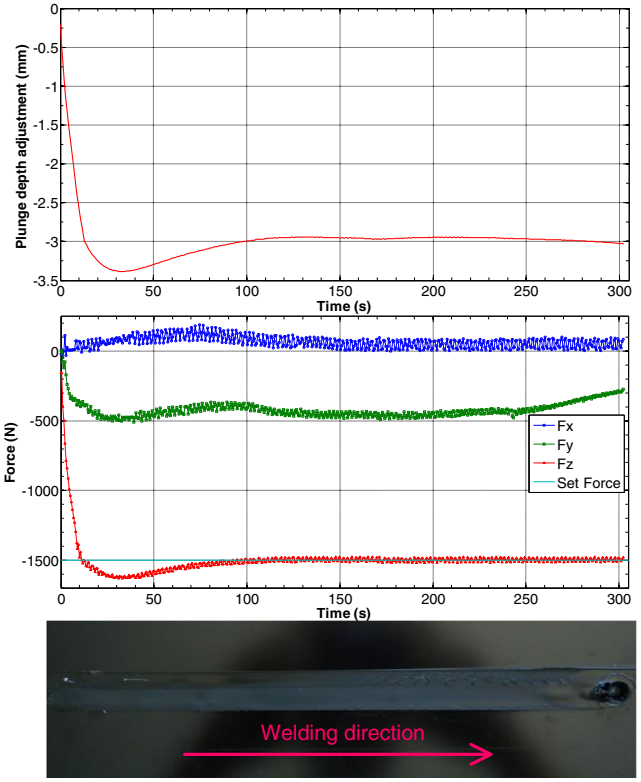

Fig. 13 Resulting weld 3: welded seam, measured loads and plunge depth adjustment during robotic FSW process using force/motion control

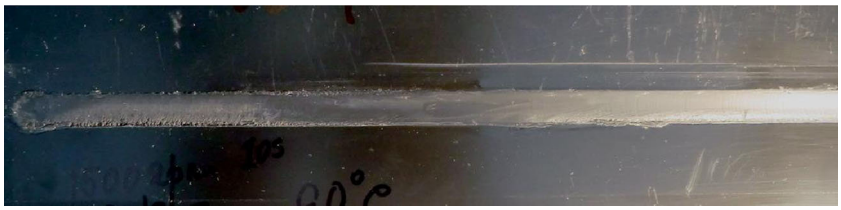

Fig. 14 Resulting weld 4: welded seam performed in a FSW machine

serve its purpose which is to serve as constraint to the molten material.

The weld 3 was performed with the same parameters as the weld 4; the only difference is that the weld 3 was performed in the robotic system and the weld 4 was performed in a FSW machine as shown in Table 4. The resulting welds present very good quality. In general, their qualities are very similar since both welds present a smooth and flat surface. The weld 3 is free of pores, and there was not a production (appearance) of burr. This weld just presents superficial degradation on the end part of the weld. This is due to the excessive heat transmitted to the surface. Since the FSW tool has high thermal inertia and the heating system just controls the warming and not the cooling, sometimes, the surface reaches too much high temperatures. The behaviour of the force/motion control system was similar to weld 1 with the difference that in this case, the overshoot was smaller (only about −1,637 N). In this case, the rotational speed was higher and consequently more heat was generated. Weld material was more softened, leading to lower contact force (different behaviour of the plant (FSW tool/ABS plates)). The weld 4 just presents some pores together with some roughness in the beginning of the welded seam in the retreating side which is the weakest side [29]. There was some burr produced in this weld. On the whole, it can be stated that weld 3 is a little better than weld 4.

By the analysis of Figs. 11, 12 and 13, it is possible to conclude that the robotic system is perfectly stable. Because when there is a small or no variation in plunge depth, the measured axial force suffers a very small variation. The global conclusion is that force/motion control improves FSW quality and is a condition to perform robotic FSW.

6 Conclusion and future work

The complete concept and design of a novel FSW robotic platform for welding polymeric materials has been presented. Experimental results demonstrate that it is possible to weld plastics with an acceptable level of quality using a robotic FSW platform aided by force/motion control and tuned with appropriate process parameters. On the other hand, it was concluded that it is virtually impossible to produce quality welded seams without force/motion (for robotic FSW). Robotic FSW has a number of advantages over common FSW machines: it is more flexible, cheaper, easy and fast to setup and easy to programme. Experimental tests proved the versatility and validity of the solution. The proposed platform can be applied to weld other materials just by changing the loads capacity, the tool and the welding parameters. Future work will seek to integrate other parameters (such as traverse speed, rotational speed, temperature and vibration) in the force/motion controller. To reduce the overshoot in the beginning of the weld, it is intended to use different control parameters in the beginning of the weld and when stationary conditions are reached. Development of FSW tools for complex welding in 3D space will be a target for further research. At this moment, the authors are investigating the capacity of the platform in welding dissimilar materials.

References

1. Neto P, Pereira D, Pires JN, Moreira AP (2013) Real-time and continuous hand gesture spotting: an approach based on artificial neural networks. In: Proc 2013 I.E. Int Conf Robotic Automation (ICRA 2013), pp 178-183, Karlsruhe, Germany
2. Thomas WM, Nicholas ED, Needham JC, Church MG, Templesmith P, Dawes CJ (1991) Friction-stir butt welding. GB Patent 9125978.8, UK
3. Lee RT, Liu CT, Chiou YC, Chen HL (2013) Effect of nickel coating on the shear strength of FSW lap joint between Ni-Cu alloy and steel. J Mater Process Technol 213(1):69–74
4. Sonne MR, Tutum CC, Hattel JH, Simar A, Meester B (2013) The effect of hardening laws and thermal softening on modelling residual stresses in FSW of aluminum alloy 2024-T3. J Mater Process Technol 213(3):477–486
5. Mishra RS, Ma ZY (2005) Friction stir welding and processing. Mater Sci Eng R Rep 50:1–78
6. Gibson BT, Lammlein DH, Prater TJ, Longhurst WR, Cox CD, Ballun MC, Dharmaraj KJ, Cook GE, Strauss AM (2013) Friction stir welding: process, automation, and control. J Manuf Process, 2013
7. Fleming PA, Hendricks CE, Cook GE, Wilkes DM, Strauss AM, Lammlein DH (2010) Seam-tracking for friction stir welded lap joints. J Mater Eng Perform 19(8):1128–1132
8. Zimmer S (2008) Contribution a l'industrialisation du soudage par friction malaxage. PhD thesis, Arts et Métiers ParisTech, Paris, France
9. Okawa Y, Taniguchi M, Sugii H, Marutani Y (2006) Development of 5-axis friction stir welding system. In: Proc SICE-ICASE Int Joint Conf 2006, pp 1266-1269, Busan, Korea
10. Mustafa SK, Pey YT, Yang G, Chen I (2010) A geometrical approach for online error compensation of industrial manipulator. In: IEEE/ASME Int Conf Adv Intell Mechatron, pp 738-743, Montreal, Canada

11. Heisel U, Richter F, Wurst KH (1997) Thermal behavior of industrial robots and possibilities for errors compensation. CIRP Ann Manuf Technol 46(1):283–286
12. Gong C, Yuan J, Ni J (2000) Nongeometric error identification and compensation for robotic system by inverse calibration. Int J Mach Tool Manuf 40(14):2119–2137
13. Ruderman M, Hoffmann F, Bertram T (2009) Modeling and identification of elastic robot joints with hysteresis and backlash. IEEE Trans Ind Electron 56(10):3840–3847
14. Soron M, Lahti KE (2009) Robotic friction stir welding of complex components using RosioTM. Svetsaren 64(1):13–15
15. Fleming PA, Lammlein D, Wilkes D, Fleming K, Bloodworth T, Cook G, Strauss A, DeLapp D, Lienert T, Bement M, Prater T (2008) In-process gap detection in friction stir welding. Sens Rev 28(1):62–77
16. Yavuz H (2004) Function-oriented design of a friction stir welding robot. J Intell Manuf 15:761–775
17. Soron M, Kalaykov I (2006) A robot prototype for friction stir welding. In: Proc 2006 I.E. Conf Robot Autom Mechatron, pp 1-5
18. Smith CB (2000) Robotic friction stir welding using a standard industrial robot. In: Proc 2nd Int Symp Frict Stir Weld
19. Zhao X, Kalya P, Landers RG, Krishnamurthy K (2007) Design and implementation of a nonlinear axial force controller for friction stir welding processes. In: Proc. 2007 American Contr Conf, pp 5553-5558, New York, USA
20. Longhurst WR (2009) Force control of friction stir welding. PhD thesis, University of Vanderbilt, Nashville, TN
21. Longhurst WR, Strauss AM, Cook GE, Fleming PA (2010) Torque control of friction stir welding for manufacturing and automation. Int J Adv Manuf Technol 51:905–913
22. Longhurst WR, Strauss AM, Cook GE (2010) Enabling automation of friction stir welding: the modulation of weld seam input energy by traverse speed force control. J Dyn Syst Meas Control 132:1–11
23. Zhao X, Kalya P, Landers RG, Krishnamurthy K (2009) Path force control for friction stir welding processes. Air Force Res Lab Rep, AFRL-RX-WP-TP-2009-4127, pp 1-8, Wright-Patterson, USA
24. Marcotte O, Abeele LV (2010) 2D and 3D friction stir welding with articulated robot arm. In: Proc 8th Int Symp Frict Stir Weld 2010. Timmendorfer, Germany, pp 778–797
25. Backer JD, Christiansson AK, Oqueka J, Bolmsjö G (2012) Investigation of path compensation methods for robotic friction stir welding. Ind Robot 39(6):601–608
26. Bres A, Monsarrat B, Dubourg L, Birglen L, Perron C, Jahazi M, Baron L (2010) Simulation of friction stir welding using industrial robots. Ind Robot 37(1):36–50
27. Neto DM, Neto P (2013) Numerical modeling of friction stir welding process: a literature review. Int J Adv Manuf Technol 65(1–4):115–126
28. Crawford R, Cook GE, Strauss AM, Hartman DA (2006) Modelling of friction stir welding for robotic implementation. Int J Model Identif Control 1(1):101–106
29. Mendes N, Loureiro A, Martins C, Neto P, Pires JN (2014) Effect of friction stir welding parameters on morphology and strength of acrylonitrile butadiene styrene plate welds. Mater Des 58:457–464
30. Cook GE, Crawford R, Clark DE, Strauss AM (2004) Robotic friction stir welding. Ind Robot 31(1):55–63
31. Zimmer S, Langlois L, Goussain JC, Martin P, Bigot R (2010) Determining the ability of high payload robot to perform FSW applications. In: Proc 8th Int Symp Frict Stir Weld 2010. Timmendorfer, Germany, pp 755–762
32. Backer JD, Soron M, IIal T, Christiansson AK (2010) Friction stir welding with robot for light weight vehicle design. In: Proc 8th Int Symp Frict Stir Weld 2010, pp 14-24, Timmendorfer, Germany
33. Strombeck A, Shilling C, Santos J (2000) Robotic friction stir welding—tool technology and applications. In: Proc 2nd Frict Stir Weld Int Symp, Gothenburg, Sweden
34. Fleming PA, Hendricks CE, Wilkes DM, Cook GE, Strauss AM (2009) Automatic seam-tracking of friction stir welded T-joints. Int J Manuf Technol 45:490–495
35. Cook G, Smartt H, Mitchell J, Strauss A, Crawford R (2003) Controlling robotic friction stir welding. Weld J 82:28–34
36. Smith CB, Hinrichs JF, Crusan A (2003) Robotic friction stir welding: state of the art. In: Proc 4th Frict Stir Weld Int Symp
37. Strand SR (2004) Effects of friction stir welding on polymer microstructure. MS thesis, Brigham Young University, Provo, UT
38. Mendes N, Neto P, Pires JN, Loureiro A (2013) An optimal fuzzy-PI force/motion controller to increase industrial robot autonomy. Int J Adv Manuf Technol 68(1–4):435–441
39. Mendes N, Neto P, Pires JN, Loureiro A (2013) Discretization and fitting of nominal data for autonomous robots. Expert Syst Appl 40(4):1143–1151. doi:10.1016/j.eswa.2012.08.023
40. Neto P, Mendes N (2013) Direct off-line robot programming via a common CAD package. Robot Auton Syst 61(8):896–910

B.1. APPENDIX B1

Materials and Design 58 (2014) 457–464

Contents lists available at ScienceDirect

Materials and Design

journal homepage: www.elsevier.com/locate/matdes

Effect of friction stir welding parameters on morphology and strength of acrylonitrile butadiene styrene plate welds

N. Mendes [a], A. Loureiro [a], C. Martins [b], P. Neto [a,*], J.N. Pires [a]

[a] CEMUC – Universidade de Coimbra, Rua Luís Reis Santos, 3030-788 Coimbra, Portugal
[b] IPC/I3N – Universidade do Minho, Campus de Azurém, 4800-058 Guimarães, Portugal

ARTICLE INFO

Article history:
Received 17 December 2013
Accepted 13 February 2014
Available online 20 February 2014

Keywords:
Friction stir welding
Acrylonitrile butadiene styrene
Stationary shoulder tool
Weld defects
Morphology

ABSTRACT

The aim of this study is to examine the effect of main friction stir welding (FSW) parameters on the quality of acrylonitrile butadiene styrene (ABS) plate welds. Welds were carried out in a FSW machine, using a tool with a stationary shoulder and no external heating system. The welding parameters studied were the tool rotational speed which varied between 1000 and 1500 (rpm); the traverse speed which varied between 50 and 200 (mm/min), and the axial force ranging from 0.75 to 4 (kN). The major novelty is to study the influence of the parameter axial force on FSW of polymers. Produced welds have always a tensile strength below the base material, reaching the maximum efficiencies of above 60 (%) for welds made with higher rotational speed and axial force. Good quality welds are achieved without using external heating, when the tool rotational speed and axial force are above a certain threshold. Above that threshold the formation of cavities and porosity in the retreating side of the stir zone is avoided and the weld region is very uniform and smooth. For low rotational speed and axial force welds have poor material mixing at the retreating side and voids at the nugget. For this reason the strain at break of these welded plates is low when compared with that of base material.

1. Introduction

Friction stir welding (FSW) was initially developed by Thomas et al. [1] in the early nineties for joining soft metals, as aluminium alloys such as those of series 2XXX and 7XXX, which were generally considered unweldable or difficult to weld at that time. The weld seams produced by this method are free from defects such as cracks or porosity; it also produces low distortion as compared to fusion welding processes. This makes FSW a very attractive welding process. The traditional FSW process consists of a rotational tool, formed by a pin and a shoulder, which is inserted into the abutting surfaces of pieces to be welded and moved along the weld joint, as illustrated in Fig. 1. During the process, the pin located inside the weld joint, softs the material and enables plastic flow, causing the mixture of materials. At the same time, the shoulder placed on the surface of the seam heats and drags material from the front to the back side of the tool, prevents leakage of material out of the welding joint and smoothes the crown seam to provide a smooth surface. This process is applied mainly to butt and lap weld joints but other joint geometries can be welded.

FSW of polymers is an attractive welding process because of the characteristics conferred to the welded seam. Strand [2] compared the most common welding processes used to join polymers, concluding that FSW is the process where is achieved higher weld strength efficiency. This process enables the production of very highly efficient welded seams with low energy consumption. In addition, relatively low cost is implied, because of its low use of energy, and it does not require the addition of filler materials. Furthermore, FSW does not require skilled professionals, and can be easily automated. Nelson et al. [3] claimed that the traditional FSW tools do not give proper results in terms of weld morphology and tensile strength when applied to polymeric materials. This effect is caused by specific properties of polymeric materials, such as their low melting temperature and low thermal conductivity when compared to metals. In order to overcome these difficulties, several FSW tools with different geometries have been developed. One such example is that created by Strand [4], called hot shoe, which consists of a rotating pin and a static shoe heated by electrical resistances. This system was patented by Nelson et al. [3] and has been used to weld several polymers, namely acrylonitrile butadiene styrene (ABS), high density polyethylene (HDPE), ultra-high molecular weight polyethylene (UHMWPE), polyvinylchloride

* Corresponding author. Tel.: +351 239790700; fax: +351 239790701.
E-mail addresses: nuno.mendes@dem.uc.pt (N. Mendes), altino.loureiro@dem.uc.pt (A. Loureiro), cmartins@dep.uminho.pt (C. Martins), pedro.neto@dem.uc.pt (P. Neto), jnp@robotics.dem.uc.pt (J.N. Pires).

http://dx.doi.org/10.1016/j.matdes.2014.02.036
0261-3069/

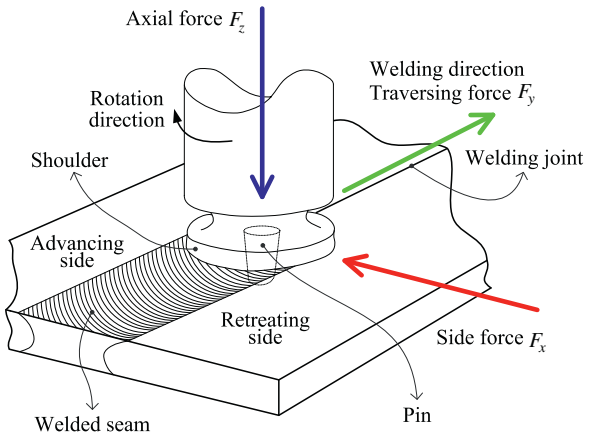

Fig. 1. Representation of the FSW process.

(PVC), polypropylene (PP), polyvinyldenefluoride (PVDF), nylon 6.6 and polytetrafluoroethylene (PTFE). The authors pointed out good results obtained in some welds, in spite of the fact that some welds have presented poor surface finish and few voids. On the other hand, Kiss and Czigány [5] succeeded in joining PP sheets by FSW using conventional milling tools, rotating in the opposite direction to that of milling operations. However, the mechanical properties of the welded seams were poor. Kiss and Czigány [5] presented a new concept of FSW tool: the viblade welding tool consisting of a vibrating blade connected to a vibrating shoe. During the welding process the blade vibrates inside the weld joint while the shoe moves in contact with the upper surface of the weld joint. Although the results of this technique were very good, it presented several drawbacks because of the complexity of the mechanism required to operate the tool, and the short working life of the blade, as concluded by Scialpi et al. [6]. Furthermore, this tool only could be used in welding joints of linear trajectory.

Aydin [7] developed a FSW tool with a larger shoulder, compared to the traditional FSW tool used to weld metallic materials, and a heating system placed at the root of the seam which enables the production of defect-free welds with a basin-like nugget zone. However, the seam welded surface was very rough, with non-aesthetic surface. The same tool concept without heating system has been used in other studies, which are presented below, to investigate the influence of some welding parameters in welded seams quality. The main drawback in the welded seams produced along these studies, as well as in the study carried out by Aydin [7], was bad surface quality of the seams. Bozkurt [8] studied the influence of FSW parameters: rotational speed, traversing speed and tilt angle on high density polyethylene (HDPE) plates. It was concluded that rotational speed is the most influent parameter in the seam quality while tilt angle is the least influent parameter. Payganeh et al. [9] studied the influence of the same parameter investigated by Bozkurt [8] and also the pin tool geometry on a polypropylene (PP) composite with 30% glass fibre. It is reported a taper pin with groove provides better results than other pin shapes. Furthermore, it is shown that larger rotational speed, lower traverse speed and larger tilt angle allows to reach better quality welded seams. In this study is clearly shown that when larger tilt angles are used, better mechanical properties of the welded seams are obtained. As easily understood, when the tilt angle increases, the axial force (Fz in Fig. 1) applied in the welding joint increases too (while the welded seam is being formed). Thus, this study opens the possibility of when higher axial force is used to perform FSW of polymers, higher quality seams are reached. Arici and Sinmaz [10] showed that defects on the seam root can be eliminated by double passes of tool on FSW of medium density polyethylene (MDPE). The influence of the pin geometry in traversing force (Fx in Fig. 1) generated by FSW of polypropylene plates was studied in Panneerselvam and Lenin [11]. The same authors [12] studied the influence of thread direction of the pin in FSW quality of nylon 6. This study concluded that the best seams are obtained when the FSW tool drives material flow towards seam root. These results confirm previous studies presented in Nelson et al. [3]. In recent studies, Kiss and Czigány [13] have proposed the use of a static shoe connected with the milling tool (similar to the hot shoe tool). This new tool has demonstrated promising results, despite not having been adequately explored yet. This is due to the complexity of the tool and the difficulty in controlling certain variables. The tool rotational speed has shown to be the most important parameter in the FSW of PP sheets as shown by Kiss and Czigány [14]. Although other parameters such as tool geometry and size, traverse speed, warming temperature and dwell time also play an important role, as they contribute to heat generation and material flow in the stir zone.

Kiss and Czigány [13] proposed a K factor depending on the rotational speed, traverse speed and tool diameter as a key condition for obtaining good quality welds in polyethylene terephthalate glycol (PETG). The K factor should range from 150 to 400, with each parameter ranging inside maximum and minimum operational limits. However, the K factor does not account for the effect of external heating or the axial force, a parameter which greatly influences the formation of defects at least in FSW of metals. Kim et al. [15] proved that increasing the tool plunge axial force (Fz in Fig. 1) in FSW of aluminium die casting alloy the weld defect size is reduced or removed. In fact, none of the previous studies approaches FSW of polymers taking into account the influence of axial force on the resultant seam. Probably, this is because most of the researchers have used milling machines in their studies, which do not allow either record or control axial force. In robotic welding systems, the axial force must be minimized due to size and cost of robots as it increases with their payload. This axial force can be reduced by increasing the heat generated in the process, adjusting tool rotational speed, and/or adding external heat.

The purpose of this research is to study the influence of rotational and traverse speeds and axial force on the FSW quality on ABS plates. This study takes into account the reduction of axial force required to obtain good quality welds, in order to develop robotic systems adapted to industrial welding of polymers. The effect of external heating is not considered in this stage of the study.

2. Materials and methods

Butt welds were produced between ABS plates of $300 \times 80 \times 6$ (mm^3). Some characteristics of the material are presented in Table 1. ABS is a light material with low glass transition temperature, which has a broad spectrum of applications, such as in the chemical and automobile industries.

A FSW tool consisting of a stationary shoulder and a conical threaded pin of 5.9 (mm) length and 10 (mm) and 6 (mm) in diameter, at the base and at the tip of the pin respectively was developed to perform the welds (Fig. 2). A long stationary shoulder was designed in order to allow heating in front of and behind the pin, although in this set of tests no external heating was applied. The shape of the shoulder is approximately rectangular with a hole in its centre (pin hole). The external dimensions of the shoulder are: 177 (mm) × 25 (mm) and its area is approximately 4396.7 (mm^2).

The welding parameters studied were rotational speed, which varied between 1000 and 1500 (rpm), traverse speed (between 50 and 200 (mm/min)), and the axial force (between 0.75 and 4 (kN)). The selection of these parameters was based on previous tests. Henceforth the welds are designated according to the

Table 1
Main properties of ABS material.

Density (g/cm^3)	Tensile strength (MPa)	Strain at break (%)	Glass transition temperature (°C)
1.04	40.5	50	105

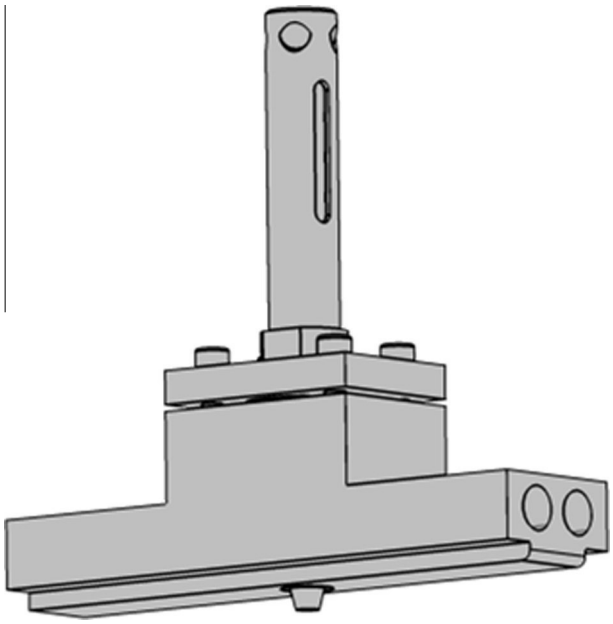

Fig. 2. FSW tool with long stationary shoulder and conical threaded pin.

following convention: letter *R* followed by rotational speed in (rpm); letter *T* followed by traverse speed in (mm/min); and letter *F* followed by the axial force in (KN). Therefore, the designation R1500T200F2 corresponds to a weld carried out with a rotational speed of 1500 (rpm), a traverse speed of 200 (mm/min) and axial force of 2 (kN). All the welds were performed in a FSW machine MTSI-Stir PDS4, which enables the recording of welding data during tests. In order to analyse the effect of tool rotational speed on weld quality, welds were performed with a constant traverse speed and axial force of 100 (mm/min) and 0.75 (KN) respectively, and a variable tool rotational speed of 1000, 1250 and 1500 (rpm). To study the effect of traverse speed, welds were produced with constant rotational speed of 1250 (rpm), axial forces between 2.0 and 3.75 (KN), and traverse speeds of 50, 100 and 200 (mm/min). The effect of axial force on the quality of the weld was investigated for constant rotational and traverse speeds of 1500 (rpm) and 100 (mm/min) respectively, and variable forces of 0.75, 2.25 and 4 (KN), although welds using other forces were also made. Although pressure is a more representative welding parameter than force, it was decided to identify the weld in relation to force. This is because pressure and force parameters are intrinsically related and the majority of the FSW equipment is parameterized by the force parameter and not pressure. In this study, the relation between pressure (*P*) and force (*F*) is given by:

$$P = \frac{F}{A_{\text{shoulder}} + A_{\text{pin cross section}}} = \frac{F}{4425(\text{mm}^2)} \quad (1)$$

where A_{shoulder} is the area of the shoulder and $A_{\text{pin cross section}}$ is the area of the pin cross section at the base of the pin.

For the morphological analysis of the welds, samples were cut out of the weld seams into 10 (μm) thick sections, using a Leitz microtome at room temperature, equipped with a perpendicular slicing glass knife. Optical transmission microscopic analyses were conducted using an Olympus BH transmittance microscope, with digital camera Leica DFC280 and software Leica application suite – LAS V4.

For mechanical tests a minimum of five tensile specimens were removed from each weld, transversely to the welding direction, and tested in a 10 (KN) universal testing machine, SHIMADZU AG-X, at room temperature, according to the ASTM: D638 standard. The samples were submitted to surface smoothing by milling in order to homogenise the thickness of the samples across the gauge section. The local strains were also determined by digital image correlation (DIC) using an Aramis 3D 5M optical system (GOM GmbH) and the procedure described in Leitão et al. [16]. Before testing, the specimens were prepared by applying a black speckle pattern randomly over the surface of the transverse samples previously painted mat white in order to enable data acquisition by DIC.

3. Results and discussion

3.1. Morphological and micrographic analyses

Visual analysis showed that almost all the welds made in this research displayed regular and smooth surface without porosity, as illustrated in Fig. 3 for a weld R1500T100F0.75. This result contradicts other studies where welded seams are full of voids, irregular or rough. The studies carried out by Scialpi et al. [17] resulted in non-flat welds where the welded seam grew out from the surface of the PP plates. The welds produced in PP composite with 30 (%) glass fibre by weight by Payganeh et al. [9] presented an extremely rough surface and in some cases they appeared to be irregular. Panneerselvam and Lenin [12] welded nylon 6 plates in which the produced welds presented a rough surface and pores in some cases.

The effect of tool rotational speed on the morphology of welds is illustrated in Figs. 4 and 5. As observed in Fig. 4 although all welds have a smooth surface, the crown formation at the weld depends on the rotational speed applied. The weld made with the lowest rotational speed (R1000T100F0.75) displayed many cavities on the retreating side (see arrow in Fig. 4(a)) suggesting that the heat generated on this side of the weld was not sufficient to promote bonding of material plastically deformed to the base material. With the increase of the rotational speed, the number of cavities decreased on the retreating side (see weld R1250T100F0.75 in Fig. 4(b)), and virtually disappeared on welds performed with 1500 (rpm), as illustrated in Fig. 4(c).

The defects present in the weld R1000T100F0.75 surface (Fig. 4(a)) extend along the entire thickness of the weld, on the retreating side, as can be seen in the micrograph of the cross section of this weld (Fig. 5(a)) which displays many cavities on the retreating side. In all micrographs the retreating side is located

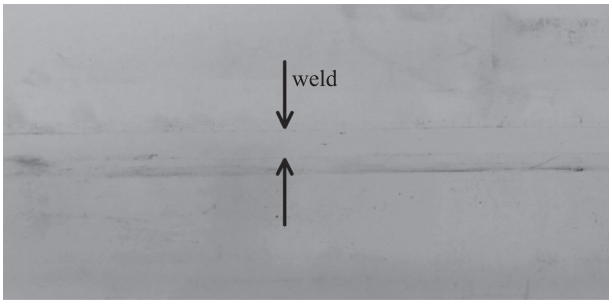

Fig. 3. Welded seam R1500T100F0.75.

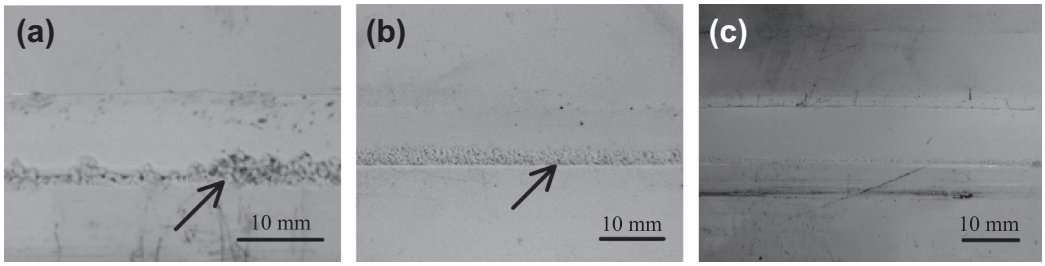

Fig. 4. Effect of rotational speed on the morphology of the weld crown: (a) R1000T100F0.75, (b) R1250T100F0.75 and (c) R1500T100F0.75.

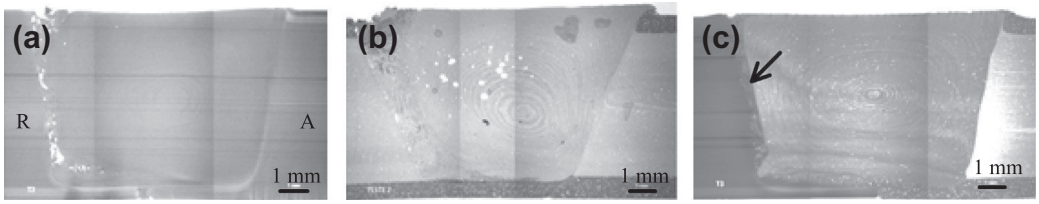

Fig. 5. Micrographs of welds performed with increasing rotational speed: (a) R1000T100F0.75, (b) R1250T100F0.75 and (c) R1500T100F0.75.

on the left, while the advancing side is on the right. This micrograph shows that the lack of bonding extends through the plate thickness. Bagheri et al. [18] have already observed that there was poor mixing of material in retreating side of FSW in ABS plates. This observation suggests that the heat generated on the retreating side is insufficient to establish bonding. This is explained by two factors:

- The heat generated on the advancing side is higher than on the retreating side, as mentioned by Aval et al. [19], who studied the effect of tool geometry on mechanical and microstructural behaviour of aluminium alloys.
- The poor thermal conductivity of ABS, which restricts heat conduction from the advancing to the retreating side.

In addition, the asymmetric flow of material in the stir zone should contribute to the formation of cavities on the retreating side. If the flow of material in the stir zone is similar to that observed in FSW of metals, the material pulled by the shoulder from the retreating to advancing sides is pushed downward within the pin diameter producing an onion ring-like structure, as mentioned by Leal et al. [20], similar to that shown in Fig. 5. However, as the temperature is lower on the retreating side, poor mixing of polymer dragged by the tool was obtained. Nandan et al. [21] show by FSW numerical simulation that in welding of mild steel material flow occurs mainly on the retreating side. The difference in material flow between advancing and retreating sides was also shown by Zhang et al. [22] using numerical simulation. Heutrier et al. [23] describe a dissymmetry between the advancing side and the retreating side of a FSW seam. According to these authors, this difference is due to the torsion and circumventing velocity fields which have different directions on the advancing and retreating sides. An element of material on the advancing side is more influenced by the vortex velocity field than an element of material on the retreating side. The vertical lines visible in the following micrographs are explained by the fact that each image is formed of several photos.

Fig. 5(b) shows that the increase of tool rotational speed to 1250 (rpm) decreased the number of cavities on the retreating side significantly, due perhaps to the increase in heat generated. However, it is still insufficient to promote complete bonding on this side. Furthermore, this image shows the presence of porosity in the nugget. This porosity is aligned with the lines of material flow and concentrated on the retreating side, suggesting that air can be trapped due to inadequate material flow. Oliveira et al. [24] suggest that voids observed in the friction spot welding of poly(methyl methacrylate) (PMMA) can be caused by thermal shrinkage, trapped air or even physicochemical structural changes such as structural water evolution.

With respect to the weld performed at the highest rotational speed (weld R1500T100F0.75), besides its excellent superficial quality, the surface is smooth and uniform and with a reduced porosity (Fig. 4(c)), as mentioned above. The micrograph shows good weld quality, without voids or porosity, and with a good mixture of material in the nugget zone, as illustrated in Fig. 5(c). However, a very narrow region of poorly mixed material can be observed on the retreating side, as shown by the arrow in Fig. 5(c). Therefore, it can be concluded that the increase in the tool rotational speed facilitates the flow and mixing of material, thus reducing the defects in the weld, although it proved insufficient in preventing poor mixing of material in a narrow zone on the retreating side.

The effect of the traverse speed on the weld crown appearance is illustrated in Fig. 6. Welds R1250T50F3.75 and R1250T100F2, made with the lowest traverse speeds, presented excellent superficial finishing, (Figs. 6a and b, respectively), unlike weld R1250T200F3.25, which presents a rough surface (Fig. 6(c)) likely caused by insufficient heat input. In fact, this weld has a ratio of rotational to traverse speeds (R (rpm)/T (mm/min)) of 6.25, while the previous welds show ratios equal to or greater than 10. This factor, as well as the excessive traverse speed, might prevent adequate heating of the shoulder. Nevertheless, no voids or porosity were observed on the surface of the welds. Thus, it can be stated that ratios of rotational/traverse speeds (R (rpm)/T (mm/min)) higher than 10 lead to good weld crown appearance. Weld R1250T100R2 was carried out between two ABS plates, one white and one black, in order to better illustrate the material flow lines. However, this procedure did not yield additional information on the micrographic analysis.

The micrographic images through the thickness direction showed onion ring-like structures in all welds, without regions of poor material mixing (Fig. 7). However, material flow vortices appear close to the root of the welds, when higher traverse speeds are applied (see Fig. 7b and c). Weld R1250T100F2 presents some porosity in the nugget, as does weld R1250T100F0.75, but unlike weld R1250T200F3.25, which was carried out with the same

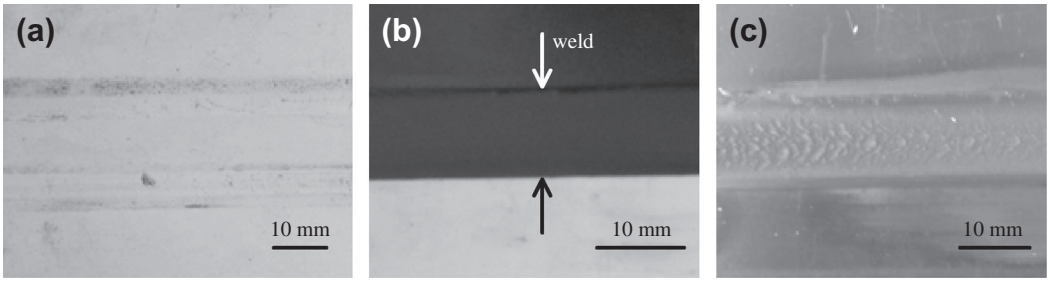

Fig. 6. Effect of traverse speed on the morphology of the weld crown: (a) R1250T50F3.75, (b) R1250T100F2 and (c) R1250T200F3.25.

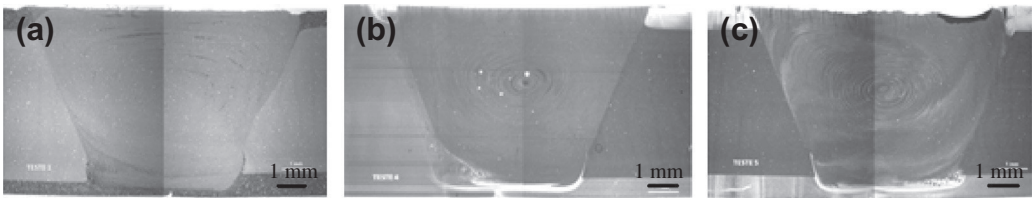

Fig. 7. Micrographs of welds performed with increasing traverse speed: (a) R1250T50F3.75, (b) R1250T100F2 and (c) R1250T200F3.25.

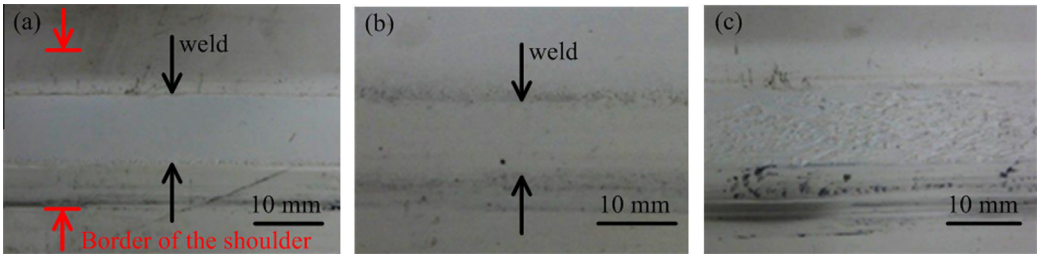

Fig. 8. Effect of axial force on the morphology of the weld crown: (a) R1500T100F0.75, (b) R1500T100F2.25 and (c) R1500T100F4.

rotational and higher traverse speed. This could be explained by the axial force applied in the latter weld, which is much greater than the force used in the weld R1250T100F2.

The effect of axial force on the quality of the weld was analysed based on welds carried out with constant rotational and traverse speeds (1500 (rpm) and 100 (mm/min) respectively), and variable axial forces of 0.75, 2.25 and 4 (KN). The crown appearance of these welds is shown in Fig. 8. The weld performed with the lowest axial force (R1500T100F0.75) displayed good superficial appearance, free of porosity on the crown surface, as shown in Fig. 8(a). The weld seam is uniform and does not present irregularities. The black line in the lower part of the image, which corresponds to the retreating side, was produced near the border of the stationary shoulder, probably due to the excessive heat generated during the process. An increase in axial load brought no substantial changes to the weld surface (see Fig. 8(b)), except for weld R1500T100F4 performed with 4 (KN), where a rough surface can be observed, as shown in Fig. 8(c). This rough surface can be explained by excessive friction between shoulder and polymer due to the high axial force for the heat input used.

The morphological observations through the thickness direction are showing that no cavities or pores formed in the stir zone of the welds (see Fig. 9). This proves that a minimum heat input is required to produce good welds, although weld R1500T100F0.75 (Fig. 9(a)) has a narrow zone of poorly mixed material on the retreating side (indicated by an arrow). This image is shown in Fig. 5(c), where the effect of tool rotational speed is evident. The combined analysis of Figs. 5 and 9 leads to the conclusion that in addition to a minimum threshold of rotational speed, i.e. a minimum amount of heat generated, a minimum axial force is also required in order to constrain the material in the stir zone, and prevent the formation of cavities, pores or zones of poorly mixed material. As in injection moulding of polymers, where a minimum threshold of pressure is needed to avoid shrinkage and porosity formation, in FSW of polymers a minimum threshold of axial force in needed to avoid the same defects and improve the mixing of material.

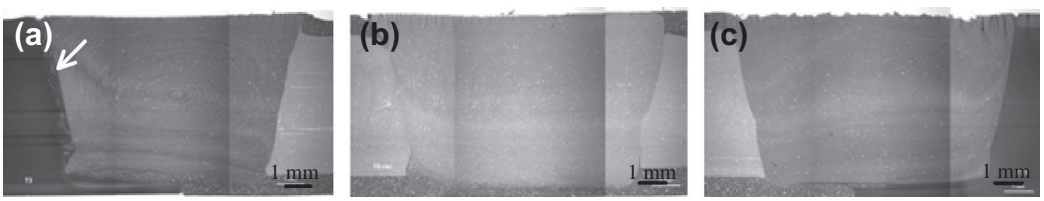

Fig. 9. Micrographs of welds performed with increasing axial force: (a) R1500T100F0.75, (b) R1500T100F2.25 and (c) R1500T100F4.

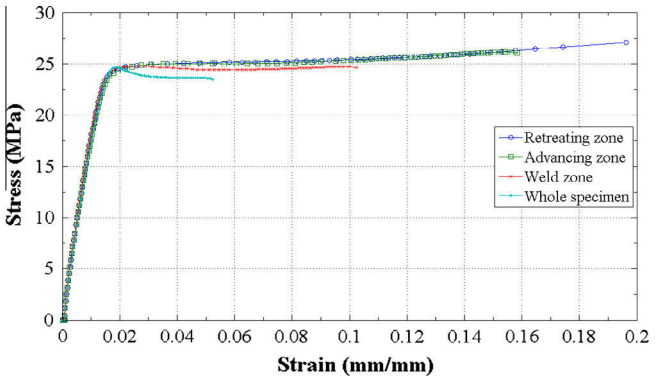

Fig. 10. Stress strain curve of the weld R1500T100F2.25.

3.2. Mechanical performance

Tensile testing was used to assess the effect of the welding parameters on mechanical properties (ultimate strength and strain at break) of the welds. Since DIC was used, the local deformation of the specimen can be considered. Fig. 10 shows a stress strain curve of the weld R1500T100F2.25 taking into account different zones of the specimen (retreating zone, advancing zone, weld zone, and whole specimen). All of these zones can be seen in detail in Fig. 12(b). In the data processing of these stress strain curves were considered mean values (strain and stress) for each zone. The retreating zone is the specimen region where maximum stain is reached. Consequently, the fracture of the sample initiates on the retreating side. The effect of tool rotational speed on stress and strain at break of welds is illustrated in Fig. 11. As this figure shows, tensile strength increases with increasing rotational speed, especially when 1500 (rpm) is applied. This result may be explained by the absent of voids on the retreating side and nugget zone of the sample (see Fig. 5). Therefore, when defects are present breakage is promoted as they work as stress concentration points. Thus, it can be concluded that the increase in rotational speed generates more heat, as stated by Strand [4], providing the proper flow of the polymer in the stir zone and preventing the formation of defects, thus increasing the strength of the welds. In general, the welds tested have a significantly lower tensile strength than the base material (Table 1), although the values obtained are similar to those of Bagheri et al. [18] in ABS welds obtained using a heated tool. This analysis complies with the work of Mostafapour and Azarsa [25] who point out that the increase in rotational speed leads to the local increase of material temperature in the joint line. Due to low thermal conduction of polymeric material, a large

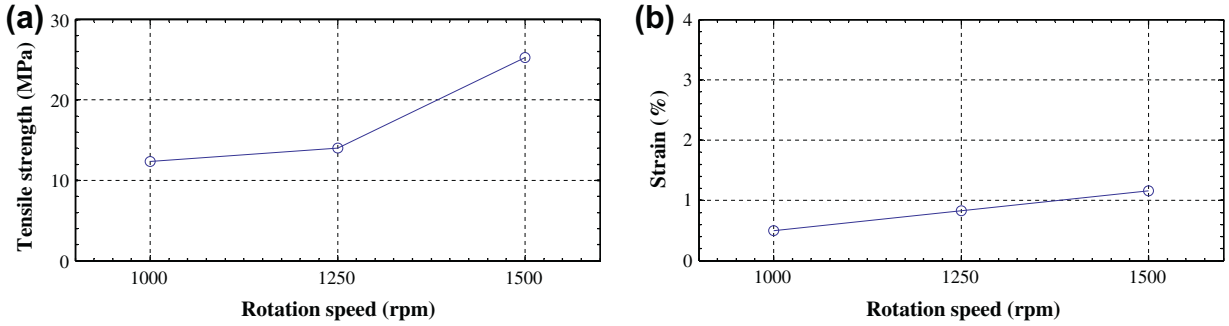

Fig. 11. Effect of tool rotational speed on: (a) tensile strength and (b) strain at break of welds.

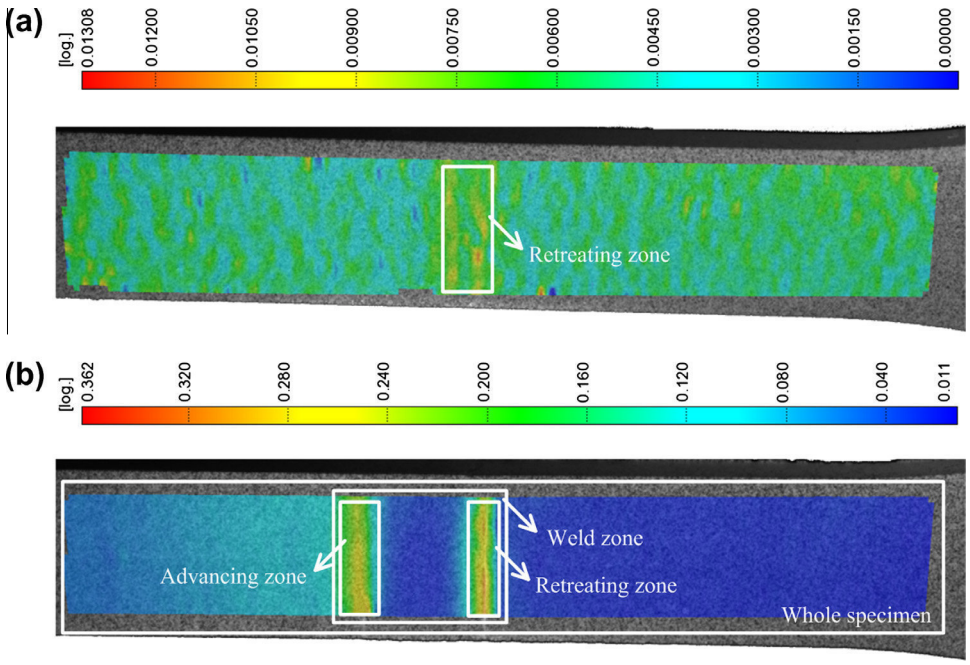

Fig. 12. Image of plastic strain of specimens: (a) R1000T100F0.75 and (b) R1500T100F2.25 just before break (Aramis image).

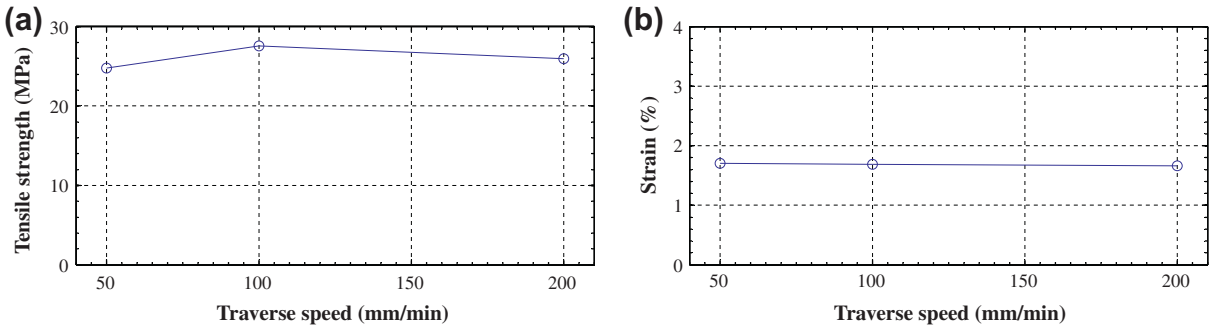

Fig. 13. Effect of tool traverse speed on: (a) tensile strength and (b) strain at break of welds.

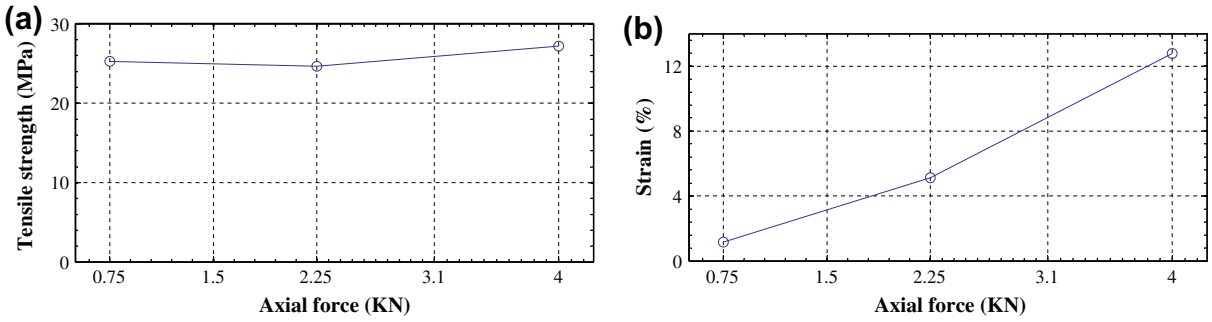

Fig. 14. Effect of tool axial force on: (a) tensile strength and (b) strain at break of welds.

amount of heat concentrates in the nugget zone. Consequently, the amount of molten material around the pin increases, and the stirring conditions are improved.

Fig. 11(b) shows that the increase in the tool rotational speed only generates a small increase in strain at break of the welds, despite being lower than the base material. This is because during the test plastic deformation concentrates at the transitions between the stir zone and the base material, mainly on the retreating side of the former where there is poor adhesion of the material, causing premature failure. Fig. 12 illustrates the actual strain field just before break on two tensile specimens removed from welds R1000T100F0.75 (Fig. 12(a)) and R1500T100F2.25 (Fig. 12(b)). The weld R1000T100F0.75 (Fig. 12(a)) has a specific zone on the retreating side with many cavities as shown in Fig. 5(a) and therefore the plastic deformation concentrates mainly on the retreating side of the weld, as shown by the yellow zone (see colour code above Fig. 12(a)). The weld R1500T100F2.25 (Fig. 12(b)) has no specific zone of poor mixing of material as shown in Fig. 9(b), and therefore the plastic deformation concentrates on both sides of the weld, as shown by the red and yellow zones (see colour code above Fig. 12(b)). The higher strain is reached in the retreating side as indicated in Fig. 10.

Regarding the influence of traverse speed on strength and strain at break of welds it is observed that there is no effect on the referred properties, at least for welds using high tool rotational speed (1250 (rpm)), as illustrated in Fig. 13. This can be explained by the poor thermal conductivity of the polymer which prevents the heat generated by the tool rotational from being transferred to the surrounding material. This is confirmed by the weld morphology that is similar in the different welds as shown in Fig. 7. Furthermore, these results comply with those of Sorensen et al. [26], who welded several polymeric materials (PP and HDPE) and concluded that traverse speed does not influence the weld quality. However, this results contradict recent results of Bagheri et al. [18], obtained on welds in ABS polymer. These authors report that the loss of strength of the welds with the increase in traverse speed is due to the poor mixing of the material caused by the reduction of the heat input from the heated shoe. In the present case no external heating system was used, and the heat was generated solely by tool rotation; no significant degradation of material mixing with increasing traverse speed could be observed, as shown in Fig. 7.

Table 2
Tensile strength efficiency (%) and strain of welds (%).

W (RPM) → F (KN) ↓	1000		1250		1500	
	Strength efficiency (%)	Strain (%)	Strength efficiency (%)	Strain (%)	Strength efficiency (%)	Strain (%)
[0.75,1.5]	31	0.51	35	0.83	62	1.16
[1.5,3.0]	43	1.22	68	1.69	61	5.12
[3.0,4.0]	54	1.73	64	1.66	67	12.79

The effect of axial force on FSW of polymers has rarely been analysed in the literature because most of the welds are carried out in milling machines, where external force control devices are required. As previously mentioned, the axial force plays an important role in controlling the formation of defects in FSW of metals. In the present case axial force influences material mixture (Fig. 9), as well as the tensile plastic performance of welds, as shown in Fig. 14. Fig. 14(a) shows that the increase in axial force does not result in any tensile strength change. However, it is observed that is essential to improve the plastic strain performance of the weld, as illustrated in Fig. 14(b). In fact, welds performed with high tool rotational speed (1500 (rpm)) and high axial force (4 (kN)) have average strain at break values of approximately 12.8 (%) unlike most of the other welds, which fail to reach 2 (%). This is because the increase in axial force promotes better material mixing on the retreating side, providing welds without a zone of weak material mixture, as shown in Fig. 9.

Nevertheless, all the specimens broke on the retreating side. This phenomenon has been studied by Bagheri et al. [18], who pointed out that material flow on advancing and retreating sides is quite different. Thus, lack of material on the retreating side can occur, which in turn increases brittleness in this zone.

The simultaneous effect of both tool rotational speed and axial force on the strength efficiency and strain of welds is shown in Table 2. The strength efficiency is the ratio between tensile strength of welds and base material. Table 2 shows that welds with strength efficiency rates above 60 (%) are reached when high tool rotational speed and axial force are used; furthermore, the axial force required to do welds with good quality decreases with increasing rotational speed. A similar effect is observed for strain, high strain performance is reached when high rotational speed and axial force are used. By the analysis of Table 2, it can be state that axial force is the most influent parameter to obtain high strain welds. Strain at break above 10 (%) is attained only in welds carried out with high tool rotational speed and axial force. The numbers between brackets in the left column of the Table 2 represent ranges of force.

The results of this study show that the strength of the weld is governed by the strength of the retreating side, which depends on the material flow in this zone. The adequate flow of material in this zone is only achieved for tool rotational speeds and axial forces above a certain threshold (rotational speed higher than 1250 (rpm) and axial force higher than 1.5 (KN)), when external heating is not used.

4. Conclusions

The aim of the present research is to study the effect of the tool rotational and traverse speeds, as well as the axial force, on the quality of welds carried out by friction stir welding on acrylonitrile butadiene styrene (ABS) plates, using a stationary shoulder tool without external heating. Based on the experimental results and discussion, the following conclusions can be drawn:

- It is feasible to produce good quality welds without any external heating.
- Tool rotational speed and axial force values above a certain threshold (rotational speed higher than 1250 (rpm) and axial force higher than 1.5 (KN)) are required to produce welds free of defects.
- Tool rotational speed generates the heat for plasticizing the polymer and promotes adequate material mixing.
- The axial force contributes to material mixing and prevents the formation of cavities in the retreating side of stir zone.
- The tensile strength and strain at break of welds is always below that of the base material.
- Welds of high strength efficiency and strain at break are achieved only when high rotational speed and high axial force are used.
- The main influence of traverse speed, when external heating is not used, is on the weld crown appearance. Good weld crown appearance is obtained when sufficient heat is provided to the welding joint. Thus, ratios of rotational / traverse speeds (R (rpm)/T (mm/min)) higher than 10 lead to good weld crown appearance.

Acknowledgements

This research is supported by FEDER funds through the program COMPETE (*Programa Operacional Factores de Competitividade*), under the project CENTRO-07-0224-FEDER-002001(MT4MOBI) and by national funds through FCT (*Fundação para a Ciência e a Tecnologia*) under the projects PEst-C/EME/UI0285/2011, PEst-C/EME/UI0285/2013, PEst-C/CTM/LA0025/2011 and the grant no. SFRH/BD/62485/2009. The authors are grateful to ThyssenKrupp Portugal – Aços e Serviços SA for the heat treatment of the FSW tools.

Appendix A. Supplementary material

Supplementary data associated with this article can be found, in the online version, at http://dx.doi.org/10.1016/j.matdes.2014.02.036.

References

[1] Thomas WM, Nicholas ED, Needham JC, Church MG, Templesmith P, Dawes CJ. Friction-stir butt welding. G.B. Patent 9125978.8, UK, 1991.
[2] Strand S. Joining plastics – can friction stir welding compete? In: Proceeding of the Electrical Insulation Conference and Electrical Manufacturing and Coil Winding Technology Conference; 2003, p. 321–6.
[3] Nelson TW, Sorenson CD, Johns CJ. Friction stir welding of polymeric materials. US Patent US6811632B2; US, 2004.
[4] Strand SR. Effects of friction stir welding on polymer microstructure. Master's Thesis, Brigham Young University, 2004.
[5] Kiss Z, Czigány T. Applicability of friction stir welding in polymeric materials. Periodica Polytech 2007;51(1):15–8.
[6] Scialpi A, Troughton M, Andrews S, De Filippis LAC. In-line reciprocating friction stir welding of plastics. Join Plast – Fügen Von Kunststoffen 2007;1:42–51.
[7] Aydin M. Effects of welding parameters and pre-heating on the friction stir welding of UHMW-Polyethylene. Polym Plast Technol Eng 2010;49:595–601.
[8] Bozkurt Y. The optimization of friction stir welding process parameters to achieve maximum tensile strength in polyethylene sheets. Mater Des 2012;35:440–5.
[9] Payganeh GH, Mostafa Arab NB, Dadgar Asl Y, Ghasemi FA, Saeidi Boroujeni M. Effects of friction stir welding process parameters on appearance and strength of polypropylene composite welds. Int J Phys Sci 2011;6(19):4595–601.
[10] Arici A, Sinmaz T. Effects of double passes of the tool on friction stir welding of polyethylene. J Mater Sci 2005;40:3313–6.
[11] Panneerselvam K, Lenin K. Investigation on effect of tool forces and joint defects during FSW of polypropylene plate. Procedia Eng 2012;38:3927–40.
[12] Panneerselvam K, Lenin K. Joining of nylon 6 plate by friction stir welding process using threaded pin profile. Mater Des 2014;53:302–7.
[13] Kiss Z, Czigány T. Effect of welding parameters on the heat affected zone and the mechanical properties of friction stir welded poly(ethylene-terephthalate-glycol). J Appl Polym Sci 2012;125:2231–8.
[14] Kiss Z, Czigány T. Microscopic analysis of the morphology of seams in friction stir welded polypropylene. Express Polym Lett 2012;6(1):54–62.
[15] Kim YG, Fujii H, Tsumura T, Komazaki T, Nakata K. Three defect types in friction stir welding of aluminum die casting alloy. Mater Sci Eng 2006;415:250–4.
[16] Leitão C, Galvão I, Leal RM, Rodrigues DM. Determination of local constitutive properties of aluminium friction stir welds using digital image correlation. Mater Des 2012;33:69–74.
[17] Scialpi A, Troughton M, Andrews S, De Filippis LAC, Viblade TM. Friction stir welding for plastics. Weld Int 2009;23(11):846–55.
[18] Bagheri A, Azdast T, Doniavi A. An experimental study on mechanical properties of friction stir welded ABS sheets. Mater Des 2013;43:402–9.
[19] Aval HJ, Serajzadeh S, Kokabi AH, Loureiro A. Effect of tool geometry on mechanical and microstructural behaviour in dissimilar friction stir welding of AA 5086–AA 6061. Sci Technol Weld Join 2011;16(7):597–604.
[20] Leal RM, Leitão C, Loureiro A, Rodrigues DM, Vilaça P. Material flow in heterogeneous friction stir welding of thin aluminium sheets: effect of shoulder geometry. Mater Sci Eng 2008;498:384–91.
[21] Nandan R, Roy GG, Lienert TJ, Debroy T. Three dimensional heat and material flow during friction stir welding of mild still. Acta Mater 2007;55:883–95.
[22] Zhang HM, Zhang Z, Chen ZT. The finite element simulation of the friction stir welding process. Mater Sci Eng 2005;403:340–8.
[23] Heutrier P, Jones MJ, Desrayaud C, Driver JH, Montheillet F, Dllehaux D. Mechanical and thermal modelling of friction stir welding. J Mater Process Technol 2006;171:348–57.
[24] Oliveira PHF, Amancio-Filho ST, dos Santos JF, Hage Jr E. Preliminary study on the feasibility of friction spot welding in PMMA. Mater Lett 2010;64(19):2098–101.
[25] Mostafapour A, Azarsa E. A study on the role of processing parameters in joining polyethylene sheets via heat assisted friction stir welding: Investigating microstructure, tensile and flexural properties. Int J Phys Sci 2012;7(4):647–54.
[26] Sorensen CD, Nelson TW, Strand SR, Johns C, Christensen J. Joining of thermoplastics with friction stir welding. In: Proceedings of ANTEC 2001, Society of Plastics Engineers, Dallas, USA; 2001, p. 1031–5.

B.2. APPENDIX B2

Materials and Design 64 (2014) 81–90

Contents lists available at ScienceDirect

Materials and Design

journal homepage: www.elsevier.com/locate/matdes

Morphology and strength of acrylonitrile butadiene styrene welds performed by robotic friction stir welding

N. Mendes [a], A. Loureiro [a], C. Martins [b], P. Neto [a,*], J.N. Pires [a]

[a] CEMUC – Universidade de Coimbra, Rua Luís Reis Santos, 3030-788 Coimbra, Portugal
[b] IPC/I3N – Universidade do Minho, Campus de Azurém, 4800-058 Guimarães, Portugal

ARTICLE INFO

Article history:
Received 14 May 2014
Accepted 14 July 2014
Available online 30 July 2014

Keywords:
Robotic friction stir welding
Acrylonitrile butadiene styrene
Stationary shoulder tool
Weld defects
Mechanical properties

ABSTRACT

The aim of this study is to examine the main factors affecting friction stir welding (FSW) of acrylonitrile butadiene styrene (ABS) plates, performed by a robotic system developed to this purpose. Welds were carried out using a tool with stationary shoulder and an external heating system. The welding parameters studied were the axial force, rotational and traverse speeds and temperature of the tool. The major novelty is to perform FSW of a polymer in a robotic system and to study the influence of the axial force on weld quality. In a robotic solution the control of axial force allows to eliminate robot positional errors and guarantee the contact between the FSW tool and the work pieces. Strength and strain properties of the welds are evaluated and correlated with the morphology of the welded zone. A comparison between welds produced in the robotic FSW system and in a dedicated FSW machine is presented. It is shown the feasibility of robotic FSW of ABS without deteriorating the mechanical properties of the welds in relation to those produced in the dedicated FSW machine.

1. Introduction

FSW of polymers is an attractive welding process due to the characteristics conferred to the welds. Strand [1] compared the most common welding processes used to join polymers, concluding that FSW is the process where it is achieved higher weld strength efficiency. This process enables the production of highly efficient welded seams with low energy consumption. In addition, relatively low cost is implied, because of its low use of energy, and it does not require the addition of filler materials. Furthermore, FSW does not require skilled professionals, and can be easily automated. The traditional FSW process is illustrated in Fig. 1. Nelson et al. [2] claimed that the traditional FSW tools do not give proper results in terms of weld morphology and tensile strength when applied to polymeric materials. This effect is caused by specific properties of polymeric materials, such as their low melting temperature and low thermal conductivity when compared to metals. In order to overcome these difficulties, several FSW tools with different geometries have been developed. One such example is that created by Strand [3], called hot shoe, which consists of a rotating pin and a static shoe heated by electrical resistances. This author pointed out good results obtained in some welds, in spite of the fact that some welds have presented poor surface finish and few voids. On the other hand, Kiss and Czigány [4] succeeded in joining polypropylene (PP) sheets by FSW using conventional milling tools, rotating in the opposite direction to that of milling operations. However, the mechanical properties of the welded seams were poor. Scialpi et al. [5] presented a new concept of FSW tool: the Viblade welding tool consisting of a vibrating blade connected to a vibrating shoe. During the welding process the blade vibrates inside the weld joint while the shoe moves in contact with the upper surface of the weld joint. Although the results of this technique were very good, it presented several drawbacks because of the complexity of the mechanism required to operate the tool, and the short working life of the blade, as concluded by Scialpi et al. [6]. Furthermore, this tool only could be used in welding joints of linear trajectory.

Aydin [7] developed a FSW tool with a larger shoulder, compared to the traditional FSW tool used to weld metallic materials, and a heating system placed at the root of the seam which enables the production of defect-free welds with a basin-like nugget zone. However, the weld crown surface was very rough, with non-aesthetic surface. The same tool concept without heating system has been used in other studies, which are presented below [8–12], to investigate the influence of some welding parameters in welded seams quality. The main drawback in the welded seams

* Corresponding author. Tel.: +351 239790700; fax: +351 239790701.
E-mail addresses: nuno.mendes@dem.uc.pt (N. Mendes), altino.loureiro@dem.uc.pt (A. Loureiro), cmartins@dep.uminho.pt (C. Martins), pedro.neto@dem.uc.pt (P. Neto), jnp@robotics.dem.uc.pt (J.N. Pires).

http://dx.doi.org/10.1016/j.matdes.2014.07.047
0261-3069/

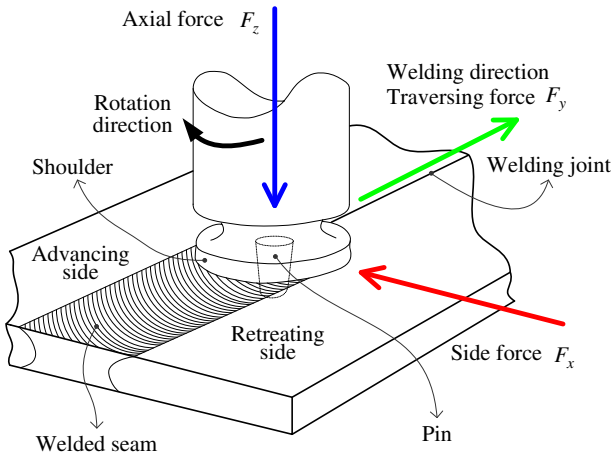

Fig. 1. Representation of the FSW process.

produced along these studies, as well as in the study carried out by Aydin [7], was bad surface quality of the welds. Bozkurt [8] studied the influence of FSW parameters: rotational speed, traversing speed and tilt angle on high density polyethylene (HDPE) plates. It was concluded that rotational speed is the most influent parameter in the seam quality while tilt angle is the least influent parameter. Payganeh et al. [9] studied the influence of the same parameter investigated by Bozkurt [8] and also the pin tool geometry on a polypropylene (PP) composite with 30% glass fibre. It is reported that a taper pin with groove provides better results than other pin shapes. Furthermore, it is shown that larger rotational speed, lower traverse speed and larger tilt angle allows to reach better quality welds. Arici and Sinmazçelýk [10] showed that defects on the seam root can be eliminated by double passes of tool on FSW of medium density polyethylene (MDPE). The influence of the pin geometry in traversing force (*Fx* in Fig. 1) generated by FSW of PP plates was studied in Panneerselvam and Lenin [11]. The same authors [12] studied the influence of thread direction of the pin in FSW quality of nylon 6. This study concluded that the best seams are obtained when the FSW tool drives material flow towards seam root. These results confirm previous studies presented in Nelson et al. [2]. Kiss and Czigány [13] have proposed the use of a static shoe connected with the milling tool (similar to the hot shoe tool). This new tool has demonstrated promising results, the best welds performed in PP and polyethylene terephthalate glycol (PETG) displayed about 90 (%) of tensile strength observed in the base material. The tool rotational speed has shown to be the most important parameter in the FSW of PP sheets as shown by Kiss and Czigány [14]. Although other parameters such as tool geometry and size, traverse speed, warming temperature and dwell time also play an important role, as they contribute to heat generation and material flow in the stir zone. Bagheri et al. [15] have studied the influence of welding parameters rotational speed, traverse speed and shoulder temperature at the beginning of the FSW process. A hot shoe tool was used in this study and the good results allowed by this tool were observed once more. However, quality welds are only reported at low traverse speed values. A recent study proposed by Pirizadeh et al. [16] presented a new concept of FSW tool named self-reacting friction stir welding (SRFSW). This tool consists of two non-rotational opposing shoulders on the crown and root sides of the joint. It was studied the influence of the process parameters tool rotational speed, tool translational speed and shape of the pin. In spite of the fact that the authors have reported good results (high weld tensile strength), they are worse than the results presented by other studies [15,17]. This is likely because the design of the FSW tool that prevents the tool operates at high rotational speed and generates enough heat to promote a strong bond.

Kiss and Czigány [13] proposed a *K* factor depending on the rotational speed, traverse speed and tool diameter as a key condition for obtaining good quality welds. The *K* factor should range from 150 to 400, with each parameter ranging inside maximum and minimum operational limits. However, the *K* factor does not account for the effect of external heating or the axial force, a parameter which greatly influences the formation of defects. Mendes et al. [17] proved that increasing the tool plunge axial force (*Fz* in Fig. 1) in FSW of ABS the weld defect size is reduced or removed and mechanical properties are improved. In fact, none of the previous studies use a robot to perform FSW of polymers and just Mendes et al. [17] present a preliminary study of the influence of axial force on the resultant welds. The use of anthropomorphic industrial robots in the FSW process can reduce the costs associated to this welding process and increase its flexibility. However, anthropomorphic industrial robots when submitted to high loads tend to present positional errors due to several factors:

- Low stiffness associated to its articulated structure.
- Vibrations due to robot structure and rotation of the tool.
- Positional error associated to the off-line programming process.

These kinds of difficulties are pointed out by Schneider et al. [18] and Leali et al. [19] in robotic machining, a manufacturing process that also requires high load capability. In this context, it is expected that the use of an industrial robot to perform FSW will require high load capabilities to produce quality welds. The majority of the published studies about FSW of polymers have been carried out in conventional milling machines that are robust machines and no positional or vibration difficulties arise.

In robotic welding systems, the axial force must be minimized due to the size and cost of robots as it increases with their payload. This axial force can be reduced by increasing the heat generated in the process, adjusting tool rotational speed, and/or adding external heat. The authors did not find any study in literature making mention to the application of anthropomorphic robots with low bearing capacity performing FSW in polymers.

This paper studies the influence of welding parameters on the microstructure and mechanical properties of welds produced in a robotic system. The welding parameters analysed are axial force, rotational speed and traverse speed. Furthermore, the influence of tool temperature in weld crown appearance is also analysed. The presented welds were performed in a robotic system which may introduce some perturbations in the FSW process due to the reduced stiffness of the mechanical structure of an anthropomorphic robot when it operates with relatively high contact forces. Because of that, robotic welds were compared with welds performed in a conventional FSW machine [17], in order to analyse the influence on the weld quality of the robotic system developed.

2. Materials and methods

Square butt welds were produced between ABS plates of $300 \times 80 \times 6$ (mm^3). Some characteristics of the material are presented in Table 1. ABS is a light material with low glass transition temperature, which has a broad spectrum of applications such as in the chemical and automobile industries.

A FSW tool consisting of a stationary shoulder and a conical threaded pin of 5.9 (mm) length and 10 (mm) and 6 (mm) in diameter, at the base and at the tip of the pin respectively, was developed to perform the welds (Fig. 2). A long stationary shoulder was designed in order to allow heating in front of and behind the

Table 1
Main properties of ABS material.

Density (g/cm^3)	Tensile strength (MPa)	Strain at break (%)	Hardness (HV0.2)	Glass transition temperature (°C)
1.04	40.5	50	11	105

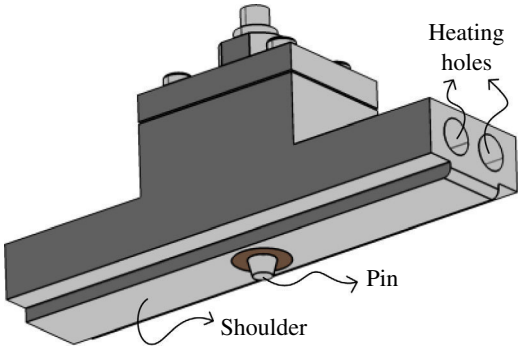

Fig. 2. FSW tool with long stationary shoulder and conical threaded pin.

pin. The shape of the shoulder is approximately rectangular with a hole in its centre (pin hole). The external dimensions of the shoulder are: 177 (mm) × 25 (mm) and its area is approximately 4396.7 (mm^2). An anvil made of steel (ST 37) was used to fix and contain melted polymer in bottom surface of the welding joint.

The welding parameters studied were rotational speed, which varied between 1000 and 1500 (rpm), traverse speed (between 50 and 200 (mm/min)), and the axial force (between 1 and 2 (kN)). The selection of these parameters was based on previous tests. Henceforth the welds are designated according to the following convention: letter *R* followed by rotational speed in (rpm); letter *T* followed by traverse speed in (mm/min); and letter *F* followed by the axial force in (kN). Therefore, the designation R1500T100F2 corresponds to a weld carried out with a rotational speed of 1500 (rpm), a traverse speed of 100 (mm/min) and axial force of 2 (kN). All the welds were performed in a robotic FSW system composed by a robot Motoman ES 165N and an in-house FSW system developed for this effect, that allows the registration of welding data during tests, as described by Mendes et al. [20].

Although pressure is a more representative welding parameter than force, it was decided to identify the weld in relation to force. This is because pressure and force parameters are intrinsically related and the majority of the FSW equipment is parameterized by the force parameter and not pressure. In this study, the relation between pressure (*P*) and force (*F*) is given by:

$$P = \frac{F}{A_{\text{shoulder}} + A_{\text{pin cross section}}} = \frac{F}{4425(\text{mm}^2)} \quad (1)$$

where A_{shoulder} is the area of the shoulder and $A_{\text{pin cross section}}$ is the area of the pin cross section at the base of the pin.

The procedure of welding consists in penetrating the FSW tool in the welding joint controlling the robotic system in positional control. In order to suppress positional errors of the robot, the FSW tool penetrates in the welding joint till the desired contact force (value of the parameter force for each weld experiment) is reached. After a Dwell time of 10 (s) the robot starts moving in the longitudinal movement, where the molten material is transferred from the leading edge to the trailing edge of the tool. During this movement the robotic system produce positional adjustments (axial penetration) controlled by a hybrid force/motion controller in order to keep the desired contact force [21]. Regarding to the heating system, the tool initially at room temperature 25 (°C) is heated during 20 (s) and let to stabilize the temperature of the tool (until the temperature starts decrease). After that, the heating system is turned on for periods of time of 3 (s) followed by a variable period of time where the temperature of the tool is stabilized. This procedure is repeated until the temperature of the tool is above 115 (°C). This procedure is performed initially (before starting welding) and during welding process. The reasons for this procedure are pointed out in Section 3.

For the morphological analysis of the welds, samples were cut out of the weld seams into 10 (μm) thick sections, using a Leitz microtome at room temperature, equipped with a perpendicular slicing glass knife. Optical transmission microscopic analyses were conducted using an Olympus BH transmittance microscope, with digital camera Leica DFC280 and software Leica application suite – LAS V4.

For mechanical tests a minimum of five tensile specimens were removed from each weld, transversely to the welding direction, and tested in a 10 (kN) universal testing machine, SHIMADZU AG-X, at room temperature, according to the **ASTM: D638** standard. The samples were submitted to surface smoothing by milling in order to homogenise the thickness of the samples across the gauge section and eliminate any defect on the crown and root of the welds. The local strains were also determined by digital image correlation (DIC) using an Aramis 3D 5M optical system (GOM GmbH). Before testing, the specimens were prepared by applying a black speckle pattern randomly over the surface of the transverse samples previously painted mat white in order to enable data acquisition by DIC.

The hardness testing methodology used to assess the effectiveness of the welds was based on the procedure detailed in [22], which presents some microhardness analysis for different polymers. This choice is due to the inexistence of a standard for Vickers microhardness of polymers. The Vickers hardness of the surface was determined with a microhardness tester (durometer ZHU 0.2 Zwick–Roell) using a Vickers diamond indenter and a 200 (g) load

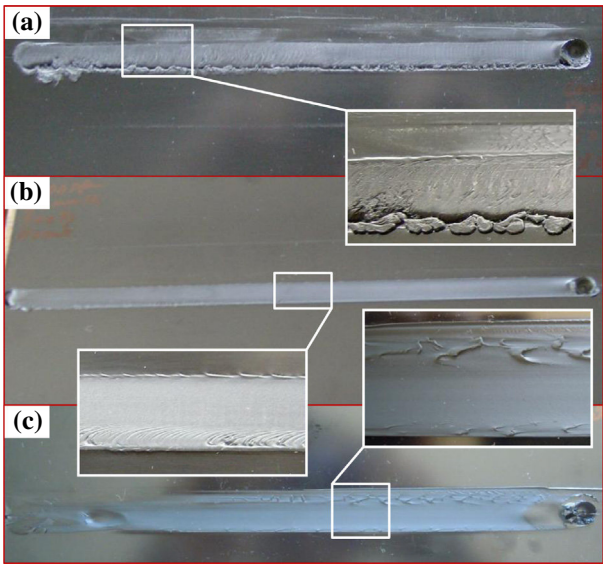

Fig. 3. Effect of temperature on the morphology of the weld crown: (a) R1500T60F1 low temperature: 90 (°C), (b) R1000T200F1 recommended temperature: 115 (°C) and (c) R1500T50F1 excessive temperature: 130 (°C).

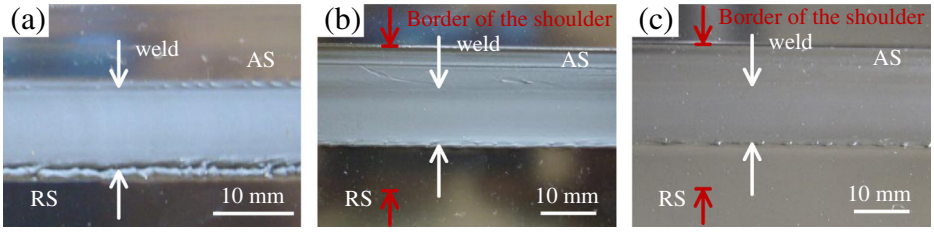

Fig. 4. Effect of axial force on the morphology of the weld crown: (a) R1000T50F1, (b) R1000T50F1.5 and (c) R1000T50F2 (AS – advancing side; RS – retreating side).

applied for 15 s. Vickers hardness measurements were made in a sequential pattern, starting on the retreating side, going through the weld nugget and finishing on the advancing side. The minimum distance between measurements is of at least 1 (mm).

3. Results

3.1. Morphological and micrographic analyses

The weld crow surface is largely influenced by the tool temperature as shown by the three weld experiments illustrated in Fig. 3. The average temperature was 90 (°C) for the first experiment (R1500T60F1, Fig. 3(a)), 115 (°C) for the second experiment (R1000T200F1, Fig. 3(b)) and 130 (°C) for the third experiment (R1500T50F1, Fig. 3(b)). The average temperature of each experiment ranges plus or minus 5 (°C). The weld crown of the first (90 (°C)) and the third (130 (°C)) experiments present some defect while the weld crown of the second (115 (°C)) experiment is practically free of defects.

The axial force has also a clear influence on the weld crown surface as well as on morphology through the thickness direction, as shown in Figs. 4 and 5, respectively. The weld produced with lower axial force (R1000T50F1) presents external and internal defects as shown in Figs. 4(a) and 5(a), respectively. The major external defect is a gap on the surface on the retreating side of the weld. This gap extends along the whole length of the weld as well as through the thickness (internal defects) of the weld. This internal defect is composed of cavities and pores on the border (stirring zone/thermo-mechanical affect zone) of the retreating side of the weld. The stirring zone is the region of the weld where melted/softened material is dragged by the FSW tool. The thermo-mechanical affect zone is the portion of polymeric material that undergoes some deformation due to heating and/or force applied by the FSW tool. Fig. 5(a) shows a weld with poor joining on the retreating side. The other two welds (R1000T50F1.5 and R1000T50F2) do not present visible external or internal defects as shown in Figs. 4(b) and (c) and 5(b) and (c), respectively. However, in these two welds is visible plastic deformation of polymeric material on the surface in the advancing side, see Fig. 4(b) and (c). The deformation on surface, which it is not considered a defect, occurs mainly on the advancing side because the polymeric material is more heated and softened on the advancing side than on retreating side [23]. Additionally, higher axial force promotes weld surface deformation by the pressure imposed to the softened material. The superficial deformation was not observed on the weld R1000T50F1 because this weld was performed at the lowest axial force, less energy is introduced into the weld and the stirred material is less softened. High compression (axial force) promotes the squeeze of the softened polymer which prevents the introduction of air into the weld and helps the cooling of the weld. Thus, shrinkage and void formation is prevented. On the other hand, high axial load increases the energy applied on the weld, leading to low cooling rate which is beneficial to weld quality (from a structural point of view and visual appearance).

Three welding conditions, R1000T100F1, R1250T100F1, R1500T100F1, were chosen to assess the influence of the tool rotational speed on weld quality. Fig. 6 shows the crown surface for the three welds and Fig. 7 shows their morphology through the thickness. While the welds R1250T100F1 and R1500T100F1, performed respectively with 1250 and 1500 (rpm), present excellent crown surface, Fig. 6(b) and (c) respectively, the weld carried out with 1000 (rpm) (R1000T100F1) presents pores and cavities on the retreating side, as shown in Fig. 6(a). Similar conclusions can be drawn by the analysis of the weld morphology through the thickness. The welds R1250T100F1 and R1500T100F1 present morphologies free of visible defects, while the weld R1000T100F1 presents lots of cavities, pores and voids on the border of the retreating side. In other words, with the increase of the rotational speed, the number of cavities on the retreating side decreased or disappeared. These defects suggest that the heat generated on the retreating side of the weld R1000T100F1 was insufficient to promote bonding of material plastically deformed to the base material. Therefore the tool rotational speed plays an important role in heat generation, as claimed by several authors, either in metals [24,25] or in polymers [7]. The concentration of defects on the retreating side is mainly related with lower heat generated on this side, as mentioned above. In fact, Heurtier et al. [24] pointed out that the material flow on the retreating and advancing sides are different and this is the main reason for the concentration of defects on the retreating side.

The effect of traverse speed on weld quality was analysed in welds R1250T50F2, R1250T100F2 and R1250T200F2, performed with traverse speeds of 50, 100 and 200 (mm/min), respectively. The welds R1250T100F2 and R1250T200F2 made with the highest traverse speeds, present excellent superficial finishing, with very smooth surface and without visible defects, see Fig. 8(b) and (c), unlike the weld R1250T50F2, Fig. 8(a), presents surface deformation and burnt material on the crown surface on the advancing side. This effect is likely caused by excessive heat input. In a previous study [17], where the welds were performed in a FSW machine, this phenomenon (burnt material) was not observed because the heat involved in the process was just generated by the friction between FSW tool and polymeric material. On the other hand, the welds presented in the current study were performed in the robotic system where the heat involved in the process beyond it is generated by the friction between FSW tool and polymeric material it is also transferred from the external heating system to the surface of the weld. This means that in the latter welds the heat input is higher than in the former welds. The welds R1250T50F2, R1250T100F2 and R1250T200F2 present ratios of rotational to traverse speeds (R (rpm)/T (mm/min)) of 25, 12.5 and 6.25, respectively. Although the dimension of the R/T ratio (1/mm) can seem non-understandable, the physical phenomenon can make this clearer. As shown above the rotational speed has a great influence in the energy generated in the welding process, thus, the rotational speed can be considered, in some way, as energy. On the other hand, the traverse speed can be understood

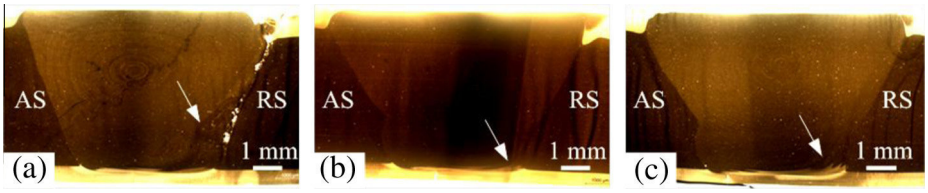

Fig. 5. Micrographs of welds performed with increasing axial force: (a) R1000T50F1, (b) R1000T50F1.5 and (c) R1000T50F2 (AS – advancing side; RS – retreating side).

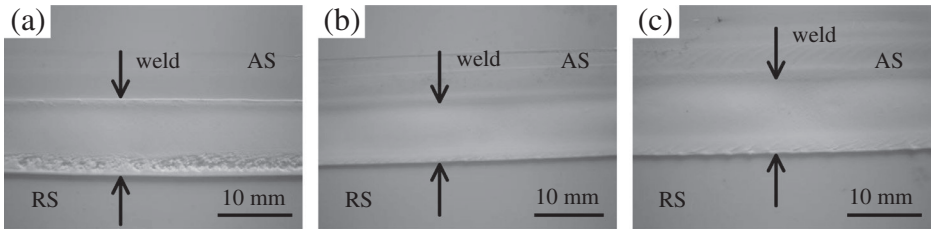

Fig. 6. Effect of rotational speed on the morphology of the weld crown: (a) R1000T100F1, (b) R1250T100F1 and (c) R1500T100F1 (AS – advancing side; RS – retreating side).

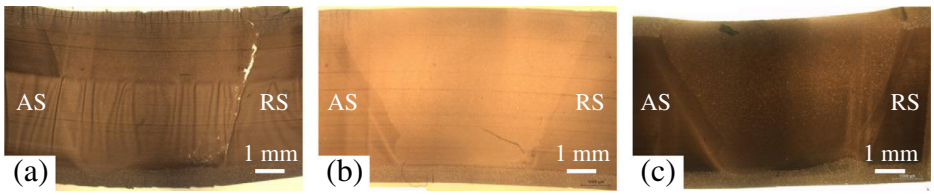

Fig. 7. Micrographs of welds performed with increasing rotational speed: (a) R1000T100F1, (b) R1250T100F1 and (c) R1500T100F1 (AS – advancing side; RS – retreating side).

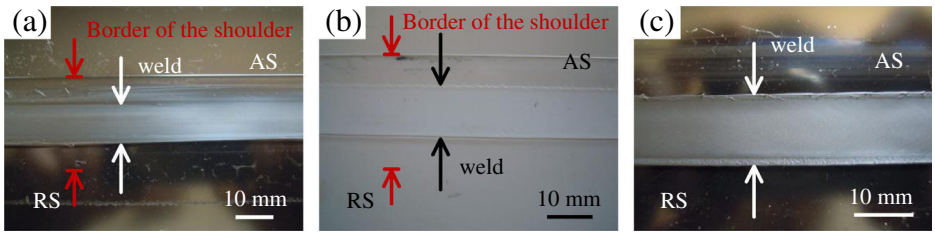

Fig. 8. Effect of traverse speed on the morphology of the weld crown: (a) R1250T50F2, (b) R1250T100F2 and (c) R1250T200F2 (AS – advancing side; RS – retreating side).

Fig. 9. Micrographs of welds performed with increasing traverse speed: (a) R1250T50F2, (b) R1250T100F2 and (c) R1250T200F2 (AS – advancing side; RS – retreating side).

as a conduction rate of that energy to the polymer. It can be concluded that the higher the R/T ratio, the higher the heat introduced into the weld. Thus, the R/T ratio of 25 on weld R1250T50F2 can be considered too high because it is visible some degradation on the weld surface, as shown in Fig. 8(a) where some scratches are visible. Taking into account all the welds shown above it can be stated that to obtain good weld crown appearance, the R/T ratio must be inferior to 20, when the FSW tool temperature is maintained at 115 (°C). The R/T ratio of 20 is obtained for the weld R1000T50F2, which displays good quality, as confirmed by the Figs. 4(c) and 5(c).

The weld R1250T200F2 that presents the best crown surface, actually, has the worst morphology through the thickness, see Figs. 8(c) and 9(c). This weld presents a lot of voids on the nugget and retreating side as well as poor mixing of polymeric material on retreating side. The morphology through the thickness of the other two welds, R1250T50F2 and R1250T100F2, do not present visible defects as shown on Fig. 9(a) and (b) respectively. Thus, the traverse speed plays also an important role in the weld quality. The R/T ratio can be used to define a threshold above which good quality welds is obtained. In the present investigation the R/T ratio must be higher than 10 in order to obtain welds with good crown

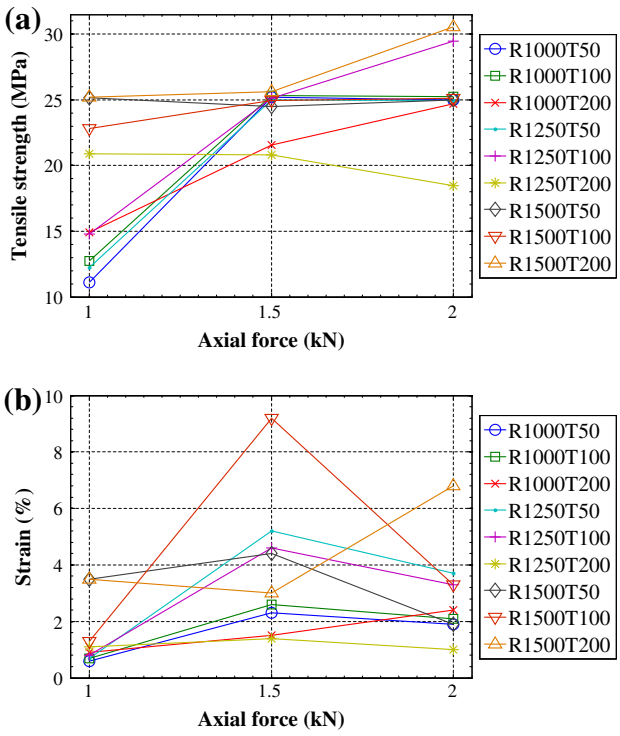

Fig. 10. Effect of axial force on: (a) the tensile strength; (b) the strain at break of the welds.

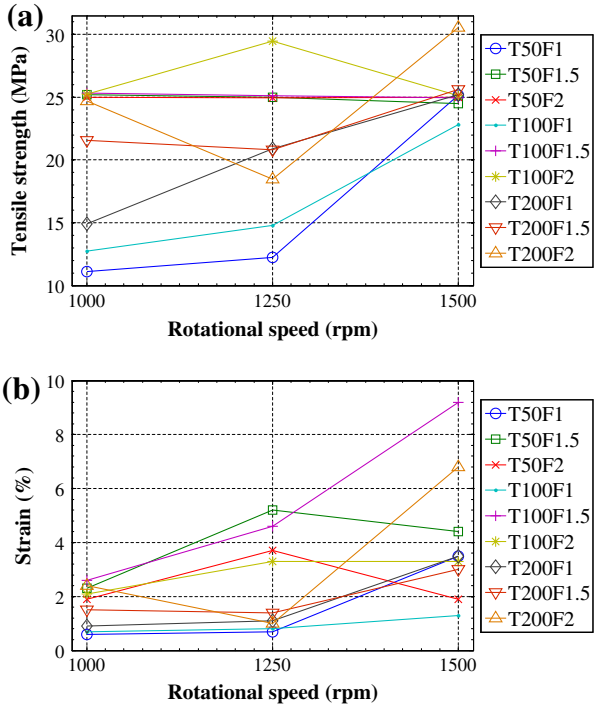

Fig. 11. Effect of rotational speed on: (a) the tensile strength; (b) the strain at break of the welds.

appearance and free of internal defects, as confirmed by the weld R1000T100F1 (Figs. 6(a) and 7(a)). The current authors reached similar conclusions in a previous study on welds performed on a FSW machine [17]. It should be mentioned that all the welds suffer of lack of penetration (Figs. 5, 7 and 9), the pin was not enough long to avoid root defects. Although the use of force control, the control of the robotic system can cause tool displacements in the axial direction, the size of the root weld defects was approximately constant (this is not well mirrored by Figs. 5, 6 and 7). This topic is not approached in this study, however, it was approached by Arici and Sinmazçelýk [10], who proposed the use of double pass to eliminate root weld defects.

3.2. Mechanical performance

The weld quality was also assessed by the ultimate tensile strength and strain at break. In all welds studied, the fracture occurred on the retreating side of the weld. It was observed that there is a general trend of weld tensile strength increase with increasing axial force, as shown in Fig. 10(a). This relation is particularly visible between the welds produced with axial force of 1 (kN) and 1.5 (kN). The tensile strength of the welds shown in Figs. 4 and 5 are represented in Fig. 10(a) by the R1000T50 curve. In this case, it is clearly visible the increase of tensile strength with increasing axial force. The weld R1000T50F1 presents the lowest tensile strength among the three weld conditions shown in Fig. 4 (R1000T50F1, R1000T50F1.5 and R1000T50F2). This behaviour is easily understood by the presence of defects on surface and retreating side of the weld R1000T50F1, Figs. 4(a) and 5(a).

As can be seen by the analysis of Fig. 10(a), the parameter axial force has a high influence on the tensile strength of the welds, mainly on the welds where less heat is generated i.e. rotational speeds are lower than 1500 (rpm). This suggests that axial force promotes reduction of the pores and voids in the weld through the thickness direction. Higher axial force promotes removal of internal weld shrinkage or dragging air into the weld, which are the main causes pointed out in the literature [26] in the formation of defects (as voids) in FSW of polymers.

Fig. 10(b) shows that the welds produced at 1 (kN) present the lowest strain followed by the welds produced at 2 (kN) which are preceded by the welds produced at 1.5 (kN). This order of

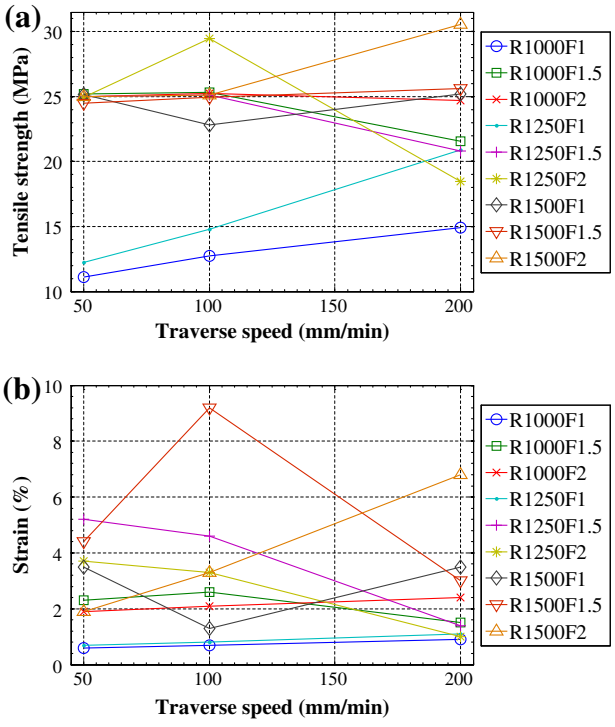

Fig. 12. Effect of traverse speed on: (a) the tensile strength; (b) the strain of the welds.

magnitude for the strain can be explained by the size of the zone of poor mixing of material, which is highlighted by an arrow in Fig. 5(a), (c) and (b), respectively. These figures allow to conclude that the larger the zone of poor mixing of material, the lower the strain of the weld.

The parameters rotational speed and axial force have similar influence on tensile strength and strain at break of welds. Fig. 11(a) shows that there is a general trend of increase tensile strength of welds with the increase of rotational speed. For instance, the tensile strength of the welds shown in Figs. 6 and 7 are represented in Fig. 11(a) by the T100F1 curve. In this case, it is visible the increase in tensile strength with the increase of rotational speed. This result is explained by the decrease of defects that act as stress concentrators. The welding parameter rotational speed provides an effect on strain similar to the effect on tensile strength, Fig. 11(b). This means that there is a tendency of increasing strain with increase of rotational speed.

It would be reckless to make any conclusion about the influence of traverse speed on tensile strength of the welds based on just some particular welding conditions. Although Bagheri et al. [15] have stated that high travel speed decreases the tensile strength, in the current study and in the study carried out by Sorensen et al. [27] seems to be excessive to make such statement. Actually, as can be seen in Fig. 12(a) in some welding condition the statement of Bagheri et al. [15] is partially verified, for example R1000F1.5 and R1250F1.5, but the other welding conditions do not reflect this effect. Unlike in the case of the welds R1000F1 and R1250F1 the opposite effect is verified.

The increase of the traverse speed leads to decreasing weld strain, as shown in Fig. 12(b). This generalisation may perhaps be justified by the different morphologies presented by the welds. The weld morphologies presented in Fig. 9 display different flow lines as observed by Strand [3], who stated that low traverse speed results in less severe flow lines, onion ring, and retreating interface. Higher traverse speeds lead to more forced material flow, which in turn prevents the mixing of material. Thus, adhesion of polymeric material on the retreating side is lower and formation of defects in this zone is promoted, as exhibited by the weld R1250T200F2 (Fig. 9(c)).

The complete spectrum of mechanical properties of welds performed in the robotic system using heated tool at 115 (°C) is presented in Table 2. The best welds present high tensile strength and reasonable strain. The weld R1500T200F2 presents the best strength efficiency, 75.5 (%). The strength efficiency is the ratio between tensile strength of the welds and base material. The weld R1500T100F1.5 presents the best strain 9.2 (%) while base material presents 50 (%). Analysing Table 2, it can be stated that high tensile strength and strain performances are reached when high rotational speed and axial force are used to produce welds.

Hardness measurement can be used to estimate relative mechanical strength of welds in metallic materials. The weld R1500T100F200 was chosen to illustrate the hardness profile measured on the cross section because it presents no morphological defects. Defects can alter the results of hardness measurement. As shown in Fig. 13, the welding hardness is unchanged in relation to the hardness of base material, about 11 (HV0.2). Consequently, hardness does not give useful information about mechanical strength of welds in ABS.

4. Discussion

4.1. Temperature

Welds with good quality must display a smooth crown without any pores or cracks, because this kind of defects is usually the main reason for fracture initiation in polymeric welds, as stated by Frassine et al. [28], who have studied the resistance to crack initiation and propagation in the fracture of polymers.

The parameter tool temperature plays an important role in FSW of polymers. As shown by Fig. 3(a), an average tool temperature of 90 (°C) provides poor weld crown appearance, where there is some porosity and formation of flash on the retreating side of the weld. In addition, the whole weld crown is rough, which means that the stirred material does not melt enough. Thus, when the cooling stage occurs, consolidation of material appears to be poor. It can be stated that to perform welds with smooth crown the tool temperature must be higher than 90 (°C). On the other hand, an average tool temperature of 130 (°C) also provides poor weld crown appearance, Fig. 3(c). In this experiment the weld crown and the thermo-mechanical affected zone on the surface (zone not stirred but affect by the temperature and pressure imposed by the shoulder) are burnt. This shows that the tool temperature of 130 (°C) is too high to perform FSW on ABS. However, high tool temperature is required to promote material mixing which explain the smoothness present in part of this weld crown. A similar effect have been reported by Bagheri et al. [15] when the initial tool temperature, before starts the welding process, assumes high values, the weld crown is burnt. It should be highlighted that while these authors only considered the tool temperature before start FSW process, the current study takes into account the tool temperature before and during the FSW process. Finally, an average tool temperature of 115 (°C) provides a quality weld crown, as shown in Fig. 3(b). The weld crown performed at 115 (°C) is smooth and free of pores. A tool temperature close the glass transition temperature of the polymer seems to be the most suitable to perform FSW.

Owing to low thermal conductivity of ABS, an increase in temperature of the tool does not imply an increase in stirred material temperature. Thus, the material that is in the interface shoulder/joint will be more affected by the tool temperature. In addition, the heat transferred between FSW tool and material occurs mainly by the shoulder than by the pin due to the fact that the shoulder area is larger. However, the pin plays an important role in the generation of heat by friction. It is expectable that the anvil has low influence on the weld quality, particularly at the root of the weld. This statement is based on the fact that ABS is a bad thermal conductor and the used anvil has a large volume that enables heat spreading for the whole anvil preventing that it reaches a level of temperature capable to cause any influence on the weld quality. It was found that higher values of rotational speed and lower values of traverse speed, without supplying external heating, promote increasing of tool temperature and consequently increasing weld crown temperature too. This increase in temperature is due to friction generated inside the FSW tool (tool mechanism) and friction generated between the pin of the tool and polymeric material. Since polymeric material is low thermal conductor, heat generated between pin and material tends to flow through the pin to the shoulder which in turn makes heat to flow/spread to the weld surface. In some welding conditions, it was found that external heating is not required because the welding process generates enough heat by friction. Moreover, in some other welding conditions without supplying external heating it is generated too much heat, leading to burnt of weld crown surface. This suggests that the use of a cooling system could improve weld quality.

Owing to the similarity of the welding parameters and material approached in this study and the ones approached by Mendes et al. [17] in a previous research, the results of both studies are compared below. In the previous study the welds were done in a FSW machine, without using any external heating. Robotic welds present in general smoother crown surface and better morphology through the thickness than the welds performed in the FSW machine, as can be realized by comparing for instance welds

Table 2
Tensile strength efficiency (%) and strain of welds (%) produced in the robotic system.

T (mm/min) ↓	R (rpm) →	1000		1250		1500	
	F (kN) ↓	Strength efficiency (%)	Strain (%)	Strength efficiency (%)	Strain (%)	Strength efficiency (%)	Strain (%)
50	1	27.4	0.6	30.2	0.7	62.2	3.5
	1.5	62.2	2.3	61.7	5.2	60.5	4.4
	2	61.7	1.9	61.6	3.7	61.7	1.9
100	1	31.5	0.7	36.5	0.8	56.3	1.3
	1.5	62.5	2.6	62.0	4.6	61.6	9.2
	2	62.3	2.1	72.8	3.3	62.0	3.3
200	1	36.8	0.9	51.6	1.1	62.2	3.5
	1.5	53.3	1.5	51.4	1.4	63.3	3.0
	2	61.0	2.4	45.6	1.0	75.5	6.8

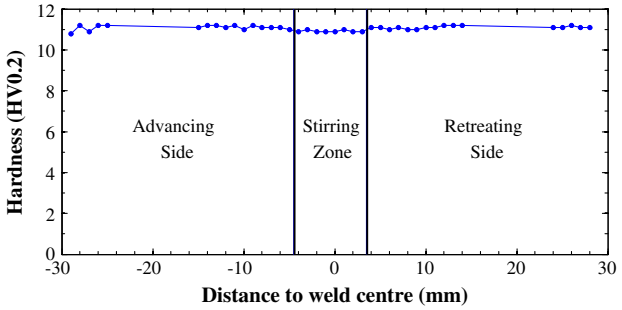

Fig. 13. Hardness profile of the weld R1500T100F200.

illustrated in Figs. 6 and 7 with welds done with similar parameters in a FSW machine, see [17]. This difference can be explained by the additional heat supplied by the tool shoulder to the welds.

4.2. Axial force

As shown above, high rotational speed generates more heat by friction and thus promotes mixing of material and adhesion to base material. If rotational speed is low the axial force is a key factor to do good welds. Fig. 10(a) shows that all welds performed with lower rotational speed (1000 and 1250 (rpm)) practically have increase in tensile strength with the increase in axial force. This effect is more visible between the welds performed at 1 (kN) and 1.5 (kN). Considering just the welds performed at high rotational speed (R1500T50, R1500T100 and R1500T200), Fig. 10(a), it appears that its tensile strength does not have significant change. These results are in good agreement with those presented by Mendes et al. [17] which demonstrate that the axial force does not cause any effect in tensile strength of welds performed with high rotational speed (1500 (rpm)).

In the current study, the strain at break of the robotic welds increases with increase of axial force, comparing the welds performed at 1 (kN) with the welds performed at 1.5 and 2 (kN). The two latter welds present clearly higher strain values than the former weld. In the previous study, the welds done using similar welding conditions (R1500T100F0.75 and R1500T100F2.25) present similar trend and strain values comparable to those welds performed in the robotic system, R1500T100F1 and R1500T100F2, respectively.

4.3. Rotational speed

The effect of the tool rotational speed on morphology of robotic welds is mirrored in a decrease of the number and size of defects with increasing rotational speed, as shown above in R1000T100F1, R1250T100F1 and R1500T100F1. The welds performed in the FSW machine with similar parameters (R1000T100F0.75, R1250T100 F0.75 and R1500T100F0.75) present exactly the same effect, i.e. the quantity and size of weld defects decrease with increase in rotational speed. The effect of the rotational speed on mechanical properties (tensile strength and strain at break) of the welds done in both systems (robotic system and FSW machine) is similar, i.e., mechanical properties increase with increasing rotational speed, as shown in Table 3. The tensile strength and strain increase as the defects in the weld decrease. It is clearly visible that the welds performed in the robotic system present better crown surface (Fig. 6) and morphology through the thickness direction (Fig. 7) than the welds performed in the FSW machine. The same effect is confirmed by the mechanical properties of the welds shown in Table 3. This effect may be explained by supplying external heat to the weld and by the slight difference of the axial force parameter which was used in the welds production.

4.4. Traverse speed

It is difficult to establish a particular relation between traverse speed and the mechanical properties of the welds. By the analysis of Fig. 12(a), it is probably that in welding conditions less favourable, i.e. where less heat is generated due to low values of rotational speed or axial force, the increase in traverse speed provides improvement of the tensile strength of the welds. However, the tensile strength of these welds is in general low. On the other hand, in welding conditions where more heat is generated, it seems that the welds do not suffer any change or suffer a small

Table 3
Tensile strength efficiency (%) and strain of welds (%) produced in the robotic system and in the FSW machine.

Weld	R1000T100F...		R1250T100F...		R1500T100F...	
	Strength efficiency (%)	Strain (%)	Strength efficiency (%)	Strain (%)	Strength efficiency (%)	Strain (%)
Robotic (F1)	31.5	0.7	36.5	0.8	56.3	1.3
Machine (F0.75)	31.0	0.5	35.0	0.8	62.0	1.2

decrease in tensile strength with increasing traverse speed. The strain property of the welds is clearly improved with decrease of the traverse speed. In the previous study, where the welds were performed in the FSW machine, just a set of welds was taken into consideration (R1250T50F3.75, R1250T100F2 and R1250T200F3 .25). It was verified that there was no significant effect on the mechanical properties of the welds with the parameter traverse speed. This was likely because all of these welds were performed at relatively high axial force which, as demonstrated above, improves weld quality.

During the welding process it was verified that low traverse speed leads to overheating or keeping of tool temperature which dismisses external heating. This phenomenon was verified in welds performed at low traverse speed (50 (mm/min)) and high axial force (1.5 or 2 (kN)) and rotational speed (1250 or 1500 (rpm)). Since this heat flux flows through the FSW tool to weld surface, as described above, it is plausible to state that traverse speed has a strong influence on temperature reached on weld crown surface. The study carried out by Bagheri et al. [15] claims that lower traverse speed leads to weld with higher tensile strength. This suggests that lower traverse speed leads to a scenario in which the shoulder and the pin heat the welding zone for a longer time, providing more heat to weld. However, Bagheri et al. [15] took into account welds which have been performed at very low traverse speeds. The welds which presented a meaningful improvement of tensile strength property were performed at 20 (mm/min). From an industrial point of view, so low traverse speed values are considered unattractive and impracticable. By this reason traverse speeds lower than 50 (mm/min) are despised. Nevertheless, comparing the results obtained in the current study with results reported by Bagheri et al. [15], it can be stated that just very low traverse speeds can really improve tensile strength of weld.

4.5. Overview

In general, the weld results performed in the robotic system are similar to the weld results performed in the FSW machine [17], where it was not used external heating. The mechanical properties of the welds performed in the robotic system display the same evolution tendencies as the welds performed in the FSW machine when the welding parameters (axial force, rotational speed and traverse speed) are changed. However, there are slightly differences between the welds performed in the robotic system and in the FSW machine that can be justified by supplying external heating to welds. This suggests that the welding parameter temperature of the FSW tool influences weld quality, mainly the weld crown surface.

5. Conclusions

The aim of the present research is to study the effect of the axial force, tool rotational and traverse speeds as well as the tool temperature, on the quality of welds carried out by FSW on ABS plates using a robotic system and a stationary shoulder tool. Furthermore, results are compared with welds performed in a FSW machine [17]. Based on the experimental results and discussion, the following conclusions can be drawn:

- It is feasible to produce good quality welds in a robotic FSW system.
- A tool temperature of 115 (°C) improves weld quality, specially the weld crown surface.
- High axial force promotes the squeeze of the molten polymeric material, preventing introduction of air into the weld and helps cooling of the weld, avoiding shrinkage and voids formation.
- High axial force improves tensile strength and strain of welds.
- The rotational speed is primarily responsible for heat generation, promoting adequate plasticizing and mixing the polymer.
- High tool rotational speed improves tensile strength and strain of welds.
- Welds free of defects present the same hardness as base material.
- To prevent lack of heat or overheating of the tool the R/T ratio must range between 10 and 20.
- A quality weld is obtained for tool temperature of 115 (°C), axial force higher than 1.5 (kN), rotational speed higher than 1250 (rpm) and low traverse speed (ranging between 50 and 100 (mm/min)).
- The welds produced in the robotic system present similar or better appearance and mechanical properties than the welds produced in the FSW machine.

Acknowledgements

This research is supported by FEDER funds through the program COMPETE (*Programa Operacional Factores de Competitividade*), under the project CENTRO-07-0224-FEDER-002001(MT4MOBI) and by national funds through FCT (*Fundação para a Ciência e a Tecnologia*) under the project PEst-C/EME/UI0285/2013 and the Grant No. SFRH/BD/62485/2009. The authors are grateful to ThyssenKrupp Portugal – Aços e Serviços SA for the heat treatment of the FSW tools and Yaskawa Ibérica for the equipment and support provided.

Appendix A. Supplementary material

Supplementary data associated with this article can be found, in the online version, at http://dx.doi.org/10.1016/j.matdes.2014.07.047.

References

[1] Strand S. Joining plastics – can friction stir welding compete? In: Proc. electr. insul. conf. electr. manuf. coil wind. technol. conf. (Cat. No. 03CH37480), IEEE; 2003. p. 321–6.
[2] Nelson TW, Sorenson CD, Johns CJ. Friction stir welding of polymeric materials. US 6811632 B2; 2004.
[3] Strand S. Effects of friction stir welding on polymer microstructure. Brigham Young University; 2004.
[4] Kiss Z, Czigány T. Applicability of friction stir welding in polymeric materials. Period Polytech Mech Eng 2007;51:15.
[5] Scialpi A, Troughton M, Andrews S, De Filippis LAC. In-line reciprocating friction stir welding of plastics. Joi Plast von Kunststoffen 2007;1:42–51.
[6] Scialpi A, Troughton M, Andrews S, De Filippis LAC. Viblade™: friction stir welding for plastics. Weld Int 2009;23:846–55.
[7] Aydin M. Effects of welding parameters and pre-heating on the friction stir welding of UHMW-polyethylene. Polym Plast Technol Eng 2010;49:595–601.
[8] Bozkurt Y. The optimization of friction stir welding process parameters to achieve maximum tensile strength in polyethylene sheets. Mater Des 2012;35:440–5.
[9] Payganeh GH, Arab NBM, Asl YD, Ghasemi FA, Boroujeni MS. Effects of friction stir welding process parameters on appearance and strength of polypropylene composite welds. Int J Phys Sci 2011;6:4595–601.
[10] Arici A, Sinmazçelýk T. Effects of double passes of the tool on friction stir welding of polyethylene. J Mater Sci 2005;40:3313–6.
[11] Panneerselvam K, Lenin K. Investigation on effect of tool forces and joint defects during FSW of polypropylene plate. Procedia Eng 2012;38:3927–40.
[12] Panneerselvam K, Lenin K. Joining of nylon 6 plate by friction stir welding process using threaded pin profile. Mater Des 2014;53:302–7.
[13] Kiss Z, Czigány T. Effect of welding parameters on the heat affected zone and the mechanical properties of friction stir welded poly(ethylene-terephthalate-glycol). J Appl Polym Sci 2012;125:2231–8.
[14] Kiss Z, Czigány T. Microscopic analysis of the morphology of seams in friction stir welded polypropylene. Express Polym Lett 2012;6:54–62.

[15] Bagheri A, Azdast T, Doniavi A. An experimental study on mechanical properties of friction stir welded ABS sheets. Mater Des 2013;43:402–9.
[16] Pirizadeh M, Azdast T, Rash Ahmadi S, Mamaghani Shishavan S, Bagheri A. Friction stir welding of thermoplastics using a newly designed tool. Mater Des 2014;54:342–7.
[17] Mendes N, Loureiro A, Martins C, Neto P, Pires JN. Effect of friction stir welding parameters on morphology and strength of acrylonitrile butadiene styrene plate welds. Mater Des 2014;58:457–64.
[18] Schneider U, Drust M, Ansaloni M, Lehmann C, Pellicciari M, Leali F, et al. Improving robotic machining accuracy through experimental error investigation and modular compensation. Int J Adv Manuf Technol 2014.
[19] Leali F, Vergnano A, Pini F, Pellicciari M, Berselli G. A workcell calibration method for enhancing accuracy in robot machining of aerospace parts. Int J Adv Manuf Technol 2014.
[20] Mendes N, Neto P, Simão MA, Loureiro A, Pires JN. A novel friction stir welding robotic platform: welding polymeric materials. Int J Adv Manuf Technol 2014.
[21] Mendes N, Neto P, Pires JN, Loureiro A. An optimal fuzzy-PI force/motion controller to increase industrial robot autonomy. Int J Adv Manuf Technol 2013;68:435–41.
[22] Poggio C, Lombardini M, Gaviati S, Chiesa M. Evaluation of Vickers hardness and depth of cure of six composite resins photo-activated with different polymerization modes. J Conserv Dent 2012;15:237–41.
[23] Nandan R, Roy GG, Lienert TJ, Debroy T. Three-dimensional heat and material flow during friction stir welding of mild steel. Acta Mater 2007;55:883–95.
[24] Heurtier P, Jones MJ, Desrayaud C, Driver JH, Montheillet F, Allehaux D. Mechanical and thermal modelling of friction stir welding. J Mater Process Technol 2006;171:348–57.
[25] Neto DM, Neto P. Numerical modeling of friction stir welding process: a literature review. Int J Adv Manuf Technol 2012;65:115–26.
[26] Oliveira PHF, Amancio-Filho ST, dos Santos JF, Hage E. Preliminary study on the feasibility of friction spot welding in PMMA. Mater Lett 2010;64:2098–101.
[27] Sorensen CD, Nelson TW, Strand S, Johns C, Christensen J. Joining of thermoplastics with friction stir welding. In: Tech. pap. Annu. Tech. Conf. Plast. Eng. Incorporated (ANTEC 2001); 2001. p. 1246–50.
[28] Frassine R, Rink M, Leggio A, Pavan A. Experimental analysis of viscoelastic criteria for crack initiation and growth in polymers. Int J Fract 1996;81:55–75.